

Investigating the role of LRRC8A in microglia and macrophage function

A thesis submitted to the University of Manchester for the degree of Doctor of Philosophy in the Faculty of Biology, Medicine and Health

2021

James R Cook

Faculty of Biology, Medicine and Health
Division of Neuroscience and Experimental Psychology

Contents

Contents	2
List of Figures	5
List of Tables	6
List of Abbreviations	7
Abstract	10
Declaration	11
Copyright Statement	12
Experimental Contributions	13
Acknowledgements	14
Chapter 1: Introduction	15
1.1 Microglia – An Overview	16
1.1.1 Microglial Ontogeny.....	17
1.1.2 Basic properties and phenotypes of microglia	18
1.2 Homeostatic microglial functions	21
1.2.1 Microglia in CNS development.....	21
1.2.2 Microglia in synaptic regulation	22
1.3 Reactive microglial effector functions	23
1.3.1 Chemotaxis and migration.....	24
1.3.2 Phagocytosis	26
1.3.3 Neuroinflammation	28
1.4 Regulation of microglial functions by ion channels	31
1.4.1 Morphology and Surveillance.....	32
1.4.2 Chemotaxis and migration.....	32
1.4.3 Phagocytosis	33
1.5 LRRC8A and the Volume Regulated Anion Channel (VRAC)	34
1.5.1 Structure and function of LRRC8 family proteins	36
1.6 VRAC functions in physiology	37
1.6.1 Role of VRAC in insulin release	38
1.6.2 Role of VRAC in immunity.....	38
1.6.3 VRAC in neuronal function	39
1.6.4 VRAC in microglial biology	40
1.7 Role of VRAC in Stroke	43
1.8 VRAC-independent functions of LRRC8A	44
1.9 Study Rationale	47
1.10 Aims	48
1.10.1 Chapter 2 – Investigating the role of VRAC in microglial physiology	48

1.10.2	Chapter 3 – Identifying novel LRRc8A-dependent signalling pathways	48
Chapter 2:	Investigating the role of VRAC in microglial physiology	49
2.1	Introduction.....	50
2.1.1	Specific Aims	51
2.2	Materials and Methods.....	52
2.2.1	Chemicals.....	52
2.2.2	Animals.....	52
2.2.3	Transcardial Perfusion	53
2.2.4	Cell Culture.....	53
2.2.5	Western Blotting.....	54
2.2.6	Regulatory volume decrease assay	54
2.2.7	Phagocytosis assays.....	55
2.2.8	In vitro motility assay	56
2.2.9	RNA Sequencing (RNA-Seq)	56
2.2.10	Acute brain slices	57
2.2.11	Lectin injection and cranial window implantation	58
2.2.12	Multiphoton imaging	58
2.2.13	Middle cerebral artery occlusion.....	59
2.2.14	Immunohistochemistry	60
2.2.15	Microglial morphology analysis	60
2.2.16	Statistics	61
2.3	Results.....	63
2.3.1	LRRc8A KO impairs volume regulation in microglia and BMDM	63
2.3.2	RNA Sequencing of primary microglia	65
2.3.3	Pathway analysis of identified DEGs	68
2.3.4	Role of VRAC in phagocytosis	71
2.3.5	VRAC inhibitors suppress phagocytosis in BMDM and microglia	71
2.3.6	VRAC is dispensable for phagocytosis	73
2.3.7	VRAC is dispensable for stochastic migration <i>in vitro</i>	75
2.3.8	DCPIB inhibits microglial chemotaxis <i>in situ</i>	77
2.3.9	VRAC does not mediate microglial chemotaxis	79
2.3.10	Microglial VRAC does not affect stroke volume or reactive morphology	82
2.3.11	VRAC does not regulate homeostatic microglial morphology	85
2.4	Discussion.....	87
2.4.1	VRAC is required for microglial volume regulation but dispensable for homeostasis.....	87
2.4.2	VRAC does not regulate phagocytosis	88
2.4.3	Cell migration and purinergic chemotaxis are independent of VRAC	89
2.4.4	VRAC does not regulate microglial morphology or ischemic damage	91
2.4.5	VRAC as a drug target for ischemic stroke	92
2.4.6	Conclusions	94
2.5	Appendix	95
Chapter 3:	Identifying novel LRRc8A-dependent signalling pathways.....	103
3.1	Introduction.....	104
3.1.1	Type I Interferons	104
3.1.2	Mechanisms of nucleotide sensing	104
3.1.3	Study rationale.....	105
3.1.4	Specific aims	106
3.2	Materials and Methods.....	107
3.2.1	Chemicals.....	107
3.2.2	Animals.....	107

3.2.3	Cell culture.....	107
3.2.4	Bone marrow derived macrophage culture	107
3.2.5	Stimulation with hypotonic or isotonic media	108
3.2.6	RNA isolation.....	108
3.2.7	Quantitative polymerase chain reaction (qPCR)	109
3.2.8	RNA Sequencing	110
3.2.9	RNA Sequencing Data Analysis.....	110
3.2.10	Western Blot.....	111
3.2.11	Statistics	112
3.3	Results.....	114
3.3.1	Hypotonicity induces transcriptomic changes which are modulated by LRR8A 114	
3.3.2	Hypotonicity-induced gene expression is differentially modulated by DCPIB and LRR8A-KO	116
3.3.3	Hypotonicity induces antiviral signalling.....	119
3.3.4	LRR8A-dependent signal modulation under hypotonic conditions.....	122
3.3.5	LRR8A restricts interferon responses following hypotonic shock.....	124
3.3.6	LRR8A modulates interferon responses independently of VRAC channel activity	125
3.3.7	LRR8A activates the PI3K-AKT pathway under hypotonic conditions	128
3.3.8	LRR8A-dependent AKT activation requires TBK1/IKKε, PKC and Fyn/Hck	130
3.3.9	LRR8A modulates interferon responses independently of PI3K-AKT	133
3.4	Discussion.....	134
3.4.1	Hypotonic shock alters macrophage physiology	134
3.4.2	Hypotonicity induces antiviral signalling.....	136
3.4.3	LRR8A modulates interferon responses following osmotic swelling	137
3.4.4	LRR8A-dependent signalling is largely independent of VRAC under hypotonic conditions	139
3.4.5	LRR8A stimulates PI3K in a PKC- and Fyn/Hck-dependent manner.....	140
3.4.6	Conclusions	143
Chapter 4:	General Discussion	144
4.1	VRAC is dispensable for multiple microglial functions.....	145
4.2	LRR8A/VRAC as a signal transducer.....	146
4.2.1	LRR8A-PI3K-AKT signalling.....	147
4.3	LRR8A restricts antiviral signalling	149
4.4	Concluding Remarks.....	151
References		153
Appendix.....		179
	Review: Is Targeting the Inflammasome a Way Forward for Neuroscience Drug Discovery?	179

Word Count: 41348

List of Figures

Figure 1.1: Homeostatic and reactive microglial functions in the CNS	31
Figure 1.2: Structure and known functions of VRAC	42
Figure 1.3: VRAC-independent signalling functions of LRRC8A	47
Figure 2.1: LRRC8A is required for volume regulation in microglia and macrophages:	64
Figure 2.2: RNA Sequencing of acutely isolated microglia from LRRC8A knockout mice	67
Figure 2.3: Enrichment analysis of LRRC8A-dependent transcriptional changes:	70
Figure 2.4: VRAC inhibitors suppress phagocytosis in primary microglia and macrophages:	72
Figure 2.5: VRAC is dispensable for phagocytosis	74
Figure 2.6: VRAC does not regulate microglial migration <i>in vitro</i> :	76
Figure 2.7: DCPIB inhibits microglial process chemoattraction:	78
Figure 2.8: VRAC is dispensable for microglial chemotaxis <i>in vivo</i> :	81
Figure 2.9: Validation of automated microglial morphology analysis.....	84
Figure 2.10: VRAC does not regulate reactive or homeostatic microglial morphology	86
Figure 2.11: Expression of chloride channel genes in WT, LRRC8A-KO and Cre microglia	95
Figure 3.1: Hypotonicity induces transcriptomic changes in BMDM:	115
Figure 3.2: Modulation of hypotonicity-induced gene expression by LRRC8A and DCPIB:	118
Figure 3.3: Hypotonicity induces wide-ranging changes in cellular physiology:	120
Figure 3.4: Antiviral response pathways are activated by hypotonic shock	121
Figure 3.5: LRRC8A modulates multiple signalling pathways independently of DCPIB:	123
Figure 3.6: LRRC8A KO exacerbates interferon responses following hypotonic shock:	126
Figure 3.7: VRAC does not mediate LRRC8A's effects on antiviral signalling:	128
Figure 3.8: LRRC8A activates AKT following hypotonic shock:	129
Figure 3.9: LRRC8A-dependent AKT activity relies on PI3K, TBK1/IKK ϵ and protein kinase C	132
Figure 3.10: PI3K-AKT signalling does not restrict hypotonicity-induced ISG expression	133
Figure 3.11: LRRC8A restricts interferon signalling following osmotic shock	138
Figure 3.12: Proposed mechanisms of LRRC8A-PI3K signalling	142

List of Tables

Table 2.1– Morphological parameters for microglial analysis	61
Table 2.2: Differentially expressed genes in WT, LRRC8A-KO and Cre microglia.....	95
Table 3.1: Primer sequences for qPCR.....	110
Table 3.2: Primary and secondary antibodies for western blot	112

List of Abbreviations

3D	Three-dimensional
A1R	Adenosine A1 receptor
aCSF	Artificial cerebrospinal fluid
AD	Alzheimer's disease
ADO	Adenosine
ANO	Anoctamin
ANOVA	Analysis of variance
ApoE	Apolipoprotein E
ATP	Adenosine triphosphate
AUC	Area under curve
A β	Amyloid-beta
BDNF	Brain-derived neurotrophic factor
BM	Bone marrow
BMDM	Bone marrow-derived macrophage
BSA	Bovine serum albumin
C1q	Complement component 1q
C3	Complement component 3
CAV1	Caveolin-1
CD	Cluster of differentiation
cGAMP	cyclic guanosine monophosphate-adenosine monophosphate cyclic guanosine monophosphate-adenosine monophosphate synthase
cGAS	
CLCN	Chloride voltage-gated channel
CLIC	Chloride intracellular channel
CNS	Central nervous system
CR3	Complement receptor 3
CSF1R	colony stimulating factor 1 receptor
CX3CL1	C-X3-C motif chemokine ligand 1
CX3CR1	C-X3-C motif chemokine receptor 1
Cxcl	C-X-C motif chemokine ligand
CyD	Cytochalasin D
DAMP	Damage-associated molecular pattern
DCPIB	4-(2-butyl-6,7-dichlor-2-cyclopentylindan-1-on-5-yl) oxobutyric acid
DEG	Differentially-expressed gene
DMEM	Dulbecco's modified eagle's medium
DMSO	Dimethyl sulphoxide
DNA	Deoxyribonucleic acid
DSB	Double-stranded break
EAA	Excitatory amino acid
Ebo	ébouriffé
ER	Endoplasmic reticulum
ERK	Extracellular signal-regulated kinase
FBS	Fetal bovine serum
FFA	Flufenamic acid

GAB2	GRB2-associated binding protein 2
GABA	Gamma-aminobutyric acid
GDNF	Glial cell-derived neurotrophic factor
GFP	Green fluorescent protein
GLT-1	Glutamine transporter 1
GRB2	Growth factor receptor bound protein 2
GS	Glutamine synthetase
GTP	Guanosine triphosphate
HSV-1	Herpes simplex virus 1
Hypo	Hypotonic
Iba1	Ionised calcium binding adapter molecule 1
IFN1R	Type-1 interferon receptor
Ifnb	Interferon beta
IFN-β	Interferon beta
IFN-γ	Interferon gamma
IGF1	Insulin-like growth factor 1
IL	Interleukin
IPA	Ingenuity pathway analysis
IRF	Interferon regulatory factor
IRS1	Insulin receptor substrate
ISG	Interferon stimulated gene
Iso	Isotonic
KO	Knockout
LPS	Lipopolysaccharide
LRRC8	Leucine-rich repeat containing 8
MACS	Magnetic cell sorting
MCAo	Middle cerebral artery occlusion
M-CSF/CSF1	macrophage-colony stimulating factor / colony-stimulating factor 1
MDA5	Melanoma differentiation-associated gene 5
MFG-E8	Milk fat globule protein E8
MPS	Mononuclear phagocyte system
NF-κB	Nuclear factor - kappa B
NKCC	Sodium potassium chloride cotransporter
NLRP3	Nacht, LRR and pyrin domain-containing 3
NPPB	5-nitro-2-(3-phenylpropylamino)benzoic acid
PAMP	Pathogen-associated molecular pattern
PBS	Phosphate-buffered saline
PCA	Principle components analysis
Pen/Strep	Penicillin / Streptomycin
PI3K	Phosphoinositide 3-kinase
PKC	Protein kinase C
PRR	Pattern recognition receptor
qPCR	Quantitative polymerase chain reaction
RBC	Red blood cell
RIG-1	Retinoic acid-inducible gene 1
RNA	Ribonucleic acid

ROS	Reactive oxygen species
RVD	Regulatory volume decrease
RVI	Regulatory volume increase
SD	Standard deviation
SEM	Standard error of the mean
STING	Simulator of interferon genes
TAK1	Transforming growth factor β -activated kinase 1
TBK1	Tank binding kinase 1
TBS	Tris-buffered saline
TGF- β	Transforming growth factor beta
THIK-1	Tandem pore domain halothane-inhibited K ⁺ channel 1
TLR	Toll-like receptor
TNF- α	Tumour necrosis factor alpha
TREM2	Triggering receptor expressed on myeloid cells 2
TRPM	Transient receptor potential melastatin
TRPV	Transient receptor potential vanilloid
TTYH	Tweety-homologue
UTP	Uridine triphosphate
V-ATPase	vacuolar H ⁺ -transporting ATPase
VCAM	vascular cell adhesion molecule 1
VRAC	Volume-regulated anion channel
WT	Wild-type
YFP	Yellow fluorescent protein

Abstract

LRRC8A is the obligatory subunit necessary for the formation of the volume-regulated anion channel (VRAC), which is a key regulator of cell volume under hypotonic conditions, as well as following cell swelling. VRAC has been proposed as a drug target for treating ischaemic stroke due to its role in excitotoxic glutamate release from astrocytes, but has also been suggested to regulate numerous aspects of microglial physiology. Microglia, the principal immune cells of the brain, are critical players in determining the course of various neuropathologies, including stroke. The role of VRAC in microglia is therefore of relevance for its utility as a drug target in CNS disease. However, current knowledge regarding the role of VRAC in determining microglial activity is based solely on studies using poorly selective channel inhibitors and requires more specific validation using genetic models. There is also some evidence that LRRC8A is able to participate in intracellular signalling cascades independently of its function as a VRAC component, though to date this phenomenon remains poorly explored. Thus, this study addressed two key questions, using a novel microglia/macrophage-targeted conditional knockout mouse model. Firstly, the role of VRAC in microglial function was assessed. Contrary to previous studies, it was found that loss of VRAC function in microglia does not affect phagocytic capacity, migration, chemotaxis or morphology. Moreover, loss of microglial VRAC did not induce major transcriptomic alterations in microglia or affect infarct volume in an experimental stroke model. Thus, this study concludes that VRAC does not contribute to a variety of key microglial functions, and VRAC could therefore be targeted as a stroke therapy without detrimentally impairing microglial function. Secondly, RNA-Sequencing was used to interrogate novel signalling pathways affected by LRRC8A following hypotonic cell swelling. These results indicated that LRRC8A is capable of modifying type-I interferon responses elicited by cell swelling, which occurs independently of the VRAC channel via a novel signalling pathway. Moreover, LRRC8A was found to activate the PI3K-AKT pathway following hypotonic swelling via two separate mechanisms differentially dependent on protein kinase C and the Src-family kinases Fyn/Hck and independent of VRAC. Thus, this study adds considerable evidence of a VRAC-independent signalling role for LRRC8A in regulating cellular physiology, which is important for interpreting genetic studies targeting LRRC8A as a component of VRAC.

Declaration

I declare that no portion of the work referred to in the thesis has been submitted in support of an application for another degree or qualification of this or any other university or other institute of learning.

James Cook

27th September 2021

Copyright Statement

- i. The author of this thesis (including any appendices and/or schedules to this thesis) owns certain copyright or related rights in it (the "Copyright") and s/he has given the University of Manchester certain rights to use such Copyright, including for administrative purposes.
- ii. Copies of this thesis, either in full or in extracts and whether in hard or electronic copy, may be made only in accordance with the Copyright, Designs and Patents Act 1988 (as amended) and regulations issued under it or, where appropriate, in accordance with licensing agreements which the University has from time to time. This page must form part of any such copies made. Presentation of Theses Policy You are required to submit your thesis electronically Page 11 of 26
- iii. The ownership of certain Copyright, patents, designs, trademarks and other intellectual property (the "Intellectual Property") and any reproductions of copyright works in the thesis, for example graphs and tables ("Reproductions"), which may be described in this thesis, may not be owned by the author and may be owned by third parties. Such Intellectual Property and Reproductions cannot and must not be made available for use without the prior written permission of the owner(s) of the relevant Intellectual Property and/or Reproductions.
- iv. Further information on the conditions under which disclosure, publication and commercialisation of this thesis, the Copyright and any Intellectual Property and/or Reproductions described in it may take place is available in the University IP Policy (see <http://documents.manchester.ac.uk/DocuInfo.aspx?DocID=24420>), in any relevant Thesis restriction declarations deposited in the University Library, the University Library's regulations (see <http://www.library.manchester.ac.uk/about/regulations/>) and in the University's policy on Presentation of Theses.

Experimental Contributions

All experiments were designed by myself with input from Dr Jack Green, as well as my supervisors Dr Catherine Lawrence and Prof. David Brough. The LRRC8A-KO mouse was created by Dr Anthony Adamson in the University of Manchester Transgenics Facility. Dr Eloise Lemarchand performed MCAo surgeries for **Figure 2.9**. Dr Jack Green assisted in managing the LRRC8A-KO mouse colony and performed the experiments presented in **Figure 3.6G,H**. Dr Anna Gray and Dr Ingo Schiessl performed cranial window implantations for intravital imaging, and provided training in intravital 2-photon imaging. Dr Leo Zeef performed initial processing and DESeq2 analyses on RNA-Seq data to generate gene-wise read counts and differential expression statistics.

Acknowledgements

My first thanks go to my primary supervisor Cath, for her incredible supervision throughout my PhD, providing guidance, support and reassurance while encouraging me to pursue my own ideas. Extra thanks go to my co-supervisor Dave, for his invaluable input and encouragement to think big.

Several aspects of my work would have been unfeasible if not for the willing technical help of Eloise, Anna and Ingo, whose expertise were vital in producing some of the most important data in this project. Particular thanks go to the best postdoc in the world, Jack Green – for the many VRAC discussions, mutual mouse support, BMDM preps, and consistently not pointing out that you had all my ideas 2 months before I had them.

Additionally, I would like to acknowledge Steven Marsden, Peter March and Roger Meadows in the Bioimaging facility, as well as Leo Zeef and Andy Hayes in the Genomics Facility for their training and expertise, and without whom this project would have been a great deal harder.

My PhD experience wouldn't have been the same without the amazing environment I found in the Brain Inflammation Group, a constant source of encouragement, support, humour, rigorous scientific discussion and extreme silliness. All members, past and present, have my gratitude for making BIG what it is – a study in how to do it right. I would like to single out Chris Hoyle for organising the Frühlingsfest funtimes, as well as Sarah Ryan and Jo Sharpe for being top people.

My final thanks go to my amazing partner and 10/10 human Abbie, for laughing at my jokes, making me outrageous quantities of tea, and making me do what I need to do, even if it involves phoning somebody. On top of that, thanks for being the reason I'm always happy.

Chapter 1: Introduction

The immune system is essential to the survival of complex multicellular animals. Whilst its name relates to its role in defence against pathogens, immune cells are known to perform myriad essential functions unrelated to host defence (Cox et al., 2021; Epelman et al., 2014). Innate immune cells, particularly macrophages, are distributed widely throughout almost every major tissue, where they assume diverse niche-dependent phenotypes (Blériot et al., 2020). These tissue-resident macrophages are often long-lived, and while they may never encounter a pathogen they nonetheless influence many aspects of tissue homeostasis and disease (Epelman et al., 2014). Often referred to as “caretakers”, tissue macrophages support normal cell turnover via phagocytosis of apoptotic cells. This role also extends to the disposal of extracellular protein complexes, lipids or particulate matter which might otherwise accumulate and impede tissue function (Okabe & Medzhitov, 2016). Besides this and other, tissue-specific functions, macrophages are major contributors to sterile inflammation, which occurs in the absence of pathogens in response to chemical or physical insults (Chen & Nuñez, 2010).

Non-communicable diseases such as cancer, vascular and ageing-related conditions are now amongst the largest contributors to global disease burden (World Health Organisation, 2021). Sterile inflammation is thought to influence the development and pathology of many such conditions, particularly stroke and other vascular events (Fu et al., 2015; Ruparelia et al., 2017), as well as Alzheimer's disease and other neurodegenerative pathologies (Heneka et al., 2014). Due to the success of immunomodulatory therapies in treating classically inflammatory conditions such as arthritis, it is hoped that the immune system will provide a druggable target for many more conditions in the future. However, notable failures including nonsteroidal anti-inflammatory drug (NSAID) trials in Alzheimer's disease (Imbimbo et al., 2010) have illustrated the need to understand the role of innate immune cells in tissue biology more thoroughly in order to select targets with better efficacy.

1.1 Microglia – An Overview

The central nervous system (CNS) is home to several types of resident immune cells (Goldmann et al., 2016; Norris & Kipnis, 2018). The largest and best-studied population are microglia, which inhabit the CNS parenchyma and are in direct contact with neurons, astrocytes and oligodendrocytes. Overall, they constitute around 5-15% of the total CNS

cellularity and are considered the main tissue macrophages of the CNS (Lawson et al., 1990). Microglia have a striking morphology, with numerous long, elaborately branching processes originating from a small, spherical cell body which consists of the nucleus surrounded by a small rim of cytoplasm. Each microglial cell occupies a discrete territory, and collectively they tile the entire CNS space.

The first such descriptions of microglia were made in 1919 by Pio del Rio-Hortega, who visualised them using a novel silver-carbonate stain of his own invention (Sierra et al., 2016). In his seminal work, he established microglia as mesodermal cells which served as the brain's resident phagocytes. He also coined the term microglia in reference to their tiny soma, the smallest of all brain cells (Sierra et al., 2019). This discovery was of particular significance since it also allowed the distinction of oligodendrocytes and microglia as separate cell types, where previously, due to inadequate staining, both cells had been conflated as a poorly characterised "third element" next to neurons and astrocytes (Sierra et al., 2019). Thus, by providing the final two pieces of the puzzle Rio-Hortega solidified the previous literature and established the four major CNS cell types as they are known today.

For much of the subsequent century, microglia received very little attention from the neuroscience community. However, recent years have seen a resurgence of interest in microglial biology, and explosive progress has been made in the past few decades in understanding their origins and function (Prinz et al., 2019). Due to their wide distribution and intimate connections to other CNS cells, microglia are of particular interest for the study of CNS immunity. Indeed, microglia are emerging as critical regulators of several aspects of brain physiology, as well as major players in the initiation and resolution of brain disease (Salter & Stevens, 2017).

1.1.1 Microglial Ontogeny

Most tissues possess resident macrophages, which for decades had been considered to differentiate from blood monocytes as part of the mononuclear phagocyte system (MPS) (Ginhoux & Guilliams, 2016). As such, the brain too was originally assumed to receive some input from the circulating pool of bone marrow-derived monocytes. This idea was supported by early studies where mice were lethally irradiated to induce bone marrow ablation and

transplanted with GFP-expressing bone marrow cells. GFP⁺ cells were then observed within the CNS of these mice, seemingly proving some BM contribution to the adult microglia population (Priller et al., 2001). However, this effect was subsequently demonstrated to be induced by both the effect of radiation on the brain and the abnormally high numbers of circulating haematopoietic precursors following the procedure (Ginhoux & Garel, 2018). When the brain was shielded during myeloablative irradiation, no engraftment of donor BM-derived cells was observed (Mildner et al., 2007). Moreover, parabiosis experiments where wild-type mice were surgically joined to share blood circulation with GFP-expressing mice confirmed that no GFP⁺ cells enter the CNS under homeostatic conditions, or on the context of neurodegeneration (Ajami et al., 2007). Finally, more recent imaging experiments in models of Alzheimer's disease have revealed that the microgliosis in this model relies on proliferation of resident microglia rather than infiltration of peripheral cells (Füger et al., 2017). Thus, microglia are now understood to renew locally without input from blood monocytes at steady-state and in some chronic pathologies.

Most tissues have now been demonstrated to contain such self-renewing macrophage populations which exist independently of adult haematopoiesis (Ginhoux & Guilliams, 2016; Yona et al., 2013). However, microglia are unique in that they derive exclusively from yolk-sac precursors which colonise the brain during early embryonic development, thus making them entirely independent from the adult haematopoietic system (Kierdorf et al., 2013). This distinction is not inconsequential, since recent studies have demonstrated that, while haematopoietic precursors or monocytes may engraft in the adult brain and assume a similar phenotype to bona fide microglia, transcriptomic and functional differences remain between the two cell types (Bennett et al., 2018; Cronk et al., 2018).

1.1.2 Basic properties and phenotypes of microglia

Microglia, like most tissue macrophages, are reliant on colony stimulating factor 1 receptor (CSFR1) signalling for survival (Erblich et al., 2011), mediated by the two cognate ligands macrophage colony stimulating factor (M-CSF/CSF1) and interleukin-34 (IL-34) (Easley-Neal et al., 2019; Kondo & Duncan, 2009; Wang et al., 2012). Microglia also express hundreds of genes comprising a unique transcriptomic signature distinguishing them both from the surrounding CNS cells and from other tissue macrophages (Gautier et al., 2012; Gosselin et

al., 2017; Hickman et al., 2013; Lavin et al., 2014; Patir et al., 2019). This specialised identity is dependent on numerous factors. Several studies have identified transforming growth factor β (TGF- β) as a critical cytokine inducing expression of microglia-specific genes and promoting their homeostatic signature (Bohlen et al., 2017; Butovsky et al., 2014; Buttgereit et al., 2016; Gosselin et al., 2017). Disrupted TGF- β signalling in microglia results in increased reactivity and partial loss of identity (Butovsky et al., 2014; Buttgereit et al., 2016). Experiments with microglia cultured *ex vivo* have indicated that combined treatment with IL-34 or CSF1 along with TGF- β results in partial, but not complete restoration of microglial signature gene expression (Bohlen et al., 2017; Butovsky et al., 2014; Gosselin et al., 2017). Thus, additional environmental cues are clearly required to instruct microglial specialisation.

A significant portion of microglial phenotypic specialisations are dedicated to supporting their role as sensors and responders in CNS injury (Hanisch & Kettenmann, 2007). Many microglial signature genes are involved in environmental surveillance, such as receptors for purines (*P2ry12*, *P2ry13*), cytokines (*Cx3cr1*) and lipids/apoptotic bodies (*Trem2/Dap12*) (Hickman et al., 2013). Additionally, microglia express diverse pattern-recognition receptors (PRRs) such as toll-like receptors (TLRs) and scavenger receptors which detect pathogen- or damage-associated molecular patterns (PAMPs/DAMPs), allowing them to sense an extremely wide variety of stimuli related to infection or tissue injury (Hickman et al., 2013; Wolf et al., 2017). One particularly remarkable adaptation was discovered in 2005 by live intracranial imaging of fluorescent microglia in CX3CR1-eGFP reporter animals. In two separate studies, the elaborately branched microglial processes, long assumed to be sessile like those of astrocytes or neurons, were in fact described to be in constant motion (Davalos et al., 2005; Nimmerjahn et al., 2005). In a process now termed “surveillance”, microglial processes exhibit dynamic rearrangements, with continuous extension and retraction of fine filopodia extending from larger branches, which themselves undergo cycles of collapse and extension at discrete locations. Thus, through their unceasing motility and extensive sensory apparatus, microglia are capable of scanning the entire CNS space on a constant basis.

These adaptations all support the ability of microglia to sense and rapidly transform in response to pathological events, in a process commonly termed “activation” (Kettenmann et al., 2011). This transformation includes alteration of the homeostatic transcriptional program

and changes in morphology which include deramification of their delicate processes and somatic hypertrophy, the extent of which depends on the strength of the stimulus (Kettenmann et al., 2011). Severe events such as cerebral ischemia can induce almost complete deramification to compact, amoeboid shapes (Heindl et al., 2018; Kettenmann et al., 2011). These morphological alterations are accompanied by gene expression changes which can include upregulation of cytokines, adhesion molecules, phagocytic receptors and enzymes geared toward specific effector functions (Hanisch & Kettenmann, 2007). Widespread microglial activation is termed microgliosis and is a hallmark of many CNS conditions. The specific transcriptional and functional changes undergone by microglia following activation are highly variable and indicate a considerable degree of functional plasticity. Indeed, recent transcriptomic studies have highlighted a variety of context-dependent states induced by specific insults and pathologies. Moreover, it is now understood that microglial phenotypes exhibit sex, age and region-dependent heterogeneity, both in disease and homeostasis (Grabert et al., 2016; Guneykaya et al., 2018; Hammond et al., 2019; Keren-Shaul et al., 2017; Li et al., 2019; Masuda et al., 2019a, 2020). Thus, microglial phenotypes are best understood as precisely tuned to their specific tissue environment, with disruptions in homeostasis eliciting dynamic changes specific to the insult in question.

Increasingly, the terminology of “resting” and “activated” cells itself is being abandoned in favour of “homeostatic” or “surveillance” microglia which exist at steady-state and “reactive” or “disease/damage-associated” microglia which exist in pathological settings (Hanisch & Kettenmann, 2007). This is mainly because the implication that “resting” microglia are dormant, inactive cells which passively await “activation” by a stimulus is incongruous with observations of extremely active, dynamic microglia at steady-state. Instead, the transition to disease or damage-associated states is increasingly described as a change in the focus of microglial activity from their homeostatic functions to controlling damage and directing immune responses. Indeed, there is evidence to support disease- or damage-associated transcriptional programmes which are activated in a variety of pathologies (Butovsky & Weiner, 2018; Chiu et al., 2013; Friedman et al., 2018; Keren-Shaul et al., 2017; Krasemann et al., 2017). In general, these disease-associated microglia (DAM) downregulate various homeostatic genes (*P2ry12*, *Tmem119*, *Gpr34*) and upregulate genes associated with

inflammation (*ApoE*, *Il1b*, *Ccl2*, *Tnf*, *C1q*), phagocytosis (*Mertk*, *Axl*, *ApoE*) and proliferation (*Csf1*, *Csf1r*), though many aspects of their phenotype will depend on the specific disease or insult in question.

1.2 Homeostatic microglial functions

Microglia have multiple emerging roles in CNS development and function, both at steady-state and in disease. Many of these roles relate to their status as immunocompetent professional phagocytes, such as clearance of apoptotic cells and debris, as well as immunosurveillance. However, recent studies have indicated a more involved role of microglia in brain function extending beyond simple maintenance duties, such as regulation of synapse formation and excitability, as well as bidirectional communication with astrocytes and neurons.

1.2.1 Microglia in CNS development

The development of a functional nervous system relies on the genesis of neurons and astrocytes/oligodendrocytes by ectodermal precursors, as well as their precise arrangement into the major brain structures and functional “wiring”. However, during CNS development many more cells are produced than are in fact required. Thus, CNS maturation requires that each structure retains the correct number of cells arranged in the correct manner, whilst superfluous and mispositioned cells are removed. Microglia impact this process on several levels by supporting the proliferation and differentiation of neural precursor cells, removing superfluous cells via phagocytosis, and by regulating cell and synapse positioning. Single-cell sequencing has revealed that developmental microglia are not only phenotypically distinct from those in the adult CNS, but also vastly more heterogeneous, presumably reflecting their diverse developmental functions (Hammond et al., 2019; Li et al., 2019; Masuda et al., 2019b).

Microglia secrete a variety of cytokines and neurotrophins including insulin-like growth factor 1 (IGF1), glial cell-derived neurotrophic factor (GDNF) and nerve growth factor (NGF), amongst others, which act to promote proliferation and differentiation of various CNS cell types. Through selective expression of secreted factors, microglia have been demonstrated to support myelination via induction of oligodendrocyte proliferation (Hagemeyer et al., 2017; Włodarczyk et al., 2017), as well as supporting the survival of specific types of neurons and their precursors (Norris & Kipnis, 2018). Conversely, there is now considerable evidence that

microglia not only remove apoptotic neural precursors which have undergone programmed cell death, they actively promote apoptosis of superfluous cells via a process of apoptosis-coupled phagocytosis, or “phagoptosis” (Brown & Neher, 2014; Cunningham et al., 2013; Wakselman et al., 2008).

Microglia are also critical for shaping CNS connectivity. Seminal studies by the Barres lab originally identified the complement system as a key mediator of synaptic refinement in the developing visual cortex (Stevens et al., 2007). In this model, low-input synapses are removed by microglia via an active process of complement-dependent phagocytosis. This phenomenon occurs widely throughout development, and disruption of microglia-mediated synapse removal through deletion of complement genes or receptors, results in functional connectivity deficits (Bialas & Stevens, 2013; Paolicelli et al., 2011; Salter & Stevens, 2017). Interestingly, recent studies have implicated complement-dependent phagocytosis as a potential mediator of synapse loss in Alzheimer’s disease and other pathologies (Hong et al., 2016; Salter & Stevens, 2017). Thus, developmental microglial functions are potentially also of relevance for treating disease in the adult CNS.

1.2.2 Microglia in synaptic regulation

Microglial processes make frequent contact with synapses as they survey the brain. What occurs during these contacts, and what consequences result, is only beginning to be understood. Nonetheless, several roles for microglia in regulating synaptic activity have so far been proposed. Firstly, microglia are suggested to regulate dendritic spine formation during learning via release of brain-derived neurotrophic factor (BDNF) (Parkhurst et al., 2013). Microglia-depleted mice therefore exhibit defects in both memory tasks and acquisition of motor tasks (Parkhurst et al., 2013). Secondly, microglial process homing to synapses has been observed to be activity-dependent (Badimon et al., 2020; Dissing-Olesen et al., 2014; Eyo et al., 2014), and recent data suggest a negative feedback loop between microglia and neurons by which microglial processes reduce synaptic excitability following contact. This occurs through an elegant bidirectional purinergic signalling axis, with ATP released following synaptic excitation serving to attract microglial processes via P2RY12 (Badimon et al., 2020; Dissing-Olesen et al., 2014; Eyo et al., 2014). Following contact, microglial ectonucleoside phosphohydrolases CD39 and CD73 hydrolyse extracellular ATP to adenosine, which lowers

excitability through synaptic A1R receptors (Badimon et al., 2020). Consequentially, microglia depletion or disruption of P2RY12, CD39 or A1R all result in increased susceptibility to seizures (Badimon et al., 2020). Thus, homeostatic microglia are a crucial regulatory component of synaptic function in the adult brain and help maintain an appropriate balance of excitatory and inhibitory signalling.

1.3 Reactive microglial effector functions

In addition to their homeostatic functions, microglia are well-equipped to sense and react to injury and cellular stress in the surrounding tissue. Depending on the type of insult, microglia will initiate a rapid response which generally involves chemotactic migration to the region in question, upregulation of effector molecules such as inflammatory and anti-inflammatory cytokines, chemokines and growth factors, as well as removal of pathogens or damaged cells by phagocytosis (**Figure 1.1**). These activities are generally understood to be adaptive, serving to limit CNS injury and promote restoration of tissue function. However, CNS diseases often coincide with maladaptive microglial activities which can prolong or exacerbate tissue injury. Thus, regulation of microglial reactivity is of great interest in treating neurological diseases.

Microglial reactivity is controlled on multiple levels by a balance of inhibitory “off” signals versus stimulatory “on” signals (Biber et al., 2007). At steady state, homeostatic phenotypes are promoted by TGF- β and reactivity suppressed by constitutive inhibitory signals. These include CD200 and CX3CL1, expressed on healthy neurons, which signal through microglial CD200R and CX3CR1 respectively to constrain their activity (Hoek et al., 2000; Manich et al., 2019; Paolicelli et al., 2014). Loss of either signalling axis therefore promotes a reactive microglial phenotype even in the absence of any tissue injury (Hoek et al., 2000; Paolicelli et al., 2014). Under conditions of stress, neurons downregulate CD200 to disinhibit microglia, and cleave CX3CL1 from its inhibitory, membrane-bound form to release a soluble ligand which acts as a microglial chemoattractant (Manich et al., 2019; Paolicelli et al., 2014). Thus expression of these inhibitory ligands is a critical means by which neurons and other CNS cells tune microglial reactivity, and disruptions in these communication lines can exacerbate microglia-mediated toxicity (Cardona et al., 2006; Manich et al., 2019).

As immunocompetent cells, microglia are sensitive to a variety of “on” signals, largely detected by pattern recognition receptors (PRRs). Tissue damage or infection induces production and release of various damage- and pathogen-associated molecular patterns (DAMPs/PAMPs), which are sensed by microglial PRRs. Multiple different classes of PRRs have been described, including toll-like receptors (TLRs), scavenger receptors such as CD36, and TREM2 (Kettenmann et al., 2011). Bacterial and fungal cell wall products, as well as extracellular nucleotides, oxidised lipids and protein aggregates can all elicit reactivity through PRR-mediated signalling pathways (Li & Wu, 2021). Damaged cells also release purines such as ATP and UTP, which signal through P2X and P2Y receptors to induce chemotactic and phagocytic responses (Brown & Neher, 2014). Microglial reactivity can also be induced by secreted factors produced by other CNS cells downstream of damage or stress signalling pathways, such as CX3CL1, CXCL10 and CCL21 (Clarner et al., 2015; Rappert et al., 2002). Thus, a variety of pathways control microglial phenotypes in CNS diseases, and the specific polarisation of microglia depends on the milieu of stimuli they encounter.

1.3.1 Chemotaxis and migration

Microglia exhibit two main forms of chemotaxis. Firstly, microglial processes are capable of rapid chemotaxis towards sources of ATP, mediated by P2RY12 receptors. P2RY12-dependent process homing is important for promoting microglial interactions with neurons and synapses during homeostasis but, is also critical under injury conditions. Focal laser ablations in brain tissue result in rapid recruitment of processes from adjacent microglia, which prevent expansion of the lesion and protect neighbouring cells (Davalos et al., 2005; Haynes et al., 2006; Hines et al., 2009). In a similar vein, small laser-induced blood-brain barrier (BBB) lesions have been observed to recruit microglial processes, which rapidly seal the breach to prevent influx of serum components to the brain (Lou et al., 2016). P2RY12 was similarly required for this process, with P2RY12-deficient mice exhibiting significantly slower closure of the BBB (Lou et al., 2016). One recent paper indicated that P2RY12 also promotes microglial process recruitment to neuronal cell bodies following intense neuronal activity, and regulates the formation of specialised purinergic signalling junctions (Cserép et al., 2020). These junctions serve to reduce neuronal calcium load and prevent excitotoxicity. P2RY12 inhibition

has therefore been shown to prevent somatic junction formation and increases infarct size in experimental stroke (Cserép et al., 2020).

The process homing responses described above are generally rapid, occurring on acute timescales of minutes to hours, without displacement of the microglial cell body. Migration of microglia, entailing movement of the entire cell, is a less well-studied phenomenon. It is likely that some subsets of developmental microglia are migratory even following the initial colonisation, given the rapid fluctuations in their density and distribution throughout various developing brain structures (Menassa & Gomez-Nicola, 2018). In adult animals, intravital imaging studies have revealed that microglia are generally static, but some rearrangements of the microglial network do occur, in addition to normal cell turnover (Eyo et al., 2018; Fügen et al., 2017). Notably, microglia rearrange more rapidly in reactive states induced by epileptic seizures, with faster turnover and greater translocation (Eyo et al., 2018). Moreover, following laser ablation to the cortex, microglia which initially contact the lesion via process chemotaxis have been observed to fully translocate towards the injury over the subsequent 12-48 hours, where they presumably phagocytose cellular debris (Eyo et al., 2018). There are also some direct reports of microglial migration in chronic pathologies. In the triple-transgenic (3xTg) mouse model of Alzheimer's disease (AD), accumulation of amyloid beta (A β) in amyloid plaques induces proliferation of plaque-adjacent microglia, followed by migration of daughter cells towards the plaque (Fügen et al., 2017). Thus, plaque-associated microglia in AD are at least partially generated via migration. Moreover, simultaneous imaging of neurons and microglia in the 3xTg model revealed that loss of cortical neurones was preceded by CX3CR1-dependent migration of nearby microglia, which clustered around the neuron in question prior to its removal (Fuhrmann et al., 2010). Interestingly, neuronal death in this model appeared to be microglia-mediated, since inhibiting microglial migration via deletion of CX3CR1 rescued neuronal loss (Fuhrmann et al., 2010).

Thus, adult microglia are clearly capable of migration both basally and in response to various pathological states. Whilst relatively few papers have documented bona fide microglial migration, it is likely a component of the microglial response to most pathologies, since effector functions such as local substance release and phagocytosis require physical proximity to be effective. With regard to treating disease, microglial migration via purinergic signalling or

CX3CR1 might present a viable therapeutic target in situations where migration is necessary to support pathological effector functions. However, precisely which disease contexts would benefit will be a matter for further study. Moreover, given the requirement for P2RY12 in various protective microglial activities, targeting this receptor would entail significant risks, most notably heightened seizure susceptibility.

1.3.2 Phagocytosis

Phagocytosis is a fundamental process regulating tissue homeostasis and is critical in resolving various pathological insults. Engulfment of any phagocytic substrate occurs via three main stages. Firstly, phagocytes must sense and move toward the particle in question, generally following a chemotactic gradient, such as lysophosphatidic acid released by apoptotic cells (Flannagan et al., 2012). Once the target is reached, receptors on the macrophage membrane bind to the target particle or cell. Viable cells generally present ligands which suppress phagocytosis, such as CD47, thus preventing engulfment (Flannagan et al., 2012). In order for phagocytosis to be initiated, pro-phagocytic ligands are required to overcome inhibitory signalling. Various pro-phagocytic ligands have been described, many of which are opsonins – soluble proteins which bind to molecules on the target particle and act as ligands for phagocyte receptors. Key opsonins include antibodies, which recognise diverse targets and ligate Fc receptors, complement, which signals through complement receptors, though others have been described (Butler et al., 2021; Rosales & Uribe-Querol, 2017). Stressed or apoptotic cells can stimulate phagocytosis by exposing phosphatidylserine, normally confined to the inner leaflet of the plasma membrane, on the cell surface, where it acts as a ligand for phagocytic opsonins including C1q, milk fat globule protein E8 (MFG-E8), and GAS6, thus promoting their engulfment (Brown & Neher, 2014). Certain particles, mainly pathogen-derived products, can simulate phagocytosis in the absence of opsonins by serving as direct ligands for phagocytic receptors (Flannagan et al., 2012). Finally, after binding of an appropriate ligand, cytoskeletal rearrangements occur, resulting in formation of a phagocytic cup, which expands until the target is completely engulfed, where it passes into endocytic compartments and is eventually degraded in phagolysosomes.

Microglia, like most macrophages, are professional phagocytes, and express a wide array of receptors capable of binding and promoting engulfment of diverse substrates. These include

toll-like receptors (TLRs), scavenger receptors, lectins, integrins (including the complement receptor CR3), Fc receptors and TREM2 (Galloway et al., 2019; Wolf et al., 2017). As previously mentioned, complement-mediated phagocytosis occurs constitutively in the CNS, especially during development. Synaptic terminals tagged by C1q are opsonised by deposition of C3b, promoting their removal by microglia expressing the C3 receptor (CD11b/CD18) (Stevens et al., 2007). Whilst this form of phagocytosis is critical for synaptic plasticity, it may also mediate synaptic loss in Alzheimer's disease and other pathologies (Galloway et al., 2019). Several papers have indicated that C1q or C3 disruption can rescue synapse loss in AD models (Hong et al., 2016; Shi et al., 2017). Moreover, some reports have indicated that microglia may directly engulf viable neurons transiently exposing phosphatidylserine as a result of cellular stress, which could contribute to neuronal death in neurodegeneration and stroke (Brown & Neher, 2014; Vilalta & Brown, 2018). Thus, some forms of phagocytosis appear to occur in a maladaptive, pathological fashion, and could be targetable in certain CNS diseases.

Despite some evidence of pathological phagocytosis, inhibiting phagocytosis can have demonstrably negative effects. In AD, microglia phagocytose amyloid beta (A β) aggregates which are thought to play a causative role in initiating neurotoxic cascades (Galloway et al., 2019; Podleśny-Drabiniok et al., 2020). As such, some papers have reported that inhibiting phagocytic pathways increases amyloid deposition following genetic overexpression or exogenous injection (Fu et al., 2012; Maier et al., 2008). Indeed, some lines of evidence point to phagocytic failure as a key prerequisite for the development of amyloid pathology: firstly, the cerebellum is noted for its resistance to amyloid accumulation and AD pathology, which correlates with an unusually phagocytic, immunovigilant phenotype in cerebellar microglia compared to those in other brain regions such as the cortex and striatum (Ayata et al., 2018; Grabert et al., 2016). Moreover, many polymorphisms associated with increased AD risk are found in genes encoding components of phagocytic pathways (Podleśny-Drabiniok et al., 2020). TREM2, for instance, is a known phagocytic receptor mediating uptake of both A β and apoptotic cells, possibly via interactions with Apolipoprotein E (ApoE), another AD risk gene (Podleśny-Drabiniok et al., 2020; Shi & Holtzman, 2018; Zhao et al., 2018). TREM2-ApoE interactions have been shown to drive phenotypic transformation of microglia to a disease-

associated state, possibly stimulated by phagocytosis of apoptotic cells (Keren-Shaul et al., 2017; Krasemann et al., 2017). Disrupting TREM2 function in AD models results in reduced microglial reactivity and, in later stages, greater pathology, though there is still some debate as to whether this reflects true phagocytosis of plaques by TREM2-expressing reactive microglia or simply containment of toxic amyloid species (Jay et al., 2015, 2017; Ulrich et al., 2014; Wang et al., 2015, 2016). Thus, there is an intimate link between microglial reactive phenotypes, phagocytic activity and overall brain pathology in AD. In other pathologies, including acute injuries, phagocytosis is also likely to provide some benefit via clearance of damaged cells and debris, thus preventing the accumulation of toxic material and paving the way for repair (Galloway et al., 2019). Phagocytosis is therefore best understood as a fundamentally beneficial process which is essential for maintaining brain function, yet which can produce damaging results if dysregulated.

1.3.3 Neuroinflammation

Inflammation is a common feature of many neurological diseases, including Alzheimer's disease, Parkinson's disease, stroke and multiple sclerosis. Inflammation is generally thought of as a protective response to tissue damage which serves to mobilise the immune system, activate local stress tolerance pathways, clear harmful material and pave the way for repair. Lack of inflammatory responses can therefore impede recovery from infection or injury. However, many cytotoxic factors can be released during inflammation, such that excessive or chronic inflammation can exacerbate tissue damage. Thus, the balance between pro- and anti-inflammatory signals is critical for effective damage resolution. Since the brain has a notoriously low regenerative capacity, balancing inflammation is of particular importance for CNS disease, since inappropriately weak or strong inflammation could lead to lifelong neuronal injury and impairment.

As the primary immunocompetent CNS cells, microglia are responsible for the initiation and propagation of neuroinflammation. As such, they express many receptors for DAMPs/PAMPs which activate a variety of inflammatory programmes. They can express a multitude of inflammatory mediators such as chemokines, cytokines, proteases, complement, opsonins and reactive oxygen species (ROS), many of which can be toxic if overproduced. Conversely, they may also upregulate anti-inflammatory factors such as interleukin 10 (IL-10) and IL-4

either alone or simultaneously. Previously macrophages were designated as either M1 (inflammatory) or M2 (anti-inflammatory) based on expression of specific markers, for instance nitric oxide synthase (NOS2; M1) or arginine synthetase (ARG1; M2). However, these classifications derived from *ex-vivo* stimulation of macrophages with a very limited array of factors (lipopolysaccharide (LPS) + interferon-gamma (IFN- γ) for M1, IL-4 + IL-10 for M2). Since macrophages *in vivo* experience a much more complex milieu of stimulants, the resulting phenotypes are understood to be considerably more nuanced, particularly given the previously mentioned consensus on microglial “activation” (Butovsky & Weiner, 2018; Martinez & Gordon, 2014; Ransohoff, 2016; Wes et al., 2016).

Ultimately, microglial phenotypes are only as relevant as their effects on other cells of the CNS. Neurons are extremely sensitive cells that require precise regulation of their extracellular environment, a function largely attributed to astrocytes and the BBB, as well as myelination by oligodendrocytes, all of which can be affected by reactive microglia. The preservation or loss of neuronal networks during inflammation therefore depends not only on microglial, but endothelial, astrocyte and oligodendrocyte responses, as well as those of the neurons themselves. This tissue-level response is complex and still largely mysterious. Nonetheless, some general mechanisms have been uncovered whereby microglial activity initiates neuroprotective or neurotoxic cascades in CNS diseases.

Neurons can be affected by microglia-derived cytokines both directly or indirectly via effects on other cell types. Direct effects of microglia on neurons include modulation of synaptic connectivity by inflammatory cytokines such as tumour necrosis factor alpha (TNF- α) and IL-1 β (Rizzo et al., 2018). These actions can lower excitatory tone, which can be protective in acute settings by restricting excitotoxic injury, yet in chronic scenarios might inhibit cognitive function and memory (Rizzo et al., 2018). In more extreme conditions, inflammation can lead to PS exposure on otherwise viable neurons and activate aberrant neurophagy, which can contribute to neuron and synapse loss (Vilalta & Brown, 2018).

Astrocytes are key targets for microglia-derived signalling molecules during inflammation and can undergo a similar phenotypic transformation known as astrogliosis, characterised by somatic hypertrophy and upregulation of growth factors, cytokines and various cytoskeletal

proteins (Sofroniew, 2014). In severe injuries, reactive astrocytes can form a barrier known as a glial scar which encapsulates damaged areas to restrict passage of immune cells, DAMPs and other toxic factors into neighbouring regions (Sofroniew, 2015). Whilst astrocytes certainly possess some capacity to sense neuronal damage, the range of ligands they detect is disputed (Cserép et al., 2020). At least in some contexts, astrocyte reactivity seems to rely on factors secreted by reactive microglia, which act as the primary sensors (Cunningham et al., 2019; Holm et al., 2012; Liddelow et al., 2017). It was recently proposed that microglia can generate either toxic (A1) or supportive (A2) astrocytes by secreting either IL-1 α or IL-1 β (respectively) alongside TNF- α and complement component 1q (C1q) (Liddelow et al., 2017). Interestingly, TNF- α , IL-1 α and C1q triple-knockout mice exhibit reduced neuronal loss in the retina following optic nerve crush. Moreover, astrocytes expressing A1 markers were detected in human tissues with various neuropathologies, suggesting that astrocyte-mediated toxicity downstream of microglial reactivity is indeed a *bona-fide* disease mechanism (Liddelow et al., 2017). However, it must be noted that both the origin and nature of the A1/A2 classification is very similar to the now-defunct M1/M2 macrophage polarisation model. It seems more likely that astrocyte reactivity *in vivo* produces a much broader range of possible states, which are likely dependent on the specific pathological context.

Many inflammatory mediators released by microglia and astrocytes target endothelial cells, which are critical regulators of brain physiology. Some inflammatory cytokines such as IL-1 β cause endothelial cells to upregulate adhesion molecules such as vascular cell adhesion molecule 1 (VCAM), as well as chemokines such as the monocyte chemoattractant CCL2. This can promote the infiltration of peripheral immune cells such as monocytes, neutrophils and lymphocytes into the brain, which can exacerbate inflammation and injury. This process can also promote permeabilization of the BBB, allowing passage of proteins and ions from the blood into the parenchyma. Serum proteins such as serum amyloid A and fibrinogen, for instance can promote inflammatory reactions in microglia and lead to local synaptic degeneration.

Neuroinflammation, particularly downstream of IL-1 β , has been linked extensively to numerous CNS diseases. A review of contributions of NLRP3-derived IL-1 β to various pathologies can be found in the **Appendix** (Swanton et al., 2018).

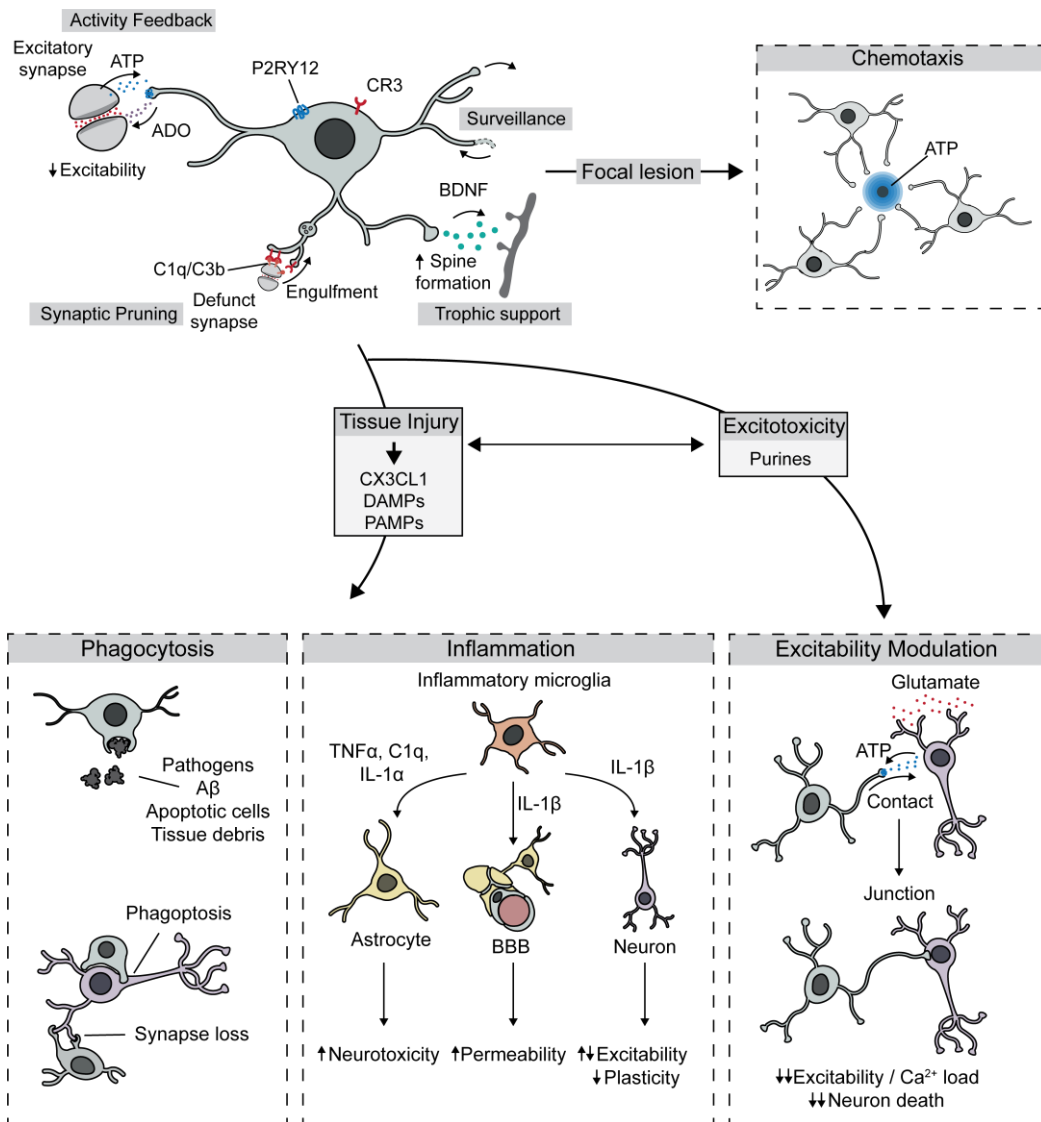


Figure 1.1: Homeostatic and reactive microglial functions in the CNS

Under homeostatic conditions, microglia engage in purinergic modulation of synaptic activity, prune defunct synapses via CR3-C3b-C1q interactions, provide immunosurveillance via process motility, and trophic support for neurons assisting in dendritic spine formation. Focal lesions induce rapid ATP-P2RY12 dependent process chemotaxis to the injured area. Following tissue injury or excitotoxic stress, microglia engage reactive programmes including phagocytosis of extracellular material, neurons and synapses, as well as inflammation which can induce astrocyte neurotoxicity, BBB permeability, as well as altering neuronal excitability and plasticity. During intense neuronal excitation microglia form P2RY12-dependent contacts with neurons, reducing their excitation and calcium load, thereby preventing excitotoxic death. ADO = adenosine, CR3 = complement receptor 3, BDNF = brain-derived neurotrophic factor.

1.4 Regulation of microglial functions by ion channels

Microglia express a variety of ion channels, some of which (e.g. THIK1) are unique to them amongst CNS cells. However, the contribution of these channels to microglial behaviour is still poorly understood. This lack of understanding may be in part due to the historical difficulty of

assaying microglia in their native environment without the use of genetically-encoded labels combined with advanced fluorescent imaging techniques. As such, much of our knowledge regarding microglial channel biology is derived from studies on neonatal microglia cultured *in vitro*, which are easily manipulated and tractable to ion channel blockers. However, due to issues such as the loss of microglial identity upon *in vitro* culture, as well as nonspecific actions of ion channel blockers, the applicability of these findings to microglial biology *in vivo* is questionable. Moreover, many roles for microglia in CNS function have only recently been described. As a result, much remains to be discovered regarding the role of ion channels in microglial biology.

1.4.1 Morphology and Surveillance

Microglia undergo dramatic changes in morphology both during development as they acquire their characteristic ramified shape, and under conditions of CNS injury, where they undergo reactive transformations including hypertrophy and deramification. Relatively little is known about regulation of microglial morphology by ion channels in either steady-state or pathological contexts, though a few key players have been determined. Microglial ramification is regulated by the cell membrane potential, with more negative potentials promoting greater ramification (Madry et al., 2018). One recent study demonstrated that potassium efflux via the two-pore domain potassium channel THIK-1 promotes ramification and surveillance *in vivo* by inducing membrane polarisation (Madry et al., 2018). Thus, ion fluxes are clearly linked to dynamic changes in microglial morphology, and any ion channel which participates in setting the membrane potential could affect microglial ramification. Previous studies have linked “stretch-activated” chloride channels to induction of microglial ramification by astrocyte-derived factors *in vitro*, though the molecular identity of the channel was not determined (Eder et al., 1998).

1.4.2 Chemotaxis and migration

Microglial chemotaxis has been proposed to rely on chloride channels, since application of the chloride channel inhibitors tamoxifen and NPPB, as well as incubation in chloride-free buffers prevent microglial process homing to laser lesions in acute brain slices (Hines et al., 2009). Whilst the application of chloride channel blockers has the potential to block ATP release channels, which are hypothesized to amplify purinergic signalling following laser

damage, the use of chloride-free buffers in this paper illustrates that this is likely not the mechanism by which chloride channels inhibit chemotaxis. Instead, a *bona fide* chloride current in microglia appears to be required. Interestingly, chloride channel blockers did not seem to affect process extension during baseline surveillance, and potassium channel blockers did not affect lesion-induced chemotaxis (Hines et al., 2009). In agreement with other work, this implies that microglial chemotaxis and baseline surveillance are differentially regulated by chloride and potassium conductance, respectively (Madry et al., 2018). Beyond these two studies, most evidence of ion channel involvement in migration comes from *in vitro* experiments, which have implicated P2X4 receptors, as well as transient receptor potential vanilloid- and muscarinic type 1 and 7 (TRPV1/TRPM7) calcium channels in mediating chemotactic responses to ATP (Izquierdo et al., 2019).

Cell migration as a whole has been studied extensively *in vitro* and is known to rely on co-ordinated activity in a variety of channels and transporters, including calcium, potassium and chloride channels, aquaporins, and various exchangers (Schwab et al., 2012). Whilst the specific transporters supporting cell migration likely vary between different cells, the overall effect is hypothesized to be one of ion import at the leading edge, and export at the trailing edge of the cell. It is proposed that these ionic fluxes promote import and export of water, thus reducing hydrostatic resistance encountered by the cell during migration and allowing extension/retraction of the cell membrane. In cultured microglia, calcium channels, Ca²⁺-activated potassium channels, and chloride channels have all been suggested to underpin migration (Eder, 2005; Luo et al., 2021; Zierler et al., 2008). Chloride channel inhibitors have also been demonstrated to inhibit chemotaxis towards the ligands CCL21 and CXCL10 mediated by CXCR3 (Rappert et al., 2002). However, since the vast majority of these studies have examined migration only in cultured neonatal microglia or microglial cell lines migrating *in vitro*, vast differences exist between these reduced preparations and microglia *in situ*, both in cellular identity and the extracellular environment. Thus, it is possible that microglia migrating *in vivo* utilize different mechanisms than those proposed here.

1.4.3 Phagocytosis

Similarly to migration, phagocytosis is a widely studied phenomenon which is known to rely on co-ordinated ion channel activity. Phagocytic shape changes are also proposed to involve

multiple channels responsible for triggering intracellular signalling pathways and cytoskeletal rearrangements, as well as supporting cell shape changes. Phagosomes also undergo rapid changes in ion concentration and pH during maturation, as phagocytes frequently produce a burst of superoxide (oxidative burst) aimed at destroying pathogens, followed by rapid acidification to aid cargo digestion by lysosomal enzymes (Flannagan et al., 2012). Thus, phagocytosis proceeds via several discrete steps, each of which involves unique ion transport requirements.

The process of target recognition and engagement has been described to rely on calcium elevations following stimulation of purinergic receptors including P2RY6, which in microglia are mediated by store-operated calcium channels and the plasma membrane calcium channel ORAI1 (Heo et al., 2015; Michaelis et al., 2015). Calcium elevation may be supported by membrane hyperpolarisation following opening of voltage-gated potassium channels (Izquierdo et al., 2019). Following target ligation, the phagocyte must create membrane protrusions supported by polymerised actin, which expand to engulf the target. These cell shape changes are suggested to require activity in both potassium and chloride channels, similarly to cell leading edge extension during migration, as well as continuing local calcium elevations (Nunes et al., 2012). Once the target has been ingested, phagosome trafficking and acidification requires import of H⁺ ions to the compartment, which is principally achieved via vacuolar H⁺-transporting ATPases (V-ATPases), but requires counterbalancing ion fluxes including accumulation of chloride, as well as efflux of sodium and other cations. As such, a large array of transporters and channels have been shown to contribute to phagosomal maturation, including voltage-gated chloride channels (CLCN3-7) and TRPML1 (Westman & Grinstein, 2021). Thus, phagocytosis depends heavily on ion transport at various stages, both as a signalling event and to support physicochemical changes during phagosome formation and maturation.

1.5 LRRC8A and the Volume Regulated Anion Channel (VRAC)

All cells possess the capacity to regulate their volume. Since most cell membranes are highly permeable to water, but orders of magnitude less permeable to ions and large osmolytes, osmolyte imbalances cause immediate osmotic water flux and subsequent swelling or

shrinkage of the cell (Hoffmann et al., 2009). Changes in cell volume can, in extreme cases, result in cell death via osmotic lysis, but may also disrupt cellular physiology in more subtle ways, for instance by modulating membrane and cytoskeletal tension. Thus, cells actively and dynamically regulate their volume to maintain optimal physical parameters for proper functioning. Volume regulation is achieved via two opposing processes, termed regulatory volume increase (RVI) and regulatory volume decrease (RVD) (Hoffmann et al., 2009). Both processes entail net gain or loss of K^+ and Cl^- , respectively, along with osmotically obliged water. Both of these ions are generally required for volume regulation in order to maintain electroneutrality, and in some cases large organic osmolytes such as taurine will contribute as well. RVI has been well characterised and is achieved by activation of Na^+/H^+ and Cl^-/HCO_3^- exchangers in some cells, or by NKCC $Na^+/K^+/2Cl^-$ cotransporters in others (Hoffmann et al., 2009). RVD was, for years, a much more mysterious process known to be reliant on K^+ and Cl^- channels, the identity of which was the subject of much speculation. It was the study of volume-sensitive channels mediating RVD which led to the identification of the volume-regulated anion channel (VRAC) as a key component of volume regulation (Strange et al., 2019).

The existence of VRAC was first suggested by two separate groups who identified volume-sensitive chloride currents in T lymphocytes and intestinal epithelial cells (Cahalan & Lewis, 1988; Hazama & Okada, 1988). This current was subsequently described in a variety of other cell types based on its electrophysiological characteristics – activation by cellular swelling (typically induced by incubation with hypotonic buffers), selectivity for anions over cations, outward rectification, and anion permeabilities corresponding to Eisenmann's sequence I ($SCN^- > I^- > NO_3^- > Br^- > Cl^- > F^-$). It was also determined that blocking this Cl^- current resulted in failure to undergo RVD and persistent swelling under hypotonic conditions (Hazama & Okada, 1988; Pedersen et al., 2015; Strange et al., 2019). For many years following these initial characterisations, the molecular identity of the channel was unknown, and the observable current referred to simply as $I_{Cl,Swell}$, in reference to its activation by cellular swelling. Over the subsequent decades, numerous candidates were proposed to carry the VRAC-dependent $I_{Cl,Swell}$ current, including CLCN3, pI_{ClIN} and P-glycoprotein, however none survived the

stringent assessments of multiple laboratories during the long search (Pedersen et al., 2015; Strange et al., 2019).

It was not until 2014 that two separate groups used genome-wide genetic screens to identify the *Lrrc8a* gene as the critical mediator of hypotonicity-induced chloride currents (Qiu et al., 2014; Voss et al., 2014). This was achieved using high-throughput screening techniques utilising cell lines expressing a halide-sensitive YFP whose fluorescence is quenched by passage of iodine through the VRAC channel under hypotonic conditions, with *Lrrc8a* identified as the only gene capable of suppressing this quenching response when knocked out. One group coined the name SWELL1 for the encoded protein (Qiu et al., 2014), though it is largely still known as LRRC8A. It was rapidly determined that loss of LRRC8A results in impaired $I_{Cl,SWELL}$ activation in electrophysiological assays and defective RVD (Qiu et al., 2014; Voss et al., 2014). Since this discovery, much progress has been made in determining the molecular mechanisms of VRAC function, and its contribution to cell and tissue physiology.

1.5.1 Structure and function of LRRC8 family proteins

Both mouse and human LRRC8A belongs to a multi-gene family consisting of five paralogues, designated LRRC8A-E. The family is putatively related to pannexins, which also serve as plasma membrane channels regulating transport of large organic solutes (Abascal & Zardoya, 2012). Each LRRC8 protein exhibits the same basic structure, with a short cytoplasmic N-terminus followed by four transmembrane domains connected by short extracellular and intracellular loops, with slight sequence variations between paralogues (**Figure 1.2A**). The C-terminus is dominated by a large leucine-rich repeat domain (LRRD), consisting of 16-17 LRRs (Kubota et al., 2004; Smits & Kajava, 2004). Whilst the N and C termini were originally hypothesised to be extracellular, more recent studies have confirmed that in fact the N-terminus and LRRD are in fact intracellular, as predicted using bioinformatics and confirmed using epitope tagging approaches (Abascal & Zardoya, 2012; Qiu et al., 2014).

A variety of recent studies have elucidated that VRAC channels are formed by hexameric assemblies of LRRC8-family proteins (Deneka et al., 2018; Kasuya et al., 2018; Kefauver et al., 2018; Kern et al., 2019; Syeda et al., 2016). Of the five members, LRRC8A is obligatory for the formation of functional channels, but LRRC8A homohexamers are themselves unable

to support VRAC currents (Gaitán-Peñas et al., 2016; Voss et al., 2014). Instead, each channel must contain at least one LRRC8A subunit along with some combination of the other four paralogues (König & Stauber, 2019). One intriguing finding by both original studies is that overexpression of LRRC8A actually inhibits VRAC activation (Qiu et al., 2014; Voss et al., 2014). Presumably, this reflects perturbed subunit stoichiometries, whereby overabundance of LRRC8A is inhibitory to channel function. Beyond this effect, no specific stoichiometric constraints have been identified for functional channel formation, and a variety of subunit compositions appear possible. Moreover, differing subunit stoichiometry can drastically alter the electrophysiological characteristics (for example, activation kinetics and conductance) and solute specificity of the resulting channel (König & Stauber, 2019).

All so far characterised VRACs are capable of transporting small anions such as Cl⁻ and I⁻, yet differ in their capacity to carry larger solutes such as nucleotides and amino acids (König & Stauber, 2019) (**Figure 1.2B**). For example, LRRC8D promotes the transport of large uncharged and even positively charged solutes such as lysine, taurine and cisplatin (Lutter et al., 2017; Planells-Cases et al., 2015; Schober et al., 2017). By contrast, LRRC8C and E confer selectivity for anionic solutes such as aspartate and glutamate (Gaitán-Peñas et al., 2016; Lutter et al., 2017; Schober et al., 2017). VRAC is also capable of supporting ATP release, which occurs most efficiently through LRRC8E-containing complexes (Gaitán-Peñas et al., 2016). LRRC8B, uniquely, has no known propensity to support large organic solute flux, but can still form functional VRACs transporting small anions (König & Stauber, 2019).

1.6 VRAC functions in physiology

VRAC is suspected to contribute to cell and tissue physiology in two main ways: firstly, volume homeostasis may be required for the normal function of some cells, particularly those experiencing high fluctuations in extracellular fluid composition or intracellular osmolyte concentrations. Secondly, VRAC transports a variety of compounds with known signalling functions, such as neurotransmitters and purines, and therefore could participate in intercellular signalling networks in a manner similar to pannexins. *Lrrc8a* mRNA is widely expressed throughout the body, including in microglia and other immune cells, as well as neurons and astrocytes, suggesting broad functionality across a variety of cell types (Qiu et

al., 2014). Indeed, several bona fide roles for VRAC in tissue homeostasis have been confirmed so far.

1.6.1 Role of VRAC in insulin release

A role for VRAC in pancreatic function was recently described using β -cell targeted LRRC8A deletion (Stuhlmann et al., 2018). Pancreatic β -cells are responsible for releasing insulin in response to blood glucose rises, in a manner which involves cell swelling and depolarisation (Best et al., 2010). β -cells exposed to high glucose concentrations undergo cell swelling, likely due to intracellular accumulation of glucose metabolites. This swelling response stimulates VRAC activity, which assists in rapid depolarisation of the cell via chloride efflux, thus stimulating fast release of insulin (Stuhlmann et al., 2018) (**Figure 1.2E**). β -cells lacking VRAC exhibit delayed insulin release following glucose stimulation, and mice lacking β -cell LRRC8A expression have impaired glucose tolerance (Stuhlmann et al., 2018). This finding illustrates the capacity for VRAC to mediate cellular functions by responding to metabolic cues and modulating membrane potential.

1.6.2 Role of VRAC in immunity

VRAC channels have recently been linked to the generation and propagation of antiviral immune responses (Lahey et al., 2020; Zhou, Chen, et al., 2020) (**Figure 1.2F**). Antiviral immunity is often dependent on recognition of cytosolic DNA, which is indicative of infection by DNA viruses. Various cytosolic DNA sensors have been described, the best-characterised of which is cyclic GMP-AMP synthase (cGAS). Upon recognition of cytosolic DNA, cGAS synthesises cyclic GMP-AMP (cGAMP) from GTP and ATP (Sun et al., 2013). cGAMP then accumulates in the cytosol, where it binds to stimulator of interferon genes (STING), which mediates responses downstream of a variety of DNA sensors (Burdette & Vance, 2013; Chen et al., 2016; Sun et al., 2013). STING is normally present on the endoplasmic reticulum membrane, yet upon binding cGAMP it assumes an active conformation traffics to an ER-golgi intermediate compartment (Chen et al., 2016; Sun et al., 2013). Active STING then recruits tank-binding kinase 1 (TBK1) and the transcription factor interferon regulatory factor 3 (IRF3) to form a complex, following which TBK1 phosphorylates IRF3 (Burdette & Vance, 2013; Fitzgerald et al., 2003). Phosphorylated IRF3 then translocates to the nucleus, where it

induces transcription of interferon beta (IFN- β), as well as interferon stimulated genes (ISGs) such as the antiviral chemokine CXCL10 (Burdette & Vance, 2013).

VRAC was shown in two separate papers to transport the cyclic dinucleotide cGAMP across the cell membrane (Lahey et al., 2020; Zhou, Chen, et al., 2020). Since cGAMP is anionic, its transport is best supported by LRRC8E and, to a lesser extent LRRC8C, and transported poorly by LRRC8D (Lahey et al., 2020; Zhou, Chen, et al., 2020). Cells incubated with extracellular cGAMP displayed upregulation of *Irf3* and *Cxcl10* mRNA, which was enhanced by treatment with hypotonic buffers, and strongly inhibited by knockout of LRRC8A or LRRC8C/E, but enhanced by knockout of LRRC8D (Lahey et al., 2020; Zhou, Chen, et al., 2020). The ability of VRAC to export and import cGAMP allows cells infected with a DNA virus to release cGAMP into the extracellular space, where it can enter neighbouring cells via VRAC and stimulate the STING-TBK1-IRF3 axis to promote antiviral signalling (**Figure 1.2F**). In support of this, HSV-1 infected cells cultured on transwell systems were able to propagate antiviral responses to uninfected cells in the lower chamber, in a manner dependent on LRRC8A (Zhou, Chen, et al., 2020). In this sense, cGAMP conductance can support the actions of IFN- β in propagating antiviral signalling to uninfected cells, thus restricting viral replication. Indeed, knockout of LRRC8E *in vivo* resulted in reduced secretion of antiviral mediators following HSV-1 infection, greater viral loads and increased morbidity (Zhou, Chen, et al., 2020). These papers demonstrate that VRAC plays a previously unappreciated role in antiviral responses to DNA viruses by supporting transfer of antiviral signalling factors between cells.

1.6.3 VRAC in neuronal function

VRAC also has several roles in brain physiology. One recent study described VRAC as a key mediator of tonic glutamate release from astrocytes (Yang et al., 2019). Astrocyte-targeted VRAC deletion via GFAP-Cre mediated recombination results in normal nervous system development but produces several defects in synaptic activity. These excitatory deficits were accompanied by impaired acquisition of memory tasks, highlighting a key contribution of VRAC channels to maintaining neuronal transmission and plasticity (Yang et al., 2019).

Two subsequent papers used a Nestin-Cre line to drive deletion of LRRC8A in neurons, astrocytes and oligodendrocytes (hereafter referred to as whole-brain knockout). Both papers reported a striking phenotype involving normal brain development followed by rapid onset of severe seizures resulting in death between the 5th and 9th postnatal week (Wilson et al., 2021; Zhou, Luo, et al., 2020). In one paper, the authors also noted significant astrogliosis in the hippocampus, an area known for its seizure susceptibility (Wilson et al., 2021). Mechanistically, defects in neurotransmitter synthesis and transport pathways were proposed to occur in KO mice, resulting in reduced GABA-ergic inhibition of CA1 pyramidal neurons and increased excitation (Wilson et al., 2021). However, this hypothesis was based mainly upon altered expression of glutamate transporter 1 (GLT1) and glutamine synthetase (GS) in KO mice and was not substantiated through rescue experiments, nor were any striking differences in neurotransmitter abundance detected between genotypes (Wilson et al., 2021). Thus, it is possible that the protein expression changes observed were incidental, and not the true source of the seizure phenotype. Moreover, it is unclear how loss of LRRC8A produced the observed changes in GLT1 and GS expression, since no link between VRAC activity and expression of these proteins has been proposed previously. It is intriguing that loss of LRRC8A in astrocytes does not produce an overt seizure phenotype, or appreciable mortality (Yang et al., 2019). The phenotype observed in whole-brain LRRC8A KO mice must therefore require neuronal and/or oligodendrocyte deletion of LRRC8A. Since no currently available Cre lines can target all neurons while sparing astrocytes, it may be some time before the exact cell type contribution of this phenotype can be determined. Nonetheless, these results highlight a critical role of LRRC8A in maintaining normal brain function.

1.6.4 VRAC in microglial biology

A number of studies have suggested roles for VRAC in regulating various aspects of microglial function. Firstly, VRAC has been suggested to regulate both cell migratory processes and microglial P2RY12-dependent chemotaxis to ATP. VRAC inhibitors have been observed to inhibit cell movement in a variety of cell types, including microglial cell lines, neutrophils, monocytes, and fibroblasts (Kim et al., 2004; Moreland et al., 2006; Schneider et al., 2008; Schwab et al., 2012; Volk et al., 2008; Zierler et al., 2008). As such, VRAC is suggested to participate in microglial migration by supporting chloride efflux at the trailing edge of the cell,

allowing for water loss and membrane retraction (Schwab et al., 2012). In this sense migration has been likened to cell volume regulation, with volume increase occurring at the leading edge and volume decrease at the trailing edge. Thus, loss of VRAC might reduce the capacity of microglia to migrate. The VRAC inhibitors tamoxifen and NPPB applied to acute brain slices are reported to inhibit microglial process convergence toward laser burns, but not to inhibit filopodial extension in the absence of a burn (Hines et al., 2009). Therefore, VRAC is also hypothesized to mediate P2RY12-dependent process chemotaxis. Given the critical role of P2RY12 in controlling a number of homeostatic microglial activities, a role for VRAC in mediating P2RY12-dependent responses could have important implications for microglial biology.

One previous study proposed that a “stretch-activated” chloride channel inhibited by common VRAC inhibitors is critical for microglial ramification in response to astrocyte-conditioned media (Eder et al., 1998). While the molecular identity of the channel was not determined, VRAC has been proposed as a likely candidate for mediating this effect (Eder et al., 1998; Mongin, 2016). VRAC has been suggested to respond to membrane stretch and may be engaged by microglia in response to local membrane deformations during ramification through the brain’s tortuous extracellular space (Mongin, 2016).

Finally, several studies have shown that VRAC inhibitors applied to microglia and microglial cell lines suppress *in vitro* phagocytosis of latex beads (Furtner et al., 2007; Harl et al., 2013) and fluorescent *E. coli* (Ducharme et al., 2007). Similar effects have also previously been demonstrated in neutrophils (Moreland et al., 2006). The role of VRAC in phagocytosis is suggested to be similar to its function during cell migration – VRAC activity is hypothesized to support chloride flux required for the formation of membrane protrusions and engulfment pseudopodia (Harl et al., 2013). VRAC may therefore support phagocytic activity, which is an important microglial function of great relevance to many brain disorders.

In summary, VRAC has been suggested to regulate a variety of critical microglial activities which could be of relevance to their function both in homeostasis and disease, and could inform future strategies aiming to modulate microglial activity therapeutically.

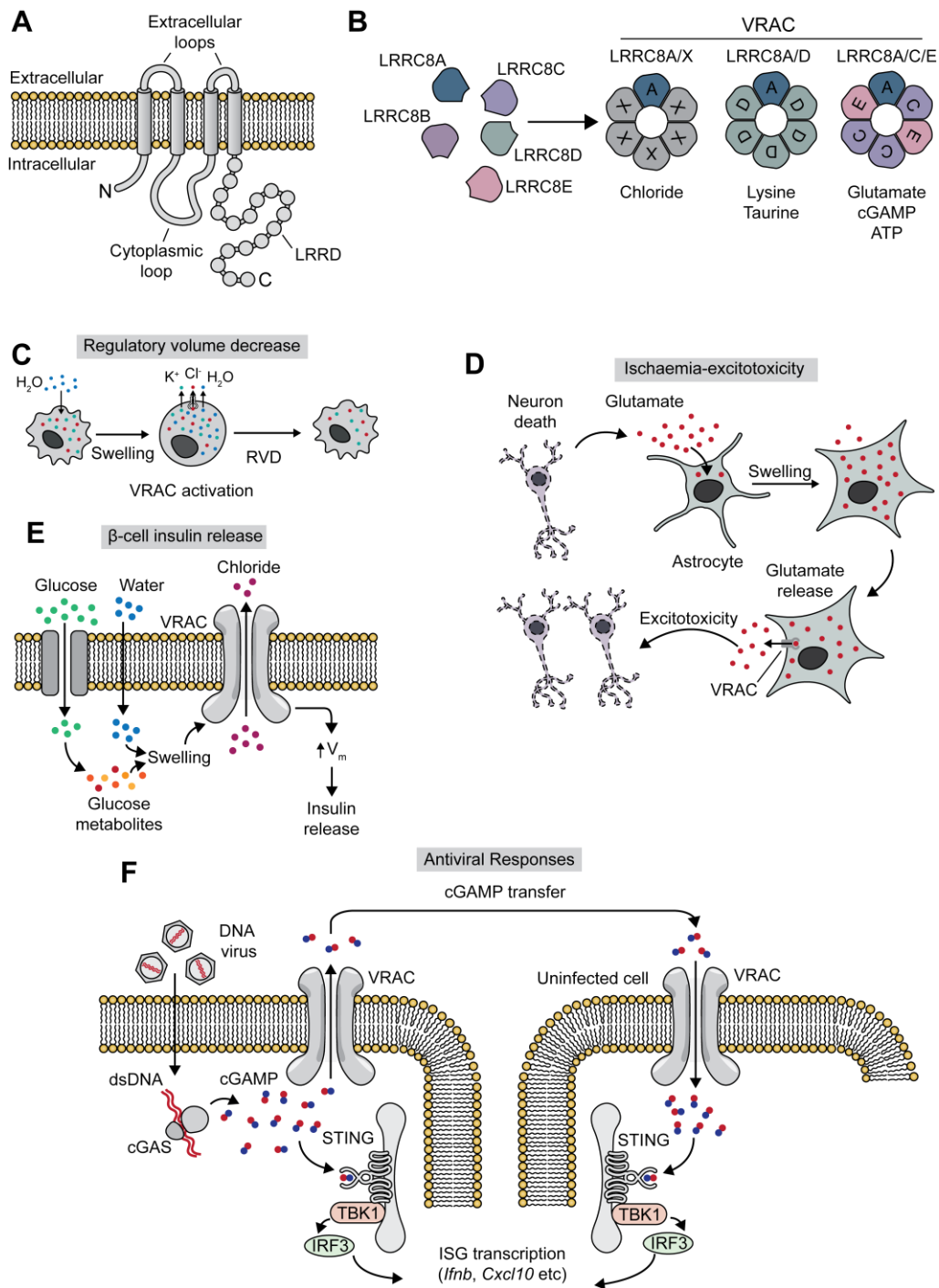


Figure 1.2: Structure and known functions of VRAC

(A) Structure of LRRRC8A, containing 4 transmembrane domains, two extracellular and one cytoplasmic loop, and the cytoplasmic c-terminal leucine-rich repeat (LRR) domain (LRRD). LRRRC8A-E have similar structures. (B) VRAC is assembled as heterohexamers containing at least one LRRRC8A in combination with up to five other paralogues. Subunit composition influences the solute specificity of the resulting channel, and specific combinations known to impart particular selectivities are shown. (C-F) VRAC functions during regulatory volume decrease (C), ischaemia-excitotoxicity (D), glucose sensing and insulin release from β cells (E), and antiviral defence via cGAS-STING (F).

However, given the historic lack of genetic tools for studying VRAC, all of the aforementioned studies have used pharmacological means to manipulate VRAC activity. Given the poor specificity of most chloride channel inhibitors, it is still uncertain whether their effects on microglia reflect VRAC inhibition or off-target activity. Thus, genetic studies are needed to clarify whether VRAC mediates microglial functions.

1.7 Role of VRAC in Stroke

VRAC may participate in pathological cascades contributing to certain diseases. The strongest evidence of pathological VRAC activity has been found for ischaemic stroke. Stroke is a leading cause of death and disability in the UK, and only one form of treatment, thrombolysis or mechanical thrombectomy, is currently available. Therefore, stroke represents one of the most pressing unmet needs in modern medicine. Ischaemic stroke results from thrombotic or embolic obstruction of a major cerebral blood vessel, resulting in interruption of blood supply to the brain region supplied by the vessel. Ischaemic conditions quickly develop within the affected area, leading to impaired glucose metabolism and ATP generation. The most severely affected region, known as the ischaemic core, experiences rapid neuronal death due to metabolic insufficiency. Neurons in the surrounding regions, known as the penumbra, are partially sustained by collateral blood flow and so experience metabolic stress but may still be viable given correct resolution of the insult. However, neuronal death in the core leads to release of intracellular osmolytes, which causes local osmotic tissue swelling known as cytotoxic edema. Moreover, excitatory amino acids (EAA) including glutamate are released by dying neurons, and initiate a subsequent wave of neuronal death due to excessive depolarization and intracellular calcium overload, known as excitotoxicity (Arundine & Tymianski, 2003).

Early studies observed that astrocyte cultures are capable of releasing large quantities of EAAs following hypotonic swelling, and noted that this could represent a pathological mechanism in stroke, given the high degree of astrocyte swelling in injured regions (Kimelberg, 2005; Kimelberg et al., 1990; Mongin, 2016). Subsequently, a model was proposed whereby astrocytes in the ischaemic penumbra accumulate glutamate and other osmolytes released by dying neurons, leading to pronounced swelling. This swelling then

stimulates VRAC opening, causing glutamate to be released back into the extracellular space, contributing to excitotoxicity (**Figure 1.2D**). During the initial ischaemia, astrocyte swelling may not cause VRAC to open, since VRAC depends on the presence of intracellular ATP for activity. Thus, severe ATP depletion inhibits VRAC activity (Mongin, 2016). However, upon restoration of blood flow following thrombolysis or thrombectomy, oxygen and glucose supply are restored, allowing ATP to accumulate once again. This is hypothesized to stimulate VRAC activity in previously ischaemic astrocytes, leading to release of intracellular glutamate (Mongin, 2016). Thus, VRAC may be a significant contributor to ischaemic injury, particularly in the ischaemic penumbra following reperfusion (Feustel et al., 2004; Mongin, 2016).

Initial studies sought to confirm this hypothesis using VRAC inhibitors to reduce extracellular accumulation of EAAs in ischaemic stroke models. Multiple studies confirmed that the VRAC inhibitors tamoxifen and DCPIB effectively reduced glutamate and aspartate release and provided striking reductions in infarct volume in experimental model of stroke (Feustel et al., 2004; Kimelberg et al., 2000, 2003; Mongin, 2016; Seki et al., 1999; Zhang et al., 2005, 2008). However, weaknesses in these studies included specificity issues surrounding VRAC inhibitors, and the fact that tamoxifen, the more potent compound, likely exhibits multiple neuroprotective effects unrelated to its role as a channel blocker. However, two recent studies have confirmed that experimental stroke in mice with either astrocyte-specific or whole-brain deletion of LRRC8A results in reduced ischaemic damage (Yang et al., 2019; Zhou, Luo, et al., 2020). As such, VRAC has emerged as a bona fide contributor to ischaemic brain damage, likely via effects on excitotoxicity. VRAC inhibition is therefore a promising avenue for future efforts in stroke treatment, and possibly other brain pathologies involving excitotoxicity, such as intracerebral hemorrhage and traumatic brain injury.

1.8 VRAC-independent functions of LRRC8A

LRRC8A is clearly capable of influencing cell and tissue physiology as a component of VRAC channels. However, several lines of evidence now suggest that LRRC8A may in some contexts act independently of the other VRAC subunits to influence cellular signal transduction (**Figure 1.3**). These VRAC-independent functions are less well-studied than those requiring

VRAC channel activity (i.e. solute transport), yet there is accumulating evidence that they may form a significant part of LRRC8A's *in vivo* significance.

LRRC8A was first identified as a protein mutated in certain forms of agammaglobulinaemia, an immunodeficiency syndrome characterised by a complete absence of circulating B cells (Sawada et al., 2003). This was ascertained to be the result of a heterozygous translocation in the *LRRC8A* gene resulting in deletion of the 3 terminal LRRs, accompanied by translation of a short stretch of intronic DNA at the C-terminus, termed LRRC8A^{Δ91/+35}. Whole-body deletion of LRRC8A in mice was subsequently shown to produce a similar, albeit more severe phenotype, with complete absence of T cells, modestly reduced B cell numbers, and an array of drastic tissue abnormalities including skin, kidney and muscle defects, growth retardation as well as extremely high pre- and post-natal mortality (Kumar et al., 2014). Mechanistically, the block on T cell development in LRRC8A-KO mice was shown to reflect defective activation of PI3K-AKT signalling in developing thymocytes, leading to aberrant apoptosis early in the maturation pathway (Kumar et al., 2014). LRRC8A was shown to associate with the Lck and Zap-70 kinases which are critical for thymocyte survival, which depended on binding to the signalling adapters GRB2 and GAB2. This study also suggested activation of the LRRC8A-GRB2-GAB2-Lck complex and subsequent recruitment of PI3K occurred in response to a ligand secreted by thymic epithelial cells, for which LRRC8A is the cognate receptor. Whilst this ligand was never identified, and to date no receptor capabilities have been conclusively proven for LRRC8A, several of the associated findings are intriguing with respect to LRRC8A biology. Firstly, LRRC8A was apparently capable of inducing PI3K activity following antibody-mediated clustering in the absence of any additional stimulation. Moreover, LRRC8A was shown to associate constitutively with Lck, ZAP-70 and GRB2-GAB2, and was able to rapidly stimulate Lck activity upon antibody binding (**Figure 1.3A**). This suggests that LRRC8A, at least partially, exists in dormant signalling complexes which can be rapidly activated by certain stimuli.

However, these results did not exclude a role for solute flux via VRAC in mediating the signalling functions of LRRC8A. This evidence came from characterisation of the *ébouiriffé* (*ebo/ebo*) mutant mouse, which was reported to harbour a frameshift mutation in the LRR domain of LRRC8A, resulting in expression of a truncated LRRC8A protein which was unable

to assemble active VRAC channels due to loss of the 13 C-terminal LRRs (Bao et al., 2018; Lalouette et al., 1996; Platt et al., 2017). While this mouse shares some characteristics with whole-body LRRC8A^{-/-} mice, the overall phenotype was much milder. Specifically, ebo/ebo mice exhibited only modestly reduced survival, no defects in T or B cell generation, no growth retardation and normal muscle development (Platt et al., 2017). Kidney, skin and liver abnormalities were, however, reported in these mice (Platt et al., 2017). This was a critical result in establishing channel-independent roles for LRRC8A *in vivo*, since expression of even truncated LRRC8A protein clearly rescues certain phenotypic characteristics associated with LRRC8A knockout, without the formation of functional VRACs.

Three further studies have investigated regulation of the PI3K pathway by LRRC8A. Firstly, it was shown that LRRC8A is necessary for activation of AKT following insulin stimulation in adipocytes, and that loss of LRRC8A impairs adipocyte hypertrophy and promotes insulin resistance (Zhang et al., 2017). The proposed mechanism by which LRRC8A regulates insulin signalling involves sequestration of GRB2 by LRRC8A, thus relieving GRB2-dependent inhibition of insulin receptor substrate (IRS)-mediated PI3K recruitment (Zhang et al., 2017) (**Figure 1.3B**). In the same study, LRRC8A was observed to co-precipitate with GRB2 and caveolin-1 (CAV1), a membrane protein enriched in caveolae, which is proposed to promote GRB2 binding to LRRC8A in response to mechanical stretch. In two separate papers, this same LRRC8A-CAV1-GRB2 interaction was suggested to promote LRRC8A-dependent stimulation of PI3K-AKT activity in response to mechanical stretch in muscle cells and endothelial cells (Alghanem et al., 2021; Kumar et al., 2020) (**Figure 1.3C**). These studies also presented some evidence of LRRC8A-dependent extracellular signal-related kinase (ERK) activation downstream of mechanical stretch. However, the mechanism for this was not investigated. While these studies also did not provide specific evidence that these LRRC8A-dependent effects were independent of VRAC conductance, it seems likely that this is the case considering the results of the studies in ebo/ebo mice. Moreover, overexpression of LRRC8A, which is well known to inhibit anion channel function by disrupting subunit stoichiometry, appeared to increase levels of AKT phosphorylation in myoblasts (Kumar et al., 2020).

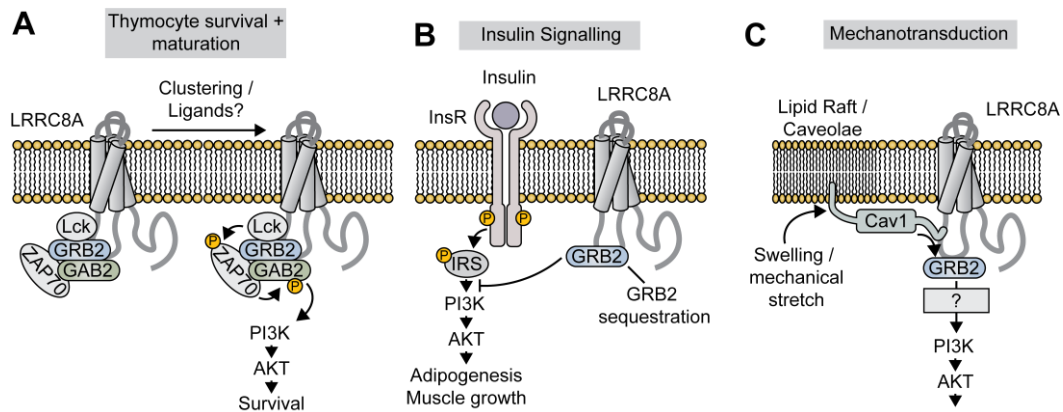


Figure 1.3: VRAC-independent signalling functions of LRRC8A

Contribution of LRRC8A to activation of the PI3K-AKT pathway in a variety of cell types. LRRC8A activates PI3K in thymocytes (A) in response to clustering or other unknown stimuli by stimulating Lck/Zap70 activity. In adipocytes (B), LRRC8A sequesters GRB2, which is a negative regulator of the insulin receptor substrate (IRS)-PI3K signalling axis. LRRC8A is also suggested to activate PI3K-AKT downstream of mechanosensing by caveolin 1 (Cav1), possibly via GRB2 (C).

Overall, there is considerable evidence that LRRC8A is necessary for induction of PI3K signalling in a variety of cell types, and contributes to cell homeostasis via mechanisms which are likely independent of its ion channel functions. However, studies in lymphocytes and adipocytes differ in their identified mechanisms of LRRC8A-dependent signalling. This suggests that LRRC8A may occupy discrete cell type-specific signalling complexes, each responding to different stimuli. Moreover, little attention has been given to the role of upstream kinase cascades in regulating LRRC8A-dependent signalling, nor downstream pathways other than PI3K which might respond to LRRC8A stimulation. Thus, much remains to be discovered regarding the role of LRRC8A as a signalling protein, and unbiased 'omics-based experiments may provide fresh insight into novel functions of LRRC8A in cellular physiology.

1.9 Study Rationale

VRAC has been suggested to regulate microglial phagocytosis, chemotaxis, migration and morphology, functions which are all relevant to CNS homeostasis and disease. Since VRAC is also suggested to be a target for treating astrocyte-dependent excitotoxicity in stroke, its functions in microglia are of interest for developing stroke therapies. However, since previous studies regarding VRAC function in microglia were conducted *in vitro* using chloride channel inhibitors with known specificity issues, there is a need for genetic studies addressing whether VRAC is the true mediator of these effects. Moreover, there have so far been no systematic

attempts to uncover novel signalling functions of LRRC8A, either as a component of VRAC or through VRAC-independent pathways. As such, the present study aimed to address the role of VRAC in regulating microglial function using a microglia-specific LRRC8A KO mouse. Subsequently, RNA-Sequencing was used to interrogate potential signalling functions of LRRC8A.

1.10 Aims

1.10.1 Chapter 2 – Investigating the role of VRAC in microglial physiology

The objective of this chapter was to clarify the contribution of VRAC to microglial function. In support of this goal, this chapter utilises a novel microglia/macrophage-specific LRRC8A knockout mouse line. Using this line, the following aims were pursued:

- Characterisation of the novel microglia-targeted *Lrrc8a^{fl/fl}:Cx3cr1^{Cre}* LRRC8A knockout mouse, in terms of LRRC8A expression and presence/absence of RVD in microglia, as well as global transcriptome profiling via RNA-Seq.
- Assess differences in microglial phagocytosis and migration/chemotaxis arising from loss of LRRC8A/VRAC using *ex-vivo* microglial cultures, acute brain slices and intravital imaging
- Determine the influence of VRAC on microglial morphology and stroke infarct volume

1.10.2 Chapter 3 – Identifying novel LRRC8A-dependent signalling pathways

The second chapter aimed to dissect novel signalling functions of LRRC8A. For this, bone-marrow derived macrophages (BMDM) from *Lrrc8a^{fl/fl}:Cx3cr1^{Cre}* and *Lrrc8a^{fl/fl}:Cx3cr1^{WT}* were used as a general immune cell model. RNA-Seq was used to assess transcriptomic differences following treatment with hypotonic media to stimulate LRRC8A-dependent signalling. Thus, the aims of this chapter were as follows:

- Perform and analyse RNA-Seq on LRRC8A-KO and WT macrophages treated with isotonic or hypotonic media
- Use upstream analysis to predict likely signalling alterations
- Validate and characterise novel signalling functions using standard cell culture techniques

Chapter 2: Investigating the role of VRAC in microglial physiology

2.1 Introduction

VRAC has been identified as a potentially promising target for treating stroke due to its role in promoting excitotoxic neuronal death following cerebral ischaemia (Mongin, 2016). However, VRAC is also suggested to support a variety of microglial functions including phagocytosis, migration and chemotaxis. Microglia are key players in determining the extent of neuronal death following stroke, and the role of VRAC in regulating their function is therefore of great relevance. Previous studies seeking to understand the role played by VRAC in microglia have done so using poorly specific pharmacological tools which are difficult to interpret conclusively. Thus, despite some suggestive evidence, there is no clear consensus on what, if any microglial functions VRAC might support, and, moving forward, genetic studies are required to clarify this point.

Currently, limited tools exist to determine VRAC function. While numerous pharmacological agents are known to inhibit VRAC, even the most specific of these drugs exert numerous off-target effects. Small interfering RNA (siRNA) can be used for knockdown studies with better specificity than drugs, yet can rarely achieve complete elimination of the target protein. Moreover, nucleotide transfection can itself alter cell physiology, particularly in immune cells such as macrophages which express immune defence mechanisms against cytosolic nucleotides. Finally, siRNA based methods are usually reserved for *in vitro* experiments, as transfection of cells *in vivo* with siRNA is challenging. Thus, there is a clear need for mouse lines allowing specific, complete LRRC8A knockout *in vivo*, allowing both *in vivo* experiments and *ex-vivo* experiments on isolated primary cells and tissues.

A constitutive LRRC8A knockout mouse line has already been described, though homozygous knockout results in a severe phenotype with high embryonic lethality, multiple tissue defects and very low survival beyond the fourth postnatal week (Kumar et al., 2014). A conditional knockout strategy deleting LRRC8A only in cell types of interest is therefore preferable in the interest of practicality and animal welfare. Fortunately, excellent targeting of microglia and tissue macrophages can be achieved via *Cx3cr1^{Cre}* recombinase-expressing mouse lines, provided the gene in question harbours LoxP sites suitable for Cre-mediated recombination (Yona et al., 2013). A macrophage-restricted conditional LRRC8A knockout mouse line was

therefore developed utilising a floxed *Lrrc8a* exon 3 in combination with the *Cx3cr1^{Cre}* recombinase (Green et al., 2020).

2.1.1 Specific Aims

This study aimed to address the role of VRAC function in microglial physiology using the novel microglia/macrophage-specific knockout mouse model created by our group. Specifically, this study sought to achieve the following:

- Characterise the microglial LRRC8A knockout mouse model to confirm the specificity and efficacy of LRRC8A ablation, and that RVD is compromised by LRRC8A KO
- Investigate whether loss of LRRC8A affects baseline microglial phenotype via transcriptomic analysis
- Determine whether LRRC8A contributes to microglial functional properties, including
 - Phagocytosis (BMDM also used to rule out cell type-specific effects)
 - Cell migration
 - ATP-dependent chemotaxis
 - Basal and reactive morphology
- Assess whether microglial LRRC8A contributes to infarct volume in the distal MCAO model of experimental stroke

2.2 Materials and Methods

2.2.1 Chemicals

DCPIB (Tocris), NPPB (Tocris), FFA (Sigma), Cytochalasin D (Sigma) and Calcein-AM (Biolegend) were obtained as powders dissolved in dimethyl sulfoxide (DMSO) to 200x concentrated stocks and stored at -20°C. pHrodo-SE (ThermoFisher) was dissolved in DMSO to 10mg/mL and stored in aliquots at -80°C. Human A β ₁₋₄₂ (Eurogentec) was dissolved in hexafluoro-2-propanol, dried into films under a rotary evaporator (Eppendorf) and stored at -80°C. Tomato lectin conjugated to DyLight 594 (Vector Biolabs) was washed twice through a centrifugal filter (10kDa MWCO) to remove sodium azide, sterile filtered and stored as a 1mg/mL stock at 4°C.

2.2.2 Animals

The *Lrrc8a^{fl/fl}* line was generated in-house using CRISPR-Cas9 as described previously (Green et al., 2020). Briefly, LoxP sites were introduced flanking exon 3 of the *Lrrc8a* gene, which contains >85% of the coding sequence. Initially a single-step procedure was attempted comprising pronuclear injection of embryos with both 3'- and 5'-targeting sgRNA-Cas9 complexes along with their respective repair templates, followed by implantation into pseudopregnant female mice. While no young harboring both 5' and 3' LoxP sequences were obtained, mice harboring the 5' LoxP site were bred to homozygosity and used as a founder colony. 5' LoxP homozygous embryos were then obtained and electroporated with the 3'-targeting sgRNA-Cas9 and repair sequence, and implanted into pseudopregnant females. The resulting young were screened for integration of the 3' LoxP sequence, and 3' + 5' LoxP harboring individuals bred to homozygosity (*Lrrc8a^{fl/fl}*).

To create a constitutive microglia/macrophage-targeted knockout model, the *Lrrc8a^{fl/fl}* line was crossed with a *Cx3cr1^{Cre}*-expressing line (Yona et al., 2013) to generate littermates homozygous for the floxed LRRC8A allele and either null (*Lrrc8a^{fl/fl}:Cx3cr1^{+/+}*) or heterozygous (*Lrrc8a^{fl/fl}:Cx3cr1^{+/Cre}*) for *Cx3cr1^{Cre}*, corresponding to WT and KO groups, respectively. A separate line of (*Lrrc8a^{+/+}:Cx3cr1^{+/Cre}*) lacking LoxP sites around *Lrrc8a* but positive for the *Cx3cr1^{Cre}* transgene were maintained for use as a control in some *in vivo* experiments, where *Cx3cr1* heterozygosity in KO mice might affect assay outcome. *Cx3cr1^{eGFP/+}* mice (originally

described by (Jung et al., 2000)) were obtained from an in-house breeding colony maintained by John Grainger. All animals were housed under standard conditions ($21 \pm 2^{\circ}\text{C}$; $55\% \pm 5\%$ humidity) in individually ventilated cages, under 12-hour light/dark cycles with *ad libitum* access to food and water. In general, all animals were between 8-36 weeks old and of mixed sex, though more specific age ranges were required for some experiments, as detailed in the respective sections. All *in vivo* work was performed in accordance with the Animals (Scientific Procedures) Act 1986 under relevant UK Home Office licenses and approved by the local Animals Welfare and Ethical Review Board (University of Manchester, UK).

2.2.3 Transcardial Perfusion

Mice were anaesthetised deeply in 2-2.5% isoflurane in a 70:30 mix of $\text{NO}_2:\text{O}_2$, and anaesthesia verified via absence of the paw withdrawal reflex. An incision was made to open the abdomen along the inferior border of the ribs. The diaphragm was then cut and the thoracic cavity exposed by bilateral incisions through the lateral portion of the ribcage. A blunt cannula was inserted into the left ventricle and clamped in place with small haemostats, following which an incision was made into the right atrium, and the mouse perfused with ice-cold solutions (PBS followed by 4% paraformaldehyde (PFA) for fixation, aCSF for acute brain slices) via a peristaltic pump at a rate of 10mL/min.

2.2.4 Cell Culture

For microglia cultures, mice were perfused with ice-cold saline and the brains collected, the cerebellum and olfactory bulb were discarded, and the remaining tissue diced into small (1-2 mm) chunks using a scalpel. Papain and DNase digestions were performed using a neural tissue dissociation kit (Miltenyi) according to the manufacturer's instructions. Following digestion, a dounce homogenizer with a loose pestle was used to dissociate the brain into a single-cell suspension, which was then pelleted at 300xg (5 min) and myelin removed by centrifugation through 30% Percoll Plus (GE Healthcare). Cells were then resuspended in MACS buffer (PBS, 0.5% BSA, 2mM EDTA) with anti-CD11b magnetic beads (Miltenyi) and incubated on a roller for 15 min. Microglia were enriched using a quadromACS separator with LS columns (Miltenyi) according to the manufacturer's instructions. After counting, $1-2 \times 10^4$ cells were spot-plated onto 96-well Cell+ anionic/cationic plates (Sarstedt) and allowed to adhere for 10 min before flooding with media. Cells were cultured for at least 7 days in

DMEM/F12 (Gibco) supplemented with 1% Penicillin/Streptomycin (Sigma), 2 mM glutamine, 10% FBS (Gibco), 50 ng/mL TGF- β 2 (Peprotech) and 20 ng/mL IL-34 (R&D Systems).

Bone marrow-derived macrophages (BMDM) were cultured by harvesting bone marrow from both femurs of each mouse, lysing red blood cells in ACK buffer, and culturing for 7 days in DMEM (10% FBS, 100 U/mL penicillin, 100 μ g/mL streptomycin) mixed 70:30 with DMEM conditioned by L929 fibroblasts.

2.2.5 Western Blotting

For western blots, cells were lysed directly in laemmli buffer (62.5 mM Tris-HCl, 2% SDS, 10% glycerol, 5% β -mercaptoethanol) and heated to 95°C for 10 min. Lysates were then separated by Tris-Glycine SDS-PAGE before transfer to polyvinylidene difluoride (PVDF) membranes (Bio-Rad). Membranes were blocked in 5% nonfat milk in phosphate-buffered saline (PBS) with 0.05% Tween-20 (PBS-T) for 1 h at room temperature before incubating overnight with mouse anti-LRRC8A (8H9, Santa Cruz, 1:100) in block buffer. Membranes were washed 3 times in PBS-T before incubating with HRP-conjugated rabbit anti-mouse (Dako) in block buffer for 1 h at room temperature. After washing 3 further times, membranes were imaged on a G:Box Chemi XX6 (Syngene) using Amersham ECL Prime chemiluminescence reagent (GE Healthcare).

For loading controls, membranes were washed and incubated with HRP-conjugated mouse anti- β -actin (Sigma) in block buffer for 1 h at room temperature, followed by washing and imaging as above.

2.2.6 Regulatory volume decrease assay

5×10^4 BMDM were seeded onto black-walled 96-well plates (Corning), whereas microglia were spot-plated onto Cell+ plates. Cells were loaded with 10 μ M calcein-AM (BioLegend) for 1h, washed three times with media and then rested for 30 min to allow calcein to equilibrate. After three further washes with isotonic buffer (132 mM NaCl, 2.5 mM KCl, 2 mM CaCl₂, 2 mM MgCl₂, 10 mM Glucose, 20 mM HEPES, pH 7.4, 312 mOsm/Kg) cells were imaged in isotonic buffer on an Eclipse Ti microscope (Nikon) equipped with a stage incubator maintaining 37°C and 5% CO₂. Calcein fluorescence was captured in the GFP channel using low laser power to minimize phototoxicity and bleaching. Live imaging was conducted using a point-visiting to

image all conditions simultaneously. One image was captured every 2 min, with hypotonic shock induced at 5 min by adding distilled water to a final dilution of 30% (218 mOsm/Kg). For quantification, fluorescent images were processed in Fiji, using a rolling-ball background subtraction (50 pixels ball size) to remove non-cell associated fluorescence. The average pixel intensity of each frame was then measured and normalized to the value of the first frame, yielding F/F_0 curves. For statistical testing, AUC values of the curves were calculated in Prism.

2.2.7 Phagocytosis assays

Phagocytosis assays were performed using an IncuCyte ZOOM (Essenbio) time-lapse microscope housed in a humidified incubator maintaining 37°C and 5% CO₂. Prior to imaging, cells were incubated in Opti-MEM (containing drugs or vehicle as specified) for 15 min. pHrodo-*E. coli* bioparticles (ThermoFisher) and pHrodo-Zymosan (ThermoFisher) were then added at a 1:10 dilution. Other prey particles were prepared and added as described below.

Human A β ₁₋₄₂ (Eurogentec) was dissolved to 10 mM in DMSO, then further diluted to 1 mM using sterile water and incubated at 37°C for 7 days. Amyloid fibrils were pelleted by centrifugation at 18,000xg for 15 min, labelled with 25 μ M pHrodo red-SE (ThermoFisher) in PBS at room temperature for 1 h, washed twice with PBS and added to cells at a final concentration of 10 μ M.

For RBC assays, whole mouse blood was collected by cardiac puncture and centrifuged briefly at 500xg to pellet cells. The pellet was then resuspended in PBS, layered onto a discontinuous percoll gradient containing 65% and 35% layers and centrifuged at 1000xg for 15 min. RBCs were recovered from the pellet, washed once with PBS, and 10⁸ cells were labelled with 50 μ M pHrodo-SE for 1 h, followed by two washes with PBS. Labelled RBCs were then opsonized with 1 μ g/mL rabbit anti-mouse RBC IgG (34-3C, Hycult) for 30 min, washed two further times with PBS, and added to cells at 10⁶ RBC per well. Un-opsonised controls were included to verify that uptake was IgG-dependent.

Following addition of particles, three images per well were captured every 15 min for a total of 3 hours, and automatically analysed using the IncuCyte software (Essenbio). Custom scripts were created which gave optimal detection for each phagocytic substrate and were run identically on all conditions. For each well, the pHrodo-positive area was normalized to the

area covered by cells (determined from the baseline image using phase confluence function) to give the phagocytic index.

2.2.8 In vitro motility assay

Microglia cultured in 96-well plates were labelled with Hoechst (Invitrogen; 1 µg/mL) in growth media for 45 min, washed with serum-free media and incubated in Opti-MEM (containing vehicle or drugs as stated) for 15 min prior to imaging. Cells were imaged on a Nikon Eclipse Ti widefield microscope with a stage incubator maintaining 37°C/5% CO₂ using both phase contrast and DAPI channels with low UV laser power to prevent toxicity. Images were obtained every 5 min for 3 h.

The fluorescent (nuclear) channel was then analysed for cell movement in ImageJ by first performing a rolling-ball background subtraction (ball radius 20) and loading the resulting images into the TrackMate plugin (Tinevez et al., 2017). To identify nuclei, LoG detection was used with a spot size of 8 µm, thresholds were empirically determined for each experiment and applied equally across all conditions. No spot filtering was necessary. Tracking was performed using the simple LAP tracker with max linking distance of 40 µm, and max gap closing distance of 70 µm over 2 frames.

2.2.9 RNA Sequencing (RNA-Seq)

Microglia were purified from 10-12-week-old female WT, KO and Cre mice via MACS and RNA isolated immediately using Purelink RNA miniprep kits (Invitrogen). Total RNA was submitted to the Genomic Technologies Core Facility (GTCF) at the University of Manchester. Quality and integrity of the RNA samples were assessed using a 2200 TapeStation (Agilent Technologies) and then libraries generated using the TruSeq® Stranded mRNA assay (Illumina, Inc.) according to the manufacturer's protocol. Briefly, total RNA (0.1-4 µg) was used as input material from which polyadenylated mRNA was purified using poly-T, oligo-attached, magnetic beads. The mRNA was then fragmented using divalent cations under elevated temperature and then reverse transcribed into first strand cDNA using random primers. Second strand cDNA was then synthesised using DNA Polymerase I and Rnase H. Following a single 'A' base addition, adapters were ligated to the cDNA fragments, and the products then purified and enriched by PCR to create the final cDNA library. Adapter indices were used

to multiplex libraries, which were pooled prior to cluster generation using a cBot instrument. The loaded flow-cell was then paired-end sequenced (76 + 76 cycles, plus indices) on an Illumina HiSeq4000 instrument. Finally, the output data was demultiplexed (allowing one mismatch) and BCL-to-Fastq conversion performed using Illumina's bcl2fastq software, version 2.20.0.422

For analysis, unmapped paired-end sequences were tested by FastQC (<https://www.bioinformatics.babraham.ac.uk/projects/fastqc/>). Sequence adapters were removed and reads were quality trimmed using Trimmomatic_0.36 (Bolger et al., 2014). The reads were mapped against the reference mouse genome (mm10/GRCm38) and counts per gene were calculated using annotation from GENCODE M21 (<https://www.gencodegenes.org/>) using STAR_2.5.3a (Dobin et al., 2013). Normalisation and differential expression was calculated with DESeq2_1.28.1 (Love et al., 2014). Differentially expressed genes between conditions (Log2 fold-change > 0.5, adjusted p-value < 0.05) were tested for pathway enrichment using the enrichR platform (Chen et al., 2013) queried via the enrichR package (<https://CRAN.R-project.org/package=enrichR>) in Rstudio.

2.2.10 Acute brain slices

Acute brain slices were prepared according to published methods (Etienne et al., 2019). Briefly, adult (8-16-week-old) Cx3cr1-eGFP mice were perfused with ice-cold oxygenated choline-artificial cerebrospinal fluid (aCSF) (110 mM choline chloride, 25 mM glucose, 25 mM NaHCO₃, 20 mM HEPES, 0.5 mM CaCl₂, 7 mM MgCl₂, 11.6 mM ascorbic acid, 3.1 mM sodium pyruvate, 2.5 mM KCl, 1.25 mM NaH₂PO₄, pH 7.4), the brain was quickly dissected, and 300 µm-thick slices cut on a VT1000S vibratome (Leica). Slices were allowed to recover in choline-aCSF at 34°C for 15 min under constant oxygenation before transfer to experimental aCSF (124 mM NaCl, 25 mM glucose, 25 mM NaHCO₃, 2 mM CaCl₂, 1 mM MgCl₂, 2.5 mM KCl, 1.25 mM NaH₂PO₄) at room temperature bubbled constantly with carbogen. Slices were used between 40-180 min after first being cut. For imaging, slices were mounted in a heated tissue chamber (Scientifica) maintained at 37°C and constantly perfused with carbogenated aCSF (3mL/min) via a peristaltic pump with inline heater. Multiphoton imaging (**2.2.12**) was performed at least 50 µm below the surface of the slice to avoid reactive microglia.

2.2.11 Lectin injection and cranial window implantation

Cranial windows were implanted as previously described (Goldey et al., 2014). Animals were anesthetized with 2.5% isoflurane in 100% O₂ and the scalp was removed over the animals left and right hemisphere. A metal head plate was mounted (Narishige CP-2, Japan) using dental cement (Sun Dental, Japan) to allow stereotaxic fixation under the 2-photon microscope. A circular piece of bone with a diameter of 3 mm was then removed using a dental drill. The dura was left intact for the whole experiment.

Prior to window implantation, tomato lectin conjugated to DyLight-594 was diluted to 50µg/mL in sterile PBS, and 200nL was injected through the dura into the cortex using a borosilicate microcapillary tube pulled to an outer tip diameter of 5µm. Injections were performed over 10 min (UltraMicroPump III, World Precision Instruments, USA), followed by a 5 min rest before the needle was withdrawn. Injection depths were between 150-250µm below the dura. Once the injection was finished, a circular coverslip (Warner Instruments, USA) was glued in place of the removed bone using dental cement (Prestige Dental, Japan).

Mice were imaged (using multiphoton, see **2.2.12**) immediately after cranial window implantation over a period of 4 hours. During this time, they were maintained under 2% isoflurane in 100% O₂ and the body temperature was maintained at 37.5 °C via a heating blanket controlled with a temperature probe (Harvard Apparatus, Kent, UK).

2.2.12 Multiphoton imaging

Imaging was conducted on both acute brain slices (**2.2.10**) and mice with implanted cranial windows (**2.2.11**) using a Leica SP8 multiphoton microscope equipped with a MaiTai Ti:Sapphire MP laser (Spectra-Physics) and an HC Fluotar L 40x water dipping lens. 1024x1024 pixel z-stacks were captured at 1.8x confocal zoom, corresponding to approximate dimensions of 180x180 µm, with Z-planes spaced 2 µm apart. For each series, 15-20 z-planes were captured, corresponding to 15-20 µm above and below the lesion. For imaging GFP, the 2-photon laser was tuned to 880 nm, and to 800 nm for imaging tomato lectin. In each case, imaging laser power was kept below 5% and 3x line averaging was used. Lesions were induced using the point bleach function in the LAS X software to illuminate a single pixel for 500 ms with laser power set to 20-30x that used for imaging. Image acquisition was then

automatically started, and z-stacks acquired 1 min apart for 10 (for Cx3cr1-eGFP brain slices) or 15 min (*in vivo* imaging).

For analysis, xyzt hyperstacks were first registered in Fiji using the turboreg plugin, and then cropped to a 120 μm x 120 μm square centred around the lesion. A median filter with a radius of 2 pixels was then applied, and background subtraction with a rolling ball radius of 50 pixels performed. Maximum-intensity z-projections were then created and a further median filter applied to smooth noise. eGFP images were then thresholded using the Huang method. For tomato lectin images, thresholds were empirically determined due to variability in the staining intensity and presence of other bright objects (e.g. blood vessels), which complicated automatic thresholding. Thresholded time-series were then analysed in MATLAB using the MGPTracker script (Gyoneva et al., 2014), which quantifies the area of a polygon in each image surrounding the lesion which is free of microglial processes. The resulting area-over-time data were then normalized to the value of the first frame for each video.

2.2.13 Middle cerebral artery occlusion

Thrombi formation and cerebral ischemia were performed using the FeCl_3 method (as a model of distal MCAo) as described previously (Le Behot et al., 2014). 12-14-week-old male mice were anesthetized with 5% isoflurane, placed in a stereotaxic device, and maintained under anesthesia with 2.5% isoflurane in a 70%:30% mixture of O_2 / N_2O . A small craniotomy (1 mm diameter) was performed on the parietal bone to expose the right middle cerebral artery (MCA). A Whatman filter paper strip soaked in FeCl_3 (30%, Sigma) was placed on the dura mater on top of the MCA for 10 min. Cerebral blood flow in the MCA territory was measured continuously by laser Doppler flowmetry (Oxford Optronix) for 1h post-occlusion, and occlusion was confirmed by a sustained drop in the doppler signal. Animals were then sutured, returned to the home cage and given access to mash placed on the cage floor. Analgesia was provided by application of EMLA cream to the scalp and subcutaneous buprenorphine (0.05 mg/kg). 24h after occlusion, mice were once more imaged using laser Doppler flowmetry for 5 minutes to confirm sustained occlusion, then culled via transcardial perfusion and brains processed for immunohistochemistry (see **2.2.14**).

2.2.14 Immunohistochemistry

For microglia immunohistochemistry, animals were anaesthetized with 2.5% isoflurane in 30:70 O₂/N₂O and transcardially perfused with cold saline solution followed by 4% PFA in 0.1 M phosphate buffer. Brains were post-fixed in 4% PFA for 24 h at 4°C, cryoprotected in 30% sucrose for 48 h at 4°C and stored at -80°C until sectioning.

For microglia morphological analyses, brains were sectioned on a cryostat to 150 µm thickness. Iba1 staining was performed on 5 randomly selected animals per genotype using published protocols (Heindl et al., 2018) with minor modifications. Briefly, sections were blocked and permeabilized overnight at room temperature in PBS with 20% DMSO, 2% normal goat serum, 1% Triton-X100 and 0.5% gelatin from cold-water fish skin (Sigma), then stained with rabbit anti-Iba1 (abcam EPR16588, 1:200) in the same buffer for 72 h at 4°C. Sections were washed 3 times for 1 h each in PBS, then incubated with Alexa-594 goat anti-rabbit IgG (Invitrogen, 1:500) and Hoechst (2.5 µg/mL) for 48 h in block buffer. After three further washes, sections were cleared by incubating with a sequence of increasingly concentrated fructose solutions to a final concentration of 80.2% w/w (SeeDB method (Ke et al., 2013)) for optimal confocal imaging (2.2.15).

For determining infarct volumes, some cryostat sections from the same mice were cut to 10 µm and stained with Cresyl violet. Infarct volume was analyzed using ImageJ and calculated as the sum of every lesion area multiplied by the distance between each section (0.5 mm).

2.2.15 Microglial morphology analysis

Cleared sections were imaged using a Leica TCS SP8 AOBS upright confocal with a 63x HCX PL Apo lens at 0.75x confocal zoom (effective magnification 47.25x). Z-stacks were acquired at 1024x1024 resolution with 0.4 µm intervals, with between 70-90 µm total depth. Stacks were positioned immediately adjacent to the infarct border in the ipsilateral cortex and at the equivalent position in the contralateral cortex for each section. Image acquisition was performed blind to experimental group.

Z-stacks were analysed in MATLAB (R2018, The MathWorks, Natick, Massachusetts, USA) using the publicly available mmqt script (Heindl et al., 2018) (<https://github.com/isdneuroimaging/mmqt>) with the default parameters on all images. This

script produces 15 morphological readouts based on simple shape volumetric measurements, skeleton analysis, and two measures of centrality derived from graph theory (**Table 2.1**). The MATLAB outputs were analysed in Rstudio (Rstudio Team, 2020) using R version 4.0.3 (R Core Team, 2020).

Table 2.1– Morphological parameters for microglial analysis

Parameter	Type	Description
Sphericity	Volumetric	3D sphericity (complexity)
Circularity	Volumetric	2D circularity
Node Volume	Volumetric	Median node volume (of each cell)
Total nodes	Skeleton	Total nodes per cell
Branching Nodes	Skeleton	Total branching nodes per cell
End nodes	Skeleton	Total end-nodes per cell
Branch nodes	Skeleton	Total nodes within branches
Nodes per branch	Skeleton	Total nodes per major branch
End nodes per branch	Skeleton	Total end nodes per major branch
Branch segments	Skeleton	Total branch segments per cell
Segments per branch	Skeleton	Total branch segments per branch
Branch length skeleton	Skeleton	Total branch length (following skeleton)
Branch sinuosity	Skeleton	Branch skeleton length / air-line length
Closeness	Centrality	Median node closeness
Betweenness	Centrality	Median node betweenness

15 morphological parameters extracted via MATLAB, based on either volumetric shape-based measurements, skeleton analysis, or graph theory centrality measures.

2.2.16 Statistics

In all experiments, statistical testing was performed with individual mice as the statistical unit (biological replicates), and n-numbers always refer to mice unless otherwise stated. Where measurements are taken from multiple cells per mouse, the average of these measurements was considered as one biological replicate. Unless otherwise specified, data were plotted and analysed in Graphpad Prism (Version 9.0). Normally distributed data (assessed via Shapiro-wilk test) are presented as mean +/- standard error of the mean (SEM), and non-normally distributed data are presented as median with interquartile range. Experiments with 2 groups were compared with a two-tailed Student's *t*-test. Comparisons between >2 experimental

groups were conducted via one-way ANOVA with Dunnet's post hoc in the case of multiple comparisons to a single control condition, or else by Tukey's post-hoc. Welch's correction was applied in case of unequal variance between groups. Experiments with two independent factors were analyzed via two-way ANOVA.

For analysis of lesion volumes following MCAO, as well as microglial morphology, all mouse surgery, staining, microscopy and computational analysis was conducted blind to mouse genotype. For intravital 2-photon imaging, no blinding was performed. For quantification of microglial chemotaxis, motility and phagocytosis, analysis was unblinded but largely automated and run with identical settings between conditions/genotypes. Unless otherwise specified, mice of mixed sex were used. MCAO experiments were conducted using only male mice, and RNA sequencing with only females.

2.3 Results

2.3.1 LRRC8A KO impairs volume regulation in microglia and BMDM

Mice homozygous for the floxed LRRC8A exon 3 (*Lrrc8a^{fl/fl}*) were crossed with CX3CR1-Cre (*Cx3cr1^{Cre/+}*) mice to produce *Lrrc8a^{fl/fl}* offspring which were either heterozygous (*Lrrc8a^{fl/fl}::Cx3cr1^{Cre/+}*) or null (*Lrrc8a^{fl/fl}::Cx3cr1^{+/+}*) for the CX3CR1-Cre knock-in, corresponding to the knockout (KO) and wild-type (WT) genotypes, respectively (**Figure 2.1A**). Since the insertion of the Cre recombinase at the *Cx3cr1* locus results in loss of one *Cx3cr1* allele, and expression of the Cre recombinase entails potential toxicity, in some experiments *Cx3cr1^{Cre/+}* mice with no LoxP sites flanking *Lrrc8a* (*Lrrc8a^{+/+}::Cx3cr1^{Cre/+}*) were included to control for CX3CR1- or Cre-dependent effects unrelated to LRRC8A function. Hereafter, this control group is denoted as “Cre”.

To confirm that LRRC8A was absent at the protein level in myeloid cells of the KO genotype, microglia and BMDM were cultured from both WT and KO mice, lysates prepared and western blots against LRRC8A performed (**Figure 2.1B**). As expected, no LRRC8A signal was observed in KO cells, indicating that LRRC8A expression was entirely ablated. Since in the CNS CX3CR1 is only expressed in microglia, LRRC8A expression should be maintained in non-microglial brain cells. To validate the specificity of the knockout in the brain, cortical lysates were prepared from WT and KO mice and LRRC8A levels assessed via western blot (**Figure 2.1B**). LRRC8A bands were observed in cortical lysates from both WT and KO mice, indicating that LRRC8A ablation in KO animals seems to be confined to microglia.

As LRRC8A was identified as the only subunit obligatory for VRAC activity (Qiu et al., 2014; Voss et al., 2014), microglia and macrophages lacking LRRC8A should also display defective VRAC activation in response to extracellular hypotonicity, resulting in impaired RVD responses. To assess whether VRAC function was impaired, WT and KO microglia were exposed to a 30% hypotonic solution (218 mOsm/Kg) and observed via time-lapse microscopy. Following hypotonic shock, visible swelling occurred in both genotypes (**Figure 2.1C**). WT cells then returned to normal volume over the subsequent 15 minutes, whereas KO cells exhibited persistent unresolved swelling (**Figure 2.1C**).

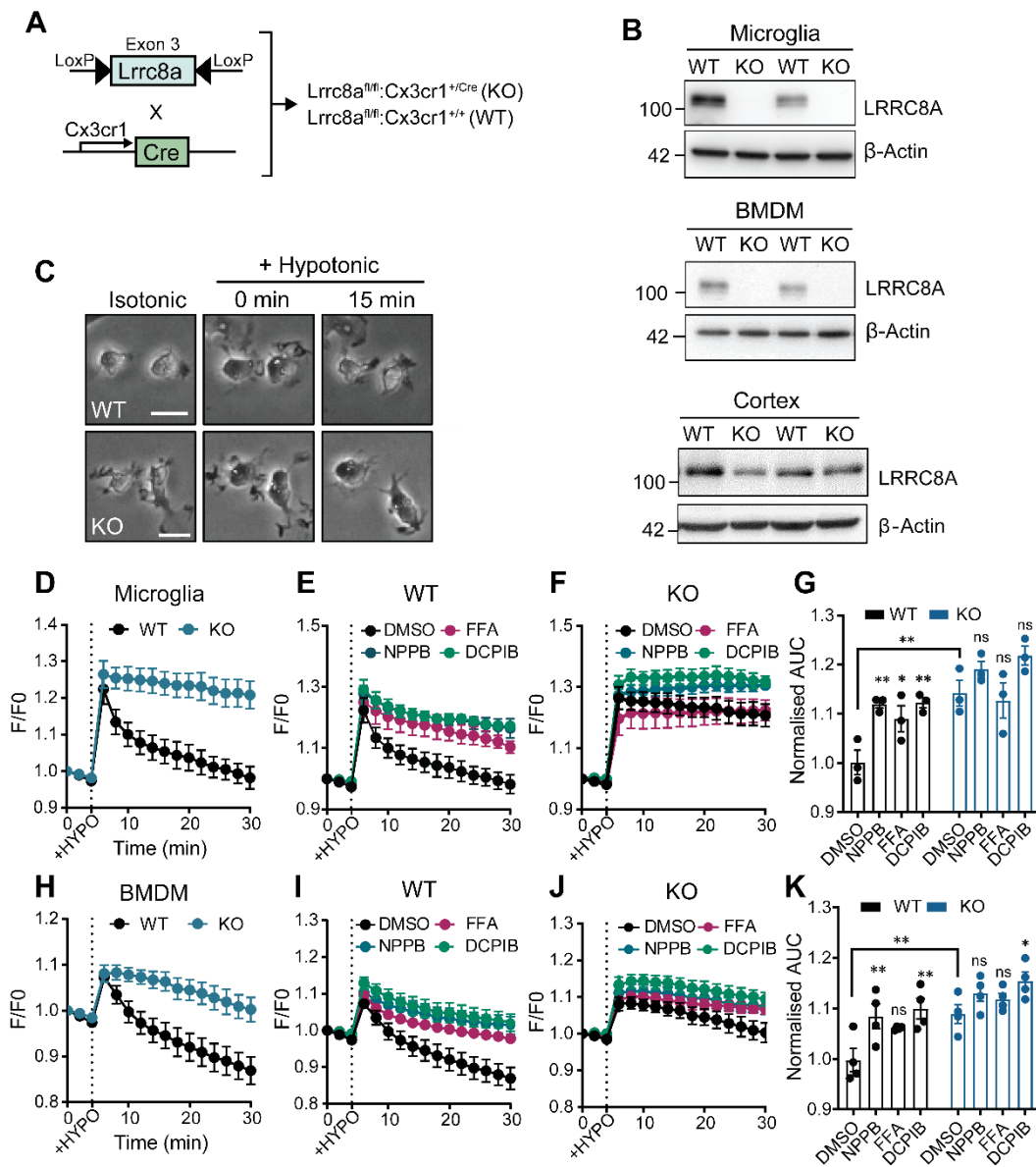


Figure 2.1: LRRRC8A is required for volume regulation in microglia and macrophages:

(A) Schematic depicting knockout generation strategy. (B) Western blots showing LRRRC8A expression in microglia, bone marrow-derived macrophages (BMDM) and whole-cortex lysate from wild-type (WT) and LRRRC8A knockout (KO) mice (representative of *n* = 4 mice) (C) Phase-contrast micrographs of WT and KO microglia at baseline (isotonic; 312 mOsm/kg) and immediately or 15 minutes after being exposed to hypotonic (218 mOsm/kg) conditions (scale bars = 20 μm) (D-F) Calcein fluorescence traces of WT and KO microglia exposed to hypotonic conditions in the presence of either vehicle (DMSO) or chloride channel blockers NPPB (100 μM), FFA (100 μM) or DCPIB (10 μM) (*n* = 3 mice). (G) Area under curve (AUC) quantification of D-F. (H-J) Calcein fluorescence traces of WT and KO BMDM exposed to hypotonic conditions in the presence of vehicle or NPPB, FFA or DCPIB (*n* = 4 mice) (K) AUC quantification of H-J. Data presented as mean ± SEM. Statistics in G,K are from one-way ANOVA with Tukey's post-hoc. * *p* < 0.05, ** *p* < 0.01

To quantify the kinetics of volume regulatory processes in both genotypes, a calcein-based RVD assay was used in both microglia and BMDM. Calcein is cell-impermeable and exhibits quenching by intracellular molecules, such that increases in cellular volume decrease the degree of fluorescence quenching due to lower molecular crowding, resulting in increased calcein signal. Therefore, changes in calcein fluorescence act as a reporter for relative cell volume following osmotic shock. Microglia and BMDM loaded with calcein-AM were exposed to hypotonic buffer, and RVD assessed via fluorescence time-lapse microscopy. The observed fluorescence intensity traces, indicative of cellular volume alterations, show that while WT cells return to normal volume within 25 minutes after application of the hypotonic solution, KO cells are entirely unable to undergo RVD (**Figure 2.1D,H**). AUC analysis of the fluorescence traces indicated a statistically significant impairment (corresponding to higher AUC) in KO cells compared to WT in both microglia and BMDM (**Figure 2.1G,K**).

To determine whether the RVD impairment in KO cells was equivalent to that produced by pharmacological chloride channel inhibition, RVD assays were also performed using the VRAC inhibitors DCPIB (10 μ M), FFA (100 μ M) and NPPB (100 μ M). Fluorescence traces (**Figure 2.1E-F, I-J**) and accompanying AUC analyses (**Figure 2.1G,K**) indicate that all three inhibitors produce significant impairment of RVD which almost exactly phenocopied LRRC8A KO. In KO cells, the inhibitors produced a slight trend toward increased AUC, which was not statistically significant in most cases, indicating that their effects on volume regulation are largely dependent on LRRC8A inhibition (**Figure 2.1G,K**). Overall, these results indicate that the Cre-lox gene targeting approach successfully ablated expression of LRRC8A at the protein level in microglia and BMDM, producing a clear functional deficit in VRAC activity. As such, the role of VRAC in microglial function should be interrogable in this model.

2.3.2 RNA Sequencing of primary microglia

Whilst much is now known about the molecular aspects of VRAC function in response to hypotonicity, its functions *in vivo* remain largely mysterious. If microglial VRAC plays a significant role in regulating any aspect of microglial physiology, or if LRRC8A itself has any such functions independently of VRAC, these might be revealed via analysis of the microglial transcriptome. RNA-sequencing was therefore performed on primary microglia acutely

isolated from WT, KO and Cre mice to reveal any perturbations of gene expression arising through loss of LRRC8A.

Samples from WT, KO and Cre mice (n=3/genotype) were sequenced on an Illumina HiSeq4000 platform to a read depth of at least 10^7 reads per sample. The microglial samples from which RNA was obtained were prepared using MACS but were not further purified via FACS (**Figure 2.2A**). Whilst MACS generally yields excellent microglial purity, possible contamination with other cell types cannot be dismissed. Therefore, following initial processing, alignment, mapping and annotation, the presence of marker genes for major CNS cell types were assessed (**Figure 2.2B**). As expected, microglial markers (*Cx3cr1*, *Tmem119* and *P2ry12*) were extremely abundant, and *Cx3cr1* reads were almost exactly halved in KO and Cre cells due to the expected heterozygosity for *Cx3cr1*. By contrast, astrocyte (*Gfap*, *Aldh111*, *Aqp4*), oligodendrocyte (*Mag*, *Mbp*, *Mog*) and neuronal (*Slc12a5*, *Snap25*, *Syt1*) markers were present at extremely low levels. To assess potential contamination with blood-derived cells such as neutrophils, which could arise by suboptimal perfusion, the markers *Ly6g*, *S100a9* and *Camp* were assessed. Whilst these genes were generally of low abundance, one KO sample showed elevated (3-4-fold) counts of all three genes compared to the other 8 samples. It is therefore possible that slight leukocyte contamination was present in this sample, though the exact extent is difficult to gauge.

To interrogate global variability between samples, principal component analysis (PCA) was conducted on the corrected, filtered gene read counts for all samples (**Figure 2.2C**). PC1 accounted for 18.5% of the total variance, and PC2 contributed 16.5%. The scree plot of the subsequent 7 components (**Figure 2.2D**) indicates that the lowest non-zero proportion was PC8, with 9.2%. This pattern is indicative of data with little overall variability between groups. Indeed, with the exception of one KO replicate, the samples do not exhibit much spatial separation along either PC1 or PC2 (**Figure 2.2C**), indicating that most of the data variability did not reflect inter-group differences.

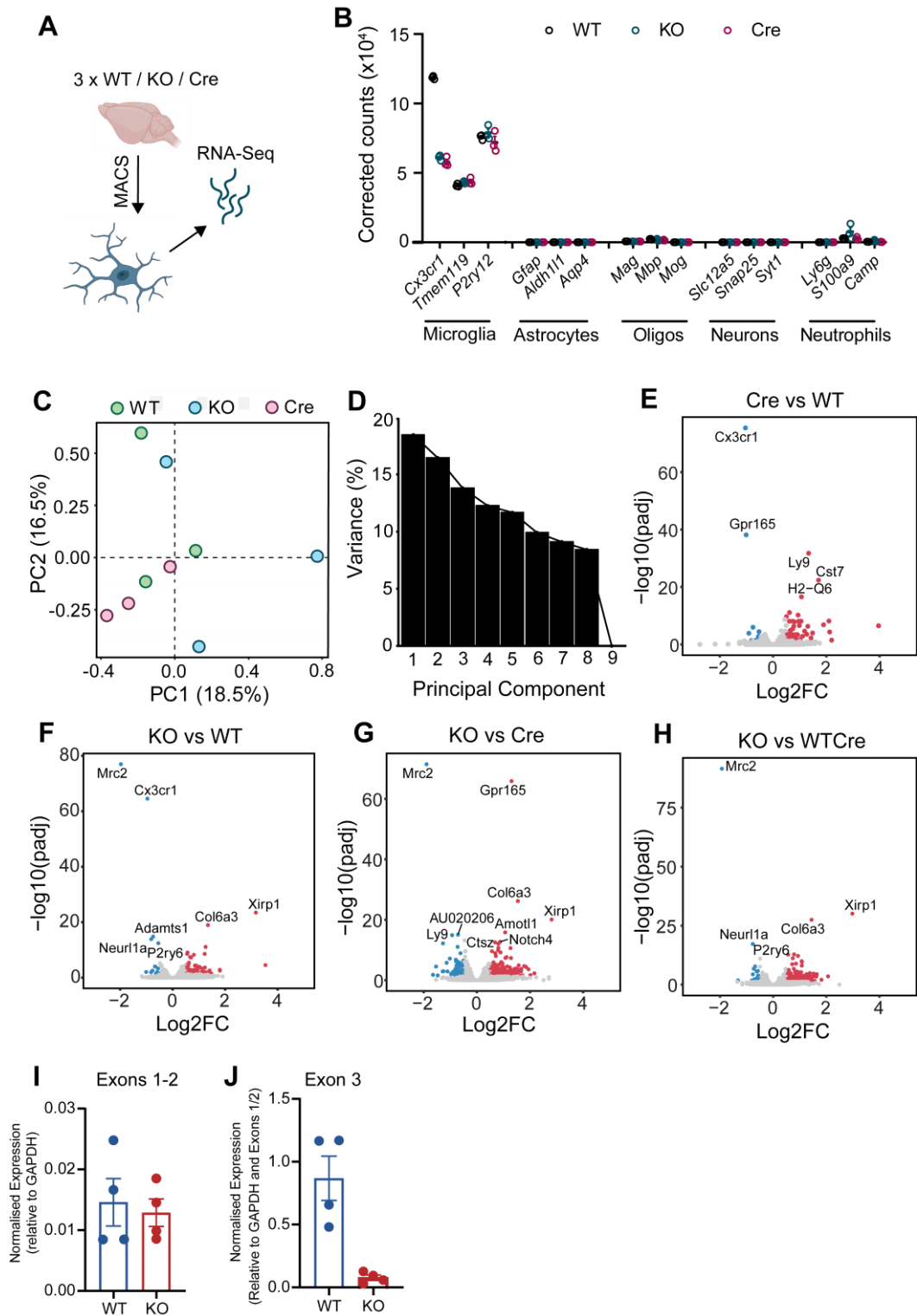


Figure 2.2: RNA Sequencing of acutely isolated microglia from LRRc8A knockout mice

(A) Schematic of microglial isolation via MACS and RNA-Seq from wild-type (WT) and LRRc8A knockout (KO) and Cre mice ($n = 3$ mice per genotype). (B) Corrected counts of marker genes for various cell types from RNA-sequencing data. (C) PCA of RNA-Seq data displaying first two components (D) Scree plot of PCA eigenvector values over the first 9 components. (E-H) Volcano plots displaying differentially expressed genes for the Cre vs WT, KO vs WT, KO vs Cre and KO vs WTCre genotype comparisons. (I-J) Expression of *Lrrc8a* exons 1-2 (I) and 3 (J) in WT and KO bone marrow derived macrophages (BMDM), as assessed by qPCR, presented as mean \pm SEM ($n = 4$).

Nonetheless, some differentially expressed genes (DEGs) were detected between groups via differential expression analysis. Four sets of tests were performed per gene, comparing expression between KO and WT cells, KO and Cre, and Cre against WT, as well as a fourth test comparing KO cells against the combined WT and Cre groups (hereafter referred to as WTCre) to isolate LRRC8A-dependent effects. DEGs were defined as having a false discovery rate (FDR)-adjusted p -value of less than 0.05 and a log₂ fold-change (Log₂FC) of greater than 0.5 in either direction. Volcano plots illustrating the genes significant at these levels are shown in **(Figure 2.2E-H)**. In total, 87 DEGs were discovered in the KO versus WT comparison, of which 17 were downregulated and 70 were upregulated **(Figure 2.2F)**. Comparing KO versus Cre microglia, 67 genes were found to be downregulated and 185 were upregulated **(Figure 2.2G)**. In Cre versus WT cells, 9 genes were downregulated and 55 were upregulated **(Figure 2.2E)**. Finally, comparing KO microglia to the WTCre group revealed 23 downregulated versus 134 upregulated genes **(Figure 2.2H)**. A full list of all identified DEGs can be found in **Table 2.2**. Of note, *Lrrc8a* does not appear to be downregulated in KO cells compared to the other two genotypes, despite being absent at the protein level and the lack of RVD in isolated microglia. Since the knockout strategy targeted only exon 3 of the *Lrrc8a* gene, it is possible that detection of *Lrrc8a* RNA in KO cells is due to continued transcription of exons 1 and 2, which cannot be translated into the full-length protein. To verify this, qPCR was performed on RNA isolated from WT and KO BMDM, with primer pairs amplifying sequences in either exons 1 and 2 or exon 3. As expected, KO cells exhibited drastically (>90%) reduced levels of exon 3, but expression of exons 1 and 2 comparable to WT **(Figure 2.2I-J)**. Thus, the *Lrrc8a* RNA detected in KO microglia likely originates from the first two exons and therefore does not imply the presence of functional LRRC8A.

2.3.3 Pathway analysis of identified DEGs

Overall, discovery of differentially expressed genes indicates that some expression differences are apparent between the three microglial genotypes. However, pinpointing LRRC8A-dependent effects requires simultaneous comparison of expression levels between the KO, WT and Cre groups. While this could be achieved using a venn-diagram approach selecting for genes significant in both the WT vs KO and KO vs Cre comparisons but nonsignificant in the Cre vs WT comparison, this method is stringent and could overlook more

subtle differences. Therefore, k-means clustering analysis was performed on all genes with FDR-adjusted p values of < 0.05 and $\log_2FC > 0.5$ for any individual genotype comparison (296 total genes). Using this method, five clusters were obtained (**Figure 2.3A**). Cluster 1 contained genes highest in the KO group compared to WT and Cre, cluster 2 consisted largely of genes downregulated in the Cre group compared to the other two. Cluster 4 contained genes downregulated in KO cells, whereas cluster 5 contained largely genes which were upregulated in the Cre group. Cluster 3 consisted of genes showing extremely high expression in one KO sample (sample 5) compared to the other eight samples. Amongst these genes in cluster 3 were the leukocyte markers *Itgal*, *S100a9* and *Ly6g*, and GO analysis indicated strong enrichment for terms including “Neutrophil-mediated immunity” and “Neutrophil degranulation” (both $p = 8.9 \times 10^{-23}$). Thus, the DEGs in cluster 3 likely reflect slight contamination with blood-derived myeloid cells in sample 5 and were therefore excluded from further downstream analyses.

To determine whether the LRRC8A-dependent gene expression changes reflect co-ordinated regulation of functional programmes in KO cells, clusters 1 and 4 were carried forward for enrichment analyses. These clusters represent upregulated and downregulated genes in the KO microglia, respectively. Cluster 4 was found to be enriched for several gene ontology biological process terms, including “positive regulation of potassium ion transport” (GO:0043268) and “positive regulation of vascular associated smooth muscle cell proliferation” (GO:1904707), the top 10 enriched terms by FDR-adjusted p -value are displayed in **Figure 2.3B**. Notably, the top 8 terms for this cluster were all enriched based on downregulated expression of 3 potassium channels (*Kcnj2*, *Kcnj9*, *Kcnj10*) and can all therefore be assumed to be redundant to one another in this case. Cluster 1 enriched primarily for terms relating to extracellular matrix organisation and amino acid transport (**Figure 2.3C**). The presence of these terms reflects upregulation of three amino acid transporters in KO cells (*Slc7a1*, *Slc7a5*, *Slc1a4*) as well as upregulation of several genes including collagens (*Col6a3*, *Col11a2*) and metalloproteinases (*Mmp2*, *Mmp28*, *Adamtsl2*). Thus, LRRC8A KO microglia may display reduced capacity for potassium transport, increased amino acid transport activity

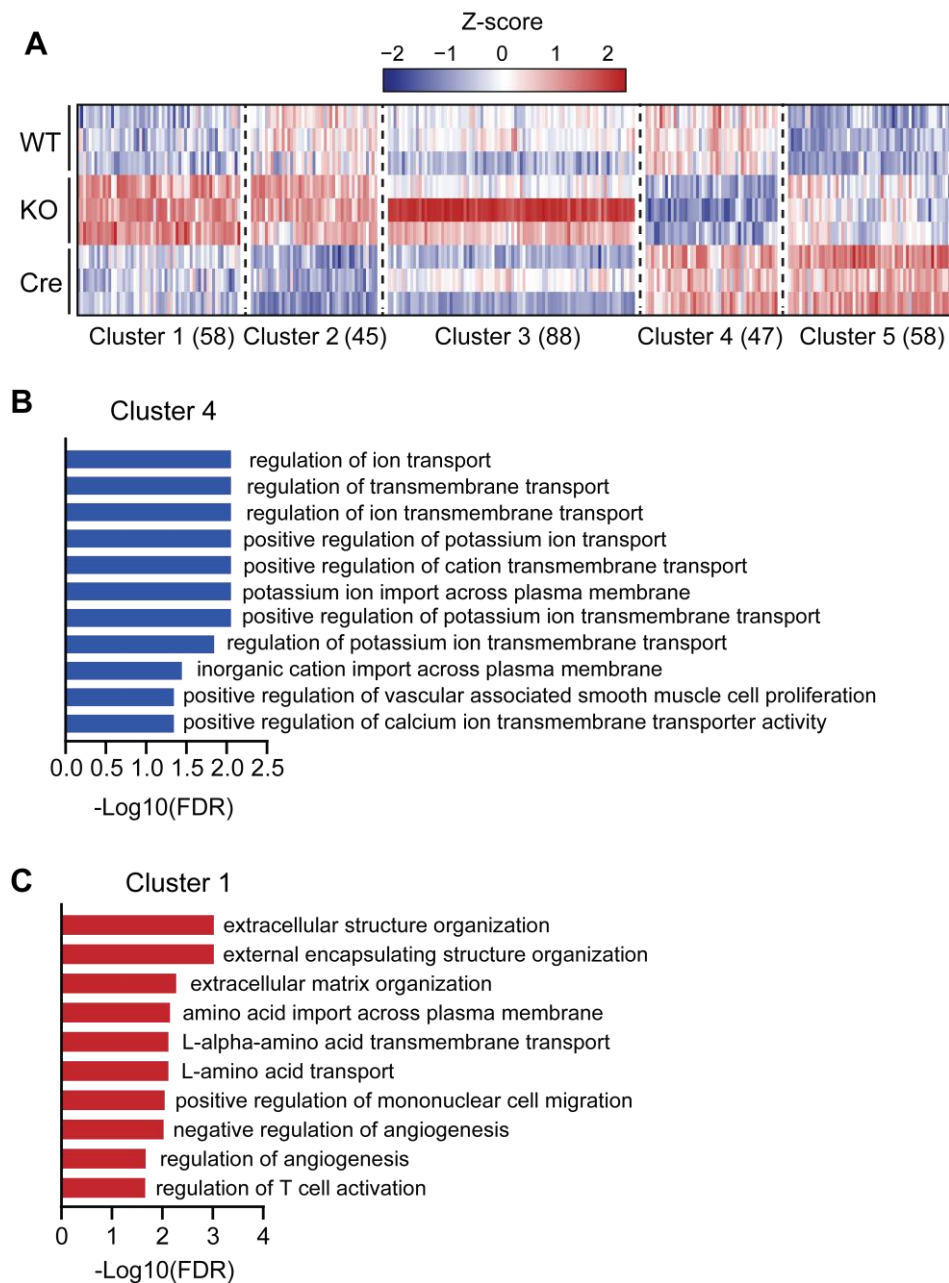


Figure 2.3: Enrichment analysis of LRRRC8A-dependent transcriptional changes:

(A) Heatmap showing differentially expressed genes between WT, LRRRC8A-KO and Cre microglia (n = 3) grouped via k-means clustering and coloured by z-score. (B-C) Gene ontology terms identified from genes in cluster 4 (B) or cluster 1, corresponding to downregulated (B) and upregulated (C) genes in LRRRC8A-KO microglia.

and altered interactions with extracellular matrix. However, it is worth noting that all of the gene sets identified via gene ontology analysis displayed relatively high (> 0.01) FDR-adjusted *p*-values, likely due to the generally low number of genes contributing to their enrichment, with many identified based only on 2-3 total genes. Moreover, the magnitude of differential

expression of these genes was also generally relatively low (0.5-1.5-fold-change). As such, it is possible that differential expression of these genes does not amount to significant functional alteration between WT and KO cells.

2.3.4 Role of VRAC in phagocytosis

Chloride channels including VRAC have been suggested to modulate microglial phagocytosis, either by facilitating cell shape changes necessary for particle engulfment, or by supporting endo-lysosomal flux and ion exchanges necessary for regulating phagosomal pH. Chloride channel inhibitors which block VRAC have been demonstrated to suppress phagocytosis of latex beads by BV-2 cells and of *E. coli* by primary microglia (Ducharme et al., 2007; Furtner et al., 2007; Harl et al., 2013). However, since these studies relied solely on chloride channel blockers, which generally lack specificity, it is still unclear whether VRAC or other channels are responsible for these effects.

2.3.5 VRAC inhibitors suppress phagocytosis in BMDM and microglia

To examine the role of VRAC in phagocytosis in real time, live-imaging assays based on engulfment of particles tagged with pH-sensitive pHrodo dyes were used. The dye fluorescence is minimal at neutral pH, but increases drastically as the environment acidifies. Therefore, only engulfed particles trafficked to acidic compartments will exhibit fluorescence, which enables live-imaging of cells to capture the kinetics of phagocytosis.

In order to verify the effect of chloride channel blockers as inhibitors of phagocytosis, primary microglia and BMDM were incubated with pHrodo-tagged fibrillar amyloid beta (fA β) or *E. coli*-derived bioparticles, respectively. Both cell types exhibited rapid uptake of their respective substrates, which was largely inhibitable by the actin depolymerising agent cytochalasin D (CyD), indicating that the signal observed reflects active phagocytic activity. Microglial uptake of fA β was dose-dependently inhibited by the chloride channel blockers NPPB and FFA, with a maximal inhibition of roughly 70% at 200 μ M for both drugs ($p < 0.0001$), which is equivalent to that achieved by CyD (**Figure 2.4A, B, G**). DCPIB exhibited a weaker effect, but still produced a significant ($p < 0.01$), roughly 30% inhibition at 20 μ M, but with no effect at lower

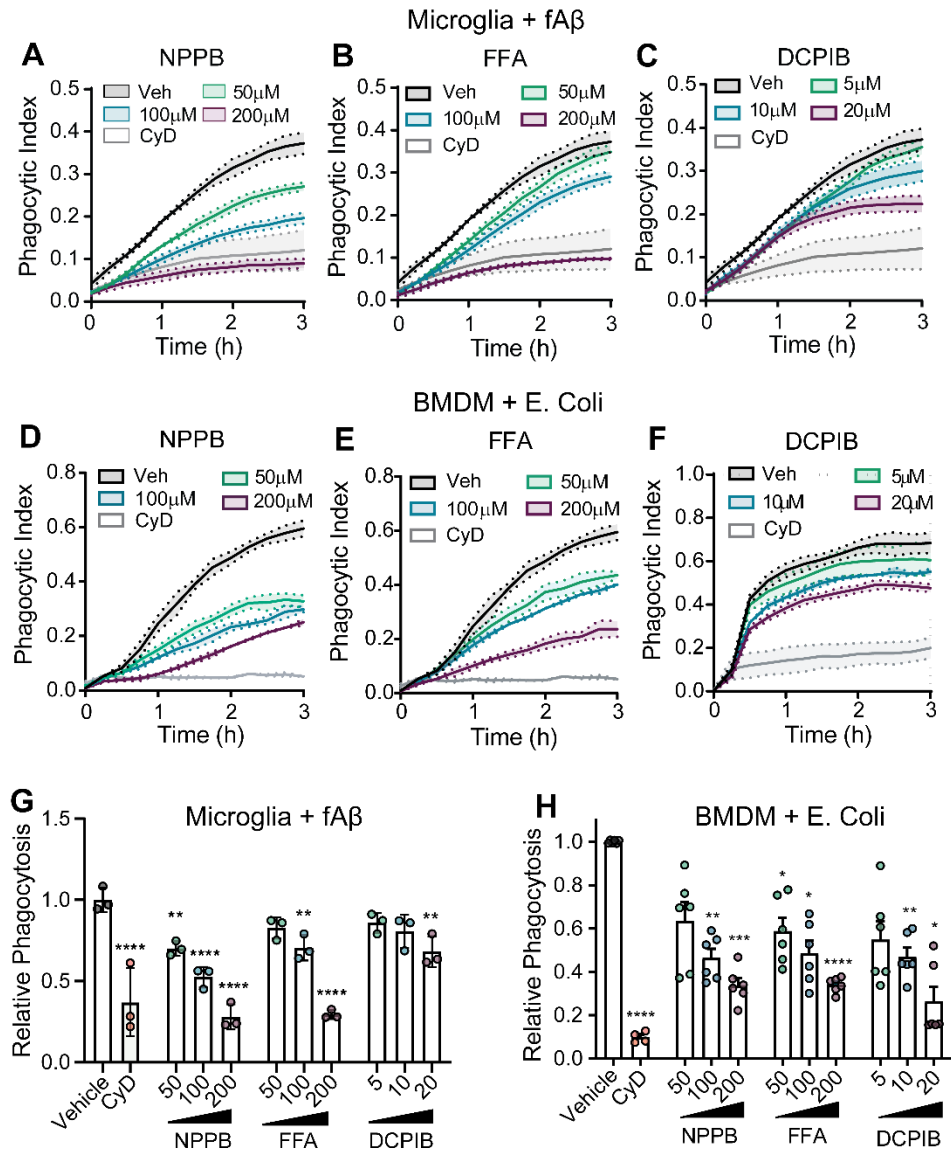


Figure 2.4: VRAC inhibitors suppress phagocytosis in primary microglia and macrophages: (A-C) Representative phagocytic uptake curves of cultured primary microglia incubated with fibrillar A β (fA β) in the presence of either vehicle (DMSO) or the VRAC inhibitors NPPB (A), FFA (B) or DCPIB (C) at varying concentrations, with cytochalasin D (CyD) as a positive control (n = 3 mice). (D-F) Representative uptake curves of bone marrow-derived macrophages (BMDM) incubated with pHrodo-tagged *E. coli*-derived particles along with either vehicle, NPPB (D), FFA (E), DCPIB (F) at varying concentrations or CyD as a positive control (n = 2 mice). (G) Area under curve (AUC) quantification of A-C, normalised to the vehicle mean. (H) AUC quantification of D-F, normalised to vehicle mean (n = 4-6 mice). Statistical comparisons were made via one-way ANOVA with Dunnett's post-hoc test * $p < 0.05$, ** $p < 0.01$, *** $p < 0.001$, **** $p < 0.0001$.

concentrations (**Figure 2.4C, G**). Similar results were obtained in BMDM ingesting *E. coli* bioparticles, with all three drugs producing dose-dependent inhibition of phagocytosis up to a maximum of roughly 65-70% (**Figure 2.4D-F, H**). Thus, phagocytosis in this model appears to be sensitive to chloride channel inhibitors, implying that VRAC could be a potential mediator of phagocytic activity.

2.3.6 VRAC is dispensable for phagocytosis

Inhibition of phagocytosis by chloride channel inhibitors indicates that chloride flux likely contributes to particle uptake, however VRAC cannot be specifically implicated due to lack of blocker specificity. Therefore, microglia and BMDM were cultured from LRRC8A KO and WT littermate mice and tested for phagocytic ability. As certain phagocytic mediators, including LRRC8A, have been demonstrated to exhibit substrate-dependent effects (Haney et al., 2018), multiple particle types were used in both microglia and BMDM to rule out cell-type or substrate-specific effects of LRRC8A deficiency. WT and KO microglia incubated with either *E. coli* bioparticles or fA β exhibited no difference in phagocytic uptake, indicating that LRRC8A appears to be dispensable for microglial phagocytosis (**Figure 2.5A-C**). WT and KO BMDM were assayed using IgG-opsonised red blood cells (IgG-RBC), *E. Coli* bioparticles or zymosan particles (**Figure 2.5D-F**). Similar to microglia, both WT and KO BMDM phagocytosed all the tested particles with identical efficiency, indicating that loss of LRRC8A, and by extension VRAC, does not impact phagocytosis of a variety of substrates.

Whilst this finding indicated that VRAC is not necessary for phagocytic activity, further experiments sought to confirm that the VRAC blockers used here and elsewhere suppress phagocytosis in a VRAC-independent manner. To achieve this, WT and KO BMDMs were exposed to chloride channel blockers and the phagocytosis assay repeated as above. Whilst robust drug effects for NPPB ($p < 0.0001$), FFA ($p < 0.0001$) and DCPIB ($p < 0.05$) were observed via two-way ANOVA, genotype effects, by contrast, were non-significant ($p > 0.05$) for all three blockers (**Figure 2.5G-I**). Moreover, no significant drug-genotype interaction effects were found for any drug. Overall, these results indicate that VRAC is neither required for phagocytosis nor responsible for the suppressive effects of chloride channel inhibitors in WT cells.

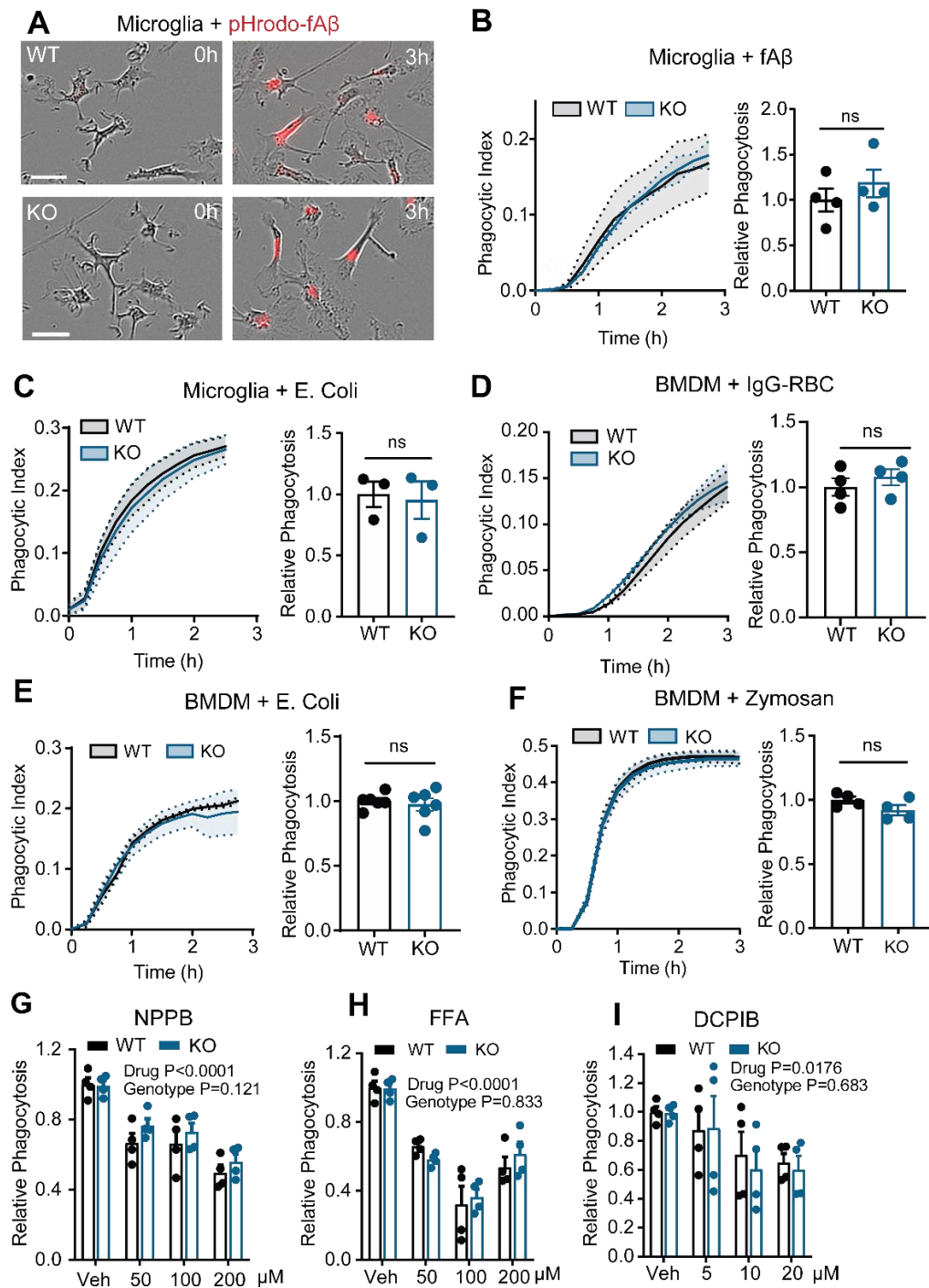


Figure 2.5: VRAC is dispensable for phagocytosis

(A) Phase-contrast and fluorescent micrographs showing uptake of pHrodo-tagged fibrillar A β (fA β) by wild-type (WT) and LRRC8A knockout (KO) microglia over 3 hours (scale bar = 30 μ m). (B-C) Representative uptake curves and pooled AUC quantification of WT and KO microglia ingesting fA β (B) and *E. Coli* bioparticles (C) (n = 3-4 mice). (D-F) Representative uptake curves and pooled AUC quantification of WT and KO bone marrow-derived macrophages (BMDM) exposed to IgG-opsonised red blood cells (IgG-RBC) (D), *E. Coli* derived bioparticles (E) or Zymosan bioparticles (F) (n = 4-6 mice). (G-H) Pooled AUC values from WT and KO BMDM ingesting *E. Coli* bioparticles in the presence of either vehicle (DMSO) or varying concentrations of the chloride channel inhibitors NPPB (G), FFA (H) or DCPIB (I) (n = 4). Statistics in B-F are from Student's *t*-test, and G-I are from two-way ANOVA.

2.3.7 VRAC is dispensable for stochastic migration *in vitro*

Cell migration has been likened to a polarized process of active volume regulation, consisting of volume increase at the leading edge and volume decrease at the trailing edge. As such, VRAC has been suggested to participate in cell migration by facilitating exchange of chloride which underpins water import/export necessary for cell movement. In support of this, a range of studies have observed that VRAC inhibitors strongly suppress migration of a variety of cell types. Additionally, VRAC blockers have been shown to inhibit P2RY12-dependent chemoattraction of microglial processes towards focal laser ablations. Thus, VRAC has been postulated as a key player in regulating ion fluxes which underpin cell migration and chemotaxis in a variety of contexts. However, given the limitations of chloride channel blockers, VRAC involvement cannot be concluded purely on this basis, and genetic studies are required to specifically address the role of VRAC in migratory activity.

To address the initial question of whether VRAC could contribute to general cell movement, as opposed to regulating a specific chemotactic pathway, primary isolated microglia were used. Primary microglia are useful in this context since, when cultured with serum, they assume a highly motile phenotype which then persists under serum-free assay conditions (Bohlen et al., 2017). In this state, they migrate stochastically in the absence of an exogenous chemotactic gradient, thus allowing the interrogation of general cell locomotion. To allow for relatively rapid, consistent quantification of cell migration over multiple conditions, a semi-automated workflow was devised, whereby cells were live-imaged over 3 hours after staining with the cell-permeable nuclear dye Hoechst 33342. The Hoechst fluorescence could then be used to identify individual nuclei and track their movement over the 3-hour period using the automated TrackMate plugin in ImageJ (**Figure 2.6A**). Using this approach, hundreds of cells per replicate/condition could be analysed automatically, circumventing both the time-intensive nature and potential sampling bias common to manual tracking.

To confirm that microglial migration *in vitro* is sensitive to VRAC inhibitors, WT microglia were assayed in the presence of either vehicle (DMSO), cytochalasin D, or varying concentrations of NPPB, FFA or DCPIB. Representative single-cell data are presented in **Figure 2.6B**, with a dose-dependent trend towards lower median migration speed apparent for all three

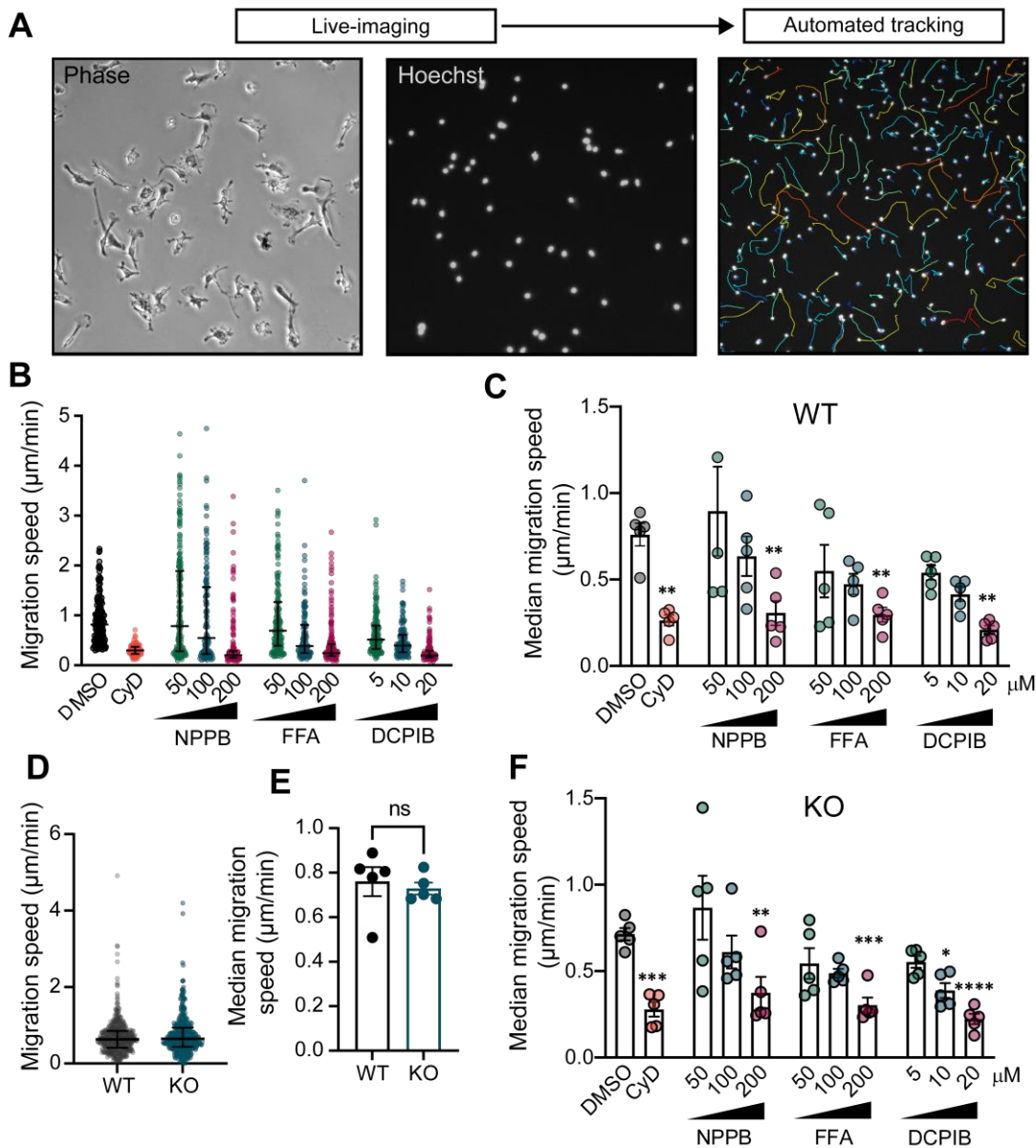


Figure 2.6: VRAC does not regulate microglial migration *in vitro*:

(A) Experimental workflow, involving live-imaging of primary microglia tagged with the nuclear dye Hoechst 33342, followed by automated tracking (B) Representative single-cell migration speeds of microglia in the presence of either vehicle (DMSO), the actin inhibitor cytochalasin D (CyD), or varying concentrations of NPPPB, FFA or DCPIB (n = 1 mouse). (C) Median migration speeds of wild-type (WT) microglia exposed to either DMSO, CyD or NPPPB, FFA or DCPIB (n = 5 mice). (D) Single-cell migration speeds of microglia from WT or LRRc8A knockout (KO) mice under baseline conditions (1428 and 1084 microglia (respectively) from n = 5 mice per genotype). (E) Median migration speeds of WT and KO microglia from each of n = 5 mice per genotype. (F) Median migration speeds of WT microglia exposed to either DMSO, CyD or NPPPB, FFA or DCPIB (n = 5 mice). Data in B,D are presented as medians with interquartile range, C,E-F are means ± SEM. Statistical comparisons were made via a Student's *t*-test (E) or one-way ANOVA with Dunnett's post-hoc (C,F). * *p* < 0.05, ** *p* < 0.01, *** *p* < 0.001, **** *p* < 0.0001

inhibitors, indicating that migration is indeed inhibited by VRAC blockers in these cells. Significant reductions in migration speed were observed at high doses of each blocker when comparing median migration speeds of all microglia from each of 5 mice (**Figure 2.6C**). The degree of inhibition obtained with these doses (roughly 60%) was comparable to that achieved by actin depolymerization via CyD, indicating an almost complete block on cell migration by these chloride channel inhibitors. To assess whether genetic ablation of LRRC8A recapitulates the effects of VRAC inhibitors, microglia from WT and KO animals were assayed in parallel. Both genotypes exhibited extremely similar migration speeds (**Figure 2.6D**), and no significant difference in migratory capacity was observed when comparing median migration speeds (**Figure 2.6E**). Moreover, NPPB, FFA and DCPIB produced significant inhibition of migration in KO cells comparable to that achieved in WT microglia (**Figure 2.6F**). Thus, it appears that VRAC is dispensable for migration of microglia *in vitro* and does not mediate the suppressive effect of chloride channel inhibitors observed in WT cells.

2.3.8 DCPIB inhibits microglial chemotaxis *in situ*

Microglia *in vivo* exhibit a strong chemotactic response to extracellular ATP, mediated by the purine receptor P2RY12. ATP release into the extracellular space can occur following cellular injury, or as a result of neuronal activity. The creation of small, focal laser ablations can serve as one such ATP source, and cause nearby microglia to extend processes towards the lesion site without any displacement of the cell body. VRAC inhibitors strongly suppress this response at concentrations which do not inhibit filopodium extension during random surveillance, and as such VRAC has been suggested to regulate P2RY12-dependent chemotaxis in a manner which may be distinct from that involved in general cell movement (Hines et al., 2009). However, no genetic studies have so far been conducted to assess whether VRAC is the true mediator of this effect.

Initial experiments sought to confirm that the more specific, gold-standard VRAC inhibitor DCPIB also inhibited microglial process chemotaxis. For this purpose, *Cx3cr1^{eGFP/+}* mice, in which microglia are strongly fluorescent, were used to create acute brain slices which can be easily assayed in the presence of drugs. Acute slices were treated with aCSF containing vehicle (DMSO) or either 10 μ M or 20 μ M DCPIB, and 2-photon laser ablations performed while capturing microglial process movements (**Figure 2.7A**). To quantify process convergence

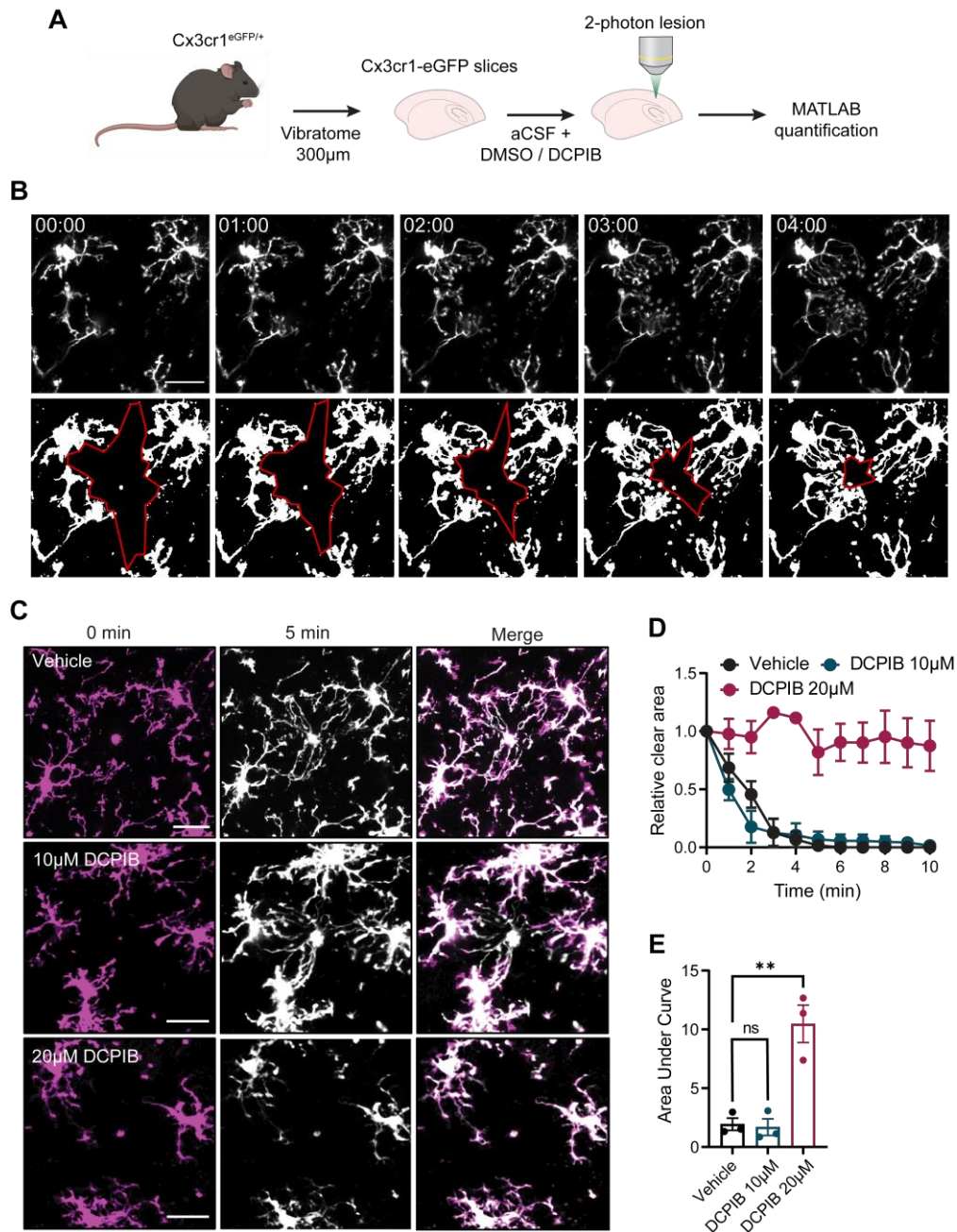


Figure 2.7: DCPIB inhibits microglial process chemoattraction:

(A) Schematic illustrating experimental workflow in $Cx3cr1^{eGFP/+}$ brain slices. (B) Original (top) and binarized (lower) frames showing microglial chemotaxis towards a focal laser ablation. Red line in lower panels denotes process-free area, scale bar = $20\mu m$. (C) Representative frames at 0 and 5 minutes post-ablation from slices treated with either vehicle (DMSO) or DCPIB at $10\mu M$ or $20\mu M$, scale bars = $20\mu m$. (D) Quantification of relative process-free area in the 10 minutes following laser ablation in slices treated with either vehicle or DCPIB at $10\mu M$ or $20\mu M$ (3-6 ablations from $n = 3$ mice per condition) (E) Area under curve quantification of D. All data presented as mean \pm SEM. Statistical comparisons in E are from one-way ANOVA with Dunnet's post-hoc. ** $p < 0.01$

towards the ablation, an automated approach described by (Gyoneva et al., 2014) was employed, whereby z-projected time series are first thresholded to produce a binary image and processed by an automated script which determines the area of a polygon surrounding the ablation which is free of microglial processes, and which shrinks over time if chemotaxis occurs (**Figure 2.7B**). Slices treated with either vehicle or 10 μ M DCPIB exhibited rapid process chemotaxis, which generally occurred within 5 minutes of the initial laser ablation (**Figure 2.7C-D**). By contrast, 20 μ M DCPIB starkly inhibited chemotaxis, such that no processes were observed to contact the lesion site, and the average process-free area remained largely unchanged throughout the 10-minute imaging period (**Figure 2.7C-D**). AUC quantification of the relative lesion areas over time confirmed that 20 μ M DCPIB produced statistically significant inhibition, whereas 10 μ M was ineffectual (**Figure 2.7E**). Thus, DCPIB is indeed capable of inhibiting microglial P2RY12-dependent chemotaxis, albeit not at low-moderate concentrations. Thus, it is conceivable that VRAC might play a role in mediating microglial chemotaxis.

2.3.9 VRAC does not mediate microglial chemotaxis

In order to address the role of VRAC in P2RY12-dependent chemotaxis directly, it is necessary to perform assays in LRRC8A KO mice. Since no drug treatments were needed for this approach, *ex vivo* brain slices were not required and intravital microscopy via cranial window implantation could be performed instead. However, one immediate issue with this approach was that the *Lrrc8a^{fl/fl}:Cx3cr1^{Cre/+}* mice bred for these experiments did not express a fluorescent label, and since the LRRC8A knockout depended on the presence of the *Cx3cr1^{Cre}* transgene, introduction of the *Cx3cr1^{eGFP}* label would result in a functional knockout of *Cx3cr1* in the KO genotype but not the WT controls. Fortunately, it is possible to fluorescently label microglia *in situ* using fluorescent lectins without the need for a fluorescent transgene (Brawek et al., 2019). To achieve this, tomato lectin conjugated to DyLight-594 was injected into the cortex prior to cranial window implantation to visualize microglia (**Figure 2.8A**). Initially, lectin injections were performed in *Cx3cr1^{eGFP/+}* mice to verify optimal labelling. Despite a lower signal to noise ratio in the lectin channel, microglial processes were still easily distinguishable and showed good concordance with the GFP signal, albeit with co-labeling of blood vessels, which lectin also binds to (**Figure 2.8B**). To confirm that the lectin signal was

of sufficient quality to enable automated analysis of microglial chemotaxis, laser ablations were performed in *Cx3cr1^{eGFP}* mice following lectin injection. Microglial processes were labelled well and retained the lectin signal during chemotaxis (**Figure 2.8C**), and produced almost identical results to the GFP channel when quantified using the automated MATLAB script (**Figure 2.8D**). Thus, lectin appears to provide satisfactory labelling for quantifying microglial chemotaxis *in vivo*.

To assess whether LRRC8A knockout affects microglial chemotaxis, WT and KO mice were subjected to the same labelling procedure and ablations performed as above. KO microglia appeared to react to laser ablations consistently and with similar velocity to WT microglia (**Figure 2.8E-F**), and AUC analysis indicated that no significant differences were apparent between the two groups (**Figure 2.8G**). As such, loss of microglial VRAC does not seemingly affect their capacity for P2RY12-dependent chemotaxis towards ATP sources.

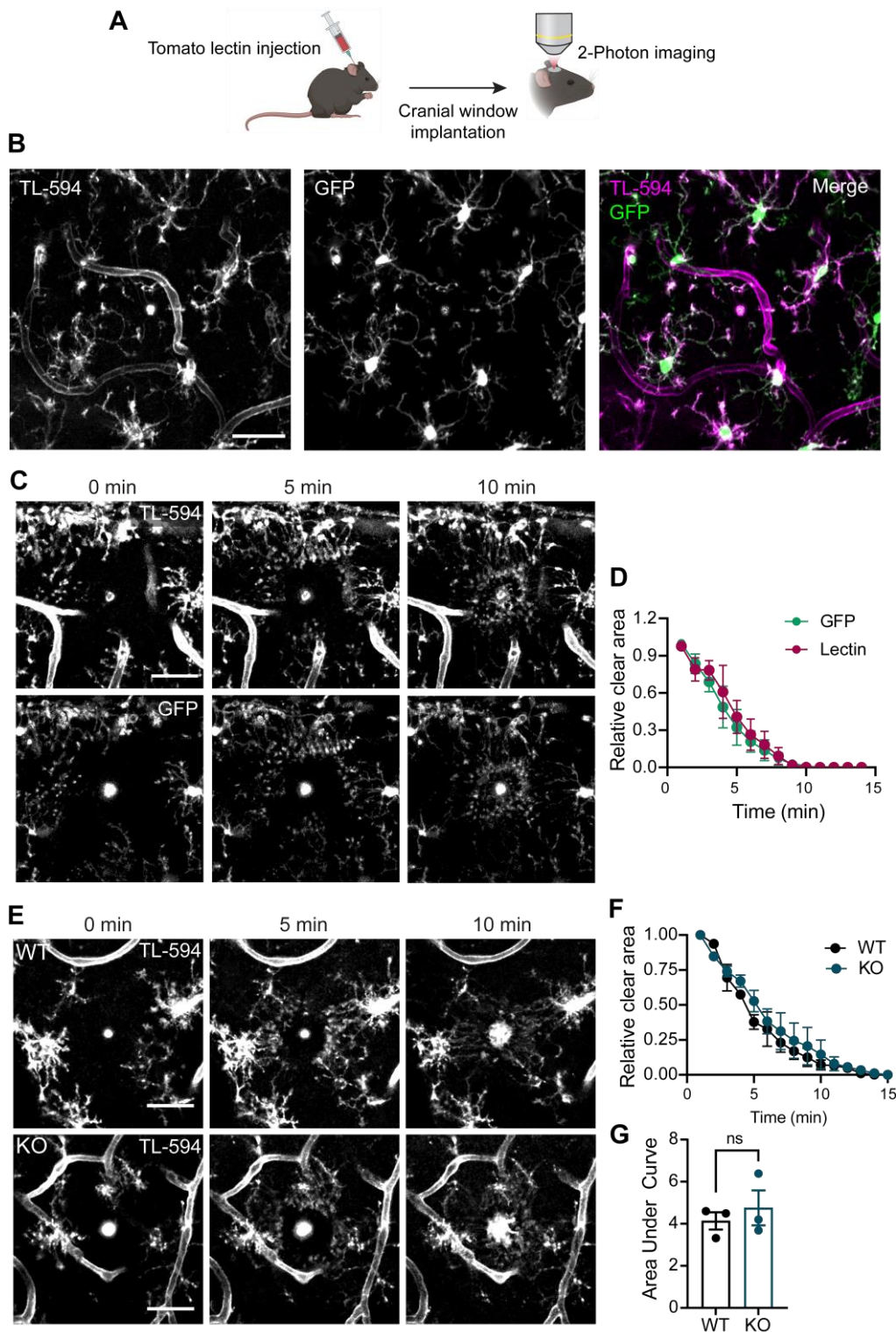


Figure 2.8: VRAC is dispensable for microglial chemotaxis *in vivo*:

(A) Schematic of tomato lectin (TL-594) injection followed by 2-photon imaging. (B) Fluorescent micrographs of TL-594 and Cx3cr1^{GFP} fluorescence in cortical microglia *in vivo*, scale bar = 30 μ m. (C) Microglia-associated tomato lectin (top) and GFP (bottom) signal during chemotaxis towards a laser ablation, scale bar = 20 μ m. (D) Chemotaxis quantification based on lectin and GFP signal in the same video (3 ablations from n = 2 mice). (E) Microglial chemotaxis in wild-type (WT) and LRRC8A knockout (KO) mice 0, 5 and 10 minutes following laser ablations, scale bar = 20 μ m. (F) Quantification of chemotaxis in WT and KO microglia (13-14 ablations from n = 3 mice each). (G) Area under curve analysis of F. Data presented as means \pm SEM. Statistical comparisons in G were made via a Student's *t*-test.

2.3.10 Microglial VRAC does not affect stroke volume or reactive morphology

Microglial morphology is dynamic, and its regulation is poorly understood. Microglia develop ramified morphologies in the mature brain, in response to brain-specific cues and astrocyte-derived factors. Ramification is known to increase with membrane polarization, in a process dependent on potassium flux via THIK-1 (Madry et al., 2018). VRAC has been suggested to regulate microglial ramification *in vitro*, though no studies have addressed this issue using genetic tools (Eder et al., 1998; Mongin, 2016). In pathological situations such as ischaemia, microglia are known to increase in volume and retract their processes, assuming a reactive, amoeboid morphology. Again, little is known about the regulation of this process by ion channels, but VRAC could regulate microglial morphology in the damaged brain by counteracting either accumulation of other osmolytes within microglia or changes in the brain extracellular environment due to neuronal injury and oedema. VRAC is also an interesting potential target for treating stroke, though it has primarily been studied with regard to its role in astrocytes (Mongin, 2016; Yang et al., 2019; Zhou, Luo, et al., 2020). Thus, it is also of interest to determine whether microglial VRAC contributes to stroke outcome. It is possible that loss of microglial VRAC could alter the extent of neuronal injury in cerebral ischemia, either by modulating the release of neuroprotective or toxic solutes, or via other effects on microglial physiology.

In initial experiments, WT, KO and Cre mice were used to check for any effect of microglial VRAC ablation on stroke infarct volume using the FeCl₃ model of permanent middle cerebral artery occlusion (MCAo). 24h post-occlusion, cresyl violet staining revealed similar infarct volumes between all three genotypes, with no significant differences detected (**Figure 2.9A**). Thus, loss of microglial VRAC did not appear to affect the extent of neuronal loss in this model of ischemia. Thick (150µm) sections from these brains were also obtained and used to determine whether loss of VRAC affected microglial reactive morphology.

Due to the highly complex 3-dimensional (3D) shape of microglia, assessment of morphological parameters can be challenging; 2-dimensional analyses often fail to discriminate salient features, whereas 3D data are often time-consuming to quantify. As such, an automated approach to morphology quantification was implemented, combining confocal microscopy with a MATLAB script which segments and reconstructs microglia in 3D, allowing

automated analysis of 23 complex shape descriptors including skeleton parameters, sphericity and volume (**Figure 2.9B, Table 2.1**)(Heindl et al., 2018). Additionally, fructose-based tissue clearing was employed to aid the acquisition of high-quality, deep z-stacks on Iba1-stained brain sections.

To verify that this strategy reliably detected morphological differences, brain sections were imaged in cortical regions both immediately adjacent to the infarct (peri-infarct) and at the equivalent position in the contralateral cortex. Since microglia in the peri-infarct region were obviously more amoeboid than those in the contralateral hemisphere (**Figure 2.9C**), these two groups should be readily distinguishable. Indeed, principal component analysis on the measurements produced by the MATLAB script displayed limited overlap between the peri-infarct and contralateral cell groups, indicating good discrimination between reactive and homeostatic cells (**Figure 2.9D**). PC1 largely reflected differences in the degree of ramification as quantified by skeletal parameters such as total number of nodes per cell (**Figure 2.9E**), whereas PC2 was influenced by volumetric parameters such as sphericity and median node volume. Three outputs with large influence over the main principal components were selected for direct comparisons: 3D sphericity, total skeletal nodes per cell, and median node volume. These three measures showed highly significant differences between the two cell groups, indicating that differences in microglial ramification and size are readily detected using this approach (**Figure 2.9F-H**).

To assess whether any differences in reactive morphology were apparent in KO microglia, cells imaged in the peri-infarct region of WT, KO and Cre mice were processed using the same pipeline (905 total cells) (**Figure 2.10A**). PCA performed on the output parameters revealed that PC1 was largely reflective of shape complexity, being most heavily influenced by sphericity, as well as variables describing the number of skeletal nodes. PC2 largely reflected the number of primary branches, since the most influential variables were related to the number of nodes per branch. Thus, extremely low PC2 scores reflect a high degree of branching, but along few primary branches. However, there was a large overlap between the three groups, indicating that most of the data variability was independent of genotype (**Figure 2.10B**).

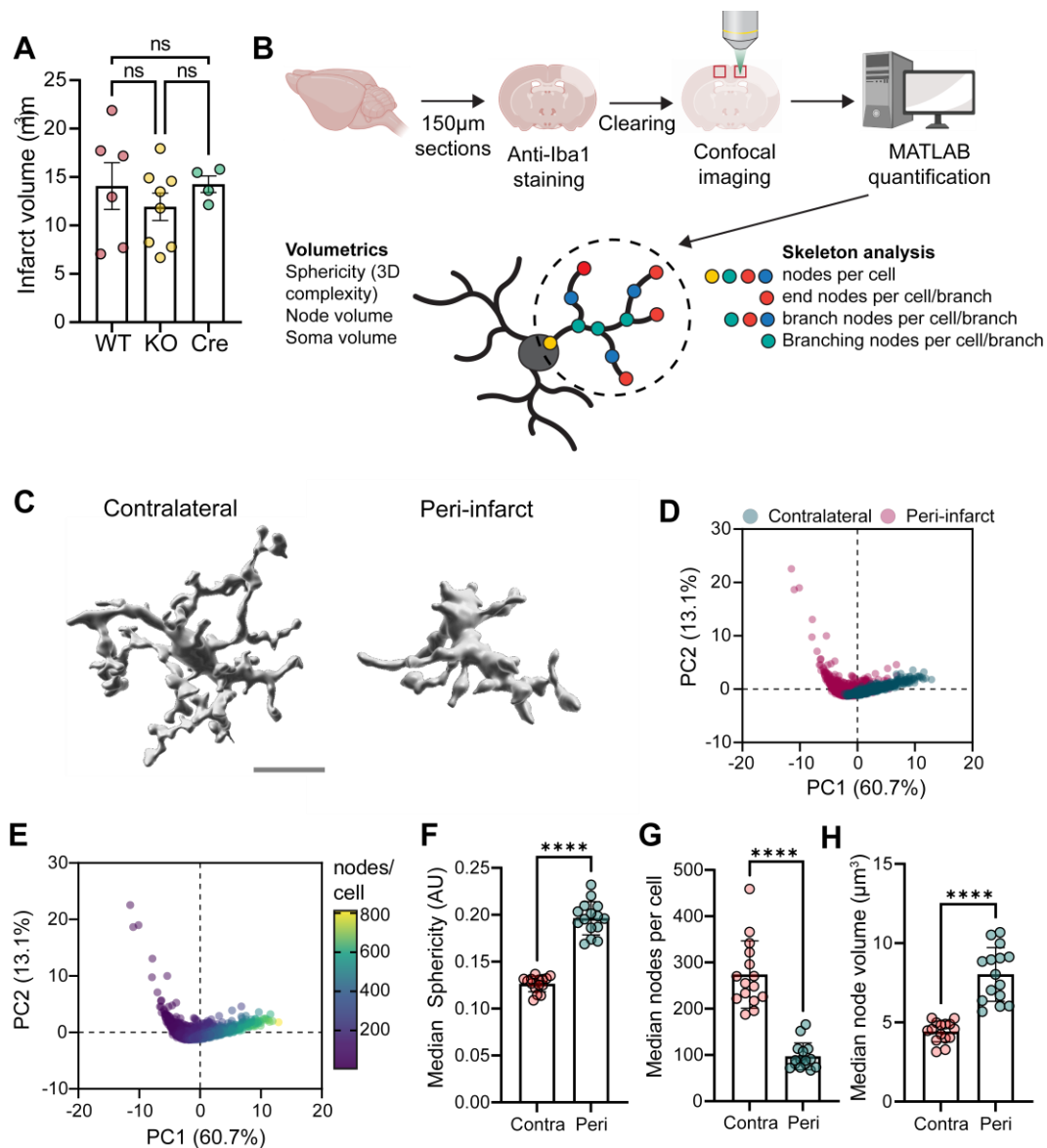


Figure 2.9: Validation of automated microglial morphology analysis

(A) Infarct volume in wild-type (WT), LRRc8A knockout (KO) and Cre control mice 24h after FeCl₃ MCAo, as assessed by cresyl violet staining (n = 4-7). (B) Thick sections of brains 24h after MCAo were stained against Iba1, cleared and imaged via confocal microscopy, followed by automated analysis in MATLAB. Schematic illustrates example parameters measured, including skeletal node types and shape descriptors. (C) 3D surface rendering of representative microglia from the contralateral (contra) or peri-infarct (peri) region. (D-E) PCA of all microglia imaged from contralateral and peri-infarct cortex, coloured by region (D) or number of skeletal nodes per cell (E). (F-H) Individual morphological parameters of contralateral or peri-infarct microglia (median values from all cells per mouse, dots represent individual mice) (n = 15). Data presented as mean ± SEM. Statistical comparisons made by one-way ANOVA (A) or Student's *t*-test (F-G). **** *p* < 0.0001

When comparing individual morphological parameters, no statistically significant differences were detected, despite a trend towards more skeleton nodes and decreased sphericity in KO cells (**Figure 2.10C-E**). Thus, loss of VRAC function does not appear to affect microglial morphology following cerebral ischemia.

2.3.11 VRAC does not regulate homeostatic microglial morphology

To investigate potential differences in morphology under homeostatic conditions, microglia were also imaged in the contralateral cortex of WT, KO and Cre mice from the MCAO study and analyzed using the same approach (**Figure 2.10F**). Initial PCA analysis indicated that, again, the three genotypes displayed large overlaps in PC scores (**Figure 2.10G**), albeit with a slight tendency towards lower PC1 scores in the KO and Cre cells. Since PC1 once again was generally reflective of skeletal complexity, this indicated a potential for increased ramification in KO and Cre microglia. When comparing individual parameters, there was a slight trend towards decreased sphericity and higher median nodes per cell in KO and Cre mice, though no significant differences were observed. As such, VRAC does not seem to contribute to the establishment or maintenance of homeostatic, ramified morphology in microglia.

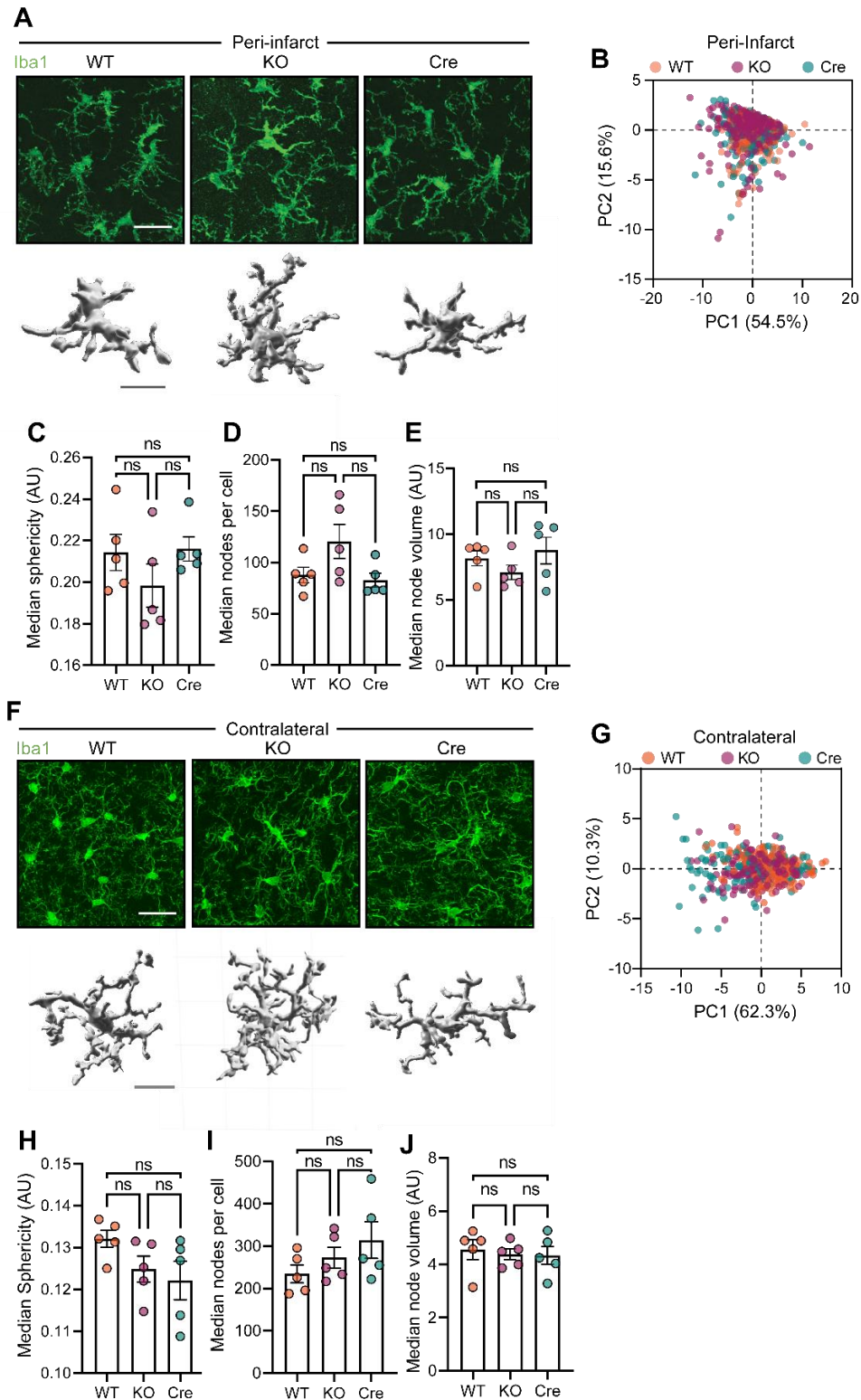


Figure 2.10: VRAC does not regulate reactive or homeostatic microglial morphology

(A,F) Representative confocal z-stacks and 3D-rendered individual cells from the peri-infarct (A) and contralateral (F) cortex of wild-type (WT), LRRC8A knockout (KO) and Cre mice 24h after MCAO. Scale bars = 20 μ m (Z-stacks) and 10 μ m (rendered cells). (B,G) PCA plots of individual cells from peri-infarct (B) and contralateral (G) cortices of WT, KO and Cre mice. (C-E, H-J) Median sphericity, nodes per cell and node volume measurements of peri-infarct (C-E) and contralateral (H-J) microglia (n = 5 mice per genotype). Statistical comparisons from one-way ANOVA, data presented as mean \pm SEM.

2.4 Discussion

2.4.1 VRAC is required for microglial volume regulation but dispensable for homeostasis

The overall aim of these experiments was to investigate the role of VRAC in microglial function. To this end, a microglial targeted knockout of LRRC8A, the obligatory VRAC subunit, was created, and initial characterisation indicated successful ablation of LRRC8A expression, which was restricted to microglia in the CNS. However, it is likely that peripheral macrophage populations were also targeted by this approach, given that LRRC8A was ablated in BMDM, and previous work with the *Cx3cr1^{Cre}* line suggested recombination in most monocyte-derived and tissue-resident macrophage populations (Yona et al., 2013). Subsequent experiments demonstrated that loss of LRRC8A resulted in defective volume regulation after hypotonic shock, thus confirming that hypotonic volume regulation is dependent on expression of functional LRRC8A-containing VRAC channels in microglia. Previous work in our lab indicated that VRAC is also required for RVD in peripheral macrophages (Green et al., 2020), which was also confirmed here via RVD assays in BMDM. Thus, microglia display a similar reliance on VRAC for volume regulation to peripheral macrophages, implying that the LRRC8A-KO microglia generated here are a suitable model for interrogating VRAC function.

One key initial question was whether VRAC (or LRRC8A itself) is required for microglial development or homeostasis, since complete LRRC8A knockout mice display extremely severe phenotypes with high embryonic and postnatal mortality along with defective generation of certain cell types, including T and B lymphocytes (Kumar et al., 2014; Platt et al., 2017). In the microglia specific conditional LRRC8A KO mice, no differences in microglial density were observed compared to control animals, nor were any gross abnormalities apparent in the mice themselves, which were born at the expected frequency and had normal appearance and size (data not shown). RNA-sequencing analysis also indicated very limited differences in gene expression arising from lack of VRAC, with normal expression of mature microglial homeostatic markers. Thus, VRAC does not appear to be required for the establishment or maintenance of a mature microglial population in the brain. These results are similar to those obtained by various groups describing relatively normal development in astrocyte-specific (Yang et al., 2019) or whole-brain (Zhou, Luo, et al., 2020) LRRC8A

knockout models. As such, VRAC function appears to be largely redundant for the development of the CNS, and for maintenance of glial cell populations throughout life. It is unclear why CNS development occurs independently of LRRC8A, whilst in whole-body LRRC8A knockout mice many other tissues display severe abnormalities.

2.4.2 VRAC does not regulate phagocytosis

Chloride channels have been suspected to regulate phagocytic activity based on experiments using chloride channel inhibitors to manipulate ion fluxes. VRAC had been a prime candidate for mediating these functions, since it is known to be expressed in microglia/macrophages and most of the agents which inhibited phagocytosis were also known VRAC blockers. Moreover, a recent CRISPR-based screen for regulators of phagocytosis indicated that LRRC8A ablation in the U937 monocytic cell line significantly inhibited phagocytosis of zymosan, as well as complement- and Fc-opsonised RBC, but not of polystyrene beads (Haney et al., 2018). This implies that any effects of gene knockouts on phagocytosis could be substrate-dependent, and as such multiple substrates were used to assess the impact of LRRC8A knockout on phagocytosis. Since no effects whatsoever were observed for any substrate, the main, immediate conclusion is that VRAC is not required for phagocytic activity. Since the substrates tested – $fA\beta$, *E. coli* bioparticles, zymosan and IgG-opsonised RBC – overlap substantially with the range of substrates reported to be affected by VRAC inhibition, the contrast between this result and previous findings likely does not reflect substrate-specific effects (Ducharme et al., 2007; Furtner et al., 2007; Haney et al., 2018; Harl et al., 2013). Moreover, the VRAC inhibitors NPPB, FFA and DCPIB were effective in reducing phagocytosis of $fA\beta$ by microglia and *E. coli* by BMDM, thus confirming that similar mechanisms to those reported are present in this model. Importantly, these drugs were found to be equally effective in WT and KO BMDMs, a fact which firmly implicates other channels in mediating their effects. Thus, while these data support a role for chloride flux in phagocytosis, they conclusively rule out a role for VRAC.

VRAC having been ruled out by the present study, the identity of the channel, or family of channels responsible for chloride transport supporting phagocytosis is likely a subject for future investigation. Analysis of microglial/macrophage transcriptomes indicates that a wide variety of channels are present, including the anoctamin family of Ca^{+} -activated chloride

channels (ANOs), chloride intracellular channels (CLICs), voltage-gated chloride channels (CLCNs) and the mysterious tweety-homolog family (TTYHs) (**Figure 2.11**). Since many channels are expressed only at very low levels in both microglia and BMDM, these seem unlikely to mediate phagocytic inhibition by chloride channel blockers. Of the expressed channels, limited data are available regarding the extent to which they are inhibited by the drugs tested here, making speculation as to possible candidates challenging. Nonetheless, the anoctamin family, of which only ANO6-8 and ANO10 are expressed at considerable levels in BMDM and microglia, appears promising since ANO6 has previously been linked to phagocytosis in macrophages (Ousingsawat et al., 2015), and can be inhibited by NPPB. Given its known sensitivity to niflumic acid, another member of the fenamate family, ANO6 can likely also be blocked by FFA, though no data are available regarding its sensitivity to DCPIB (Ousingsawat et al., 2015; White & Aylwin, 1990). It is therefore possible that the effects of chloride channel blockers on phagocytosis relate to ANO6 inhibition, yet further studies utilizing known phagocytosis inhibitors in ANO6-null mice would be required to confirm this.

One potential caveat to these experiments is the use of microglia cultured *in vitro*, since partial loss of identity is inevitable upon removal from the brain (Bohlen et al., 2017). Whilst 3D culture such as brain slices more faithfully recapitulate *in vivo* microglial biology, they are technically inflexible compared to 2D culture, and live-imaging experiments involving multiple conditions become costly and time-consuming. Microglia from mature brains cultured with brain-mimicking cytokines are demonstrably more similar to mature microglia than cell lines, neonatal microglia or cultured macrophages (Bohlen et al., 2017; Butovsky et al., 2014). Thus, the use of microglia from adult animals in conjunction with TGF- β and IL-34 containing media represents the current gold-standard 2D culture approach, and a fair compromise between technical flexibility and biological relevance.

2.4.3 Cell migration and purinergic chemotaxis are independent of VRAC

Chloride flux has been proposed as a key regulator of cell migration, both as a general mediator of cell movement, and as a specific component of P2RY12-dependent process chemotaxis in microglia (Hines et al., 2009; Izquierdo et al., 2019; Schwab et al., 2012). VRAC has been proposed as a key mediator of these effects due largely to overlapping

pharmacology, but this involvement has never been confirmed genetically. Thus, the present study aimed to address the role of VRAC in both stochastic migration and ATP-dependent microglial chemotaxis.

VRAC is suggested to support cell migration by allowing flux of chloride across the plasma membrane of migrating cells, which allows local influx and efflux of water, thus creating local changes in cell volume which permit cell polarization and extension of the leading edge, as well as retraction of the trailing edge (Schwab et al., 2012; Zierler et al., 2008). In this sense, migration has been likened to a coupled process of simultaneous volume increase and decrease analogous to that which occurs during osmotic stress (Schwab et al., 2012). Thus, by token of its role in osmotic volume control, VRAC has also been proposed to regulate cell movement. This proposed function was initially addressed using highly motile cultures of microglia from WT and KO animals to assess any differences in cell motility between the two genotypes. Similarly to experiments assessing phagocytosis, chloride channel blockers did indeed appear to inhibit cell migration *in vitro*, yet did so regardless of VRAC expression, displaying equal inhibition in WT and KO microglia. Moreover, WT and KO cells displayed identical migratory capacity. This result argues against the model of migration as a process analogous to osmotic volume control, since osmotic volume control was severely impaired in KO cells, yet migration was unaffected. Thus, a key point arising from this study is that cell volume changes resulting from osmotic stimuli and those involved in cellular functions such as phagocytosis and migration likely occur via different mechanisms.

Chloride flux via VRAC had also been thought to regulate P2RY12-dependent microglial process chemotaxis, a key function of microglia *in vivo*. However, LRRC8A-KO mice exhibited no defects in process convergence toward 2-photon laser ablations *in vivo*, despite this same form of chemotaxis having been inhibited by DCPIB in *ex vivo* brain slices. It is tempting to speculate that DCPIB inhibits process chemotaxis in brain slices via the same mechanism by which VRAC blockers inhibit microglial migration *in vitro*, since in both cases microglia cease even random movements and appear completely immobile on exposure to high doses. However, elucidation of the specific channels responsible for this effect will require further study.

P2RY12-dependent chemotaxis is a significant mechanism by which microglia influence brain physiology. Recently, P2RY12 was shown to mediate the formation of specialized junctions between microglial processes and neuronal somata (Cserép et al., 2020). Under conditions of stress such as ischemia, these contacts mediate reductions in neuronal calcium load and increase neuronal survival. Consequently, acute inhibition of microglial P2RY12 increases ischemic stroke damage (Cserép et al., 2020). Since VRAC does not regulate P2RY12-dependent chemotaxis, pharmacological VRAC inhibition should not inhibit the formation of these junctions or P2RY12-dependent neuroprotection.

2.4.4 VRAC does not regulate microglial morphology or ischemic damage

The role of ion fluxes in determining microglial morphology is still poorly defined, other than one or two key principles. In the present study, no differences were observed in the morphology of either homeostatic or reactive microglia upon microglial VRAC ablation. This result implies that, contrary to previous findings, VRAC does not regulate microglial ramification. The previously reported effect of chloride channel blockers on preventing microglial ramification *in vitro* is perhaps not surprising considering the effects observed in this study, whereby high doses of inhibitors appear to prevent the creation of membrane protrusions, thus completely inhibiting migration and chemotaxis. A role for chloride in protrusion formation has been proposed previously, and may also form the basis of phagocytic inhibition by chloride channel blockers (Harl et al., 2013; Schwab et al., 2012; Zierler et al., 2008). As such, the idea that chloride transport underpins local cell shape changes required for diverse microglial activities including establishment of mature morphology is supported by the data presented here, with the caveat that this mode of chloride transport is in fact distinct from the VRAC-mediated $I_{Cl}(\text{swell})$ proposed by most prior studies.

It is also interesting that loss of VRAC appears to have little impact on microglial morphology following ischemia. As such, it seems that VRAC currents are not required to maintain microglial viability by counteracting cellular swelling due to brain oedema or changes in osmolyte balance upon microglial activation. It is tempting to speculate that, due to the lack of differences in morphology, microglial polarization and phenotype are also unchanged between WT and KO microglia following MCAo. However, this would require validation at the level of gene expression or surface markers to be conclusive.

In either case, it is important to note that infarct volumes following MCAo were not altered by LRRC8A knockout. Thus, any functional differences in microglia arising from VRAC ablation are clearly not sufficient to alter ischemic damage at least at an acute time point (24h). It has previously been suggested that VRAC can mediate EAA release from microglia, which could prove neurotoxic in stroke settings (Harrigan et al., 2008; Schlichter et al., 2011). These results therefore imply that, since no differences in infarct volume were observed, EAA release from microglia is either independent of VRAC, or else is not overtly pathological in stroke. However, one key consideration around this finding is that the FeCl₃ thrombotic stroke model used here induces permanent vessel occlusion, with an absence of significant reperfusion (Karatas et al., 2011), whereas both studies implicating astrocyte VRAC in modulating stroke infarct volume have used transient MCAo models (Yang et al., 2019; Zhou, Luo, et al., 2020). Due to these differences in the extent of reperfusion, and since VRAC-dependent EAA release is suspected to occur mostly in the ischemic penumbra, as opposed to the ischemic core, direct comparison between these models with respect to VRAC is challenging (Mongin, 2016). As such, the use of a transient MCAo model might be more interpretable with respect to the role of EAA release from microglia in determining ischemic damage.

2.4.5 VRAC as a drug target for ischemic stroke

VRAC is of increasing interest in the field of stroke, since astrocytic VRAC has been shown to mediate pathological EAA release and promote excitotoxicity in ischemia (Yang et al., 2019; Zhou, Luo, et al., 2020). Ablation of microglial VRAC, by contrast, did not cause any difference in the extent of brain damage in stroke. Combined with the fact that no VRAC dependence was observed for microglial phagocytosis or P2RY12-dependent chemotaxis, this result supports the idea that VRAC could serve as a therapeutic target in ischemic injury, since protective microglial functions occur independently of VRAC. Therefore, selective VRAC inhibitors could reduce excitotoxic EAA release without compromising microglia-mediated neuroprotection. Indeed, previous studies have indicated that DCPIB exerts neuroprotective actions when administered in a rat model of transient MCAo, reducing both glutamate accumulation and infarct size, which also supports earlier data reporting similar effects of tamoxifen, another known VRAC inhibitor (Kimmelberg et al., 2000; Zhang et al., 2005, 2008).

Notably, DCPIB provides no benefit upon intravenous administration, presumably reflecting poor CNS penetration (Zhang et al., 2008).

With respect to microglia, it is interesting to note that both DCPIB and tamoxifen inhibit microglial process chemotaxis, yet both are protective in stroke models (Kimelberg et al., 2000; Zhang et al., 2005, 2008). One possible explanation is that the beneficial effect of reducing EAA release outweighs the detrimental consequences of preventing process chemotaxis (Cserép et al., 2020). Indeed, since P2RY12-dependent process homing is activity-dependent and protects neurons by curbing excess excitation, it is also possible that VRAC inhibitors reduce neuronal calcium load enough to eliminate the need for such somatic contacts entirely. Alternatively, since relatively high concentrations of DCPIB and tamoxifen (20 μ M and 40 μ M, respectively) were required to inhibit process chemotaxis in brain slices (Hines et al., 2009), it may be the case that the concentration of these drugs (which was not generally measured *in vivo*) was simply insufficient to inhibit chemotaxis in stroke models, yet retained significant inhibition of EAA release. This uncertainty could be clarified in future by studies examining the effect of P2RY12 inhibition on infarct volumes in mice with brain-specific VRAC deletion, but would be aided by the development of compounds capable of targeting VRAC without inhibiting microglial chemotaxis.

Whilst these, and previous data support the development of VRAC as a drug target for treating stroke, another key point is that new compounds with greater selectivity for VRAC over other channels would be of great benefit moving forward. DCPIB is currently the gold-standard inhibitor, yet still exhibits considerable off target activity - it has been shown to inhibit tweety homologue channels (Han et al., 2019), and likely also inhibits CLIC-family channels given its structural similarity to IAA-94, a known CLIC inhibitor. Moreover, the data presented here and elsewhere demonstrate dramatic VRAC-independent effects on cell physiology, including inhibition of phagocytosis, cell motility, chemotaxis and NLRP3 inflammasome activation at 10-20 μ M, which is the standard concentration used for functional VRAC studies (Furtner et al., 2007; Green et al., 2020). Whilst the mechanism mediating these effects is unclear, DCPIB clearly displays activity at other chloride channels, which undermines its utility as a tool for manipulating VRAC. Moreover, previous papers have reported inhibition of glutamate transport pathways and modulation of potassium currents by even low doses of DCPIB

(Bowens et al., 2013; Lv et al., 2019; Minieri et al., 2013). Thus, it is increasingly difficult to interpret studies using any chloride channel inhibitor with respect to VRAC function, and the field would benefit greatly from new, more selective VRAC inhibitors.

2.4.6 Conclusions

Overall, these results argue against VRAC as a fundamental regulator of microglial physiology. Microglial VRAC is seemingly unnecessary for phagocytosis, cell migration, chemotaxis and morphology, and does not alter other microglial functions sufficiently to affect infarct volume. Given previous studies implicating swelling-activated chloride currents in various cellular functions, these results highlight the need for validation of inhibitor-based data using more specific genetic techniques. In this vein, future studies will likely seek to determine which channels underpin suppression of microglial functions by chloride channel inhibitors, as this could inform future strategies aimed at modulating immune functions in the brain. However, this may prove difficult given the likelihood of redundancy between chloride channels, particularly those of the same family. Thus, a good strategy might involve combinatorial targeting of multiple channels simultaneously, which could be compatible with high-throughput screening strategies. VRAC itself may also prove a good drug target for some CNS pathologies involving astrocyte swelling, and given the right inhibitor, could be targeted without altering several microglial functions.

A major question raised by this study is what, if any, microglial functions VRAC does regulate. It is unclear what events stimulate microglial VRAC activity *in vivo*, and for what purpose. Since blood osmolyte concentrations are tightly regulated, large, rapid ionic imbalances on the scale of hypotonic challenge *in vitro* likely do not occur *in vivo*. Thus, it is questionable to what extent VRAC is required for volume regulation under most circumstances. Since VRAC is known to transport various molecules involved in cellular signalling, it may be that VRAC's primary function in microglia *in vivo* relates to signal transduction, albeit in contexts which are yet to be established.

2.5 Appendix

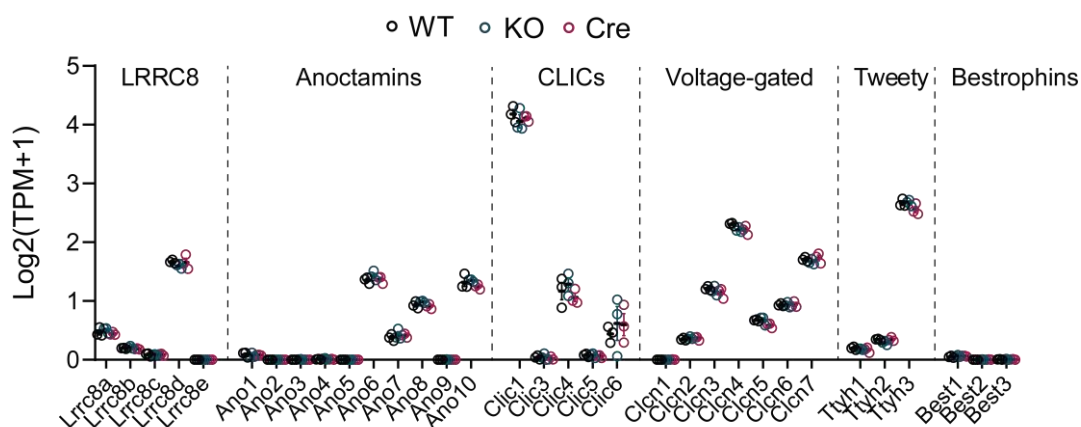


Figure 2.11: Expression of chloride channel genes in WT, LRRc8A-KO and Cre microglia
Expression levels given in $\log_2(\text{transcripts per million} + 1)$ of major chloride channel genes in wild-type (WT), LRRc8A knockout (KO) and Cx3cr1-Cre (Cre) microglia, as quantified by RNA-Seq. $n = 3$. Lrrc8a mRNA still detected in KO microglia due to continued transcription of exons 1 and 2 (see Figure 2.2)

Table 2.2: Differentially expressed genes in WT, LRRc8A-KO and Cre microglia

KO vs WT Microglia			Cre vs WT Microglia		
Symbol	Log2FC	padj	Symbol	Log2FC	padj
Mrc2	-1.97	1.07E-77	Cx3cr1	-1.04	3.92E-76
Cx3cr1	-0.96	2.80E-65	Gpr165	-1.01	7.10E-39
Xirp1	3.17	3.32E-24	Ly9	1.34	1.78E-32
Col6a3	1.34	1.09E-19	Cst7	1.71	4.22E-23
Adams1	-0.74	1.49E-15	H2-Q6	1.07	2.82E-17
Neur1a	-0.82	1.32E-14	Cd34	0.62	8.05E-12
P2ry6	-0.55	3.85E-13	Tmem181b-ps	7.01	3.40E-11
Adamts12	1.26	8.35E-12	Arl5c	0.94	6.28E-11
Cd34	0.57	8.54E-10	H2-D1	0.50	2.17E-10
Lag3	0.55	2.53E-09	Pdcd1	2.10	7.33E-09
Mlph	0.55	2.53E-09	Chst1	0.96	8.35E-09
Mymk	1.22	2.66E-09	Cd22	1.05	8.35E-09
Amotl1	0.81	5.60E-09	Slamf9	0.62	8.75E-09
Prl	-26.70	1.14E-08	Pxdc1	0.74	8.75E-09
Tmem44	0.67	3.76E-08	Sp100	0.80	1.60E-08
Notch4	0.70	5.58E-08	Lox	1.90	1.49E-07
Serpinf1	0.62	4.08E-06	Hcar2	0.99	2.67E-07
Cdh23	0.52	2.56E-05	Gm32312	3.96	3.21E-07
Gm32312	3.54	2.98E-05	H2-Q7	0.78	4.98E-07
Mmp2	0.60	3.85E-05	Ildr2	1.30	4.98E-07
Atf5	0.85	4.19E-05	Sema6d	-0.75	1.09E-06
Hlf	0.90	4.27E-05	Epb4113	0.74	3.85E-06
Liph	-0.68	9.44E-05	Naalad2	0.65	1.33E-05
Vash1	-0.66	9.77E-05	Gm4951	1.18	2.35E-05

Xdh	1.02	0.000124	Upk1b	-0.53	3.76E-05
Il1b	0.53	0.000175	Rxrg	2.13	4.80E-05
Tmem154	1.23	0.000224	Sfi1	0.65	0.000106
Cdkn1a	0.54	0.000344	Lrguk	1.48	0.000107
2510009E07Rik	-0.56	0.000514	Gm13889	-0.91	0.000134
Arsg	0.54	0.000514	Tnfsf8	1.26	0.000295
S100a6	1.12	0.00052	H2-Q5	0.67	0.000362
Cpq	0.60	0.00083	AC154187.1	0.89	0.000362
Plbd1	0.92	0.00083	Cdkn1a	0.53	0.000417
Slc16a9	0.95	0.001248	Parp3	0.81	0.00044
Lgals3	0.83	0.001279	Gpr162	0.92	0.000476
Fyn	0.53	0.001499	Prkar1b	0.74	0.000501
Ccl12	0.57	0.001508	Slc39a4	0.72	0.000636
Gpnmb	1.80	0.001508	Hao	0.87	0.000859
Mmp28	0.70	0.001518	A130077B15Rik	0.71	0.000953
Slc1a4	0.89	0.001882	Tnfsf13b	0.73	0.001093
Trp53i11	0.52	0.00265	Fblim1	0.53	0.001374
Gm11545	1.41	0.00265	Tmem154	1.11	0.00148
Gm27008	1.80	0.002866	Nbea	-0.55	0.001803
Sp100	0.53	0.002912	Rgs7bp	-0.51	0.0025
Pfkm	-0.77	0.002962	Rnf24	0.65	0.003075
Pacsin1	0.71	0.003601	Hebp1	0.53	0.003281
Itgae	0.91	0.004215	Bcl2a1a	0.68	0.003551
Serpine1	0.88	0.004454	Gcnt2	0.55	0.003674
Folr2	0.61	0.005253	Alb	1.42	0.00533
Gm4951	0.92	0.005887	Osgin1	0.69	0.008918
Ear2	1.19	0.007043	Zmynd15	0.70	0.010455
Rell1	0.87	0.007674	Hpn	0.55	0.015054
Nptxr	-1.01	0.00873	Amer2	0.82	0.017128
Amer2	0.87	0.009281	Chst2	1.01	0.020509
Itgal	0.87	0.009975	Arhgap15	0.75	0.023861
Klf11	-0.59	0.01019	Aoah	0.51	0.030006
Plekhh2	-0.82	0.010314	Pde8b	0.50	0.030965
Vstm4	1.31	0.011643	Tex11	2.20	0.033217
Pglyrp1	1.08	0.013168	Igsf9	0.83	0.033878
Itgb2l	1.16	0.013194	G530011O06Rik	0.91	0.036009
Gh	-14.95	0.018144	Bace1	-0.65	0.036926
Osgin1	0.66	0.018144	Nlrc5	0.60	0.036926
Al662270	1.07	0.018577	Vangl1	-0.81	0.045729
Trerf1	1.19	0.01858	Ccdc122	0.88	0.046286
Retnla	1.27	0.01858			
Serpinb1a	1.34	0.018817			
Afdn	0.75	0.019929			
Syne1	0.80	0.021828			
Cd300lf	0.87	0.024751			
Aprt	-0.53	0.025812			

Pde10a	1.29	0.02645
Emilin1	0.81	0.028172
Cxcr2	1.19	0.028172
Cd24a	0.90	0.028236
Hist1h2bc	0.53	0.02872
Igf2bp2	-0.63	0.029893
Ccr2	0.60	0.030198
Cyp4f18	0.93	0.030468
Creb5	0.77	0.03103
Emilin2	0.86	0.033513
Hbegf	-0.55	0.035207
Rxrg	1.48	0.035643
Asns	1.37	0.036535
Soat2	0.95	0.037604
Chil1	1.23	0.039908
Efcab6	1.33	0.04775

KO vs Cre Microglia

Symbol	Log2FC	padj
Mrc2	-1.89456	3.35E-72
Gpr165	1.305492	1.27E-66
Col6a3	1.543632	6.26E-27
Xirp1	2.815399	8.40E-21
Amotl1	1.065983	1.50E-16
AU020206	-0.71127	8.73E-16
Ly9	-0.93324	1.29E-15
Notch4	0.874557	2.02E-13
Myo18b	0.685564	3.06E-13
Cst7	-1.27737	6.43E-13
Tmem44	0.808943	8.91E-13
Neurl1a	-0.72475	9.61E-12
Tmem181b-ps	-6.96407	1.86E-11
Serpinf1	0.809151	2.05E-11
Hlf	1.267004	2.42E-11
Khdrbs3	0.800722	1.25E-10
MIph	0.567309	2.57E-10
Sema6d	0.892206	6.60E-10
Lat2	-0.61684	1.23E-09
Actn1	0.691991	1.23E-09
Slc7a5	0.714166	1.01E-08
Adcy8	1.118585	2.38E-08
Pacsin1	1.076798	4.32E-08
Slc1a4	1.2862	4.75E-08
Hcar2	-1.01732	7.20E-08
Hebp1	-0.79078	1.70E-07

KO vs WTCre Microglia

Symbol	Log2FC	padj
Mrc2	-1.9321	3.25E-92
Xirp1	2.98029	8.14E-31
Col6a3	1.44405	3.38E-28
Neurl1a	-0.76941	5.89E-18
Notch4	0.786794	1.44E-13
MIph	0.560862	1.73E-13
Amotl1	0.934614	6.92E-13
Tmem44	0.737909	6.62E-12
Adamtsl2	1.072998	1.20E-10
Mymk	1.083065	2.45E-10
Atf5	0.858511	1.28E-09
Serpinf1	0.715321	2.28E-09
Hlf	1.076884	8.99E-09
Vash1	-0.68262	1.84E-08
Liph	-0.73124	1.95E-07
Serpine1	0.777251	1.95E-07
Fyn	0.587495	5.79E-07
AU020206	-0.57718	1.53E-06
2510009E07Rik	-0.61996	2.55E-06
Pacsin1	0.889209	2.67E-06
Slc7a5	0.607873	4.13E-06
Lgals3	0.827175	4.89E-06
Plbd1	0.964362	5.65E-06
S100a6	1.05123	5.65E-06
Trp53i11	0.5721	9.06E-06
Ear2	1.379167	1.35E-05

Rc3hb2	-0.51319	3.44E-07	Xdh	0.930364	1.50E-05
Arl5c	-0.75266	5.55E-07	Mmp28	0.671729	2.01E-05
Liph	-0.78002	6.61E-07	Retnla	1.522391	2.18E-05
Adamts12	0.919425	1.06E-06	Actn1	0.555501	2.33E-05
2510009E07Rik	-0.67778	1.24E-06	Trerf1	1.259053	3.86E-05
Pecam1	0.62647	1.30E-06	Gm27008	1.640157	3.86E-05
Gpr162	-1.13742	1.74E-06	Pfkm	-0.76643	4.36E-05
H2-Q6	-0.66089	1.89E-06	Itgal	1.006953	4.36E-05
Gm23935	0.616354	2.23E-06	Slc16a9	0.850147	6.11E-05
Mymk	0.966765	3.05E-06	Pecam1	0.527887	6.57E-05
Vash1	-0.71095	3.39E-06	Itgb2l	1.287657	7.19E-05
Spns2	-0.58674	3.83E-06	Gm11545	1.292439	7.48E-05
Atf5	0.868923	4.75E-06	Folr2	0.59524	8.25E-05
Ahnak	0.730232	8.33E-06	Gpnmb	1.634687	9.57E-05
Fyn	0.638755	8.70E-06	Adamts1	-0.56605	0.000134
Ccdc162	0.809161	9.40E-06	Syne1	0.864694	0.000166
Ear2	1.57477	1.25E-05	Pglyrp1	1.150465	0.000166
Anapc15	-0.75443	1.44E-05	Myo18b	0.511729	0.000273
Hpn	-0.77024	1.62E-05	Cd24a	1.067745	0.000278
Dpp7	-0.54652	1.62E-05	Cxcr2	1.366013	0.000303
Cass4	0.62411	2.24E-05	Epx	2.066192	0.000303
Trp53i11	0.62571	2.25E-05	Rel1	0.832865	0.000318
Retnla	1.784617	2.26E-05	Spn	1.017278	0.000337
Itgal	1.144443	2.79E-05	Efcab6	1.375281	0.000338
Lox	-1.53664	3.08E-05	Afdn	0.740918	0.000375
Epb41l3	-0.673	3.08E-05	Lrg1	1.619885	0.000417
Mical3	0.541462	3.73E-05	Asns	1.511038	0.000418
Igkc	1.851698	4.25E-05	Fgfr1	0.624971	0.000466
Plbd1	1.004302	4.86E-05	Chil1	1.440405	0.000466
Upk1b	0.502974	6.29E-05	Vim	0.614485	0.000486
Fat3	0.756671	6.30E-05	Aprt	-0.53091	0.000593
Cd24a	1.244378	6.30E-05	Mcemp1	1.222364	0.000594
Prl	-20.2806	6.61E-05	Emilin2	0.926119	0.00088
Ache	-0.6682	6.90E-05	Gadl1	0.750583	0.000939
Anxa2	0.947576	7.03E-05	Adcy8	0.823077	0.000939
Ccl2	0.512465	0.000133	Adam8	0.906752	0.00104
Sema4b	0.504091	0.000138	Cfp	0.594772	0.001114
Casc4	0.63226	0.000138	Anxa2	0.772779	0.00119
Mcemp1	1.468148	0.000139	Igf2bp2	-0.61116	0.001514
Tiam1	0.551236	0.000178	Lrrc4	0.814234	0.001763
Bace1	0.874452	0.000195	Plp2	1.050103	0.002126
Itgb2l	1.414151	0.000201	Mthfd2	0.585799	0.002614
Chil1	1.672749	0.000203	Emb	0.625319	0.00273
Parp3	-0.80954	0.00022	Acap1	1.360569	0.00273
Rnf24	-0.72046	0.000223	Khdrbs3	0.563852	0.003105
Lrg1	1.943442	0.000248	Cyfp2	0.838724	0.003118

Cxcr2	1.540693	0.000266	Ccdc88c	1.090068	0.003325
Dpy19l3	0.510516	0.000348	Atp8b4	1.186652	0.003851
Klk8	-0.55082	0.00036	Glipr2	1.152926	0.003881
Lgals3	0.824374	0.000381	Anxa1	1.24919	0.004058
Vangl1	1.06585	0.000417	Itgae	0.747022	0.004287
Crispld2	1.343331	0.000537	Ccdc162	0.615668	0.004299
Pygm	0.911311	0.000638	Cd44	0.733392	0.004332
Neo1	0.759265	0.000671	Rasgrp2	0.903354	0.00439
Pnma2	1.418066	0.000671	Fpr2	1.303343	0.004436
Pglyrp1	1.218506	0.000823	Plxna1	0.534003	0.004576
Lrrc4	0.964503	0.000827	Plac8	1.060317	0.004576
Fblim1	-0.52016	0.000882	Gm28512	0.830729	0.005326
Cyfp2	1.005208	0.000931	Lrrk2	0.898395	0.005326
S100a6	0.992319	0.001089	A830008E24Rik	-0.69029	0.005534
Lrguk	-1.25648	0.0011	Scarf2	-0.52253	0.005714
St8sia6	-0.81454	0.0011	Ache	-0.52552	0.005725
Jam3	0.734503	0.001167	Hspb3	-0.71641	0.005949
Syne1	0.920898	0.001205	Soat2	0.907416	0.006117
Pdcd1	-1.28607	0.001208	Podxl2	0.79213	0.007147
Spn	1.137118	0.001208	Kcnj10	-0.61172	0.007496
Pfkm	-0.7662	0.001211	Wfdc21	1.212476	0.007934
Ehd1	0.517501	0.001244	Elane	1.420032	0.008547
Xdh	0.848886	0.001244	Dhrs9	1.818482	0.008547
Cnn2	0.552328	0.001248	Igkc	1.357144	0.008953
G530011O06Rik	-1.10427	0.001265	Jam3	0.582181	0.009457
Asns	1.663717	0.001271	Sertad1	-0.53275	0.009552
Trerf1	1.325737	0.001343	Fcna	0.509399	0.009769
Kcnj10	-0.73749	0.001409	Ly6g	1.272431	0.010617
Speg	-0.51254	0.001455	Adgrg3	1.436712	0.010785
Bmp1	0.624603	0.001481	G0s2	1.11091	0.010793
Mmp28	0.650117	0.001481	Plvap	0.770508	0.011289
S100a11	1.067114	0.001506	Pi16	1.124405	0.011302
Ncs1	0.529079	0.001591	Slc1a4	1.080965	0.011662
Ildr2	-0.89098	0.001614	Bmp1	0.500264	0.012071
Gm13889	0.762644	0.001759	Clec4d	1.196273	0.012071
Gpatch11	0.626806	0.00177	Rnf144a	1.089538	0.012258
H2-Q7	-0.53477	0.001779	D630045J12Rik	0.509521	0.012571
Scarf2	-0.62494	0.00179	Cd300lb	0.790932	0.01308
Fpr2	1.548521	0.001907	Arl4d	-0.62324	0.013624
Emilin2	0.993603	0.002087	Neo1	0.578131	0.013704
Hspb3	-0.84659	0.002284	S100a11	0.851392	0.013704
Kcnj2	-0.54259	0.002396	Mgst1	0.887913	0.014312
Cfp	0.647356	0.002583	S100a8	1.286681	0.015656
Abcg3	-0.57022	0.002731	Ctla2b	-1.3266	0.016164
Plxna1	0.624272	0.003066	Crispld2	0.987637	0.016906
I830127L07Rik	1.311689	0.003355	Tle2	-0.63165	0.017997

Slc7a1	0.610771	0.003841	I830127L07Rik	1.047795	0.017997
Folr2	0.580712	0.003938	Nptxr	-0.81148	0.01808
Kcnj9	-0.90393	0.00416	Ccr2	0.524169	0.019877
Prkar1b	-0.61688	0.00416	Slc25a24	0.859662	0.019877
Arap2	0.566206	0.004172	Tet1	0.535587	0.021098
Fgfr1	0.667505	0.004172	Vstm4	0.980947	0.021408
Gprasp2	0.519666	0.004761	Napsa	0.772507	0.0216
Napsa	0.982343	0.004771	9830107B12Rik	1.469486	0.0224
A830008E24Rik	-0.78923	0.005114	Fcnb	1.485144	0.023674
Dhrs9	2.165352	0.005362	Ahnak	0.506772	0.025869
Cd22	-0.59551	0.005476	Sfn1	1.196041	0.026008
Anxa1	1.407557	0.005476	Adgre5	0.614474	0.026208
Mthfd2	0.62383	0.0056	Il1r2	0.981252	0.026932
Plac8	1.186642	0.0056	Gm14548	1.566194	0.028664
Gsto1	-0.51965	0.005761	S100a9	1.270477	0.029323
Gpnmb	1.494081	0.005761	Anapc15	-0.54356	0.030404
G0s2	1.3083	0.006313	Hebp1	-0.55346	0.030576
Ccdc88c	1.210896	0.006372	Padi4	1.093069	0.03175
Gm15564	0.653657	0.006785	Alox15	1.382104	0.03251
Gm27008	1.516647	0.006785	Cd177	1.338383	0.033117
Podxl2	0.937663	0.007182	Mmp25	0.975581	0.033838
Akt3	-0.62761	0.007358	Sgms2	0.711156	0.034141
Tnfsf8	-0.96864	0.007445	Gda	1.283938	0.034543
Gm11545	1.18867	0.007746	Prtn3	1.311006	0.034543
Rell1	0.797742	0.007787	Lpcat4	0.995924	0.035462
Slc16a9	0.764016	0.007817	Hr	1.060945	0.035507
Acap1	1.471608	0.008279	Rrm2	1.080598	0.038277
Afdn	0.732938	0.008637	Col11a2	0.758026	0.038769
Glipr2	1.264184	0.008724	Lmtk2	0.68488	0.042333
Efcab6	1.414521	0.008724	Mmp8	1.256823	0.042333
Tet1	0.653649	0.008903	Arhgef37	1.315302	0.042333
Mki67	0.748041	0.00891	Pygm	0.65226	0.04294
Plp2	1.133611	0.009979	Serpnb1a	1.025409	0.044076
Cd44	0.777292	0.010053	Lyz1	1.309351	0.044076
Fcgr4	-0.5448	0.011161	Olfm1	0.553394	0.04503
Aprt	-0.52565	0.011178	Trim67	1.315728	0.045678
Pkib	-0.56643	0.01158	Ccdc8	0.607028	0.046413
Gadl1	0.785811	0.01158	Runx3	0.711202	0.048402
Slc39a12	0.511259	0.012501	Syt3	-0.70122	0.048603
Rasgrp2	0.969129	0.012536			
Arl4d	-0.7109	0.012556			
Ptprd	1.337621	0.013764			
Ly6g	1.427457	0.013764			
Pi16	1.273557	0.013839			
Cldn11	1.393567	0.013839			
Atp8b4	1.242564	0.014161			

Mycl	0.5886	0.014231
Emb	0.63912	0.014231
Lefty1	-0.64156	0.015497
Htra3	0.707512	0.015497
Adgre5	0.704869	0.015759
Gm21887	-1.65222	0.016761
Sertad1	-0.55293	0.017304
Wfdc21	1.314913	0.017304
Gm16118	-0.86313	0.017442
Gda	1.523556	0.017709
Zbtb20	0.500423	0.017734
Chst2	-0.94501	0.017803
A130077B15Rik	-0.53228	0.018183
Fcna	0.564423	0.019479
Tnfsf13b	-0.55152	0.020143
Jchain	2.014845	0.021482
Aldh1l2	0.795084	0.0216
Igf2bp2	-0.59377	0.021965
Lrrk2	0.93404	0.022059
Nbl1	0.717786	0.023848
Il12rb2	-0.95506	0.02412
Atp8b1	0.668007	0.024245
Tle2	-0.70693	0.024319
Adgrg3	1.581791	0.02531
Fcnb	1.721623	0.025871
Rflnb	0.868743	0.025982
Ctla2b	-1.47417	0.026589
Pygl	0.516411	0.027228
Igsf9	-0.77685	0.027429
Hp	1.495516	0.028948
Elane	1.531148	0.029477
Rnf144a	1.179734	0.030101
Tmem52	0.661224	0.03076
Clec4d	1.263182	0.032027
Bcl2l2	-0.5678	0.033469
Soat2	0.870221	0.033885
D630045J12Rik	0.550445	0.034473
Slc25a24	0.987363	0.034718
Gsr	0.577026	0.034844
Lilra6	1.629893	0.03715
Mmp8	1.457184	0.037263
Serpine1	0.676522	0.038721
Slfn1	1.337621	0.039059
Cdc42ep3	-0.71393	0.03923
S100a8	1.398739	0.040283
Cc2d2a	0.621564	0.040651

Adra2a	1.140353	0.041742
Acpp	1.553461	0.042584
Gm15964	-0.88323	0.045205
Lmnb1	0.571732	0.045205
Cd300lb	0.833509	0.045205

Microglia from WT, LRRC8A-KO (KO) and Cre mice (n = 3) were isolated via MACS and RNA sequenced (see **2.2.9**). Differential expression analysis was conducted (**2.2.9**) and genes found to be significant between each genotype pair are listed here. WTCre is a composite group consisting of both WT and Cre samples.

Chapter 3: Identifying novel LRRC8A- dependent signalling pathways

3.1 Introduction

3.1.1 Type I Interferons

Interferons are critical cytokines which regulate multiple facets of innate and adaptive immunity, though are primarily noted for their role in viral pathologies. Three families of interferons have been described, known simply as types I, II and III. Only one type II interferon – IFN- γ - is known, and is expressed predominantly by adaptive immune cells (McNab et al., 2015). Type III interferons are a relatively recent discovery consisting of the multi-gene IFN- λ family, and appear to act primarily on endothelial cells, the main cell type which express the type III interferon receptor (McNab et al., 2015). Type I interferons consist of IFN- α (multiple subtypes) and IFN- β , as well as IFN- ϵ and IFN- κ , in mice, though more types have been described in humans and other mammals (Platanias, 2005). Importantly, all type I interferons exhibit considerable structural homology and signal through a common receptor, known as the interferon α/β receptor (IFNAR) (Platanias, 2005). Whilst IFN- α is predominantly produced by plasmacytoid dendritic cells and acts systemically to mobilise adaptive immunity, IFN- β can be produced by most cell types (Ivashkiv & Donlin, 2014; Siegal et al., 1999). IFN- β is induced rapidly following recognition of immunogenic nucleotides by PRRs, and acts on neighbouring cells to promote transcription of interferon-stimulated genes (ISGs), many of which have antiviral and immunostimulatory functions (Schneider et al., 2014). Thus, IFN- β is critically important in propagating antiviral responses from infected cells to the neighbouring tissue and promotes antiviral functions of both innate and adaptive immune cells (Ivashkiv & Donlin, 2014; McNab et al., 2015).

3.1.2 Mechanisms of nucleotide sensing

Macrophages, and indeed most cells, express a variety of mechanisms for sensing nucleotides. Detection of immunogenic nucleotides activates response pathways which vary depending on the type of molecule (e.g. RNA and DNA of varying composition) and its localisation (e.g. extracellular or cytosolic), though almost all sensing pathways induce IFN- β and a subset of ISGs via phosphorylation of IRF3, which is expressed constitutively in most cell types (Honda et al., 2006). IRF3 is primarily phosphorylated by TBK1 as the final step in most pathways, though TBK1 can be activated via a variety of different routes depending on the sensor in question (Fitzgerald et al., 2003; McWhirter et al., 2004). DNA and RNA present

in the extracellular space or in engulfed cargo are detected by TLRs 3, 7, 8 and 9 in endosomes, which signal through the adapters TRIF and MyD88 to induce IRF3 phosphorylation via TBK1, as well as activation of NF- κ B (Kawai & Akira, 2010; McNab et al., 2015). TLR4 may also induce IRF-dependent responses via TRIF in response to certain ligands, such as the bacterial endotoxin lipopolysaccharide (Kawai & Akira, 2010; McNab et al., 2015).

The presence of cytosolic nucleotides is detected by a separate array of sensors binding both DNA and RNA and promoting IRF3 phosphorylation via overlapping pathways. Cytosolic RNA is sensed primarily by retinoic acid inducible gene 1 (RIG-1) and melanoma-differentiation-associated gene 5 (MDA5), both of which signal via mitochondrial antiviral signalling protein (MAVS), which directly activates TBK1 to induce IRF3-dependent transcription (Kato et al., 2006; McNab et al., 2015). Various sensors for cytosolic DNA have been described, the best-studied of which are cGAS and DNA-dependent activator of interferon regulatory factors (DAI/ZBP1), though many others have been suggested (Paludan & Bowie, 2013; Sun et al., 2013; Takaoka et al., 2007). Importantly, most proposed sensors of cytosolic DNA mediate their effects by activating STING, an ER-membrane protein which, upon activation, recruits TBK1 to form a signalling complex phosphorylating IRF3 (Burdette & Vance, 2013). Thus, the STING-TBK1-IRF3 axis represents a convergent pathway essential to many forms of immune response. Whilst most studies have focused on microbial challenge, there is an increasing body of evidence implicating STING-dependent DNA sensing in generating inflammatory responses to sterile insults (Decout et al., 2021). These include cancer signalling, tissue infarction, and cellular stress due to inflammatory cytokine exposure (Decout et al., 2021; Zhu et al., 2019).

3.1.3 Study rationale

There have been various intriguing hints in the literature that LRRC8A and VRAC engage in a wide variety of signalling functions amongst different cells and tissues. While novel signalling functions of LRRC8A/VRAC likely remain to be discovered, no studies have so far undertaken systematic, unbiased attempts to identify signal transduction events involving LRRC8A/VRAC. Thus, the present study aimed to identify previously unrecognised signalling pathways depending on LRRC8A/VRAC using RNA sequencing. Most studies seeking to understand

the function of LRRC8A have done so with respect to its obligatory involvement in VRAC channel activity. However, multiple lines of evidence now support VRAC-independent signalling by LRRC8A in a variety of contexts. As such, this study further attempts to delineate between signalling mediated via VRAC-dependent solute flux and signalling arising from LRRC8A-dependent protein-protein interactions occurring independently of the VRAC channel.

Little is known about regulation of VRAC and LRRC8A with respect to their signalling functions. However, VRAC is known to be activated by cell swelling and mechanostimulation. Moreover, VRAC gating is understood to depend on sequences contained in the cytoplasmic portions of LRRC8A, implying that LRRC8A-dependent protein-protein interactions should also be stimulated by cell swelling. Thus, cell swelling was used as a stimulus aimed at producing robust signalling mediated by both LRRC8A and VRAC. Cell swelling was stimulated using extracellular hypotonicity, since this produces robust swelling in the absence of overt cellular injury (e.g. due to hypoxia or other insults). Some previous literature has indicated that macrophage phenotypes can be modulated by hyper-osmotic environments, but no studies have so far examined the effect of hypo-osmolarity on macrophage function. Therefore, a secondary objective of this study was to determine the effect hypotonic stress on macrophage phenotype, which could provide some insight into novel physiological situations which might engage VRAC *in vivo*. This study used BMDMs as a general immune cell model due to the large numbers of cells obtainable per mouse, which makes them suitable for large-scale *in vitro* experiments.

3.1.4 Specific aims

This study aims to investigate several important issues with respect to LRRC8A function in macrophages, specifically:

- Characterise the transcriptomic response to osmotic swelling in macrophages
- Investigate potential signalling pathways altered by LRRC8A under hypotonic conditions
- Establish whether LRRC8A-dependent signalling is dependent on VRAC function

3.2 Materials and Methods

3.2.1 Chemicals

Unless otherwise stated, cell culture solutions and media were obtained from Gibco. DCPIB was purchased from Tocris, NPPB from Cayman Chemical and FFA from Sigma. Unless otherwise specified, kinase inhibitors were purchased from Cayman Chemical. A151, H151, poly(dA:dT) and 2'3'-cGAMP were from Invivogen.

3.2.2 Animals

Lrrc8a^{fl/fl}:Cx3cr1^{Cre/+} (KO), *Lrrc8a^{fl/fl}:Cx3cr1^{+/+}* (WT), and *Lrrc8a^{+/+}Cx3cr1^{Cre/+}* (Cre) were bred in-house as described previously (2.2.2). Animals were kept in individually ventilated cages maintained at 55 ± 10% humidity and a 12-hour light/dark cycle with access to food and water *ad libitum*. Mice were used between the ages of 2-6 months. Where possible, littermates were used for experiments comparing WT and KO mice. For each experiment, n-numbers are stated in figure legends.

3.2.3 Cell culture

Unless otherwise stated, all cell culture experiments were performed in a laminar flow cabinet under sterile conditions. All cell incubations were performed in a humidified incubator maintaining 37°C with 5% CO₂. BMDM standard media was DMEM (Gibco) supplemented with 10% heat-inactivated FBS (Gibco) and 100U/mL penicillin with 100µg/mL streptomycin. BMDM growth media consisted of a 2:1 mix of fresh standard media to standard media conditioned by L929 fibroblasts, which secrete M-CSF. Serum-free media consisted of DMEM with penicillin and streptomycin only.

3.2.4 Bone marrow derived macrophage culture

Mice were deeply anaesthetised with 2% isoflurane in 70% NO₂/30% O₂ and culled by cervical dislocation. The femurs were dissected and muscle removed, and the cleaned bones placed in ice-cold DMEM. Under sterile conditions, the distal femur head was removed with scissors, exposing the marrow. A collection tube was then made by placing a 0.5mL Eppendorf inside a larger 1.5mL tube. A small hole was created in the bottom of the inner tube using a 25G needle, and the femurs placed inside the 0.5mL tube with the cut end facing down. 100µL PBS was pipetted into the lower tube, and marrow collected by centrifuging for

5s at 2000xg. The marrow was resuspended in DMEM and passed through a 70µm cell strainer and pelleted (5 min at 2000 xg), then resuspended in 3mL ACK buffer (Gibco) for 2-3 minutes to lyse red blood cells. 9mL DMEM was then added to neutralise the ACK buffer, and the marrow cells recovered by centrifugation (5 min at 2000xg). For culturing, the cells were resuspended in 30mL growth media, placed in a T225 tissue culture flask and incubated for 5-7 days, with 15mL growth media added on day 3.

Once confluent, flasks of BMDM were harvested by scraping with a sterile cell scraper. The cell suspensions were recovered by centrifugation (5 min at 2000xg) and resuspended in fresh standard media to a density of 10^6 cells/mL and seeded in tissue culture plates. BMDM were then incubated overnight to promote attachment and assayed the following day.

3.2.5 Stimulation with hypotonic or isotonic media

For hypotonic/isotonic stimulations, BMDM were first changed to serum-free media containing drugs or vehicle (DMSO) where applicable, and incubated for 15 minutes. Hypotonic (Hypo) conditions were induced by adding an equal volume of sterile, low-endotoxin cell culture-grade water (Hyclone), or for isotonic (Iso) controls sterile PBS (without $\text{Ca}^{2+}/\text{Mg}^{2+}$) was used. Thus, hypotonic stimulation entailed a 50% reduction in medium osmolarity, whereas isotonic stimulation maintained osmolarity but the concentration of media components such as amino acids, glucose and Ca^{2+} were still reduced by 50% as in the hypotonic condition. In experiments using drugs, these were present in both the media and added PBS/water. For AKT phosphorylation experiments, cells were serum-starved for 1h prior to beginning the assay.

3.2.6 RNA isolation

For RNA extractions, Purelink DNA/RNA purification kits (Invitrogen) were used according to the manufacturer's instructions. DNase/RNase free barrier pipette tips were used throughout. In brief, BMDM were immediately placed on ice, media removed and replaced with 350µL lysis buffer containing 0.1% β-mercaptoethanol (Sigma). One volume of ice-cold 70% ethanol was added, and the lysate loaded onto spin columns, which were spun for 30s at 14,000xg. One wash with wash buffer 1 was performed, then 80µL of Purelink DNase I (Invitrogen) was added to each column and incubated for 15 minutes at room temperature. One more wash

with wash buffer 1 and two washes with wash buffer 2 were then performed, and the membrane dried by centrifuging for 2 minutes at 14,000xg. 30 μ L DNase/RNase-free water was then added to each membrane and incubated for 5 minutes. RNA was recovered by centrifuging for 2 minutes at 14,000xg into a clean 1.5mL Eppendorf tube. RNA concentration was determined using a NanoDrop T1000 spectrophotometer (ThermoFisher Scientific).

3.2.7 Quantitative polymerase chain reaction (qPCR)

To generate cDNA libraries for qPCR, SuperScript III kits (Invitrogen) were used according to the manufacturer's instructions. Briefly, 200ng RNA was combined with 1nmol dNTPs (Bioline) and 50ng random hexamers (Invitrogen), and heated to 65°C for 5 minutes in a Prime Elite thermocycler (Techne). 1 μ L SuperScript III was then added to each reaction, along with 1 μ L RNaseOUT (Invitrogen), 1 μ L DTT and 4 μ L 5x first-strand reaction buffer (Invitrogen). This mixture was reacted in a thermocycler for 60 minutes at 50°C followed by inactivation at 70°C for 15 minutes. The resulting cDNA was diluted to 1.66ng/mL with water for use in qPCR reactions.

For qPCR, a reaction mix was created by combining 5 μ L SYBR Green master mix (Invitrogen) with 1 μ L each of 700nM forward and reverse primers (200nM final concentration) per well. This mix was aliquoted into a MicroAmp 384-well optical PCR plate (Applied Biosystems), and cDNA added in triplicate wells per sample by pipetting 3 μ L (5ng total cDNA) under the rim of each well to prevent mixing. For each primer pair, a standard curve was also run consisting of 4 10-fold serial dilutions of neat cDNA obtained from BMDM transfected with poly(dA:dT). The plate was then sealed and centrifuged briefly (30s at 500xg) to combine the cDNA and reaction mix. The plate was immediately assayed on a 7900HT Fast Real-Time PCR machine (Applied Biosystems) for 40 cycles with standard settings. Each sample was always run with the housekeeping gene GAPDH as a loading control.

Data were exported to Microsoft excel, where the standard curves were first used to estimate primer efficiency by first calculating the slope of the Ct values versus the negative log(10) dilution of cDNA. Efficiency was then determined as $10^{(-1/\text{slope})}$. For each sample, the average Ct value between the three replicates was calculated and used to estimate total cDNA abundance as follows: $\text{abundance} = \text{primer efficiency}^{(-\text{Ct})}$. Sample-wise abundances were

first normalised to GAPDH abundance to correct for loading differences, then further normalised to a control condition (typically untreated or isotonic-treated cells) to give fold-change values. Primer sequences are given in **Table 3.1** below.

Table 3.1: Primer sequences for qPCR

Gene	Direction	Sequence (5'-3')
<i>Ifnb1</i>	Forward	TGGGAGATGTCCTCAACTGC
	Reverse	CCAGGCGTAGCTGTTGTA CT
<i>Cxcl10</i>	Forward	CCACGTGTTGAGATCATTGCC
	Reverse	TCACTCCAGTTAAGGAGCCC
<i>Gapdh</i>	Forward	CAGTGCCAGCCTCGTCC
	Reverse	CAATCTCCACTTTGCCACTGC
<i>Rsad2</i>	Forward	TGGTTCAAGGACTATGGGGAGT
	Reverse	CTTGACCACGGCCAATCAGA
<i>Il1b</i>	Forward	CCACAGACCTTCCAGGAGAATG
	Reverse	GTGCAGTTCAGTGATCGTACAGG
<i>Ccl7</i>	Forward	CCCTGGGAAGCTGTTATCTTCAA
	Reverse	CTCGACCCACTTCTGATGGG

Primer sequences identified via Primer-BLAST (<https://www.ncbi.nlm.nih.gov/tools/primer-blast/>) against *Mus musculus* mRNA transcript sequences indicated. Primers were chosen to span exon-exon junctions in all cases except *Ifnb1*, which is a single-exon gene.

3.2.8 RNA Sequencing

RNA was submitted to the genomic technologies core facility at the University of Manchester, sequenced and differential expression analysis conducted as described in **2.2.9**.

3.2.9 RNA Sequencing Data Analysis

Gene-wise read count data were analysed in Rstudio 1.4 (R Core Team, 2021). Initial filtering was conducted to remove genes which did not achieve at least 50 corrected counts in at least 3 samples. Subsequently, for each comparison differentially expressed genes were identified based on Log₂FC values of > 0.5 in either direction and FDR-adjusted *p* value (*p*_{adj}) < 0.05. Heatmaps were created using the pheatmap package, and volcano plots generated using ggplot.

Gene set enrichments were conducted using the EnrichR platform queried through the EnrichR R package from Rstudio. Results were exported to Microsoft Excel for further processing in Prism (visualisation) or Cytoscape (enrichment maps). For enrichment maps, Cytoscape 3.1.9 was used, running the enrichmentmap package. Data were first processed in excel to conform to the expected format, including (for each significant gene set) the name, direction (+1 or -1

for upregulated versus downregulated gene sets, respectively), FDR-adjusted p value and tab-delimited list of genes identified in each set. Using this data, clusters were built from significant ($p_{adj} < 0.05$) gene sets using the yfiles organic layout, with Jaccard + Overlap edge calculation (cutoff 0.43). The resulting enrichment map was manually labelled according to common biological themes within each cluster, and the layout altered slightly for easier annotation and clarity.

K-means clustering was performed on DEGs identified between the WT Hypo and KO Hypo conditions as follows: sample-wise gene counts were averaged to produce mean counts for each condition, from which Z-scores were calculated using the `scale()` function, and the resulting matrix clustered using the `kmeans()` function with a k value of 5. Thus, genes were assigned to clusters based on the overall average expression pattern between conditions, thereby reducing the influence of batch effects and intra-group variability on cluster generation.

Ingenuity Pathway Analysis (IPA) was run on the indicated DEG classes to infer causal changes in upstream regulators. Briefly, the analysis was run using the default settings, and upstream analysis was restricted to all regulator types excluding non-endogenous chemicals, considering only high-confidence (i.e. experimentally validated) causal relationships. IPA performs two steps in regulator analyses – initially a list of the highest-confidence regulators is created based on known regulators whose known gene expression effects best overlap with the gene perturbations in the dataset. Next, known relationships between regulators are used to identify likely regulator networks which co-operatively explain the identified gene expression changes and identify putative master regulators. These causal networks were extracted and graphed, focusing on kinases and transcription factors with Z-scores of >2 in either direction, corresponding to activated and suppressed regulators, respectively. Genes predicted to be affected by each master regulator were extracted from the table of regulators produced by IPA. Only regulators with network bias-adjusted p values of < 0.05 were considered.

3.2.10 Western Blot

For protein extraction, cells were placed on ice immediately, media aspirated and lysed in a small volume of laemmli buffer (62.5mM Tris-HCl, 10% glycerol, 5% β -mercaptoethanol, 2%

SDS and 0.002% bromophenol blue) with 10% PhosStop (Roche). Lysates were collected into tubes and denatured by boiling at 95°C for 10 minutes. Proteins were then separated on 10% Tris-glycine polyacrylamide gels and transferred to PVDF membranes. Membranes were blocked in tris-buffered saline (TBS) with 0.05% Tween-20 (TBST) with 5% BSA for one hour, before incubating with primary antibody (see **Table 3.2**) in block buffer overnight at 4°C with constant rolling. Membranes were then washed 3x in TBST for 5 minutes each and incubated with anti-rabbit IgG HRP-conjugated secondary antibody for 1h at room temperature in block buffer. Following 3 more washes, bands were visualised on a G:Box Chemi XX6 (Syngene) with using Amersham ECL Prime chemiluminescence substrate (GE Healthcare).

For phosphorylated protein blots, two separate gels were run simultaneously, and probed separately for phosphorylated and total protein. Following initial imaging, membranes were incubated with HRP-conjugated anti- β -actin loading control antibody and re-imaged following 3 additional washes. For densitometry analysis, the intensity of phosphorylated and total protein bands was calculated in ImageJ and normalised to the intensity of their respective β -actin control. Then, the normalised phospho-band intensity was divided by the normalised total protein intensity, and the resulting phospho/total ratios centred by dividing by the mean value for each gel.

Table 3.2: Primary and secondary antibodies for western blot

Target	Host	Supplier	Concentration
AKT (phospho-S473)	Rabbit	Cell Signalling #9271	1:1000
AKT (total)	Rabbit	Cell Signalling #9272	1:1000
TBK1 (phospho-S172)	Rabbit	Cell Signalling #5483	1:1000
TBK1 (Total)	Rabbit	Cell Signalling #3504	1:1000
Phospho-PKC substrate	Rabbit	Cell Signalling #6967	1:1000
Rabbit IgG (HRP secondary)	Goat	Dako #P0448	1:1000
β -Actin (HRP conjugated)	Mouse	Sigma #A2228	1:20,000

3.2.11 Statistics

Unless otherwise stated, data were analysed in GraphPad Prism 9.0 (GraphPad). Data with two independent groups were compared via Student's *t* test. Where >2 conditions were present, one-way or two-way ANOVA was performed. For comparing all conditions to one

control condition, Dunnet's *post-hoc* test was used, and for any other comparisons Tukey's test was used. Data were checked for normal distribution using Shapiro-Wilk tests and for equal standard deviation using Brown-Forsythe tests. Where non-normal distribution or unequal SD were present, an appropriate transformation (e.g. log₁₀) was applied prior to testing. Data are presented as mean ± SEM. All data points represent individual mice.

3.3 Results

3.3.1 Hypotonicity induces transcriptomic changes which are modulated by LRRC8A

LRRC8A/VRAC function in macrophages remains largely mysterious. Its role as a mediator of cell volume reduction in the context of osmotic swelling has been well demonstrated, yet it is unclear what physiological or pathological scenarios this function might be relevant to *in vivo*. Thus, these experiments sought to establish what cellular pathways are altered following swelling induced by osmotic stress, with a view to inferring likely roles of swelling responses in macrophage function *in vivo*. Moreover, using LRRC8A-KO mice, roles for VRAC (or LRRC8A itself) in regulating these processes could be examined.

In an initial pilot experiment, RNA-sequencing was used to assess what, if any, transcriptomic differences might occur between WT and KO macrophages under conditions of hypotonicity. Primary BMDMs generated from WT, KO and Cre mice were either lysed in the absence of stimulus to check for any baseline differences between genotypes, or after a 4h treatment with 50% hypo-osmotic media (WT and KO only) (**Figure 3.1A**). Initial analysis of the resulting gene-wise read counts was conducted via PCA, which indicated close clustering of the three unstimulated groups (**Figure 3.1B**). By contrast, the WT and KO groups stimulated with hypotonic media separated from the unstimulated groups and from each other along PC1, with the hypotonic-stimulated KO cells exhibiting an apparently greater distance from the unstimulated controls. This analysis indicates that, whilst the unstimulated BMDMs are very similar, hypotonicity induces transcriptomic changes which are differentially regulated between WT and KO cells.

Differential expression analysis confirmed that the unstimulated cells were highly similar, with extremely low numbers of differentially expressed genes (DEGs; Log₂-fold change > 0.5 and FDR-adjust *p* value < 0.05) between KO and WT (2 genes), KO and Cre (6 genes), and Cre vs WT cells (4 genes) (data not shown). Hypotonic treatment induced a large transcriptomic response, with 6315 differentially expressed genes detected between hypotonic-stimulated and control WT cells (3473 upregulated, 2842 downregulated) (**Figure 3.1C**).

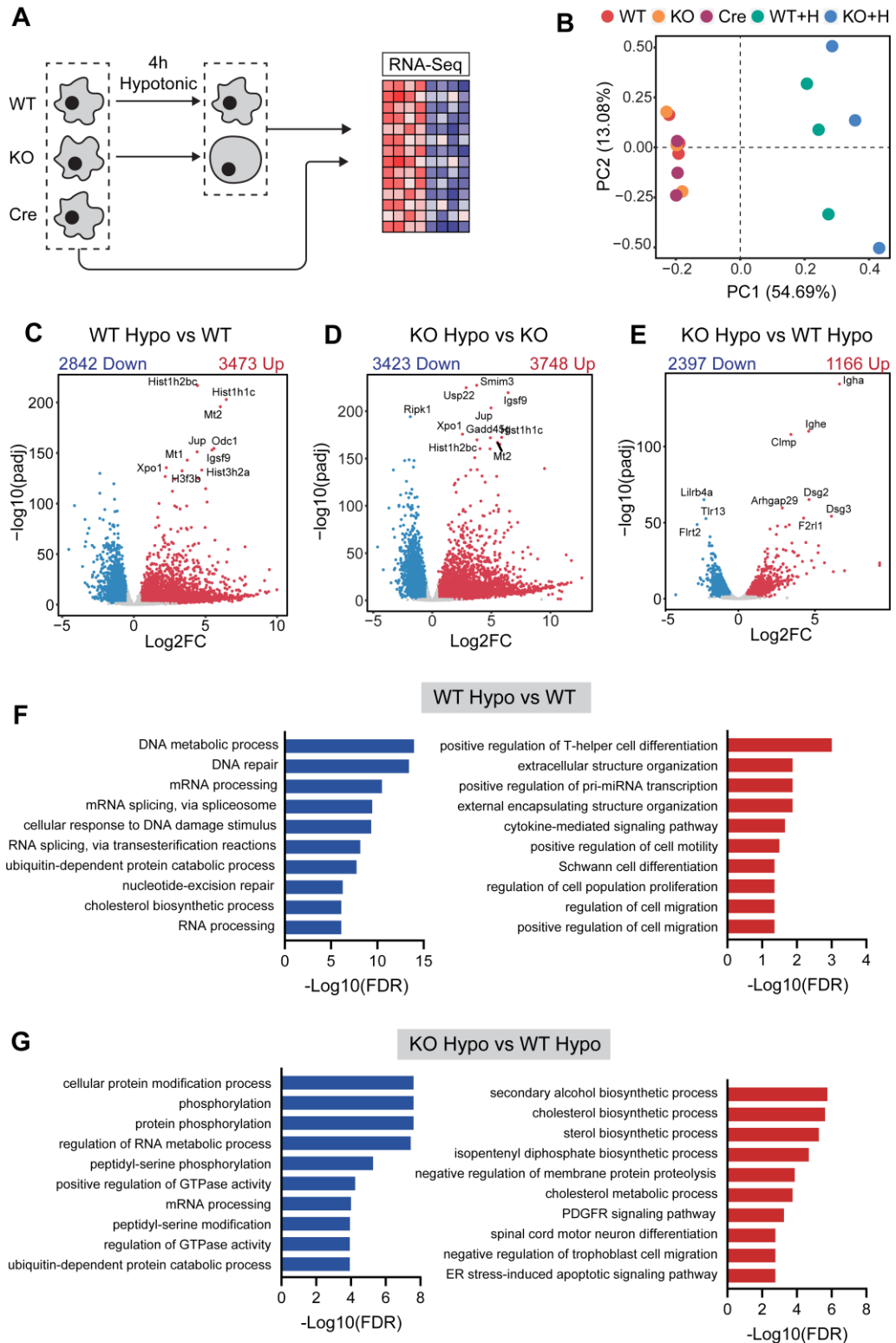


Figure 3.1: Hypotonicity induces transcriptomic changes in BMDM:

(A) $n = 3$ Wild-type (WT), LRR8A knockout (KO) and Cre bone marrow-derived macrophages (BMDM) were sequenced following either no stimulation or 4h stimulation with 50% hypotonic (hypo) media (WT and KO only). (B) PCA of gene expression changes between the 5 groups. (C-E) Volcano plots showing differentially regulated genes identified between hypotonic and unstimulated WT cells (C), Hypotonic versus unstimulated KO cells (D) or between WT and KO cells under hypotonic conditions (E). (F-G) Downregulated (blue) and upregulated (red) gene sets identified in WT cells stimulated with hypotonic media (F), and between hypotonic stimulated KO and WT cells (G). H = hypotonic.

Similarly, KO cells exhibited 7171 differentially expressed genes upon hypotonic stimulation (3748 upregulated, 3423 downregulated) (**Figure 3.1D**). Substantial differences in the response to hypotonicity were also observed between WT and KO cells, with 3563 total genes differentially expressed, of which 1166 were upregulated and 2397 were downregulated (**Figure 3.1E**). Thus, not only does hypotonicity elicit large changes in patterns of gene transcription, LRRC8A exerts a significant influence over the response.

Enrichment analysis of hypotonicity-induced DEGs identified in WT cells indicated downregulation of various pathways, including DNA and RNA metabolic processes, as well as cholesterol biosynthesis. Upregulated pathways suggested some regulation of immune responses, including cell migration and cytokine signalling (**Figure 3.1F**). Enrichments performed on differentially expressed genes between WT and KO cells under hypotonic conditions suggested relative downregulation of genes involved in protein modification and RNA metabolism, and upregulation of various biosynthetic processes (**Figure 3.1G**). As such, these results suggest that osmotic swelling induces co-ordinated changes in gene expression reflecting altered cellular functions which are, to some extent, controlled by LRRC8A. Thus, this model produces clear LRRC8A-dependent effects on macrophage physiology which could provide some insight into its functions *in vivo*.

3.3.2 Hypotonicity-induced gene expression is differentially modulated by DCPIB and LRRC8A-KO

To gain a deeper insight into the role of LRRC8A in modulating the response to hypotonicity, one further sequencing experiment was performed. In this round, WT and KO cells were stimulated with hypotonic media in the presence or absence of DCPIB to block VRAC channel activity (**Figure 3.2A**). A control group consisting of WT cells stimulated with PBS was also included (WT Iso control), though no KO PBS control was included due to the extreme similarity between the two genotypes at baseline. The inclusion of DCPIB should enable delineation of VRAC-dependent effects (i.e. those resulting from differential activity of the VRAC channel) from LRRC8A-dependent effects arising through altered signalling and independent of channel activity. The resulting expression data appeared broadly similar to the pilot experiment (**Figure 3.1**), with PCA analysis indicating large hypotonicity-dependent effects and separate clustering of WT and KO cells along PC1 and, in this dataset, along PC2

(**Figure 3.2B**). DCPIB treatment induced a shift in WT cells along PC1, but not PC2, and did not appear to phenocopy the effect of LRRC8A KO. Expectedly, the effect of DCPIB in KO cells was less pronounced.

Differential expression analysis again uncovered large numbers of DEGs in both hypotonic-stimulated WT and KO cells compared to PBS, and to each other, confirming the presence of a large hypotonicity effect with significant modulation by LRRC8A (**Figure 3.2C-E**). Many genes differentially expressed in the first round of sequencing were also identified as DEGs in this round, confirming that hypotonicity induces a robust, reproducible effect. Interestingly, DCPIB treatment resulted in comparatively few differentially expressed transcripts in WT cells compared to LRRC8A KO, and also induced a significant number of DEGs in KO cells (**Figure 3.2F-G**). Thus, DCPIB did not appear to mimic the effect of LRRC8A ablation particularly strongly and exhibited considerable off-target effects in LRRC8A-KO cells. These data imply that the effect of LRRC8A ablation on hypotonicity-induced gene expression patterns may be largely independent of VRAC channel activity.

To characterise the cellular response to hypotonicity, DEGs identified in WT cells stimulated with hypotonicity (**Figure 3.3A**) were used for enrichment analysis, searching the KEGG, Reactome, MSigDB, WikiPathways and Gene Ontology databases for enriched terms via the EnrichR platform (Chen et al., 2013). Large numbers of significantly enriched gene sets were found for both upregulated and downregulated genes, the 10 most highly significant of which in either direction are displayed in **Figure 3.3B-C**. The highest confidence upregulated gene sets point to regulation of inflammatory responses, including interferon signalling, as well as genes related to hypoxia (**Figure 3.3B**), whereas the top downregulated gene sets are dominated by those relating to mRNA processing (**Figure 3.3C**). Due to the presence of many highly similar gene sets, a better overview of the landscape of the response can be obtained using an enrichment map (**Figure 3.3D**), whereby gene sets were clustered by degree of gene overlap and labelled according to common themes between sets. This visualisation additionally highlighted a variety of differentially regulated gene sets, such as those related to cholesterol biosynthesis, DNA repair, cell cycle and proteostasis.

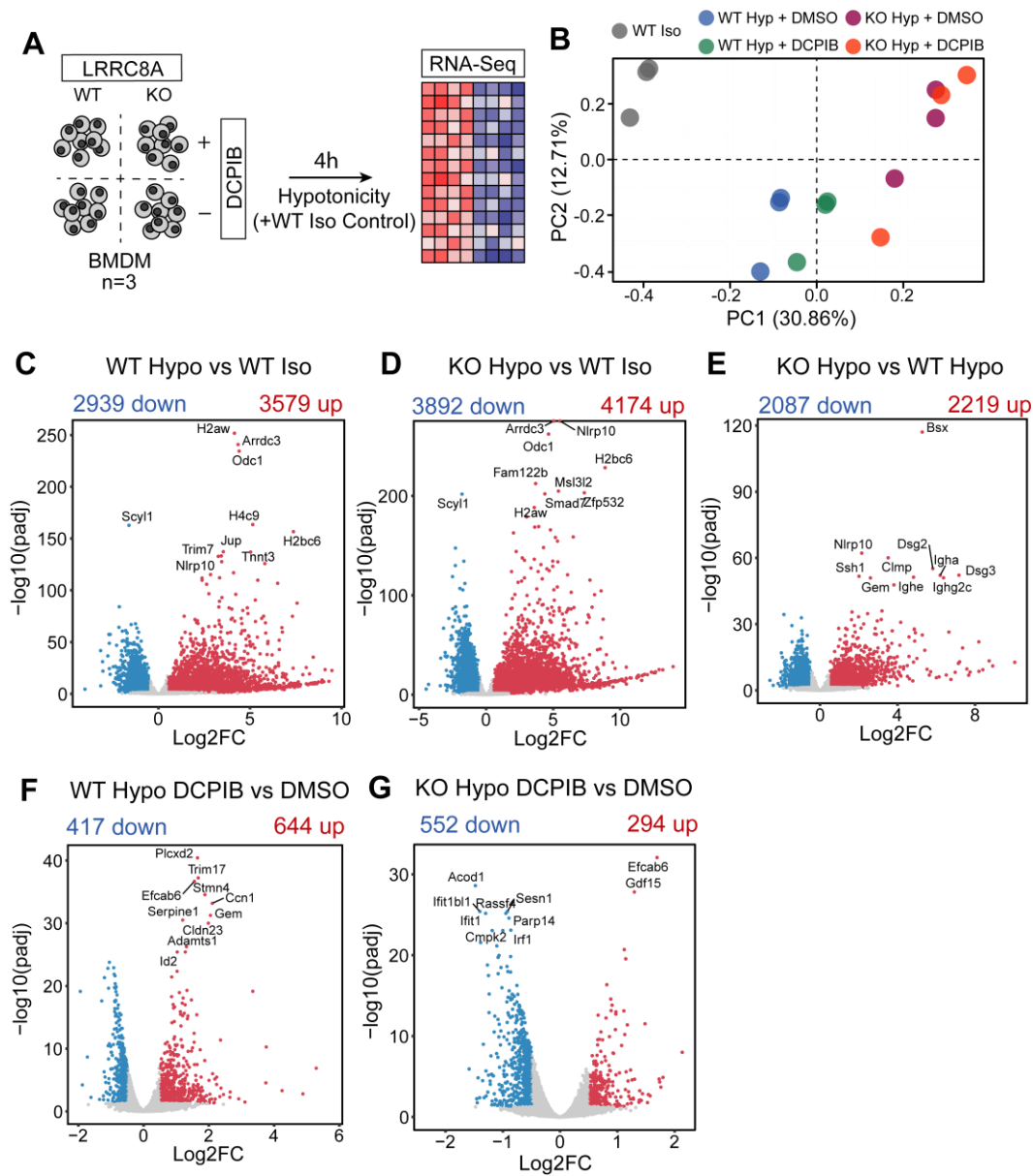


Figure 3.2: Modulation of hypotonicity-induced gene expression by LRRC8A and DCPIB: (A) Bone marrow-derived macrophages (BMDM) from $n = 3$ wild-type (WT) and LRRC8A knockout (KO) mice were stimulated with 50% hypotonic (hypo) media containing either vehicle (DMSO) or $10\mu\text{M}$ of the VRAC channel blocker DCPIB. A WT group stimulated with isotonic (iso) media was included as a control. (B) PCA plot of gene expression variability between the 5 experimental groups (C-G) Volcano plots showing differentially expressed genes identified between WT cells stimulated with iso or hypo media (C), Hypotonic-treated KO cells versus WT isotonic (D), KO versus WT hypotonic-treated cells (E), WT (F) or KO (G) cells treated with hypotonic media containing DCPIB versus DMSO.

As expected, there was also a large cluster of upregulated gene sets related to interferon signalling, as well as some indicating regulation of inflammation and apoptosis. Overall, these data indicate that hypotonicity induces a wide range of effects on cellular physiology.

3.3.3 Hypotonicity induces antiviral signalling

Given the extensive transcriptomic effects of hypotonic shock, ingenuity pathway analysis (IPA) was used to gain insight into what signalling pathways might be responsible for the effects observed. Initially, DEGs identified between hypotonic and isotonic-treated WT cells (**Figure 3.2C**) were considered, and causal networks of likely regulators were identified in IPA. The 10 transcription factors and kinases with the highest positive and negative Z-scores are shown in **Figure 3.4A**. Interestingly, some of regulators predicted to be activated by hypotonicity are core components of antiviral signalling pathways (IRF2/3/7, STAT1, TAK1), and some predicted to be inhibited are known antagonists of these pathways (SPDEF, TRIM24). Moreover, the transcription factor SREBF2, which controls cholesterol biosynthetic genes, was predicted to be repressed following hypotonic shock, which is also known to occur following interferon stimulation (Robertson & Ghazal, 2016). Other activated regulators for this dataset included sensors of cytosolic nucleotides (MAVS, RIG-1, cGAS and DNA-PK), which are known to activate IRF-dependent transcriptional responses via STING, as well as interferon beta (IFNB1) and the DNA damage sensors ATM/ATR and p53 (**Figure 3.4B**). Thus, this analysis implies that hypotonic shock induces some degree of antiviral response, which may relate to activation of DNA sensors. Accordingly, a large number of genes with known antiviral effector functions (**Figure 3.4C**), as well as genes known to be interferon-responsive (**Figure 3.4D**), were upregulated following hypotonic shock. Additionally, induction of various cytokines, chemokines, and other genes involved in inflammatory responses was observed (**Figure 3.4E**). Whilst most interferon genes were not present at detectable levels, interferon beta was significantly upregulated (**Figure 3.4E**). Thus, the transcriptional response to hypotonic swelling is consistent with induction of an antiviral state, likely mediated by DNA sensing pathways.

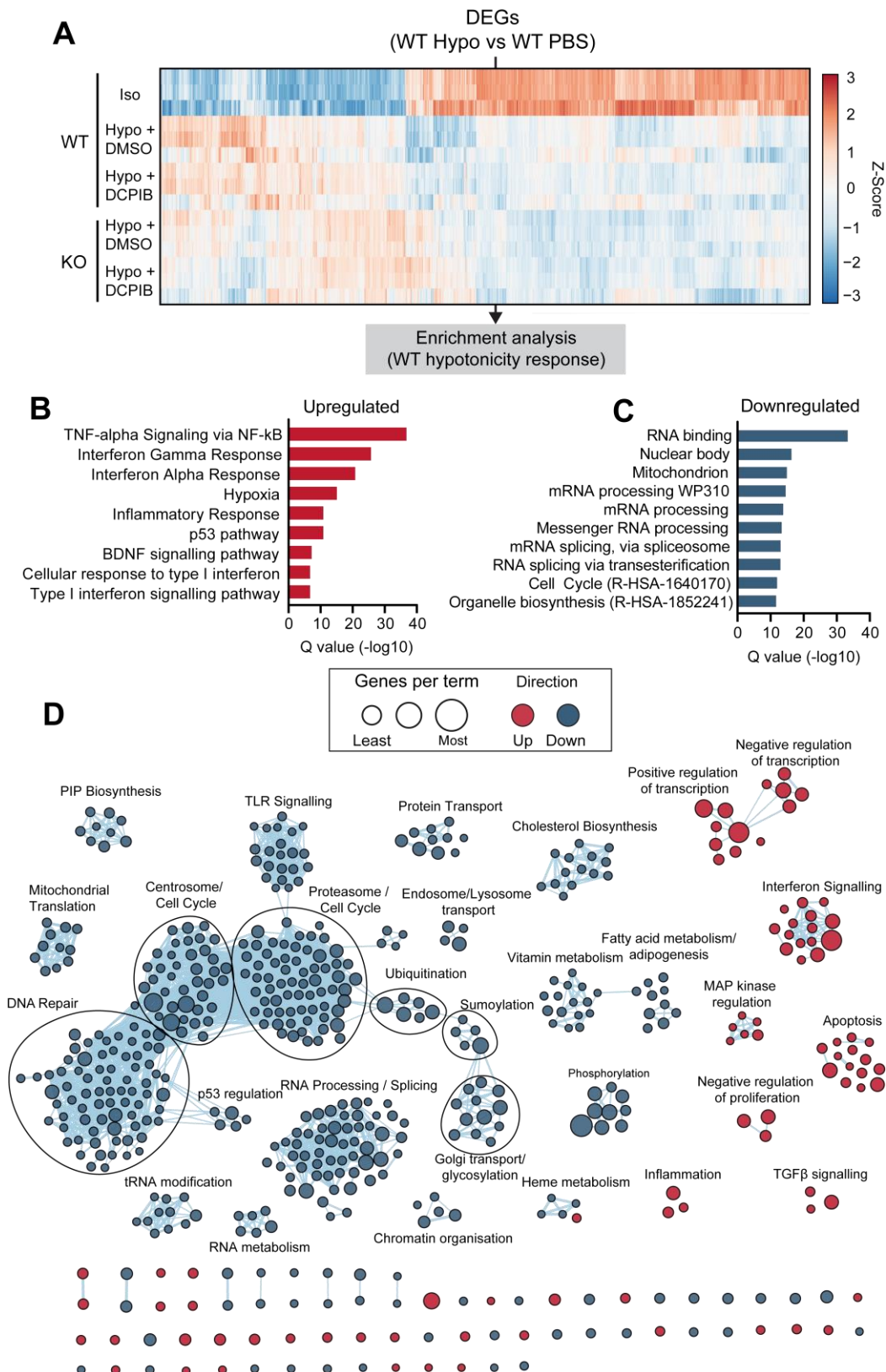


Figure 3.3: Hypotonicity induces wide-ranging changes in cellular physiology:

(A) Heatmap displaying expression patterns of genes found to be significant in the wild-type (WT) hypotonic (hypo) vs WT isotonic (iso) comparison (Figure 3.2C) and used for enrichment analysis. (B-C) Top 10 upregulated (B) and downregulated (C) gene sets identified between WT Hypo vs WT PBS groups, by adjusted p value (Q value). (D) Enrichment map showing all identified upregulated (red) and downregulated (blue) gene sets responsive to hypotonicity. Nodes represent gene sets, connected by lines indicating the degree of overlap between sets, and clustered by similarity.

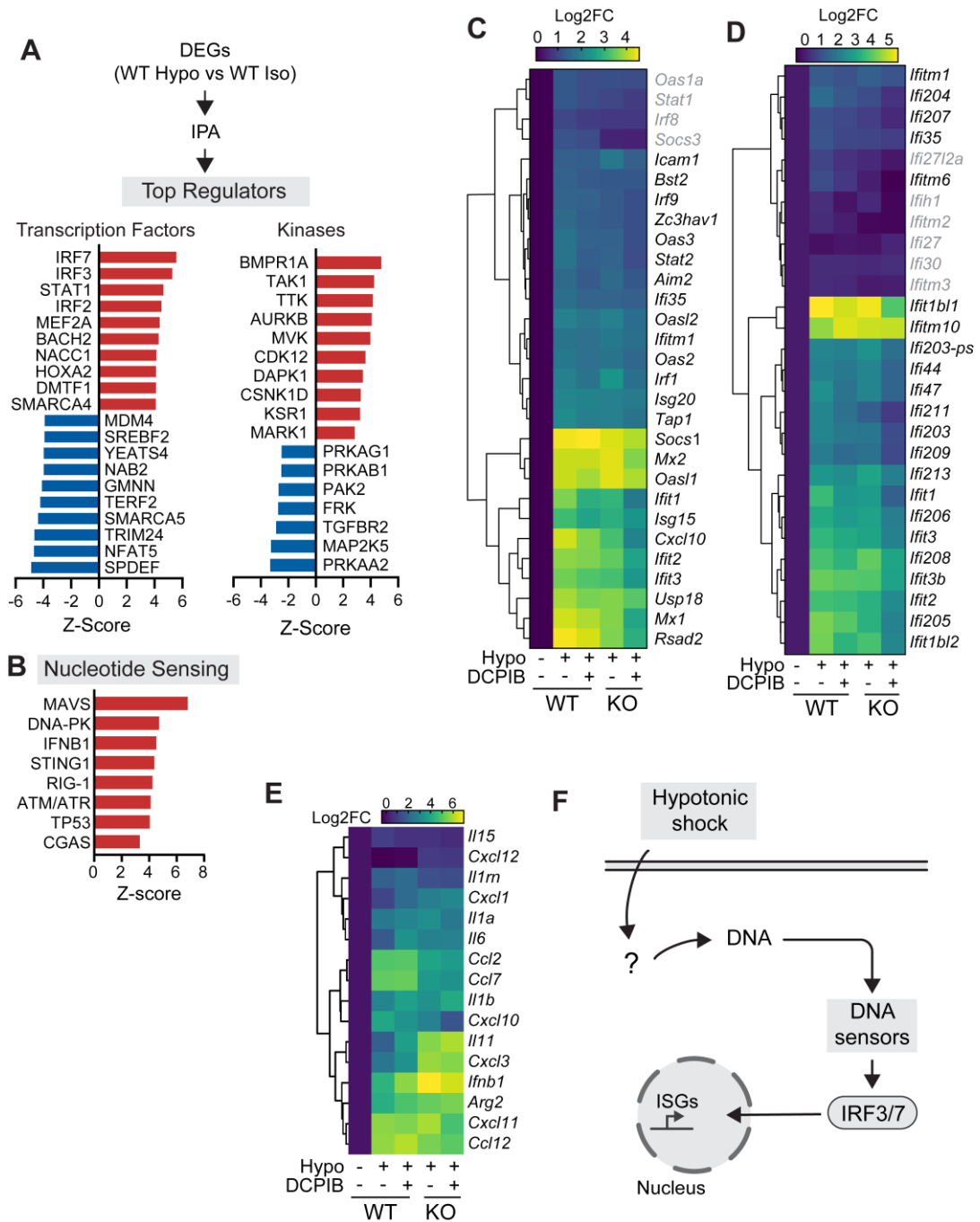


Figure 3.4: Antiviral response pathways are activated by hypotonic shock

(A) Differentially expressed genes between hypotonic (Hypo)- and isotonic (Iso)-stimulated wild-type (WT) bone marrow-derived macrophages (BMDM) (Figure 3.2C) were analysed via IPA and causal regulators predicted with adjusted p values < 0.05 identified. The top 10 transcription factors and kinases with positive and negative z-scores are given, ordered by z-score. (B) Additional regulators involved in nucleotide sensing, ordered by z-score. (C-E) Heatmaps of gene expression data for genes involved in antiviral defence (C), genes stimulated by interferons (D) and selected inflammatory genes (E). Expression across all groups is displayed, genes in black/grey denote significant/non-significant FDR-adjusted p values for the WT hypo vs WT iso comparison, respectively. Log2 fold-change (Log2FC) values were calculated relative to the WT iso condition. (F) Schematic displaying proposed signalling pathways based on IPA regulator analysis.

3.3.4 LRRC8A-dependent signal modulation under hypotonic conditions

To examine the role of LRRC8A in mediating the transcriptomic response to hypotonicity, DEGs identified between the WT and KO hypotonic-treated cells groups were analysed. For this analysis, upregulated and downregulated genes could not be designated simply based on the fold-change value between the two groups, since this could indicate either exacerbation or reduction of the response observed in WT cells. Therefore, K-means clustering was performed to build gene clusters reflecting overall expression patterns between WT isotonic, WT hypotonic and KO hypotonic samples. Using this approach, 5 main clusters were apparent, corresponding to responses exaggerated (clusters 1 and 3), or blunted (clusters 2 and 4) by LRRC8A KO (**Figure 3.5A**). Cluster 5 consisted largely of genes downregulated only in KO cells treated with hypotonicity. To focus on transcriptional perturbations requiring LRRC8A (i.e. reduced/absent in KO cells), clusters 2 and 4 were analysed to identify LRRC8A-dependent signalling pathways via IPA. This analysis predicted reduced activity in the antiviral transcription factors IRF3/7, as well as increased activity at various negative regulators of interferon signalling (SPDEF, NLRC5, ARID5A), thus implying that the presence of LRRC8A modulates generation of the antiviral response in hypotonic conditions (**Figure 3.5B**). Interestingly, this analysis also predicted defective activity downstream of various kinases well-known for their important signalling functions, including the Src family kinase Fyn, the MAP kinase TAK1, and protein kinase C delta (PRKCD). Most strikingly, three components of the PI3K complex (PIK3R1/2, PIK3CD) were predicted to have decreased activation, as well as the downstream kinase PDK2 and the upstream adapter GAB1 (**Figure 3.5C-D**). Additionally, the transcription factor FOXO4, which known to be inhibited by AKT downstream of PI3K, was also predicted to be activated. As such, these data imply that LRRC8A modulates various signalling pathways upon hypotonic stimulation, and may contribute to the induction of antiviral responses. Since a number of genes regulated by IRF3 were also identified as PI3K targets by IPA, it is also possible that PI3K signalling modulates IRF3-dependent responses under hypotonic conditions (**Figure 3.5E**).

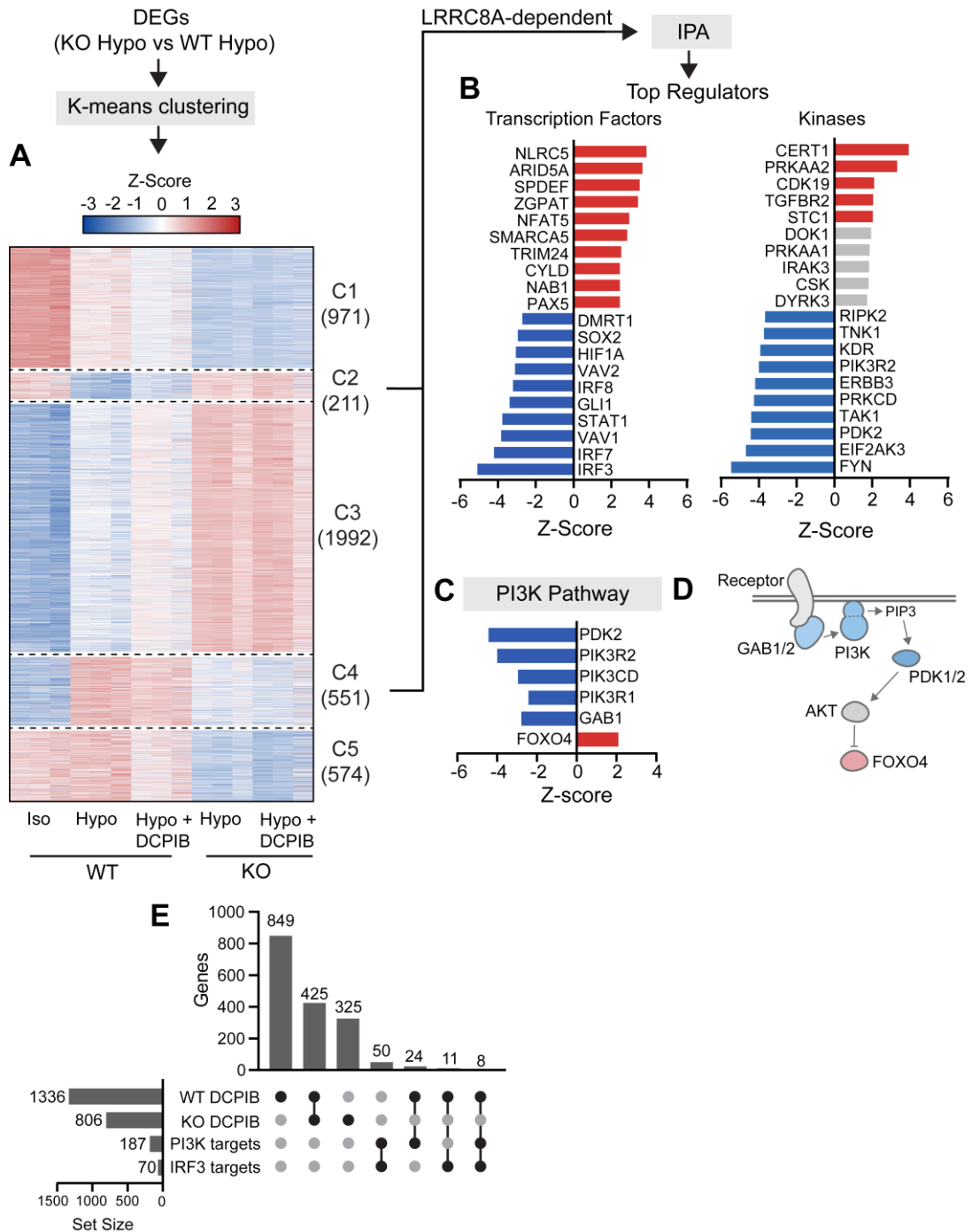


Figure 3.5: LRR8A modulates multiple signalling pathways independently of DCPIB:

(A) Heatmap visualising the results of K-means clustering for DEGs significant between the LRR8A knockout (KO) hypotonic (hypo) and wild-type (WT) hypo conditions in bone marrow-derived macrophages (BMDM). (B) Top regulators identified via IPA for the LRR8A-dependent response (clusters 2 and 4). (C-D) Regulators from the PI3K pathway predicted to be altered under hypotonic conditions, ordered by predicted z-score (C) and depicted in a schematic (D). (E) UpSet plot displaying intersectionality between genes significantly altered by DCPIB in WT and KO cells (WT DCPIB and KO DCPIB, respectively), as well as PI3K pathway and IRF3 targets identified in clusters 2 and 4. Total set size is displayed on the left-hand graph, and the number of genes for each intersection (depicted by dots and connecting lines) is represented in the top graph.

To examine whether LRRC8A-dependent effects were related to VRAC channel activity or to unrelated signalling functions, the effect of LRRC8A knockout was contrasted with the effect of DCPIB treatment in both WT and KO cells, according to the following criteria: each perturbation significant between KO and WT Hypo-treated cells was considered DCPIB-sensitive if DCPIB treatment elicited a statistically significant change in the same direction in WT cells, but failed to do so in KO cells. Overall, of the 4299 DEGs identified between KO and WT hypo-treated cells, only 1336 were affected by DCPIB treatment in WT cells. Of these, 425 were also perturbed in the same direction in KO cells and therefore likely reflected activity at targets other than LRRC8A. Thus, only 911 genes appeared to be truly DCPIB-sensitive in this dataset. Of these genes, there was little overlap with PI3K or IRF3 targets identified in clusters 2 and 4, implying that LRRC8A-dependent modulation of PI3K and interferon responses is likely independent of VRAC channel function (**Figure 3.5D**).

3.3.5 LRRC8A restricts interferon responses following hypotonic shock

To further investigate the putative role of hypotonicity in generating interferon responses, as well as their modulation by LRRC8A, timecourse experiments were conducted whereby WT and KO BMDMs were stimulated with either isotonic or hypotonic media for 1, 2, 4 or 6 hours, and expression of the IRF3 targets interferon- β (*Ifnb*) and *Cxcl10* quantified by qPCR. Significantly enhanced expression of *Ifnb* was detected in KO cells compared to WT, beginning at 4 hours after hypotonic shock and maintained at 6h (**Figure 3.6A**). Indeed, WT cells did not appear to significantly induce *Ifnb* at any time point. By contrast, *Cxcl10* was significantly upregulated in both WT and KO cells by 4h and was significantly higher in KO cells compared to WT at 6h, but not earlier (**Figure 3.6B**). Increased expression of the interferon-stimulated genes *Rsad2* (**Figure 3.6C**) and *Ccl7* (**Figure 3.6D**) and the inflammatory cytokine *Il1b* (**Figure 3.6E**) was also observed 6h after hypotonic shock in both WT and KO cells, with significantly greater induction in KO than WT for all three genes. Additionally, phosphorylation of the IRF3 activator TBK1 at Ser172 was increased in KO cells relative to WT at 4 and 6 hours post-hypotonic stimulation (**Figure 3.6F**). As such, these data confirm that a type-I interferon response is activated in BMDM under hypotonic conditions via TBK1, which likely signals through IRF3. Moreover, loss of LRRC8A exacerbates the interferon response via a mechanism likely acting upstream of TBK1.

Since the previous analysis indicated that DNA-sensing pathways might underly the interferon response in hypotonicity (**Figure 3.4**), further experiments were conducted using the DNA mimetic A151, which antagonises DNA sensing, as well as the STING inhibitor H151. Hypotonicity-induced expression of both *Ifnb* and *Cxcl10* was significantly inhibited by both compounds in KO cells (**Figure 3.6G,H**). Despite a similar trend toward inhibition of *Cxcl10* expression in WT cells, no significant differences were observed, which may reflect much lower hypotonic induction in this group (**Figure 3.6H**). This result confirms that hypotonicity-induced antiviral signalling results from DNA-dependent activation of STING-TBK1, in a manner which is drastically increased by LRRC8A KO. To check whether LRRC8A also affects interferon responses to exogenous DNA, WT and KO BMDM were transfected with poly dA:dT under normal conditions and secretion of IFN- β measured by ELISA. As expected, both genotypes exhibited significantly increased IFN- β secretion upon poly(dA:dT) transfection, yet no differences in IFN- β protein secretion were observed between the two genotypes (**Figure 3.6I**). This implies that LRRC8A is not a universal regulator of antiviral signalling, and likely modulates interferon responses in a context-specific manner requiring particular stimuli.

3.3.6 LRRC8A modulates interferon responses independently of VRAC channel activity

Having observed a strong effect of LRRC8A deletion in promoting exaggerated interferon responses to hypotonic shock, subsequent experiments explored the idea that this may occur due to defective VRAC activity in LRRC8A KO cells. LRRC8A-containing VRACs are known to modulate cGAS-dependent STING activation by conducting cGAMP across the plasma membrane (Lahey et al., 2020; Zhou, Chen, et al., 2020). It is therefore possible that the increased interferon response in KO cells results from reduced cGAMP release downstream of DNA-dependent cGAS activation, resulting in increased intracellular cGAMP accumulation. However, it is unclear whether BMDMs conduct cGAMP in sufficient quantities to produce such an effect. To assess the relative permeability of BMDM to cGAMP, WT and KO BMDM were incubated with cGAMP under either isotonic or hypotonic conditions for 3h, and expression of *Ifnb* and *Cxcl10* assessed by qPCR. L929 fibroblast cells, which are known to transport cGAMP well, were included in parallel as a comparison cell type (Zhou, Chen, et al., 2020).

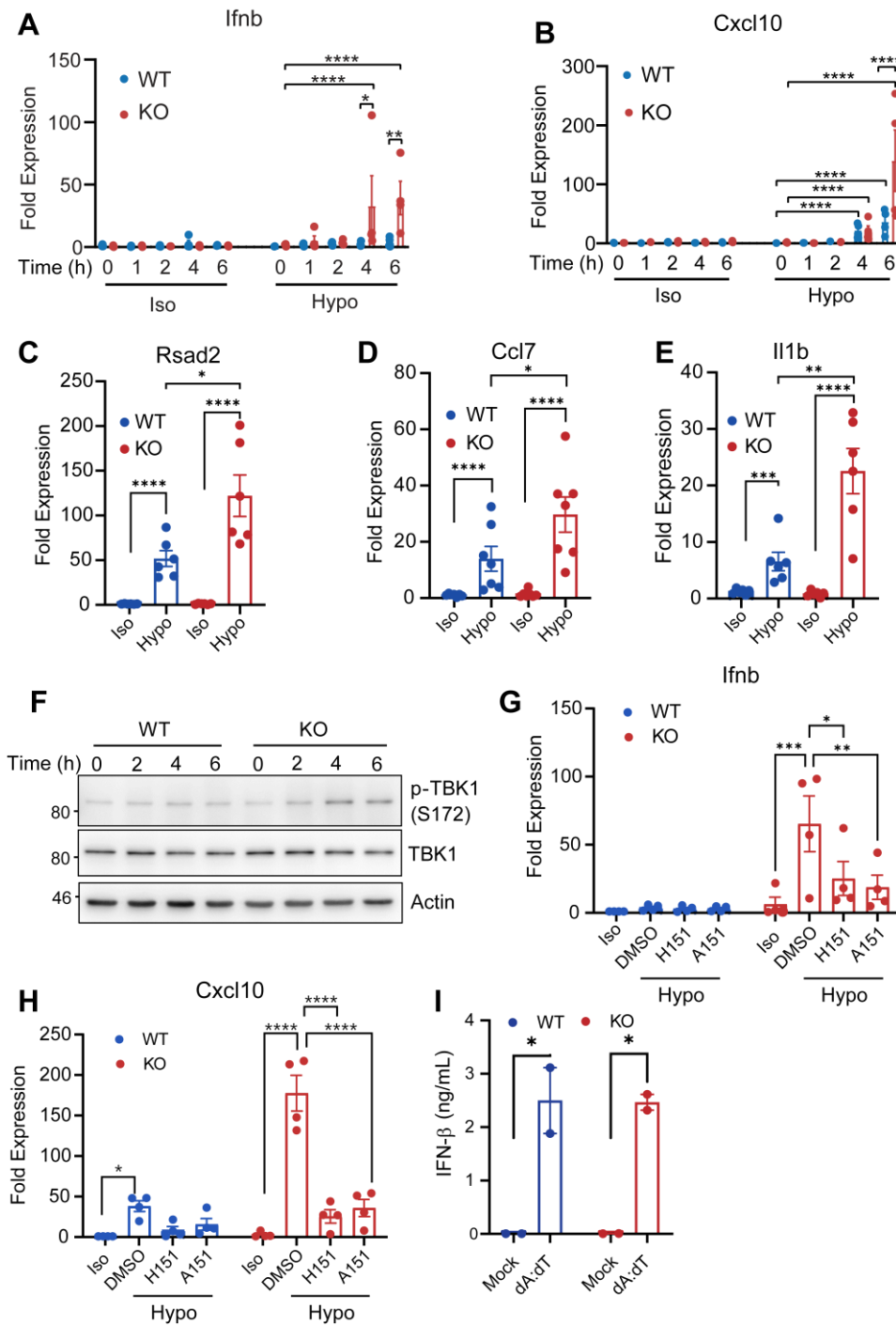


Figure 3.6: LRR8A KO exacerbates interferon responses following hypotonic shock: (A,B) Timecourse of interferon beta (*Ifnb*; A) and *Cxcl10* (B) expression of mRNA following treatment of wild-type (WT) and LRR8A knockout (KO) bone marrow-derived macrophages (BMDM) with 50% hypotonic (Hypo) or isotonic (Iso) media (n = 4). (C-E) mRNA expression of *Rsad2* (C), *Ccl7* (D) and *Il1b* (E) in WT and KO BMDM after 6h treatment with isotonic or hypotonic media. (F) Western blot showing total and phosphorylated (Ser172) TBK1 at in WT and KO BMDM at various timepoints following either PBS or hypo treatment (representative of n = 3). (G,H) Expression of *Ifnb* (G) and *Cxcl10* (H) mRNA in WT and KO BMDM at 6h following treatment with isotonic or hypotonic media containing either vehicle (DMSO), the STING inhibitor H151 (10 μ M) or the DNA mimetic A151 (1 μ M) (n = 4). (I) IFN- β protein secretion from WT and KO BMDM either mock-transfected or transfected with poly(dA:dT) for 6h (n = 2). Data are presented as mean \pm SEM. Expression data were acquired via qPCR, normalised to GAPDH expression for each sample, and within each experiment to the WT PBS condition. Statistics in A-E and G-I are from two-way ANOVA with Dunnet's post-hoc. * $p < 0.05$, ** $p < 0.01$, *** $p < 0.001$, **** $p < 0.0001$.

Indeed, L929 cells responded well to cGAMP, particularly under hypotonic conditions, displaying roughly 150-fold induction of *Irfn* and 700-fold induction of *Cxcl10* (**Figure 3.7A,B**). While WT BMDM also exhibited small (10-20-fold) but statistically significant induction of *Irfn* and *Cxcl10* in response to cGAMP, this was extremely low compared to L929 cells, indicating generally poor cGAMP permeability in BMDM (**Figure 3.7A,B**). KO cells did not exhibit significant responses to cGAMP under any conditions tested. Thus, while BMDM do appear to transport small quantities of cGAMP, they do so with very low efficiency, particularly compared with L929 cells, in which cGAMP is readily transported. This apparent lack of cGAMP permeability may reflect high expression of LRRC8D and low levels of LRRC8E in BMDM, which is an unfavourable configuration for cGAMP transport (**Figure 3.7C**). Thus, these data suggest that defective release of intracellular cGAMP is not the mechanism by which LRRC8A-KO exacerbates interferon responses to hypotonic shock.

It is also possible that loss of LRRC8A could affect antiviral signalling under hypotonic conditions due to defective cell volume regulation, or due to other effects depending on solute transport. To assess whether other ion channel-dependent effects could contribute to restriction of antiviral signalling, WT and KO BMDM were treated with isotonic or hypotonic media in the presence of either vehicle or the VRAC inhibitors DCPIB, NPPB or FFA. *Irfn* expression was generally unaffected by VRAC inhibition in WT cells, though trends towards reduction were observed in KO cells (significant for FFA only) (**Figure 3.7D**). VRAC inhibitors produced trends towards *Cxcl10* reduction in both genotypes, though the only statistically significant reduction was for NPPB in KO cells (**Figure 3.7E**). Thus, blocking VRAC channel activity in WT cells does not reproduce the effect of LRRC8A KO on antiviral signalling, which suggests that defective cell volume regulation or solute transport is not the primary cause of enhanced interferon responses in KO cells. As such, these data, along with the transcriptomic analysis (**Figure 3.5E**), imply that LRRC8A-dependent modulation of antiviral signalling occurs independently of the VRAC channel.

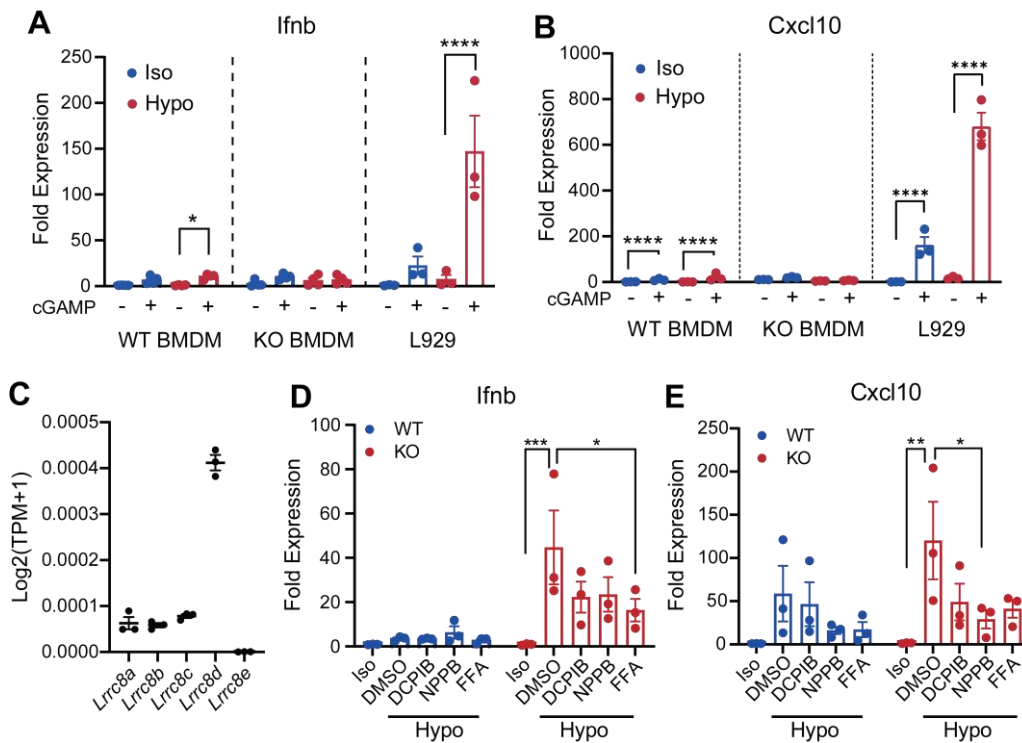


Figure 3.7: VRAC does not mediate LRRC8A's effects on antiviral signalling:

(A, B) Expression of *Ifnb* (A) and *Cxcl10* (B) mRNA in wild-type (WT) and LRRC8A knockout (KO) bone marrow-derived macrophages (BMDM) and L929 cells following 3 hours' incubation with either isotonic (Iso) or hypotonic (Hypo) media with or without 5µg/mL cGAMP (n = 3-4). (C) Expression of VRAC subunit genes in WT BMDM assessed by RNA-Seq. TPM = transcripts per million. (D,E) Expression of *Ifnb* (D) and *Cxcl10* (E) mRNA in WT and KO BMDM following a 6h stimulation with PBS or hypotonic media containing either vehicle (DMSO) or the VRAC inhibitors DCPIB (10µM), NPPB (100µM) or FFA (100µM) (n = 3). Data are presented as mean ± SEM. Statistics in A-B and D-E are from two-way ANOVA with Sidak's (A-B) or Dunnet's (D-E) *post-hoc*. * $p < 0.05$, ** $p < 0.01$, *** $p < 0.001$, **** $p < 0.0001$.

3.3.7 LRRC8A activates the PI3K-AKT pathway under hypotonic conditions

Analysis of the transcriptomic response to hypotonicity indicated a potential defect in PI3K signalling in KO cells, which may also be linked to regulation of interferon responses (see 3.3.4). This is intriguing considering LRRC8A's proposed role in linking PI3K-AKT activation to events such as insulin receptor signalling and mechanosensation. To establish whether hypotonic shock also induces LRRC8A-dependent PI3K activation, WT BMDM were stimulated with isotonic or hypotonic conditions for 5, 30, 60 or 120 minutes and the lysates probed for AKT phosphorylation via western blot. In WT cells AKT phosphorylation appeared stable under isotonic conditions, but hypotonic shock induced rapid, apparently biphasic increases in phospho-AKT (Figure 3.8A). Densitometry analysis confirmed that statistically significant increases were present, primarily at 5 minutes and 2h post-stimulation, with less consistent effects at intermediate timepoints which did not achieve statistical significance

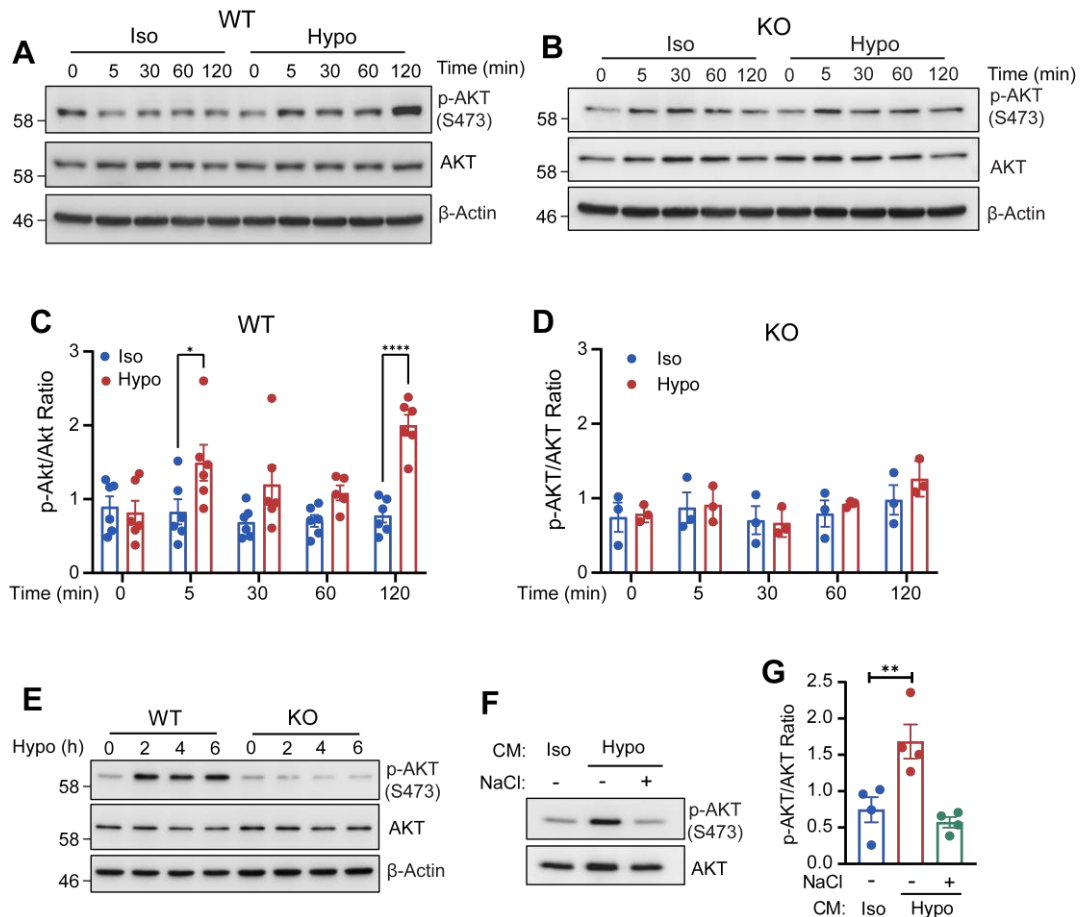


Figure 3.8: LRR8A activates AKT following hypotonic shock:

(A) Timecourse of total AKT and phosphorylated (S473) AKT (pAKT) levels following either isotonic (iso) or hypotonic stimulation of wild-type (WT) bone marrow-derived macrophages (BMDM; representative of $n = 6$). (B) Timecourse of total and phosphorylated AKT levels in LRR8A knockout (KO) BMDM following isotonic or hypotonic stimulation (representative of $n = 3$). (C-D) Densitometry analysis of relative AKT phosphorylation after PBS or hypotonic stimulation in WT (C) and KO (D) BMDM ($n = 6$ and 3 , respectively). (E) Extended timecourse of total and phosphorylated AKT levels following hypotonic shock in WT and KO BMDM (representative of $n = 3$). (F) AKT phosphorylation following 2h treatment with conditioned media (CM) from cells stimulated with either PBS or hypotonicity for 2h, along with hypo-conditioned media with osmolarity corrected by NaCl (representative of $n = 4$). (G) Densitometry quantification of (F). Data are presented as mean \pm SEM. Statistics in C-D are from 2-way ANOVA with Sidak's *post-hoc*, G are from one-way ANOVA with Tukey's *post-hoc*. * $p < 0.05$, ** $p < 0.01$, **** $p < 0.0001$.

(Figure 3.8C). To determine whether this effect relies on LRR8A, KO cells were then assayed in the same manner. Strikingly, in KO cells hypotonicity failed to activate AKT phosphorylation at any time point, thus confirming that AKT activation in this context is entirely reliant on LRR8A (Figure 3.8B,D). Extended assays were also performed, confirming that LRR8A-dependent AKT phosphorylation persists up to at least 6h following hypotonic stimulation, though the degree of induction plateaus after 2h (Figure 3.8E).

AKT activation following hypotonic shock appeared to be somewhat biphasic, exhibiting an early peak at 5 minutes followed by a later, more persistent induction by 2h post-hypotonicity. Considering previously described work linking LRRC8A to PI3K induction in response to insulin and other secreted factors, it seems plausible that the later peak in AKT activity could be caused by receptor-dependent events in response to secreted factors released following hypotonic shock. If this were true, it would be possible that the later defect in AKT induction in KO cells relates either to insufficient ligand release by KO cells, or to a specific LRRC8A-receptor interaction in the recipient cell which could be studied further. To establish whether secreted ligands contribute to AKT activation in this model, WT BMDM were stimulated with PBS or hypotonicity for 2h, and the conditioned media transferred to naïve WT cells for a further 2h. The conditioned media induced AKT phosphorylation in the recipient cells, however when the osmolarity was corrected via addition of NaCl, this stimulation was abolished (**Figure 3.8F,G**). Therefore, AKT stimulation in this model likely occurs without input from paracrine or autocrine signalling pathways, and instead reflects internally generated signals.

3.3.8 LRRC8A-dependent AKT activation requires TBK1/IKK ϵ , PKC and Fyn/Hck

LRRC8A is clearly able to engage channel-independent signalling cascades to activate PI3K-AKT signalling following hypotonic shock. LRRC8A-PI3K signalling has been described previously, but the only well-characterised pathways involving LRRC8A are those activated by secreted ligands such as insulin, which likely do not contribute to AKT activation under hypotonic conditions (**Figure 3.8F**). Therefore, it is unclear what pathways stimulate LRRC8A-dependent AKT activity in this model. Since multiple kinases were predicted to exhibit blunted activity in KO cells under hypotonic conditions in the IPA analysis (**Figure 3.5**) it is possible that these might be involved in LRRC8A-dependent signalling involving PI3K-AKT.

To gain insight into the events surrounding LRRC8A-dependent AKT stimulation, DCPIB and the PI3K inhibitor LY294002 were initially used to assess the involvement of VRAC channel activity PI3K in AKT activation during hypotonic shock in WT cells. Due to the possibility that the biphasic AKT activation under hypotonic conditions represents two differently regulated pathways, both 5- and 120-minute timepoints were tested. LY294002 completely abolished AKT activity under hypotonic conditions at both timepoints, whereas DCPIB had no effect at either, thus confirming PI3K-dependent, but VRAC-independent AKT signalling downstream

of LRRC8A (**Figure 3.9A**). Next, inhibitors for a variety of kinases predicted to be altered in the IPA analyses (TAK1, Fyn, focal adhesion kinase (FAK), TBK1/IKK ϵ and PKC) were tested for their effects on hypotonicity-induced AKT phosphorylation. Initially, a 5 minute hypotonic shock was used to induce AKT activation, since this more closely mirrors the stimulations used in previous papers (Kumar et al., 2020, 2014). Interestingly, Takinib (TAK1 inhibitor), PP2 (Fyn/Lck/Hck inhibitor) and GSK2256098 (FAK inhibitor) did not reduce AKT phosphorylation, whereas MRT67307 (TBK1/IKK ϵ inhibitor) and Gö6983 (PKC inhibitor) almost entirely prevented AKT activation (**Figure 3.9B**). Thus, both TBK1/IKK ϵ and PKC appear to be necessary for rapid LRRC8A-dependent AKT activity. TBK1/IKK ϵ have been demonstrated to phosphorylate AKT directly at S473 in a context-specific manner (Xie et al., 2011). As such, it is likely that these kinases act downstream of LRRC8A/PI3K. PKC, however, is known to mediate rapid responses to diverse stimuli, and has been linked previously to VRAC activity under hypotonic conditions (Chou et al., 1998; Gong et al., 2004). It is therefore feasible that PKC acts upstream of LRRC8A in mediating AKT activation. To confirm that PKC activity is indeed induced by hypotonicity, WT and KO BMDM were stimulated with isotonic or hypotonic media and lysates probed with an antibody which recognises the serine-phosphorylated (R/K)XpSX(R/K) PKC target motif of cellular PKC substrates. Whilst several bands were detected in these blots, only one band at roughly 80kDa appeared to be sensitive to the tested stimulations (**Figure 3.9C**). This band increased in intensity at 5 minutes post-stimulation with both isotonic and hypotonic media, but returned to baseline intensity by 120 minutes. This pattern was confirmed to be significant by densitometry targeting this band specifically (**Figure 3.9D**). Thus, PKC activity appears to be acutely increased by fluid addition to BMDM cultures irrespective of osmolarity or LRRC8A expression. This result suggests that, while PKC is required for LRRC8A-dependent PI3K-AKT activity, increases in PKC activity do not translate directly to increased AKT phosphorylation. Instead, basal PKC activity may simply be permissive for assembly of LRRC8A-containing signalling complexes.

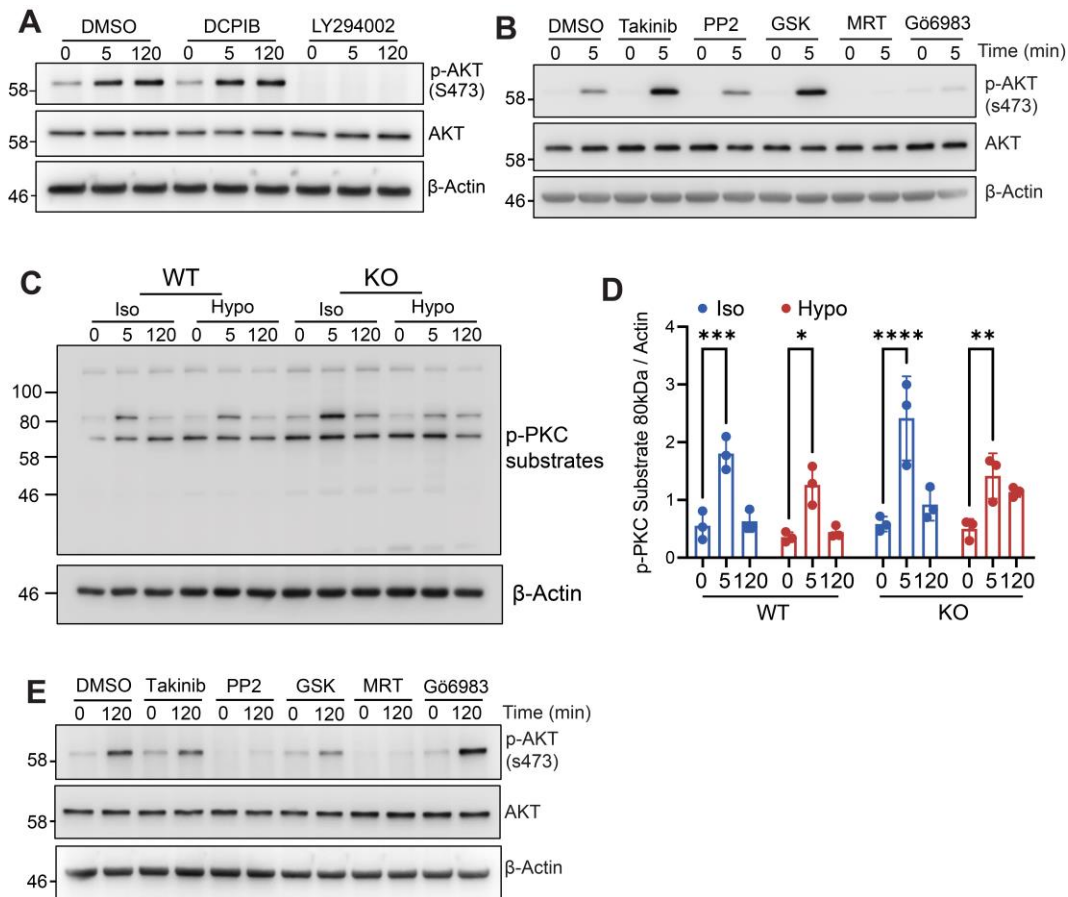


Figure 3.9: LRRc8A-dependent AKT activity relies on PI3K, TBK1/IKKε and protein kinase C
(A) Total and phosphorylated (S473) AKT in bone marrow-derived macrophages (BMDMs) stimulated hypotonic (hypo) media containing vehicle, the VRAC inhibitor DCPIB (10μM) or the PI3K inhibitor LY294002 (10μM) for 0, 5 or 120 minutes. **(B)** Total and phosphorylated AKT levels in BMDM treated with hypotonic media containing either vehicle (DMSO) or Takinib, PP2, GSK2256098 (GSK), MRT67307 (MRT) or G66983 (all 10μM) **(C)** Phosphorylated PKC substrates (R/KXSXR/K) in WT and LRRc8A-KO (KO) BMDM 0, 5 or 120m following stimulation with isotonic (Iso) or hypotonic (Hypo) media **(D)** Densitometry quantification of **(C)** (n = 3). **(E)** total and phosphorylated AKT levels in WT BMDM treated with hypotonic media for 2h using the same inhibitor panel as in **(B)**. All blots are representative of n = 3-4. Data in **D** are presented as mean ± SEM, statistics are from two-way ANOVA with Dunnet's *post-hoc*. * $p < 0.05$, ** $p < 0.01$, *** $p < 0.001$, **** $p < 0.0001$.

Having demonstrated the involvement of PKC and TBK1/IKKε in LRRc8A-dependent AKT activation acutely (5 minutes) after hypotonic shock, the possibility was considered that the later peak in AKT activity at 2h post-stimulation may be differently regulated. Therefore, BMDMs were treated with hypotonic media for 0 or 120 minutes while exposed to the same inhibitor panel, and the lysates probed for AKT activation. In this experiment, AKT phosphorylation was once again blocked by MRT67307, and was sensitive to PP2, but not to G66983 (**Figure 3.9E**). Thus, delayed AKT activation 120 minutes after hypotonicity occurs independently of PKC and is instead dependent on Fyn/Lck/Hck activity, as well as continuing

to require TBK1/IKK ϵ . These data therefore suggest that LRRC8A activates the PI3K-AKT pathway downstream of various distinct signalling events which are contextually regulated.

3.3.9 LRRC8A modulates interferon responses independently of PI3K-AKT

Given the stark effect of LRRC8A deficiency on hypotonicity-induced PI3K pathway activation (**Figure 3.8**), and the apparent overlap between PI3K and IRF3-regulated genes identified via IPA (**Figure 3.5**), it is possible defective PI3K signalling mediates the enhanced interferon responses observed in KO cells. To assess this, WT and KO BMDM were treated with either isotonic or hypotonic media for 6h, in the presence of the AKT inhibitor MK-2206 or the PI3K inhibitor LY294002. LY294002 is also known to inhibit DNA-dependent protein kinase (DNA-PK), which is capable of eliciting STING-TBK1 responses in some contexts. Thus, NU7441, a DNA-PK inhibitor, was also included to control for DNA-PK inhibition by LY294002. Neither AKT, PI3K nor DNA-PK inhibition affected expression of *Ifnb* or *Cxcl10* in WT or KO cells. As such, these data suggest that LRRC8A modulates hypotonicity-induced interferon responses via a mechanism independent of PI3K and AKT. Moreover, it can also be concluded that the interferon response observed under hypotonic conditions is independent of DNA-PK.

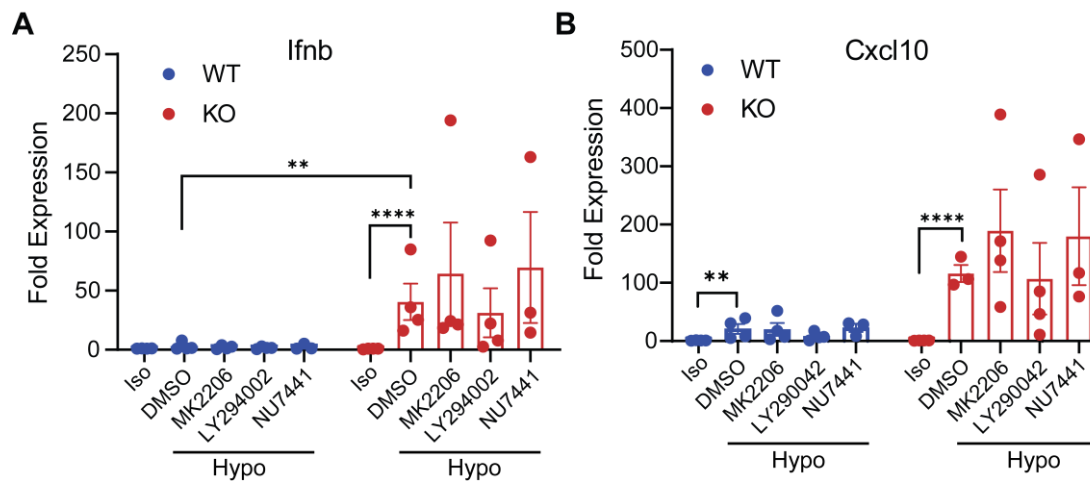


Figure 3.10: PI3K-AKT signalling does not restrict hypotonicity-induced ISG expression (A,B) *Ifnb* (A) and *Cxcl10* (B) mRNA expression in wild-type (WT) and LRRC8A knockout (KO) bone marrow-derived macrophages (BMDM) stimulated for 6h with either isotonic (Iso) or hypotonic (Hypo) media containing vehicle (DMSO), the AKT inhibitor MK-2206 (10 μ M), the PI3K inhibitor LY294002 (10 μ M), or the DNA-PK inhibitor NU7441 (100nM) (n = 3-4). Data presented as mean \pm SEM. Statistics are from two-way ANOVA with Dunnet's post-hoc. ** $p < 0.01$, **** $p < 0.0001$.

3.4 Discussion

LRRC8A has poorly understood functions in regulating cellular physiology via both VRAC-dependent and -independent pathways. In this study, we used high-throughput sequencing to identify cellular functions and pathways impacted by LRRC8A. Analysis of the resulting transcriptomic data suggested that LRRC8A deletion had wide-ranging effects on cellular signalling following hypotonic swelling, including significant modulation of the PI3K pathway (**Figure 3.12**) and a type-I interferon response (**Figure 3.11**). Subsequent assays confirmed that LRRC8A deletion resulted in an exacerbated interferon response under hypotonic conditions and defective activity in the PI3K pathway. Finally, it was shown that LRRC8A modulates antiviral signalling independently of both the VRAC channel and the PI3K pathway.

3.4.1 Hypotonic shock alters macrophage physiology

RNA sequencing was performed on WT and LRRC8A KO BMDM after incubation in either isotonic or hypotonic conditions. The resulting sequencing data revealed that hypotonicity induces drastic alterations in gene expression, to a degree which was previously unappreciated. Through enrichment analyses, it was found that a variety of pathways were altered, including downregulation of RNA processing genes and mitochondrial translation, as well as metabolic pathways including cholesterol synthesis and genes involved in vitamin metabolism. Upregulated functions were dominated by inflammatory and stress response pathways, indicating that macrophages may view strong alterations in osmolarity as a danger signal. This result echoes that of a recent paper highlighting oscillatory mechanical stress as a polarisation cue in macrophages, whereby long-term exposure to pulsatile hydrostatic pressure induces expression of various inflammatory genes involved in immune responses (Solis et al., 2019). Indeed, mechanosensation was shown to be critical for expression of neutrophil chemoattractants by lung-infiltrating monocytes, thus contributing to bacterial clearance in a mouse model of pneumonia (Solis et al., 2019). Thus, it is possible that osmolarity or cell swelling provide similar cues to macrophages in specific tissue microenvironments and may be important for generating or enhancing inflammatory responses in some contexts. Indeed, both hypertonic and hypotonic conditions have been demonstrated to induce activation of the NLRP3 and NLRC4 inflammasomes, respectively, though in both cases relatively severe osmolarity alterations of $\pm 70\%$ were required (Compan

et al., 2012; Green et al., 2020; Ip & Medzhitov, 2015; Perregaux et al., 1996). Less drastic fluctuations in osmolarity might serve to enhance the effects of other concomitant signals arising from tissue damage or infection, as was the case for cyclical force, which increased IL-1 β release following NLRP3 inflammasome activation in BMDM, yet by itself induced only modest (20-fold) induction of *IL-1 β* mRNA (Solis et al., 2019). As such, it would be of interest to determine whether hypotonic stress modulates macrophage priming mediated by PAMPs such as LPS, dsDNA or poly(I:C).

It seems unlikely that most tissues would regularly experience such drastic changes in osmolarity as those frequently used *in vitro* and in the present study. One exception is perhaps the kidney, which relies on generating osmotic gradients to regulate global water balance. Indeed, fluctuating sodium concentrations in the kidney have been linked to orchestration of local immune responses, with high sodium levels inducing recruitment of inflammatory monocyte-derived macrophages (Berry et al., 2017; Fehrenbach & Mattson, 2020). While most studies linking osmolyte balance to macrophage inflammatory polarisation have focused on hyperosmolarity, the data presented here suggest that hypoosmolarity could also induce similar effects. Precisely which tissues and pathologies might provide cues via hypotonic response pathways is still unclear, but the most obvious candidates are likely barrier sites such as the skin, gut or airway epithelia, which are vulnerable to fluctuations in osmolarity and are of high immunological importance.

It is also important to consider that stimuli other than osmotic fluctuations could potentially induce responses similar to that characterised here, since it is possible that much of the transcriptional response to hypotonicity relies on sensory events which also respond to other stimuli. Indeed, the identity of the cellular “sensor” of hypotonicity is still a matter of some debate, but likely consists of multiple convergent pathways (Pedersen et al., 2011). Only one protein kinase, ASK3 (MAP3K15), has so far been demonstrated to respond directly to osmolarity, exhibiting increased autophosphorylation and activation with decreasing osmotic strength (Naguro et al., 2012). Other proposed sensors of hypotonic stress include membrane stretch-activated channels such as TRPM7 and TRPV4 as well as membrane-associated kinases such as EGFR and integrin-associated signalling complexes (Krause et al., 1996; Pedersen et al., 2011; Plant, 2014). Thus, cells respond to hypotonicity with a variety of

contextually regulated signalling events, many of which in fact detect phenomena related to cell swelling, such as membrane deformation or cytoskeletal tension. Cell swelling is known to occur following various insults including hypoxia, exposure to toxins and mechanical injury. It is therefore possible that much of the transcriptomic response characterised here in osmotically swollen cells is in fact common to many pathologies. In this sense, it is intriguing that LRRC8A exerts such a large influence over the hypotonic response, seemingly independently of its role as a component of VRAC, and thus also potentially independently of osmolarity.

3.4.2 Hypotonicity induces antiviral signalling

While the transcriptomic perturbations elicited by osmotic swelling in WT BMDM were extensive, and suggested widespread functional alterations, the most significantly enriched pathways via both gene set analysis and regulator predictions in IPA were related to interferon signalling. This encompassed upregulation of a variety of antiviral genes, inflammatory cytokines and the type-I interferon *Ifnb*. Moreover, cholesterol biosynthetic genes and RNA processing pathways were downregulated, which is consistent with induction of an antiviral state (Robertson & Ghazal, 2016). Since antiviral responses are generally the result of DNA/RNA sensing events, and given the lack of any exogenous nucleotide sources in this model, it was assumed that the response must be elicited by self-DNA. This is supported by the identification of nucleotide sensors as likely mediators in IPA, and inhibition of the response by A151, an immunosuppressive oligonucleotide which antagonises immunogenic DNA sensors. Thus, osmotic shock appears to activate a DNA-dependent antiviral transcriptional programme.

Two key questions regarding the mechanism of this response remain. Firstly, it is unclear which DNA sensor is responsible, although since the response is inhibited by the STING inhibitor H151 and appears to engage TBK1, it can be concluded that the sensing pathway culminates in the STING-TBK1-IRF3 axis (see **Figure 3.11**). However, since STING acts downstream of many different DNA sensing events, the specific pathway activated by osmotic swelling requires further study (Atianand & Fitzgerald, 2013). Secondly, the mechanism by which self-DNA is rendered immunogenic by osmotic shock has not previously been described and may be an interesting avenue for future studies. It is possible that hypotonic swelling

induces release of mtDNA from mitochondria, prompting recognition by cytosolic DNA sensors. However, it is also feasible that osmotic shock causes mislocalisation of nuclear DNA, to the same effect. In support of the latter mechanism, hyperosmotic stress has been demonstrated to induce double-stranded breaks (DSBs) in genomic DNA (Kültz & Chakravarty, 2001). Hypoosmotic conditions have also been shown to induce DNA damage in HeLa cells, though this appeared to be primarily localised to the nucleolus (Velichko et al., 2019). Thus, it is possible that osmotic stress induces DNA release from the nucleus following DSB formation, activating cytosolic DNA sensing pathways, or that STING is directly stimulated by nuclear kinases following DSB detection (Dunphy et al., 2018).

3.4.3 LRRC8A modulates interferon responses following osmotic swelling

Perhaps the most significant finding in the present study was that LRRC8A KO appeared to exacerbate expression of *Ifnb* and *Cxcl10*, as well as *Rsad2*, *Ccl7* and *Il1b* after prolonged exposure to hypotonic conditions (see 3.3.5). This was somewhat surprising, since analysis of the RNA-Seq dataset suggested that many known targets of antiviral signalling cascades were reduced in KO cells. This discrepancy is likely due to the fact that the sequencing experiments were performed 4h after hypotonic shock, whereas timecourse validation experiments revealed that, for instance, increased expression of *Cxcl10* mRNA in KO cells was only apparent after 6h, with no effect observed at previous timepoints. Thus, 4h post-stimulation may have been suboptimal for characterising the relative extent of ISG induction. It is still possible that some ISGs are less highly induced in KO cells than WT even after 6h, though this would require separate validation.

Initially, it was hypothesised that loss of LRRC8A caused increased ISG expression either via increased retention of cGAMP downstream of cGAS activity, or by compromising RVD, leading to unresolved, persistent swelling, thus inducing a larger response. However, inhibiting VRAC with blockers at concentrations which block RVD failed to replicate this effect, suggesting that LRRC8A limits the antiviral response in this model independently of its effects on cell volume. Moreover, transport of antiviral signalling molecules such as cGAMP via the VRAC pore is also unlikely to be the mechanism, since it was also demonstrated that BMDMs are poorly permeable to cGAMP. These data therefore point to ion channel-independent effects of LRRC8A on antiviral signalling, which has not previously been shown to occur.

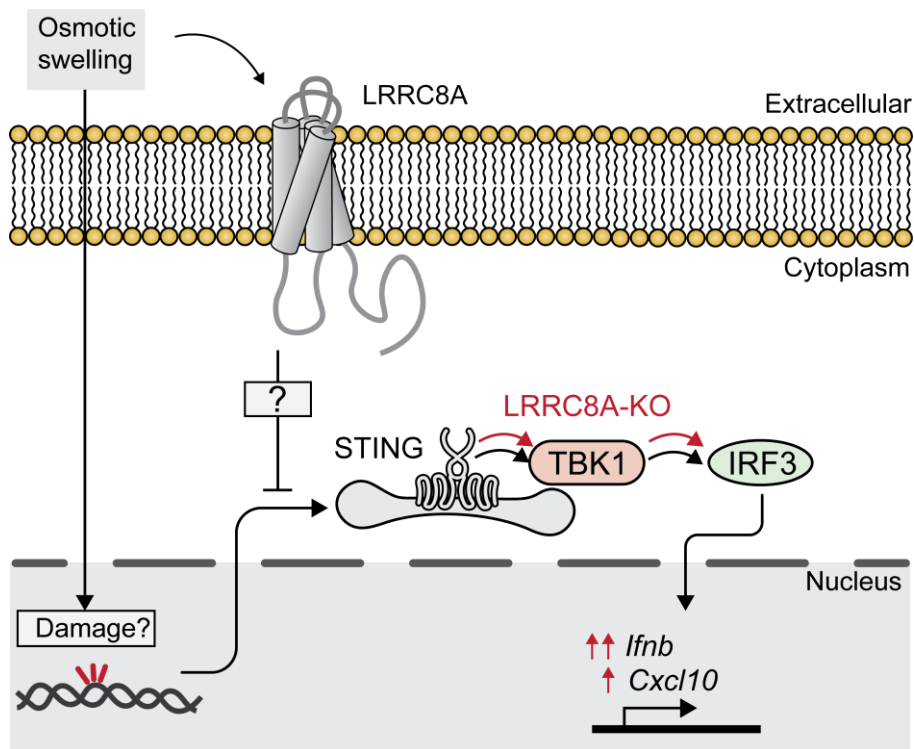


Figure 3.11: LRRC8A restricts interferon signalling following osmotic shock

Osmotic swelling was demonstrated to induce DNA- and STING-dependent induction of TBK1-IRF3 signalling, which may be the result of DNA damage. LRRC8A antagonises this pathway via an unknown mechanism independently of the VRAC channel. Thus, LRRC8A-KO results in greatly enhanced expression of *Ifnb* and moderately increased expression of *Cxcl10* following hypotonic shock.

Whilst LRRC8A expression clearly modulated interferon responses under hypotonic conditions, no differences in IFN- β secretion were observed between WT and KO cells transfected with poly(dA:dT) in normal isotonic media, suggesting that LRRC8A-dependent regulation of interferon responses is likely to be context-specific. Since LRRC8A KO BMDMs exhibited minimal gene expression differences compared to WT controls in isotonic media, it appears that LRRC8A does not exert appreciable signalling functions at baseline in BMDM. This accounts for the fact that LRRC8A does not modulate DNA-induced interferon secretion under isotonic conditions. As such, it is likely the case that LRRC8A only affects antiviral signalling in the presence of stimuli such as hypotonicity which engage its signalling functions.

The precise mechanism by which LRRC8A KO aggravates antiviral responses is still unclear. Activation of the PI3K pathway is currently the only signalling event known to occur in an LRRC8A-dependent, VRAC-independent manner in a variety of contexts. IPA analysis indicated that PI3K targets overlapped significantly with LRRC8A-sensitive IRF3-induced

genes. Therefore, a role for PI3K in suppressing antiviral signalling downstream of LRRC8A was hypothesised. Although LRRC8A-dependent PI3K activity was robustly induced in osmotically swollen WT cells, inhibiting PI3K and AKT activity did not affect the extent of *Irfn* and *Cxcl10* induction by osmotic shock in either WT or KO BMDM. Therefore, LRRC8A must suppress osmotic shock-induced interferon responses via a novel signalling pathway independent of PI3K-AKT (**Figure 3.11**).

3.4.4 LRRC8A-dependent signalling is largely independent of VRAC under hypotonic conditions

Another surprising result provided by this sequencing experiment is that, although LRRC8A KO cells exhibit significant alterations in transcriptome following osmotic shock, the addition of DCPIB to WT cells only weakly phenocopies this effect. Indeed, the majority of genes altered in KO cells compared to WT were insensitive to DCPIB. Of the DCPIB-sensitive genes identified, a significant fraction were clearly altered nonspecifically, since a comparable change was detected in the absence of LRRC8A. It could be argued that the concentration of DCPIB used here (10 μ M) might have been too low to fully block VRAC channel activity, since the many studies of VRAC function are performed with 20 μ M DCPIB. However, in our BMDM cultures, 10 μ M was sufficient to block RVD following osmotic shock, to an extent comparable with LRRC8A KO. It was also observed that 20 μ M DCPIB induces a wide range of effects on microglial and BMDM physiology which were unrelated to VRAC activity. Thus, 10 μ M was used to minimise nonspecific effects, yet likely still inhibited VRAC-dependent solute flux and volume control. Consistent with this idea, the VRAC inhibitors NPPB and FFA also failed to phenocopy the effect of LRRC8A-KO on ISG expression, despite clearly inhibiting RVD, indicating that insufficient blocker concentration is unlikely to account for the discrepancy between LRRC8A-KO and DCPIB-treated cells.

Whilst some channel-independent effects of LRRC8A have been described, studies of LRRC8A function have overwhelmingly focused on VRAC biology. These results suggest that VRAC-independent signalling may be of equal, if not greater functional significance than VRAC-mediated activity. Moreover, given that PI3K-AKT inhibition did not phenocopy the effect of LRRC8A-KO on ISG expression, it is likely that additional LRRC8A-controlled pathways beyond PI3K remain to be found. The identity of these pathways is of significant

interest and will likely form the basis of future studies. With this in mind, it is interesting to note that the results of the IPA regulator analysis indicated potential roles for Fyn, TAK1 and PKC, amongst others, in mediating LRRC8A-dependent gene expression. Of these, TAK1 has previously been shown to be activated by hypotonic shock, where it mediates NLRP3 inflammasome activation (Compan et al., 2012). It is therefore possible that LRRC8A modulates TAK1 function, or vice-versa. Fewer studies have linked Fyn to osmotic signalling, though Src-family kinases in general have been suggested to be activated following osmotic stress (Barfod et al., 2005; Pedersen et al., 2011).

3.4.5 LRRC8A stimulates PI3K in a PKC- and Fyn/Hck-dependent manner

Given the previously described interaction between LRRC8A and the PI3K pathway, as well as the transcriptomic analysis indicating that PI3K may mediate hypotonic signalling downstream of LRRC8A, PI3K pathway activity was investigated. In initial experiments, it was confirmed that osmotic swelling activates PI3K-dependent AKT phosphorylation in WT cells, and that LRRC8A was required for this effect. This result builds on previous studies demonstrating that LRRC8A stimulates PI3K activity in response to insulin, mechanical stretch and LRRC8A ligation with antibodies (Alghanem et al., 2021; Kumar et al., 2020, 2014). Since swelling induces membrane stretch, it may be that rapid PI3K activity following osmotic shock is stimulated by mechanosensitive pathways via LRRC8A. However, this is a poorly understood phenomenon, and the possibility of additional upstream kinases generating LRRC8A-dependent signals has received little attention. Therefore, subsequent experiments sought to establish whether other regulators identified via IPA might be required for LRRC8A stimulation of the PI3K pathway. These experiments identified TBK1/IKK ϵ and PKC as essential for rapid LRRC8A-induced AKT phosphorylation. Of these, it is likely that TBK1/IKK ϵ act as a non-canonical AKT kinase downstream of PI3K under hypotonic conditions, as has been shown previously for other stimuli (Xie et al., 2011).

The involvement of PKC in regulating LRRC8A signalling is intriguing, since it has been reported to be required for VRAC activity and RVD in some cell types (Chou et al., 1998; Gong et al., 2004). PKC activity was found to increase acutely following BMDM stimulation, albeit in a non-osmosensitive manner and independently of LRRC8A. Since addition of isotonic fluid to BMDM elicited increases in PKC activity, but not AKT phosphorylation, it appears that

increased PKC activity alone is not sufficient to stimulate the LRRC8A-PI3K pathway. It is therefore possible that PKC fulfils a permissive role whereby PKC activity is necessary for association between LRRC8A and other proteins which regulate PI3K activation, but does not directly trigger activity of the complex. This role of PKC as an upstream regulator of LRRC8A signalling is also supported by the fact that PKC activity appeared to be independent of LRRC8A expression. Thus, these data support a model whereby PKC is required for the formation of LRRC8A-containing signalling complexes which activate rapidly upon stimulation with hypotonic media to elicit downstream changes in PI3K activity.

It is also intriguing that stimulation of the PI3K pathway by LRRC8A following osmotic swelling occurred biphasically, with both a rapid and delayed peak in activity. Whilst the initial activity likely occurs downstream of osmosensing or mechanosensing cascades due to cell swelling, it is unclear what causes the second, later peak at 2h post-stimulation. Media transfer experiments demonstrated that autocrine ligand release is unlikely to cause the delayed peak, suggesting it likely results from delayed intracellular signalling events following hypotonic shock. Experiments using kinase inhibitors revealed that the delayed peak in AKT activity is sensitive to PP2, but not to PKC inhibition, thus suggesting a different mode of signalling to that of the early peak. PP2 inhibits the Src family kinases Fyn, Lck and Hck, of which only Fyn and Hck were detectable at the mRNA level in these cells via RNA-Seq. Thus, Fyn or Hck probably mediate delayed LRRC8A-dependent AKT activation after osmotic shock. It is tempting to speculate that Fyn is the more likely mediator of LRRC8A-dependent signalling based on its predicted association with LRRC8A-dependent transcriptional alterations in the IPA analysis, though this will require further study to validate. Interestingly, PP2 was also shown to inhibit AKT phosphorylation following antibody-mediated LRRC8A clustering in thymocytes, though this effect was proposed to be due to inhibition of Lck. In thymocytes, LRRC8A associates constitutively with the Lck/Zap-70 complex which stimulates PI3K activation upon LRRC8A clustering. However, constitutive association between LRRC8A and Fyn/Hck in BMDM seems unlikely, since PP2-sensitive AKT phosphorylation did not occur until 2h post-stimulation. Moreover, it is unclear whether Fyn/Hck act upstream or downstream of LRRC8A in this signalling pathway, which is a key point requiring further study. It is possible that LRRC8A associates with Fyn/Hck and stimulates their activity, as was shown for Lck in

thymocytes, yet it is equally feasible that Fyn/Hck regulate LRRC8A or its associated proteins as is likely the case for PKC.

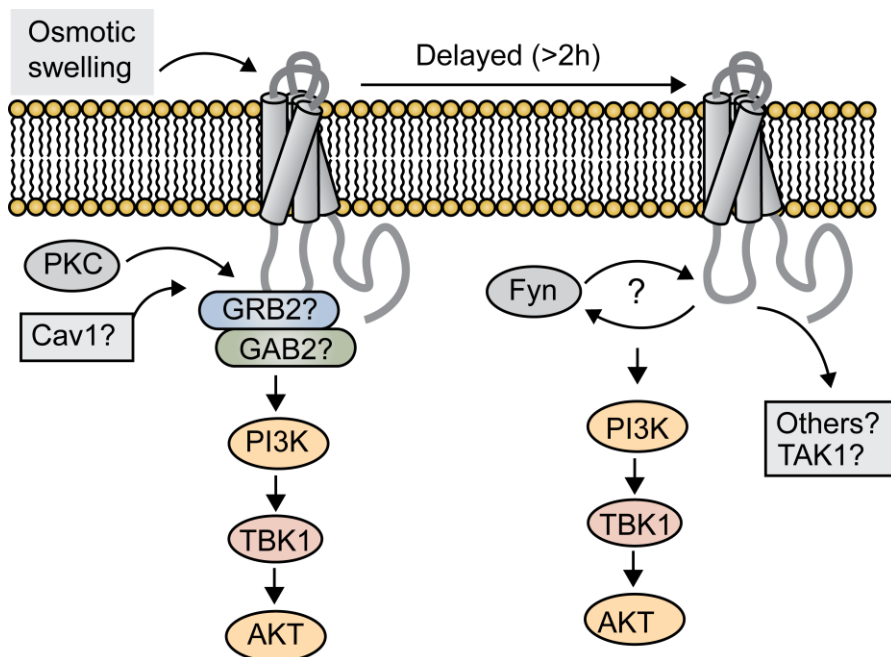


Figure 3.12: Proposed mechanisms of LRRC8A-PI3K signalling

LRRC8A likely signals to PI3K in two distinct waves following hypotonic shock. The first, transient wave occurs rapidly following swelling and requires PKC signalling, whereas the second is delayed yet persistent, and requires Fyn/Hck. Both pathways require TBK1/IKK ϵ to activate AKT, likely downstream of PI3K. Either pathway may require additional proteins such as GRB2/GAB2 or Caveolin-1, and may also activate signalling pathways other than PI3K.

Overall, these data point to a previously unappreciated degree of diversity in signalling pathways engaging LRRC8A. Two separate pathways involving PKC and Fyn/Hck were demonstrated to stimulate PI3K activation via LRRC8A in a temporally regulated manner following osmotic cell swelling. The exact relationship between LRRC8A, PKC and Fyn/Hck with respect to PI3K signalling remains to be determined and would be an interesting avenue for further studies. This study also determined that, while the PI3K pathway is regulated by LRRC8A in more ways than previously thought, LRRC8A also engages other signalling pathways whose identity is yet to be determined, at least one of which is capable of modulating interferon signalling.

3.4.6 Conclusions

Overall, this study adds significantly to our understanding of osmotic shock as an environmental danger signal which instructs macrophage phenotype. Specifically, that osmotic shock induces a DNA-dependent antiviral response via STING, in addition to various alterations in metabolic, DNA and RNA processing pathways, as defined by RNA-Seq. Moreover, this study reveals significant signalling functions of LRRC8A which likely occur independently of VRAC activity, and which can modulate interferon responses via an as-yet undescribed pathway. These results raise key issues regarding the cellular function of LRRC8A. Firstly, that LRRC8A likely engages additional signalling cascades independently of PI3K signalling. Secondly, LRRC8A may stimulate the PI3K pathway in more contexts than previously appreciated, which could be relevant to survival signalling in both developmental and pathological contexts.

Chapter 4: General Discussion

The present study aimed to address two primary issues with respect to the biology of VRAC using a novel microglia/macrophage-targeted LRRC8A knockout mouse line. Firstly, the role of VRAC-dependent chloride flux in regulating microglial phenotype and effector functions was investigated. Contrary to prior work in this area, it was found that VRAC is entirely dispensable for numerous aspects of microglial biology it was previously thought to regulate. This finding has implications for treating CNS diseases in which VRAC has been identified as a potential drug target due to its role in astrocyte physiology, since astrocyte VRAC could likely be targeted without impairing microglia. Secondly, transcriptomic experiments were performed in WT and LRRC8A-KO BMDM under hypotonic conditions in an attempt to uncover novel functions of LRRC8A/VRAC. These data highlighted several important points, including a large influence of LRRC8A on gene expression which appeared to be largely independent of VRAC. Subsequent experiments revealed that LRRC8A exerts pleiotropic effects on interferon signalling and the PI3K pathway via mechanisms which do not require VRAC-dependent solute flux. These data have numerous implications for the study of LRRC8A/VRAC biology going forward, including the stringent requirement for genetic studies and a great need for new, more specific pharmacological inhibitors.

4.1 VRAC is dispensable for multiple microglial functions

VRAC channels have, for some time, been postulated as targets for preventing excessive neuronal death in stroke due to their proposed function in releasing glutamate from astrocytes (Mongin, 2016). There is also a great deal of interest in targeting microglia therapeutically, since microglia have been shown to regulate numerous aspects of stroke physiology. VRAC was, until recently, also thought to regulate activation of the NLRP3 inflammasome, which promotes maturation and release of the inflammatory cytokine IL-1 β from inflammatory macrophages/microglia (Daniels et al., 2016; Green et al., 2020). A fenamate NSAID which is known to inhibit VRAC was shown to prevent neurological deficits in a mouse model of Alzheimer's disease by inhibiting NLRP3 (Daniels et al., 2016), and earlier work suggested other pleiotropic functions of VRAC in supporting microglial phagocytosis, chemotaxis, morphology and migration (Ducharme et al., 2007; Eder, 2005; Eder et al., 1998; Furtner et al., 2007; Harl et al., 2013; Hines et al., 2009; Zierler et al., 2008). Thus, rationale was established for the creation of a microglia-targeted LRRC8A knockout mouse model to allow

more thorough validation of VRAC's contribution to microglial physiology. In a recently published paper, our group used this mouse model to establish that VRAC does not in fact mediate NLRP3 inflammasome activation by most stimuli, and that previous work with VRAC inhibitors likely reflects actions on other chloride channels (Green et al., 2020). In a similar vein, the present work clarifies that other long-held associations between VRAC and microglial physiology are also most likely spurious correlations arising from lack of blocker specificity. Indeed, VRAC appeared to be largely dispensable for survival, transcriptomic identity, phagocytic activity, chemotaxis and migration in microglia. In fact, the only point on which this and the aforementioned study agree with previous literature is that VRAC is necessary for RVD following hypotonic shock (Green et al., 2020). These two studies therefore highlight the stringent need to verify inhibitor-based data with genetic tools in order to ensure correct interpretation with respect to individual mediators.

One key point arising from both studies is that chloride flux is almost certainly a central mediator of both microglial physiology and NLRP3 activity. Chloride channels are therefore of great relevance to various disease processes, and their pharmacological inhibition could be either beneficial or detrimental to disease outcome. Whilst VRAC can be dismissed as a core regulator of microglial physiology, the data here invite future study as to the true identity of the responsible chloride channels. Moreover, the present work also suggests that VRAC can be inhibited in the CNS without impairing microglial function, provided a suitably selective inhibitor is used. Overall, these results represent a significant refinement of the current knowledge surrounding both chloride channels in innate immunity and VRAC biology.

4.2 LRRRC8A/VRAC as a signal transducer

Numerous studies have uncovered indisputable requirements for LRRRC8A and VRAC channel function in a variety of cell types. One common theme emerging from these studies is that VRAC can be activated by diverse stimuli such as cell swelling and inflammatory cytokines, through a variety of mechanisms involving protein-protein interactions and phosphorylation events. Moreover, many of the proposed effects of VRAC are unrelated to its role in maintaining cell volume during osmotic shock, and instead support signal transduction by transporting factors such as ATP, neurotransmitters and cGAMP, or via effects on cell

membrane potential. However, several studies have provided evidence, albeit somewhat indirectly, of signalling functions fulfilled by LRRC8A which do not require assembly of a functional VRAC channel, though these have generally been limited to LRRC8A-dependent stimulation of the PI3K pathway. The present study therefore considered the possibility that LRRC8A/VRAC has novel signalling functions not yet described, and attempted to shed some light on this issue via transcriptomic analysis of gene expression in WT and LRRC8A KO BMDM treated with isotonic or hypotonic buffers. Hypotonic swelling was used as a stimulus in this experiment due to its relative simplicity and its well-described capacity to robustly activate VRAC.

The results of this study demonstrated three major points. Firstly, that hypotonic swelling induces wide-ranging effects on cellular physiology, including apparent polarisation of BMDM to an antiviral state. Secondly, LRRC8A-KO significantly modified the transcriptomic response to hypotonicity, indicating significant influence of LRRC8A/VRAC over cellular signal transduction. Finally, experiments using DCPIB to block the VRAC channel indicated that in fact VRAC blockade poorly mimicked the effect observed in LRRC8A-KO, which suggests a significant degree of VRAC-independent activity downstream of LRRC8A. Subsequent investigations revealed that LRRC8A likely engages multiple downstream signalling pathways in a manner independent of VRAC, stimulating both PI3K activity and as-yet uncharacterised pathways which modulate macrophage antiviral signalling.

4.2.1 LRRC8A-PI3K-AKT signalling

During the course of this study, several refinements to the current model of LRRC8A-dependent signalling were discovered. Firstly, hypotonicity-induced PI3K-AKT activation was demonstrated to be insensitive to DCPIB, thus demonstrating that LRRC8A-dependent stimulation of PI3K occurs independently of VRAC. This had, in principle, been implied by previous literature comparing phenotypes in LRRC8A^{-/-} versus ebouirffe mutant mice, though this line of reasoning is complicated by the different genetic backgrounds of the two mouse strains and the potential for some residual VRAC activity in the ebouirffe mutant (Kumar et al., 2014; Platt et al., 2017). Thus, the present study provides the first direct evidence that LRRC8A can engage signalling pathways independently of the VRAC channel. Moreover, new molecular players in the LRRC8A-PI3K-AKT pathway were discovered using inhibitors of

PKC, TBK1/IKK ϵ and Fyn/Hck, and it was shown that PKC and Fyn/Hck dependent pathways are separate, with distinct kinetics following hypotonic shock. Overall, this study complements the existing literature on this topic by demonstrating the existence of diverse participants in the LRRC8A-PI3K signalling axis. A major question posed by these results is whether the pathways engaged by LRRC8A to activate PI3K in this model also involve the same adapter proteins and interactors suggested by previous studies – namely GAB2, GRB2 and Caveolin 1. It is likely that the two temporally distinct waves of AKT activation in this model reflect assembly of discrete signalling complexes, and it would be illuminating in future studies to assess the relative contribution of these known LRRC8A-interacting proteins to both the rapid and delayed PI3K-AKT activating events. It is feasible that there exists a “core” group of adapter proteins which are universally required for LRRC8A signalling, and which can recruit additional components and kinases in a context-specific manner to drive distinct responses.

In a more general sense, much remains to be discovered regarding the ability of LRRC8A to stimulate intracellular signalling. Firstly, it is unknown which regions of LRRC8A mediate the protein interactions necessary for engaging the PI3K-AKT pathway. The cytoplasmic loop appears to be the best candidate, since thymocyte AKT activation is maintained in ebouirffe animals lacking most of the LRR domain (Platt et al., 2017). The cytoplasmic loop also contains several known phosphorylation sites, including serine 217, which is phosphorylated by stimuli including insulin and lipopolysaccharide (LPS) (Humphrey et al., 2013; Weintz et al., 2010). Since neither insulin nor LPS are known to induce VRAC activity, yet insulin receptor signalling requires LRRC8A, it is tempting to speculate that this phospho-site regulates protein interactions which support intracellular signalling cascades. However, this would require specific validation, which could be assessed via targeted mutation.

Identification of the regions and residues which regulate VRAC-independent signalling by LRRC8A could prove invaluable for future efforts to understand LRRC8A biology, since it may allow the creation of mutant constructs which are VRAC-competent but defective in signalling functions, and vice-versa. Indeed, VRAC-incompetent constructs which retain intracellular signalling capabilities may already exist, since some labs have undertaken mutagenesis experiments to probe residues required for VRAC assembly and gating, yet likely have not assessed whether constructs lacking VRAC activity are capable of supporting PI3K signalling

(Bertelli et al., 2021; Qiu et al., 2014; Yamada & Strange, 2018). Creation or identification of these tools would allow VRAC channel functions to be clearly delineated from LRRC8A signalling functions both in cell models and *in vivo* without reliance on chloride channel inhibitors, and thus would prove enormously helpful moving forward.

4.3 LRRC8A restricts antiviral signalling

In this study, osmotic stress was shown to induce a robust type-I interferon response in BMDM, which was dependent on DNA sensing and STING, and exacerbated by loss of LRRC8A. Mechanistically, inhibition of the VRAC channel did not recapitulate the enhanced response seen in the LRRC8A-KO cells, nor did inhibition of hypotonicity-induced PI3K signalling, the only well-characterised VRAC-independent LRRC8A function. Thus, it can be concluded that LRRC8A modulates macrophage phenotype following hypotonic stress by suppressing interferon responses through a novel VRAC-independent signalling axis.

This is an intriguing result, since LRRC8A has only been previously linked to interferon signalling via VRAC-dependent transport of cGAMP. Thus, this study provides a novel mechanism by which LRRC8A might modify inflammatory and antiviral signalling. Key areas which should be addressed in future work include the pathway of STING-TBK1 activation following osmotic stress, and the mechanism by which this is enhanced LRRC8A-KO. Whilst this study eliminated DNA-PK as a potential mediator, several further avenues remain to be explored. One recent paper described the existence of a noncanonical STING activation pathway following DNA damage, mediated by the nuclear kinase ataxia-telangiectasia mutated (ATM), along with p53 and IFI16 (Dunphy et al., 2018). Since osmotic stress has been previously observed to damage DNA, and p53 and ATM were highlighted as potential regulators of the osmotic response via IPA, it is possible that this mechanism is activated under hypotonic conditions. Future work could address this hypothesis using inhibitors of ATM, which were demonstrated to suppress DNA-damage induced STING activation (Dunphy et al., 2018). The data presented here also strongly imply the existence of a novel signalling axis connecting LRRC8A to STING activity. Exactly which kinases and intermediates constitute this pathway should also be addressed by future work. The results of the transcriptomic analysis will likely form a good starting point in identifying these mediators, and

it may be informative to perform further unbiased 'omics analyses such as phospho-proteomics on WT and LRRC8A-KO cells under hypotonic conditions to identify LRRC8A-dependent changes in kinase regulatory sites.

Regardless of the specific mechanism, it is clear that LRRC8A is capable of modulating certain forms of interferon response independently of VRAC, though it is unclear in which situations this might occur *in vivo*. Largely this can be attributed to uncertainty regarding the contexts and stimuli which induce LRRC8A signalling. Since LRRC8A-KO did not appear to affect IFN- β secretion following transfection of poly(dA:dT), it can be assumed that LRRC8A only regulates certain forms of inflammatory response and/or only does so under specific conditions. The present study demonstrates that cell swelling is likely one such condition, and previous research has indicated that mechanical stimulation may also induce LRRC8A-dependent effects. What other stimuli or insults might induce LRRC8A-dependent modulation of antiviral responses remains to be determined. However, one promising prospect is that of cancer signalling. Since high LRRC8A expression has been linked to greater proliferation and poor prognosis in a variety of cancer types (Kurashima et al., 2021; Lu et al., 2019; Zhang et al., 2018), it is interesting to consider that certain cancer niches may induce chronic stimulation of LRRC8A.

The results of this study suggest that, in cancer cells, stimulation of LRRC8A could both suppress immunogenic interferon responses to DNA damage and promote survival signalling and invasion via PI3K. A role for LRRC8A in mediating cancer signalling is particularly intriguing given its link to PKC, Src kinases and TBK1/IKK ϵ , which are known to drive oncogenic signalling pathways when dysregulated. However, cancer cells are also known to import chemotherapeutics such as cisplatin through VRAC, and low expression of LRRC8A has therefore also been linked to increased drug resistance (Planells-Cases et al., 2015). Thus, the role of LRRC8A/VRAC as a cancer target is disputed, which may reflect different functions depending on the specific cell type on question. It is possible that in some cancers the signalling milieu favours pro-oncogenic functions of LRRC8A, whereas in others LRRC8A may not contribute to oncogenic signalling and instead forms drug-transporting VRAC channels which aid in treatment. In this sense, it is also relevant to consider whether LRRC8A is capable of engaging PI3K and other signalling pathways whilst simultaneously participating

in VRAC channels, or whether these functions are mutually exclusive. Similarly, it is possible that VRAC channel activity and LRRC8A signalling are differentially regulated by upstream kinases and adapter proteins, which could enable them to be specifically targeted. Thus, further characterisation of signalling events both upstream and downstream of LRRC8A is of interest for future studies.

4.4 Concluding Remarks

Perhaps the most universally relevant issue arising from this study is the ability of LRRC8A to drastically alter cellular signalling pathways in a manner independent of the VRAC channel and associated solute flux. This result highlights that a critical distinction should be drawn between LRRC8A and VRAC, which are often taken as synonymous with respect to their cellular functions. An increasing number of groups are now utilising genetic LRRC8A targeting strategies when studying VRAC to circumvent the specificity issues of VRAC blockers. This is undoubtedly necessary, particularly given the drastic contrast between the results presented here and previous literature regarding microglia. However, our results urge that these studies should be interpreted with caution and should not be considered unambiguous with respect to VRAC, given the distinct possibility of LRRC8A-dependent effects which occur in a VRAC-independent manner. As such, the continued use of VRAC inhibitors as an orthogonal validation strategy is required, and VRAC functions should be identified based on convergent phenotypes arising both from pharmacological VRAC blockade and to genetic ablation of LRRC8A.

In a similar vein, it has become increasingly clear that VRAC inhibitors display a great deal of nonspecific activity which complicates their use, both scientifically and therapeutically. In the present study, even DCPIB, the most selective VRAC inhibitor, was shown to completely inhibit microglial chemotaxis, cell migration, and to moderately suppress phagocytosis at 20 μ M, which is a concentration frequently used by VRAC biologists in cellular assays. Indeed, a variety of effects on gene expression were observed in LRRC8A-KO cells via RNA-Seq even at 10 μ M, which is the lowest concentration used routinely for studying VRAC. The nonspecificity of VRAC inhibitors is already a known issue, and this study adds to the increasing evidence that even DCPIB is largely unreliable as a tool for interrogating VRAC

function in the absence of genetic validation. The identification or creation of novel more selective VRAC inhibitors will therefore be of great benefit for studying and targeting VRAC biology.

Future studies building on the present work should focus primarily on elucidating the mechanism by which LRRC8A suppresses hypotonicity-induced STING activity. Determining the specific signalling events modulated by LRRC8A in this pathway will likely be useful for uncovering novel LRRC8A-regulated processes *in vivo*.

References

- Abascal, F., & Zardoya, R. (2012). LRRC8 proteins share a common ancestor with pannexins, and may form hexameric channels involved in cell-cell communication. *BioEssays: News and Reviews in Molecular, Cellular and Developmental Biology*, *34*(7), 551–560. <https://doi.org/10.1002/bies.201100173>
- Ajami, B., Bennett, J. L., Krieger, C., Tetzlaff, W., & Rossi, F. M. V. (2007). Local self-renewal can sustain CNS microglia maintenance and function throughout adult life. *Nature Neuroscience*, *10*(12), 1538–1543. <https://doi.org/10.1038/nn2014>
- Alghanem, A. F., Abello, J., Maurer, J. M., Kumar, A., Ta, C. M., Gunasekar, S. K., Fatima, U., Kang, C., Xie, L., Adeola, O., Riker, M., Elliot-Hudson, M., Minerath, R. A., Grueter, C. E., Mullins, R. F., Stratman, A. N., & Sah, R. (2021). The SWELL1-LRRC8 complex regulates endothelial AKT-eNOS signaling and vascular function. *ELife*, *10*, e61313. <https://doi.org/10.7554/eLife.61313>
- Arundine, M., & Tymianski, M. (2003). Molecular mechanisms of calcium-dependent neurodegeneration in excitotoxicity. *Cell Calcium*, *34*(4–5), 325–337. [https://doi.org/10.1016/s0143-4160\(03\)00141-6](https://doi.org/10.1016/s0143-4160(03)00141-6)
- Atianand, M. K., & Fitzgerald, K. A. (2013). Molecular Basis of DNA Recognition in the Immune System. *The Journal of Immunology*, *190*(5), 1911–1918. <https://doi.org/10.4049/jimmunol.1203162>
- Ayata, P., Badimon, A., Strasburger, H. J., Duff, M. K., Montgomery, S. E., Loh, Y.-H. E., Ebert, A., Pimenova, A. A., Ramirez, B. R., Chan, A. T., Sullivan, J. M., Purushothaman, I., Scarpa, J. R., Goate, A. M., Busslinger, M., Shen, L., Losic, B., & Schaefer, A. (2018). Epigenetic regulation of brain region-specific microglia clearance activity. *Nature Neuroscience*, *21*(8), 1049–1060. <https://doi.org/10.1038/s41593-018-0192-3>
- Badimon, A., Strasburger, H. J., Ayata, P., Chen, X., Nair, A., Ikegami, A., Hwang, P., Chan, A. T., Graves, S. M., Uweru, J. O., Ledderose, C., Kutlu, M. G., Wheeler, M. A., Kahan, A., Ishikawa, M., Wang, Y.-C., Loh, Y.-H. E., Jiang, J. X., Surmeier, D. J., ... Schaefer, A. (2020). Negative feedback control of neuronal activity by microglia. *Nature*, *586*(7829), 417–423. <https://doi.org/10.1038/s41586-020-2777-8>
- Bao, J., Perez, C. J., Kim, J., Zhang, H., Murphy, C. J., Hamidi, T., Jaubert, J., Platt, C. D., Chou, J., Deng, M., Zhou, M.-H., Huang, Y., Gaitán-Peñas, H., Guénet, J.-L., Lin, K., Lu, Y., Chen, T., Bedford, M. T., Dent, S. Y. R., ... Benavides, F. (2018). Deficient LRRC8A-dependent volume-regulated anion channel activity is associated with male infertility in mice. *JCI Insight*, *3*(16), e99767. <https://doi.org/10.1172/jci.insight.99767>

- Barfod, E. T., Moore, A. L., Melnick, R. F., & Lidofsky, S. D. (2005). Src Regulates Distinct Pathways for Cell Volume Control through Vav and PhospholipaseC γ *. *Journal of Biological Chemistry*, 280(27), 25548–25557. <https://doi.org/10.1074/jbc.M411717200>
- Bennett, F. C., Bennett, M. L., Yaqoob, F., Mulinyawe, S. B., Grant, G. A., Hayden Gephart, M., Plowey, E. D., & Barres, B. A. (2018). A Combination of Ontogeny and CNS Environment Establishes Microglial Identity. *Neuron*, 98(6), 1170-1183.e8. <https://doi.org/10.1016/j.neuron.2018.05.014>
- Berry, M. R., Mathews, R. J., Ferdinand, J. R., Jing, C., Loudon, K. W., Wlodek, E., Dennison, T. W., Kuper, C., Neuhofer, W., & Clatworthy, M. R. (2017). Renal Sodium Gradient Orchestrates a Dynamic Antibacterial Defense Zone. *Cell*, 170(5), 860-874.e19. <https://doi.org/10.1016/j.cell.2017.07.022>
- Bertelli, S., Remigante, A., Zuccolini, P., Barbieri, R., Ferrera, L., Picco, C., Gavazzo, P., & Pusch, M. (2021). Mechanisms of Activation of LRRC8 Volume Regulated Anion Channels. *Cellular Physiology and Biochemistry: International Journal of Experimental Cellular Physiology, Biochemistry, and Pharmacology*, 55(S1), 41–56. <https://doi.org/10.33594/000000329>
- Best, L., Brown, P. D., Sener, A., & Malaisse, W. J. (2010). Electrical activity in pancreatic islet cells: The VRAC hypothesis. *Islets*, 2(2), 59–64. <https://doi.org/10.4161/isl.2.2.11171>
- Bialas, A. R., & Stevens, B. (2013). TGF- β signaling regulates neuronal C1q expression and developmental synaptic refinement. *Nature Neuroscience*, 16(12), 1773–1782. <https://doi.org/10.1038/nn.3560>
- Biber, K., Neumann, H., Inoue, K., & Boddeke, H. W. G. M. (2007). Neuronal ‘On’ and ‘Off’ signals control microglia. *Trends in Neurosciences*, 30(11), 596–602. <https://doi.org/10.1016/j.tins.2007.08.007>
- Blériot, C., Chakarov, S., & Ginhoux, F. (2020). Determinants of Resident Tissue Macrophage Identity and Function. *Immunity*, 52(6), 957–970. <https://doi.org/10.1016/j.immuni.2020.05.014>
- Bohlen, C. J., Bennett, F. C., Tucker, A. F., Collins, H. Y., Mulinyawe, S. B., & Barres, B. A. (2017). Diverse requirements for microglial survival, specification, and function revealed by defined-medium cultures. *Neuron*, 94(4), 759-773.e8. <https://doi.org/10.1016/j.neuron.2017.04.043>
- Bolger, A. M., Lohse, M., & Usadel, B. (2014). Trimmomatic: A flexible trimmer for Illumina sequence data. *Bioinformatics (Oxford, England)*, 30(15), 2114–2120. <https://doi.org/10.1093/bioinformatics/btu170>
- Bowens, N. H., Dohare, P., Kuo, Y.-H., & Mongin, A. A. (2013). DCPIB, the proposed selective blocker of volume-regulated anion channels, inhibits several glutamate transport

- pathways in glial cells. *Molecular Pharmacology*, 83(1), 22–32. <https://doi.org/10.1124/mol.112.080457>
- Brawek, B., Olmedillas Del Moral, M., & Garaschuk, O. (2019). In Vivo Visualization of Microglia Using Tomato Lectin. *Methods in Molecular Biology (Clifton, N.J.)*, 2034, 165–175. https://doi.org/10.1007/978-1-4939-9658-2_12
- Brown, G. C., & Neher, J. J. (2014). Microglial phagocytosis of live neurons. *Nature Reviews Neuroscience*, 15(4), 209–216. <https://doi.org/10.1038/nrn3710>
- Burdette, D. L., & Vance, R. E. (2013). STING and the innate immune response to nucleic acids in the cytosol. *Nature Immunology*, 14(1), 19–26. <https://doi.org/10.1038/ni.2491>
- Butler, C. A., Popescu, A. S., Kitchener, E. J. A., Allendorf, D. H., Puigdellívol, M., & Brown, G. C. (2021). Microglial phagocytosis of neurons in neurodegeneration, and its regulation. *Journal of Neurochemistry*, 158(3), 621–639. <https://doi.org/10.1111/jnc.15327>
- Butovsky, O., Jedrychowski, M. P., Moore, C. S., Cialic, R., Lanser, A. J., Gabriely, G., Koeglsperger, T., Dake, B., Wu, P. M., Doykan, C. E., Fanek, Z., Liu, L., Chen, Z., Rothstein, J. D., Ransohoff, R. M., Gygi, S. P., Antel, J. P., & Weiner, H. L. (2014). Identification of a unique TGF- β -dependent molecular and functional signature in microglia. *Nature Neuroscience*, 17(1), 131–143. <https://doi.org/10.1038/nn.3599>
- Butovsky, O., & Weiner, H. L. (2018). Microglial signatures and their role in health and disease. *Nature Reviews Neuroscience*, 19(10), 622–635. <https://doi.org/10.1038/s41583-018-0057-5>
- Buttgereit, A., Lelios, I., Yu, X., Vrohligs, M., Krakoski, N. R., Gautier, E. L., Nishinakamura, R., Becher, B., & Greter, M. (2016). Sall1 is a transcriptional regulator defining microglia identity and function. *Nature Immunology*, 17(12), 1397–1406. <https://doi.org/10.1038/ni.3585>
- Cahalan, M. D., & Lewis, R. S. (1988). Role of potassium and chloride channels in volume regulation by T lymphocytes. *Society of General Physiologists Series*, 43, 281–301.
- Cardona, A. E., Pioro, E. P., Sasse, M. E., Kostenko, V., Cardona, S. M., Dijkstra, I. M., Huang, D., Kidd, G., Dombrowski, S., Dutta, R., Lee, J.-C., Cook, D. N., Jung, S., Lira, S. A., Littman, D. R., & Ransohoff, R. M. (2006). Control of microglial neurotoxicity by the fractalkine receptor. *Nature Neuroscience*, 9(7), 917–924. <https://doi.org/10.1038/nn1715>
- Chen, E. Y., Tan, C. M., Kou, Y., Duan, Q., Wang, Z., Meirelles, G. V., Clark, N. R., & Ma'ayan, A. (2013). Enrichr: Interactive and collaborative HTML5 gene list enrichment analysis tool. *BMC Bioinformatics*, 14, 128. <https://doi.org/10.1186/1471-2105-14-128>

- Chen, G. Y., & Nuñez, G. (2010). Sterile inflammation: Sensing and reacting to damage. *Nature Reviews Immunology*, *10*(12), 826–837. <https://doi.org/10.1038/nri2873>
- Chen, Q., Sun, L., & Chen, Z. J. (2016). Regulation and function of the cGAS–STING pathway of cytosolic DNA sensing. *Nature Immunology*, *17*(10), 1142–1149. <https://doi.org/10.1038/ni.3558>
- Chiu, I. M., Morimoto, E. T. A., Goodarzi, H., Liao, J. T., O’Keeffe, S., Phatnani, H. P., Muratet, M., Carroll, M. C., Levy, S., Tavazoie, S., Myers, R. M., & Maniatis, T. (2013). A neurodegeneration-specific gene-expression signature of acutely isolated microglia from an amyotrophic lateral sclerosis mouse model. *Cell Reports*, *4*(2), 385–401. <https://doi.org/10.1016/j.celrep.2013.06.018>
- Chou, C.-Y., Shen, M.-R., Hsu, K.-S., Huang, H.-Y., & Lin, H.-C. (1998). Involvement of PKC- α in regulatory volume decrease responses and activation of volume-sensitive chloride channels in human cervical cancer HT-3 cells. *The Journal of Physiology*, *512*(2), 435–448. <https://doi.org/10.1111/j.1469-7793.1998.435be.x>
- Clarner, T., Janssen, K., Nellessen, L., Stangel, M., Skripuletz, T., Krauspe, B., Hess, F.-M., Denecke, B., Beutner, C., Linnartz-Gerlach, B., Neumann, H., Vallières, L., Amor, S., Ohl, K., Tenbrock, K., Beyer, C., & Kipp, M. (2015). CXCL10 triggers early microglial activation in the cuprizone model. *Journal of Immunology (Baltimore, Md.: 1950)*, *194*(7), 3400–3413. <https://doi.org/10.4049/jimmunol.1401459>
- Compan, V., Baroja-Mazo, A., López-Castejón, G., Gomez, A. I., Martínez, C. M., Angosto, D., Montero, M. T., Herranz, A. S., Bazán, E., Reimers, D., Mulero, V., & Pelegrín, P. (2012). Cell Volume Regulation Modulates NLRP3 Inflammasome Activation. *Immunity*, *37*(3), 487–500. <https://doi.org/10.1016/j.immuni.2012.06.013>
- Cox, N., Pokrovskii, M., Vicario, R., & Geissmann, F. (2021). Origins, Biology, and Diseases of Tissue Macrophages. *Annual Review of Immunology*, *39*(1), 313–344. <https://doi.org/10.1146/annurev-immunol-093019-111748>
- Cronk, J. C., Filiano, A. J., Louveau, A., Marin, I., Marsh, R., Ji, E., Goldman, D. H., Smirnov, I., Geraci, N., Acton, S., Overall, C. C., & Kipnis, J. (2018). Peripherally derived macrophages can engraft the brain independent of irradiation and maintain an identity distinct from microglia. *The Journal of Experimental Medicine*, *215*(6), 1627–1647. <https://doi.org/10.1084/jem.20180247>
- Cserép, C., Pósfai, B., Lénárt, N., Fekete, R., László, Z. I., Lele, Z., Orsolits, B., Molnár, G., Heindl, S., Schwarcz, A. D., Ujvári, K., Környei, Z., Tóth, K., Szabadits, E., Sperlág, B., Baranyi, M., Csiba, L., Hortobágyi, T., Maglóczy, Z., ... Dénes, Á. (2020). Microglia monitor and protect neuronal function through specialized somatic purinergic junctions. *Science*, *367*(6477), 528–537. <https://doi.org/10.1126/science.aax6752>

- Cunningham, C., Dunne, A., & Lopez-Rodriguez, A. B. (2019). Astrocytes: Heterogeneous and Dynamic Phenotypes in Neurodegeneration and Innate Immunity. In *Neuroscientist* (Vol. 25, Issue 5, pp. 455–474). SAGE Publications Inc. <https://doi.org/10.1177/1073858418809941>
- Cunningham, C. L., Martínez-Cerdeño, V., & Noctor, S. C. (2013). Microglia Regulate the Number of Neural Precursor Cells in the Developing Cerebral Cortex. *The Journal of Neuroscience*, 33(10), 4216–4233. <https://doi.org/10.1523/JNEUROSCI.3441-12.2013>
- Daniels, M. J. D., Rivers-Auty, J., Schilling, T., Spencer, N. G., Watremez, W., Fasolino, V., Booth, S. J., White, C. S., Baldwin, A. G., Freeman, S., Wong, R., Latta, C., Yu, S., Jackson, J., Fischer, N., Koziel, V., Pillot, T., Bagnall, J., Allan, S. M., ... Brough, D. (2016). Fenamate NSAIDs inhibit the NLRP3 inflammasome and protect against Alzheimer's disease in rodent models. *Nature Communications*, 7(1), 12504. <https://doi.org/10.1038/ncomms12504>
- Davalos, D., Grutzendler, J., Yang, G., Kim, J. V., Zuo, Y., Jung, S., Littman, D. R., Dustin, M. L., & Gan, W.-B. (2005). ATP mediates rapid microglial response to local brain injury in vivo. *Nature Neuroscience*, 8(6), 752–758. <https://doi.org/10.1038/nn1472>
- Decout, A., Katz, J. D., Venkatraman, S., & Ablasser, A. (2021). The cGAS–STING pathway as a therapeutic target in inflammatory diseases. *Nature Reviews Immunology*, 21(9), 548–569. <https://doi.org/10.1038/s41577-021-00524-z>
- Deneka, D., Sawicka, M., Lam, A. K. M., Paulino, C., & Dutzler, R. (2018). Structure of a volume-regulated anion channel of the LRRC8 family. *Nature*, 558(7709), 254–259. <https://doi.org/10.1038/s41586-018-0134-y>
- Dissing-Olesen, L., LeDue, J. M., Rungta, R. L., Hefendehl, J. K., Choi, H. B., & MacVicar, B. A. (2014). Activation of neuronal NMDA receptors triggers transient ATP-mediated microglial process outgrowth. *The Journal of Neuroscience: The Official Journal of the Society for Neuroscience*, 34(32), 10511–10527. <https://doi.org/10.1523/JNEUROSCI.0405-14.2014>
- Dobin, A., Davis, C. A., Schlesinger, F., Drenkow, J., Zaleski, C., Jha, S., Batut, P., Chaisson, M., & Gingeras, T. R. (2013). STAR: Ultrafast universal RNA-seq aligner. *Bioinformatics*, 29(1), 15–21. <https://doi.org/10.1093/bioinformatics/bts635>
- Ducharme, G., Newell, E. W., Pinto, C., & Schlichter, L. C. (2007). Small-conductance Cl⁻ channels contribute to volume regulation and phagocytosis in microglia. *European Journal of Neuroscience*, 26(8), 2119–2130. <https://doi.org/10.1111/j.1460-9568.2007.05802.x>
- Dunphy, G., Flannery, S. M., Almine, J. F., Connolly, D. J., Paulus, C., Jønsson, K. L., Jakobsen, M. R., Nevels, M. M., Bowie, A. G., & Unterholzner, L. (2018). Non-

- canonical Activation of the DNA Sensing Adaptor STING by ATM and IFI16 Mediates NF- κ B Signaling after Nuclear DNA Damage. *Molecular Cell*, 71(5), 745-760.e5. <https://doi.org/10.1016/j.molcel.2018.07.034>
- Easley-Neal, C., Foreman, O., Sharma, N., Zarrin, A. A., & Weimer, R. M. (2019). CSF1R Ligands IL-34 and CSF1 Are Differentially Required for Microglia Development and Maintenance in White and Gray Matter Brain Regions. *Frontiers in Immunology*, 10, 2199. <https://doi.org/10.3389/fimmu.2019.02199>
- Eder, C. (2005). Regulation of microglial behavior by ion channel activity. *Journal of Neuroscience Research*, 81(3), 314–321. <https://doi.org/10.1002/jnr.20476>
- Eder, C., Klee, R., & Heinemann, U. (1998). Involvement of stretch-activated Cl⁻ channels in ramification of murine microglia. *The Journal of Neuroscience: The Official Journal of the Society for Neuroscience*, 18(18), 7127–7137.
- Epelman, S., Lavine, K. J., & Randolph, G. J. (2014). Origin and Functions of Tissue Macrophages. *Immunity*, 41(1), 21–35. <https://doi.org/10.1016/j.immuni.2014.06.013>
- Erblich, B., Zhu, L., Etgen, A. M., Dobrenis, K., & Pollard, J. W. (2011). Absence of colony stimulation factor-1 receptor results in loss of microglia, disrupted brain development and olfactory deficits. *PloS One*, 6(10), e26317. <https://doi.org/10.1371/journal.pone.0026317>
- Etienne, F., Mastrolia, V., Maroteaux, L., Girault, J.-A., Gervasi, N., & Roumier, A. (2019). Two-photon Imaging of Microglial Processes' Attraction Toward ATP or Serotonin in Acute Brain Slices. *JoVE (Journal of Visualized Experiments)*, 143, e58788. <https://doi.org/10.3791/58788>
- Eyo, U. B., Mo, M., Yi, M.-H., Murugan, M., Liu, J., Yarlagadda, R., Margolis, D. J., Xu, P., & Wu, L.-J. (2018). P2Y₁₂R-Dependent Translocation Mechanisms Gate the Changing Microglial Landscape. *Cell Reports*, 23(4), 959–966. <https://doi.org/10.1016/j.celrep.2018.04.001>
- Eyo, U. B., Peng, J., Swiatkowski, P., Mukherjee, A., Bispo, A., & Wu, L.-J. (2014). Neuronal Hyperactivity Recruits Microglial Processes via Neuronal NMDA Receptors and Microglial P2Y₁₂ Receptors after Status Epilepticus. *The Journal of Neuroscience*, 34(32), 10528–10540. <https://doi.org/10.1523/JNEUROSCI.0416-14.2014>
- Fehrenbach, D. J., & Mattson, D. L. (2020). Inflammatory macrophages in the kidney contribute to salt-sensitive hypertension. *American Journal of Physiology-Renal Physiology*, 318(3), F544–F548. <https://doi.org/10.1152/ajprenal.00454.2019>
- Feustel, P. J., Jin, Y., & Kimelberg, H. K. (2004). Volume-regulated anion channels are the predominant contributors to release of excitatory amino acids in the ischemic cortical penumbra. *Stroke*, 35(5), 1164–1168. <https://doi.org/10.1161/01.STR.0000124127.57946.a1>

- Fitzgerald, K. A., McWhirter, S. M., Faia, K. L., Rowe, D. C., Latz, E., Golenbock, D. T., Coyle, A. J., Liao, S.-M., & Maniatis, T. (2003). IKKepsilon and TBK1 are essential components of the IRF3 signaling pathway. *Nature Immunology*, *4*(5), 491–496. <https://doi.org/10.1038/ni921>
- Flannagan, R. S., Jaumouillé, V., & Grinstein, S. (2012). The Cell Biology of Phagocytosis. *Annual Review of Pathology: Mechanisms of Disease*, *7*(1), 61–98. <https://doi.org/10.1146/annurev-pathol-011811-132445>
- Friedman, B. A., Srinivasan, K., Ayalon, G., Meilandt, W. J., Lin, H., Huntley, M. A., Cao, Y., Lee, S.-H., Haddick, P. C. G., Ngu, H., Modrusan, Z., Larson, J. L., Kaminker, J. S., Brug, M. P. van der, & Hansen, D. V. (2018). Diverse Brain Myeloid Expression Profiles Reveal Distinct Microglial Activation States and Aspects of Alzheimer's Disease Not Evident in Mouse Models. *Cell Reports*, *22*(3), 832–847. <https://doi.org/10.1016/j.celrep.2017.12.066>
- Fu, H., Liu, B., Frost, J. L., Hong, S., Jin, M., Ostaszewski, B., Shankar, G. M., Costantino, I. M., Carroll, M. C., Mayadas, T. N., & Lemere, C. A. (2012). Complement component C3 and complement receptor type 3 contribute to the phagocytosis and clearance of fibrillar A β by microglia. *Glia*, *60*(6), 993–1003. <https://doi.org/10.1002/glia.22331>
- Fu, Y., Liu, Q., Anrather, J., & Shi, F.-D. (2015). Immune interventions in stroke. *Nature Reviews Neurology*, *11*(9), 524–535. <https://doi.org/10.1038/nrneurol.2015.144>
- Füger, P., Hefendehl, J. K., Veeraraghavalu, K., Wendeln, A.-C., Schlosser, C., Obermüller, U., Wegenast-Braun, B. M., Neher, J. J., Martus, P., Kohsaka, S., Thunemann, M., Feil, R., Sisodia, S. S., Skodras, A., & Jucker, M. (2017). Microglia turnover with aging and in an Alzheimer's model via long-term in vivo single-cell imaging. *Nature Neuroscience*, *20*(10), 1371–1376. <https://doi.org/10.1038/nn.4631>
- Fuhrmann, M., Bittner, T., Jung, C. K. E., Burgold, S., Page, R. M., Mitteregger, G., Haass, C., LaFerla, F. M., Kretschmar, H., & Herms, J. (2010). Microglial Cx3cr1 knockout prevents neuron loss in a mouse model of Alzheimer's disease. *Nature Neuroscience*, *13*(4), 411–413. <https://doi.org/10.1038/nn.2511>
- Furtner, T., Zierler, S., & Kerschbaum, H. H. (2007). Blockade of chloride channels suppresses engulfment of microspheres in the microglial cell line, BV-2. *Brain Research*, *1184*, 1–9. <https://doi.org/10.1016/j.brainres.2007.09.057>
- Gaitán-Peñas, H., Gradogna, A., Laparra-Cuervo, L., Solsona, C., Fernández-Dueñas, V., Barrallo-Gimeno, A., Ciruela, F., Lakadamyali, M., Pusch, M., & Estévez, R. (2016). Investigation of LRRC8-Mediated Volume-Regulated Anion Currents in Xenopus Oocytes. *Biophysical Journal*, *111*(7), 1429–1443. <https://doi.org/10.1016/j.bpj.2016.08.030>

- Galloway, D. A., Phillips, A. E. M., Owen, D. R. J., & Moore, C. S. (2019). Phagocytosis in the Brain: Homeostasis and Disease. *Frontiers in Immunology*, *10*, 790. <https://doi.org/10.3389/fimmu.2019.00790>
- Gautier, E. L., Shay, T., Miller, J., Greter, M., Jakubzick, C., Ivanov, S., Helft, J., Chow, A., Elpek, K. G., Gordonov, S., Mazloom, A. R., Ma'ayan, A., Chua, W.-J., Hansen, T. H., Turley, S. J., Merad, M., Randolph, G. J., & Immunological Genome Consortium. (2012). Gene-expression profiles and transcriptional regulatory pathways that underlie the identity and diversity of mouse tissue macrophages. *Nature Immunology*, *13*(11), 1118–1128. <https://doi.org/10.1038/ni.2419>
- Ginhoux, F., & Garel, S. (2018). The mysterious origins of microglia. *Nature Neuroscience*, *21*(7), 897–899. <https://doi.org/10.1038/s41593-018-0176-3>
- Ginhoux, F., & Williams, M. (2016). Tissue-Resident Macrophage Ontogeny and Homeostasis. *Immunity*, *44*(3), 439–449. <https://doi.org/10.1016/j.immuni.2016.02.024>
- Goldey, G. J., Roumis, D. K., Glickfeld, L. L., Kerlin, A. M., Reid, R. C., Bonin, V., Schafer, D. P., & Andermann, M. L. (2014). Removable cranial windows for long-term imaging in awake mice. *Nature Protocols*, *9*(11), 2515–2538. <https://doi.org/10.1038/nprot.2014.165>
- Goldmann, T., Wieghofer, P., Jordão, M. J. C., Prutek, F., Hagemeyer, N., Frenzel, K., Amann, L., Staszewski, O., Kierdorf, K., Krueger, M., Locatelli, G., Hochgerner, H., Zeiser, R., Eelman, S., Geissmann, F., Priller, J., Rossi, F. M. V., Bechmann, I., Kerschensteiner, M., ... Prinz, M. (2016). Origin, fate and dynamics of macrophages at central nervous system interfaces. *Nature Immunology*, *17*(7), 797–805. <https://doi.org/10.1038/ni.3423>
- Gong, W., Xu, H., Shimizu, T., Morishima, S., Tanabe, S., Tachibe, T., Uchida, S., Sasaki, S., & Okada, Y. (2004). CIC-3-independent, PKC-dependent Activity of Volume-sensitive Cl⁻ Channel in Mouse Ventricular Cardiomyocytes. *Cellular Physiology and Biochemistry*, *14*(4–6), 213–224. <https://doi.org/10.1159/000080330>
- Gosselin, D., Skola, D., Coufal, N. G., Holtman, I. R., Schlachetzki, J. C. M., Sajti, E., Jaeger, B. N., O'Connor, C., Fitzpatrick, C., Pasillas, M. P., Pena, M., Adair, A., Gonda, D. D., Levy, M. L., Ransohoff, R. M., Gage, F. H., & Glass, C. K. (2017). An environment-dependent transcriptional network specifies human microglia identity. *Science (New York, N.Y.)*, *356*(6344), eaal3222. <https://doi.org/10.1126/science.aal3222>
- Grabert, K., Michoel, T., Karavolos, M. H., Clohisey, S., Baillie, J. K., Stevens, M. P., Freeman, T. C., Summers, K. M., & McColl, B. W. (2016). Microglial brain region-dependent diversity and selective regional sensitivities to aging. *Nature Neuroscience*, *19*(3), 504–516. <https://doi.org/10.1038/nn.4222>

- Green, J. P., Swanton, T., Morris, L. V., El-Sharkawy, L. Y., Cook, J., Yu, S., Beswick, J., Adamson, A. D., Humphreys, N. E., Bryce, R., Freeman, S., Lawrence, C., & Brough, D. (2020). LRRRC8A is essential for hypotonicity-, but not for DAMP-induced NLRP3 inflammasome activation. *ELife*, 9. <https://doi.org/10.7554/eLife.59704>
- Guneykaya, D., Ivanov, A., Hernandez, D. P., Haage, V., Wojtas, B., Meyer, N., Maricos, M., Jordan, P., Buonfiglioli, A., Gielniewski, B., Ochocka, N., Cömert, C., Friedrich, C., Artiles, L. S., Kaminska, B., Mertins, P., Beule, D., Kettenmann, H., & Wolf, S. A. (2018). Transcriptional and Translational Differences of Microglia from Male and Female Brains. *Cell Reports*, 24(10), 2773-2783.e6. <https://doi.org/10.1016/j.celrep.2018.08.001>
- Gyoneva, S., Davalos, D., Biswas, D., Swanger, S. A., Garnier-Amblard, E., Loth, F., Akassoglou, K., & Traynelis, S. F. (2014). Systemic inflammation regulates microglial responses to tissue damage in vivo. *Glia*, 62(8), 1345–1360. <https://doi.org/10.1002/glia.22686>
- Hagemeyer, N., Hanft, K.-M., Akriditou, M.-A., Unger, N., Park, E. S., Stanley, E. R., Staszewski, O., Dimou, L., & Prinz, M. (2017). Microglia contribute to normal myelinogenesis and to oligodendrocyte progenitor maintenance during adulthood. *Acta Neuropathologica*, 134(3), 441–458. <https://doi.org/10.1007/s00401-017-1747-1>
- Hammond, T. R., Dufort, C., Dissing-Olesen, L., Giera, S., Young, A., Wysoker, A., Walker, A. J., Gergits, F., Segel, M., Nemes, J., Marsh, S. E., Saunders, A., Macosko, E., Ginhoux, F., Chen, J., Franklin, R. J. M., Piao, X., McCarroll, S. A., & Stevens, B. (2019). Single-Cell RNA Sequencing of Microglia throughout the Mouse Lifespan and in the Injured Brain Reveals Complex Cell-State Changes. *Immunity*, 50(1), 253-271.e6. <https://doi.org/10.1016/j.immuni.2018.11.004>
- Han, Y.-E., Kwon, J., Won, J., An, H., Jang, M. W., Woo, J., Lee, J. S., Park, M. G., Yoon, B.-E., Lee, S. E., Hwang, E. M., Jung, J.-Y., Park, H., Oh, S.-J., & Lee, C. J. (2019). Tweety-homolog (Ttyh) Family Encodes the Pore-forming Subunits of the Swelling-dependent Volume-regulated Anion Channel (VRAC_{swell}) in the Brain. *Experimental Neurobiology*, 28(2), 183–215. <https://doi.org/10.5607/en.2019.28.2.183>
- Haney, M. S., Bohlen, C. J., Morgens, D. W., Ousey, J. A., Barkal, A. A., Tsui, C. K., Ego, B. K., Levin, R., Kamber, R. A., Collins, H., Tucker, A., Li, A., Vorselen, D., Labitigan, L., Crane, E., Boyle, E., Jiang, L., Chan, J., Rincón, E., ... Bassik, M. C. (2018). Identification of phagocytosis regulators using magnetic genome-wide CRISPR screens. *Nature Genetics*, 50(12), 1716–1727. <https://doi.org/10.1038/s41588-018-0254-1>
- Hanisch, U.-K., & Kettenmann, H. (2007). Microglia: Active sensor and versatile effector cells in the normal and pathologic brain. *Nature Neuroscience*, 10(11), 1387–1394. <https://doi.org/10.1038/nn1997>

- Harl, B., Schmölzer, J., Jakab, M., Ritter, M., & Kerschbaum, H. H. (2013). Chloride channel blockers suppress formation of engulfment pseudopodia in microglial cells. *Cellular Physiology and Biochemistry: International Journal of Experimental Cellular Physiology, Biochemistry, and Pharmacology*, 31(2–3), 319–337. <https://doi.org/10.1159/000343370>
- Harrigan, T. J., Abdullaev, I. F., Jourd'heuil, D., & Mongin, A. A. (2008). Activation of microglia with zymosan promotes excitatory amino acid release via volume-regulated anion channels: The role of NADPH oxidases. *Journal of Neurochemistry*, 106(6), 2449–2462. <https://doi.org/10.1111/j.1471-4159.2008.05553.x>
- Haynes, S. E., Hollopeter, G., Yang, G., Kurpius, D., Dailey, M. E., Gan, W.-B., & Julius, D. (2006). The P2Y₁₂ receptor regulates microglial activation by extracellular nucleotides. *Nature Neuroscience*, 9(12), 1512–1519. <https://doi.org/10.1038/nn1805>
- Hazama, A., & Okada, Y. (1988). Ca²⁺ sensitivity of volume-regulatory K⁺ and Cl⁻ channels in cultured human epithelial cells. *The Journal of Physiology*, 402, 687–702. <https://doi.org/10.1113/jphysiol.1988.sp017229>
- Heindl, S., Gesierich, B., Benakis, C., Llovera, G., Duering, M., & Liesz, A. (2018). Automated Morphological Analysis of Microglia After Stroke. *Frontiers in Cellular Neuroscience*, 12. <https://doi.org/10.3389/fncel.2018.00106>
- Heneka, M. T., Kummer, M. P., & Latz, E. (2014). Innate immune activation in neurodegenerative disease. *Nature Reviews Immunology*, 14(7), 463–477. <https://doi.org/10.1038/nri3705>
- Heo, D. K., Lim, H. M., Nam, J. H., Lee, M. G., & Kim, J. Y. (2015). Regulation of phagocytosis and cytokine secretion by store-operated calcium entry in primary isolated murine microglia. *Cellular Signalling*, 27(1), 177–186. <https://doi.org/10.1016/j.cellsig.2014.11.003>
- Hickman, S. E., Kingery, N. D., Ohsumi, T. K., Borowsky, M. L., Wang, L. C., Means, T. K., & El Khoury, J. (2013). The microglial sensome revealed by direct RNA sequencing. *Nature Neuroscience*, 16(12), 1896–1905. <https://doi.org/10.1038/nn.3554>
- Hines, D. J., Hines, R. M., Mulligan, S. J., & Macvicar, B. A. (2009). Microglia processes block the spread of damage in the brain and require functional chloride channels. *Glia*, 57(15), 1610–1618. <https://doi.org/10.1002/glia.20874>
- Hoek, R. M., Ruuls, S. R., Murphy, C. A., Wright, G. J., Goddard, R., Zurawski, S. M., Blom, B., Homola, M. E., Streit, W. J., Brown, M. H., Barclay, A. N., & Sedgwick, J. D. (2000). Down-regulation of the macrophage lineage through interaction with OX2 (CD200). *Science (New York, N.Y.)*, 290(5497), 1768–1771. <https://doi.org/10.1126/science.290.5497.1768>

- Hoffmann, E. K., Lambert, I. H., & Pedersen, S. F. (2009). Physiology of Cell Volume Regulation in Vertebrates. *Physiological Reviews*, 89(1), 193–277. <https://doi.org/10.1152/physrev.00037.2007>
- Holm, T. H., Draeby, D., & Owens, T. (2012). Microglia are required for astroglial toll-like receptor 4 response and for optimal TLR2 and TLR3 response. *GLIA*, 60(4), 630–638. <https://doi.org/10.1002/glia.22296>
- Honda, K., Takaoka, A., & Taniguchi, T. (2006). Type I Inteferon Gene Induction by the Interferon Regulatory Factor Family of Transcription Factors. *Immunity*, 25(3), 349–360. <https://doi.org/10.1016/j.immuni.2006.08.009>
- Hong, S., Beja-Glasser, V. F., Nfonoyim, B. M., Frouin, A., Li, S., Ramakrishnan, S., Merry, K. M., Shi, Q., Rosenthal, A., Barres, B. A., Lemere, C. A., Selkoe, D. J., & Stevens, B. (2016). Complement and microglia mediate early synapse loss in Alzheimer mouse models. *Science (New York, N.Y.)*, 352(6286), 712–716. <https://doi.org/10.1126/science.aad8373>
- Humphrey, S. J., Yang, G., Yang, P., Fazakerley, D. J., Stöckli, J., Yang, J. Y., & James, D. E. (2013). Dynamic adipocyte phosphoproteome reveals that Akt directly regulates mTORC2. *Cell Metabolism*, 17(6), 1009–1020. <https://doi.org/10.1016/j.cmet.2013.04.010>
- Imbimbo, B. P., Solfrizzi, V., & Panza, F. (2010). Are NSAIDs Useful to Treat Alzheimer's Disease or Mild Cognitive Impairment? *Frontiers in Aging Neuroscience*, 2, 19. <https://doi.org/10.3389/fnagi.2010.00019>
- Ip, W. K. E., & Medzhitov, R. (2015). Macrophages monitor tissue osmolarity and induce inflammatory response through NLRP3 and NLRC4 inflammasome activation. *Nature Communications*, 6(1), 6931. <https://doi.org/10.1038/ncomms7931>
- Ivashkiv, L. B., & Donlin, L. T. (2014). Regulation of type I interferon responses. *Nature Reviews Immunology*, 14(1), 36–49. <https://doi.org/10.1038/nri3581>
- Izquierdo, P., Attwell, D., & Madry, C. (2019). Ion Channels and Receptors as Determinants of Microglial Function. *Trends in Neurosciences*, 42(4), 278–292. <https://doi.org/10.1016/j.tins.2018.12.007>
- Jay, T. R., Hirsch, A. M., Broihier, M. L., Miller, C. M., Neilson, L. E., Ransohoff, R. M., Lamb, B. T., & Landreth, G. E. (2017). Disease Progression-Dependent Effects of TREM2 Deficiency in a Mouse Model of Alzheimer's Disease. *The Journal of Neuroscience: The Official Journal of the Society for Neuroscience*, 37(3), 637–647. <https://doi.org/10.1523/JNEUROSCI.2110-16.2016>
- Jay, T. R., Miller, C. M., Cheng, P. J., Graham, L. C., Bemiller, S., Broihier, M. L., Xu, G., Margevicius, D., Karlo, J. C., Sousa, G. L., Cotleur, A. C., Butovsky, O., Bekris, L., Staugaitis, S. M., Leverenz, J. B., Pimplikar, S. W., Landreth, G. E., Howell, G. R.,

- Ransohoff, R. M., & Lamb, B. T. (2015). TREM2 deficiency eliminates TREM2+ inflammatory macrophages and ameliorates pathology in Alzheimer's disease mouse models. *The Journal of Experimental Medicine*, 212(3), 287–295. <https://doi.org/10.1084/jem.20142322>
- Jung, S., Aliberti, J., Graemmel, P., Sunshine, M. J., Kreutzberg, G. W., Sher, A., & Littman, D. R. (2000). Analysis of fractalkine receptor CX(3)CR1 function by targeted deletion and green fluorescent protein reporter gene insertion. *Molecular and Cellular Biology*, 20(11), 4106–4114. <https://doi.org/10.1128/MCB.20.11.4106-4114.2000>
- Karatas, H., Erdener, S. E., Gursoy-Ozdemir, Y., Gurer, G., Soylemezoglu, F., Dunn, A. K., & Dalkara, T. (2011). Thrombotic distal middle cerebral artery occlusion produced by topical FeCl₃ application: A novel model suitable for intravital microscopy and thrombolysis studies. *Journal of Cerebral Blood Flow & Metabolism*, 31(6), 1452–1460. <https://doi.org/10.1038/jcbfm.2011.8>
- Kasuya, G., Nakane, T., Yokoyama, T., Jia, Y., Inoue, M., Watanabe, K., Nakamura, R., Nishizawa, T., Kusakizako, T., Tsutsumi, A., Yanagisawa, H., Dohmae, N., Hattori, M., Ichijo, H., Yan, Z., Kikkawa, M., Shirouzu, M., Ishitani, R., & Nureki, O. (2018). Cryo-EM structures of the human volume-regulated anion channel LRRC8. *Nature Structural & Molecular Biology*, 25(9), 797–804. <https://doi.org/10.1038/s41594-018-0109-6>
- Kato, H., Takeuchi, O., Sato, S., Yoneyama, M., Yamamoto, M., Matsui, K., Uematsu, S., Jung, A., Kawai, T., Ishii, K. J., Yamaguchi, O., Otsu, K., Tsujimura, T., Koh, C.-S., Reis e Sousa, C., Matsuura, Y., Fujita, T., & Akira, S. (2006). Differential roles of MDA5 and RIG-I helicases in the recognition of RNA viruses. *Nature*, 441(7089), 101–105. <https://doi.org/10.1038/nature04734>
- Kawai, T., & Akira, S. (2010). The role of pattern-recognition receptors in innate immunity: Update on Toll-like receptors. *Nature Immunology*, 11(5), 373–384. <https://doi.org/10.1038/ni.1863>
- Ke, M.-T., Fujimoto, S., & Imai, T. (2013). SeeDB: A simple and morphology-preserving optical clearing agent for neuronal circuit reconstruction. *Nature Neuroscience*, 16(8), 1154–1161. <https://doi.org/10.1038/nn.3447>
- Kefauver, J. M., Saotome, K., Dubin, A. E., Pallesen, J., Cottrell, C. A., Cahalan, S. M., Qiu, Z., Hong, G., Crowley, C. S., Whitwam, T., Lee, W.-H., Ward, A. B., & Patapoutian, A. (2018). Structure of the human volume regulated anion channel. *ELife*, 7, e38461. <https://doi.org/10.7554/eLife.38461>
- Keren-Shaul, H., Spinrad, A., Weiner, A., Matcovitch-Natan, O., Dvir-Szternfeld, R., Ulland, T. K., David, E., Baruch, K., Lara-Astaiso, D., Toth, B., Itzkovitz, S., Colonna, M., Schwartz, M., & Amit, I. (2017). A Unique Microglia Type Associated with Restricting

- Development of Alzheimer's Disease. *Cell*, 169(7), 1276-1290.e17. <https://doi.org/10.1016/j.cell.2017.05.018>
- Kern, D. M., Oh, S., Hite, R. K., & Brohawn, S. G. (2019). Cryo-EM structures of the DCPIB-inhibited volume-regulated anion channel LRRC8A in lipid nanodiscs. *ELife*, 8, e42636. <https://doi.org/10.7554/eLife.42636>
- Kettenmann, H., Hanisch, U.-K., Noda, M., & Verkhratsky, A. (2011). Physiology of Microglia. *Physiological Reviews*, 91(2), 461–553. <https://doi.org/10.1152/physrev.00011.2010>
- Kierdorf, K., Erny, D., Goldmann, T., Sander, V., Schulz, C., Perdiguero, E. G., Wieghofer, P., Heinrich, A., Riemke, P., Hölscher, C., Müller, D. N., Luckow, B., Brouwer, T., Debowski, K., Fritz, G., Opdenakker, G., Diefenbach, A., Biber, K., Heikenwalder, M., ... Prinz, M. (2013). Microglia emerge from erythromyeloid precursors via Pu.1- and Irf8-dependent pathways. *Nature Neuroscience*, 16(3), 273–280. <https://doi.org/10.1038/nn.3318>
- Kim, M.-J., Cheng, G., & Agrawal, D. K. (2004). Cl⁻ channels are expressed in human normal monocytes: A functional role in migration, adhesion and volume change. *Clinical and Experimental Immunology*, 138(3), 453–459. <https://doi.org/10.1111/j.1365-2249.2004.02635.x>
- Kimelberg, H. K. (2005). Astrocytic swelling in cerebral ischemia as a possible cause of injury and target for therapy. *Glia*, 50(4), 389–397. <https://doi.org/10.1002/glia.20174>
- Kimelberg, H. K., Feustel, P. J., Jin, Y., Paquette, J., Boulos, A., Keller, R. W., & Tranmer, B. I. (2000). Acute treatment with tamoxifen reduces ischemic damage following middle cerebral artery occlusion. *Neuroreport*, 11(12), 2675–2679. <https://doi.org/10.1097/00001756-200008210-00014>
- Kimelberg, H. K., Goderie, S. K., Higman, S., Pang, S., & Waniewski, R. A. (1990). Swelling-induced release of glutamate, aspartate, and taurine from astrocyte cultures. *The Journal of Neuroscience: The Official Journal of the Society for Neuroscience*, 10(5), 1583–1591.
- Kimelberg, H. K., Jin, Y., Charniga, C., & Feustel, P. J. (2003). Neuroprotective activity of tamoxifen in permanent focal ischemia. *Journal of Neurosurgery*, 99(1), 138–142. <https://doi.org/10.3171/jns.2003.99.1.0138>
- Kondo, Y., & Duncan, I. D. (2009). Selective reduction in microglia density and function in the white matter of colony-stimulating factor-1-deficient mice. *Journal of Neuroscience Research*, 87(12), 2686–2695. <https://doi.org/10.1002/jnr.22096>
- König, B., & Stauber, T. (2019). Biophysics and Structure-Function Relationships of LRRC8-Formed Volume-Regulated Anion Channels. *Biophysical Journal*, 116(7), 1185–1193. <https://doi.org/10.1016/j.bpj.2019.02.014>

- Krasemann, S., Madore, C., Cialic, R., Baufeld, C., Calcagno, N., El Fatimy, R., Beckers, L., O'Loughlin, E., Xu, Y., Fanek, Z., Greco, D. J., Smith, S. T., Tweet, G., Humulock, Z., Zrzavy, T., Conde-Sanroman, P., Gacias, M., Weng, Z., Chen, H., ... Butovsky, O. (2017). The TREM2-APOE pathway drives the transcriptional phenotype of dysfunctional microglia in neurodegenerative diseases. *Immunity*, *47*(3), 566-581.e9. <https://doi.org/10.1016/j.immuni.2017.08.008>
- Krause, U., Rider, M. H., & Hue, L. (1996). Protein Kinase Signaling Pathway Triggered by Cell Swelling and Involved in the Activation of Glycogen Synthase and Acetyl-CoA Carboxylase in Isolated Rat Hepatocytes. *Journal of Biological Chemistry*, *271*(28), 16668–16673. <https://doi.org/10.1074/jbc.271.28.16668>
- Kubota, K., Kim, J. Y., Sawada, A., Tokimasa, S., Fujisaki, H., Matsuda-Hashii, Y., Ozono, K., & Hara, J. (2004). LRRC8 involved in B cell development belongs to a novel family of leucine-rich repeat proteins. *FEBS Letters*, *564*(1–2), 147–152. [https://doi.org/10.1016/S0014-5793\(04\)00332-1](https://doi.org/10.1016/S0014-5793(04)00332-1)
- Kültz, D., & Chakravarty, D. (2001). Hyperosmolality in the form of elevated NaCl but not urea causes DNA damage in murine kidney cells. *Proceedings of the National Academy of Sciences of the United States of America*, *98*(4), 1999–2004. <https://doi.org/10.1073/pnas.98.4.1999>
- Kumar, A., Xie, L., Ta, C. M., Hinton, A. O., Gunasekar, S. K., Minerath, R. A., Shen, K., Maurer, J. M., Grueter, C. E., Abel, E. D., Meyer, G., & Sah, R. (2020). SWELL1 regulates skeletal muscle cell size, intracellular signaling, adiposity and glucose metabolism. *ELife*, *9*, e58941. <https://doi.org/10.7554/eLife.58941>
- Kumar, L., Chou, J., Yee, C. S. K., Borzutzky, A., Vollmann, E. H., von Andrian, U. H., Park, S.-Y., Hollander, G., Manis, J. P., Poliani, P. L., & Geha, R. S. (2014). Leucine-rich repeat containing 8A (LRRC8A) is essential for T lymphocyte development and function. *The Journal of Experimental Medicine*, *211*(5), 929–942. <https://doi.org/10.1084/jem.20131379>
- Kurashima, K., Shiozaki, A., Kudou, M., Shimizu, H., Arita, T., Kosuga, T., Konishi, H., Komatsu, S., Kubota, T., Fujiwara, H., Okamoto, K., Kishimoto, M., Konishi, E., & Otsuji, E. (2021). LRRC8A influences the growth of gastric cancer cells via the p53 signaling pathway. *Gastric Cancer*, *24*(5), 1063–1075. <https://doi.org/10.1007/s10120-021-01187-4>
- Lahey, L. J., Mardjuki, R. E., Wen, X., Hess, G. T., Ritchie, C., Carozza, J. A., Böhnert, V., Maduke, M., Bassik, M. C., & Li, L. (2020). LRRC8A:C/E Heteromeric Channels Are Ubiquitous Transporters of cGAMP. *Molecular Cell*, *80*(4), 578-591.e5. <https://doi.org/10.1016/j.molcel.2020.10.021>
- Lalouette, A., Lablack, A., Guenet, J.-L., Montagutelli, X., & Segretain, D. (1996). Male Sterility Caused by Sperm Cell-Specific Structural Abnormalities in Ebouiriffé, a New Mutation

- of the House Mouse¹. *Biology of Reproduction*, 55(2), 355–363. <https://doi.org/10.1095/biolreprod55.2.355>
- Lavin, Y., Winter, D., Blecher-Gonen, R., David, E., Keren-Shaul, H., Merad, M., Jung, S., & Amit, I. (2014). Tissue-resident macrophage enhancer landscapes are shaped by the local microenvironment. *Cell*, 159(6), 1312–1326. <https://doi.org/10.1016/j.cell.2014.11.018>
- Lawson, L. J., Perry, V. H., Dri, P., & Gordon, S. (1990). Heterogeneity in the distribution and morphology of microglia in the normal adult mouse brain. *Neuroscience*, 39(1), 151–170. [https://doi.org/10.1016/0306-4522\(90\)90229-w](https://doi.org/10.1016/0306-4522(90)90229-w)
- Le Behot, A., Gauberti, M., Martinez De Lizarrondo, S., Montagne, A., Lemarchand, E., Repesse, Y., Guillou, S., Denis, C. V., Maubert, E., Orset, C., & Vivien, D. (2014). Gplba-VWF blockade restores vessel patency by dissolving platelet aggregates formed under very high shear rate in mice. *Blood*, 123(21), 3354–3363. <https://doi.org/10.1182/blood-2013-12-543074>
- Li, D., & Wu, M. (2021). Pattern recognition receptors in health and diseases. *Signal Transduction and Targeted Therapy*, 6(1), 1–24. <https://doi.org/10.1038/s41392-021-00687-0>
- Li, Q., Cheng, Z., Zhou, L., Darmanis, S., Neff, N. F., Okamoto, J., Gulati, G., Bennett, M. L., Sun, L. O., Clarke, L. E., Marschallinger, J., Yu, G., Quake, S. R., Wyss-Coray, T., & Barres, B. A. (2019). Developmental Heterogeneity of Microglia and Brain Myeloid Cells Revealed by Deep Single-Cell RNA Sequencing. *Neuron*, 101(2), 207–223.e10. <https://doi.org/10.1016/j.neuron.2018.12.006>
- Liddelow, S. A., Guttenplan, K. A., Clarke, L. E., Bennett, F. C., Bohlen, C. J., Schirmer, L., Bennett, M. L., Münch, A. E., Chung, W.-S., Peterson, T. C., Wilton, D. K., Frouin, A., Napier, B. A., Panicker, N., Kumar, M., Buckwalter, M. S., Rowitch, D. H., Dawson, V. L., Dawson, T. M., ... Barres, B. A. (2017). Neurotoxic reactive astrocytes are induced by activated microglia. *Nature*, 541(7638), 481–487. <https://doi.org/10.1038/nature21029>
- Lou, N., Takano, T., Pei, Y., Xavier, A. L., Goldman, S. A., & Nedergaard, M. (2016). Purinergic receptor P2RY12-dependent microglial closure of the injured blood–brain barrier. *Proceedings of the National Academy of Sciences of the United States of America*, 113(4), 1074–1079. <https://doi.org/10.1073/pnas.1520398113>
- Love, M. I., Huber, W., & Anders, S. (2014). Moderated estimation of fold change and dispersion for RNA-seq data with DESeq2. *Genome Biology*, 15(12), 550. <https://doi.org/10.1186/s13059-014-0550-8>

- Lu, P., Ding, Q., Li, X., Ji, X., Li, L., Fan, Y., Xia, Y., Tian, D., & Liu, M. (2019). SWELL1 promotes cell growth and metastasis of hepatocellular carcinoma in vitro and in vivo. *EBioMedicine*, *48*, 100–116. <https://doi.org/10.1016/j.ebiom.2019.09.007>
- Luo, L., Song, S., Ezenwukwa, C. C., Jalali, S., Sun, B., & Sun, D. (2021). Ion channels and transporters in microglial function in physiology and brain diseases. *Neurochemistry International*, *142*, 104925. <https://doi.org/10.1016/j.neuint.2020.104925>
- Lutter, D., Ullrich, F., Lueck, J. C., Kempa, S., & Jentsch, T. J. (2017). Selective transport of neurotransmitters and modulators by distinct volume-regulated LRRC8 anion channels. *Journal of Cell Science*, *130*(6), 1122–1133. <https://doi.org/10.1242/jcs.196253>
- Lv, J., Liang, Y., Zhang, S., Lan, Q., Xu, Z., Wu, X., Kang, L., Ren, J., Cao, Y., Wu, T., Lin, K. L., Yung, K. K. L., Cao, X., Pang, J., & Zhou, P. (2019). DCPIB, an Inhibitor of Volume-Regulated Anion Channels, Distinctly Modulates K2P Channels. *ACS Chemical Neuroscience*, *10*(6), 2786–2793. <https://doi.org/10.1021/acscemneuro.9b00010>
- Madry, C., Kyrargyri, V., Arancibia-Cárcamo, I. L., Jolivet, R., Kohsaka, S., Bryan, R. M., & Attwell, D. (2018). Microglial Ramification, Surveillance, and Interleukin-1 β Release Are Regulated by the Two-Pore Domain K⁺ Channel THIK-1. *Neuron*, *97*(2), 299–312.e6. <https://doi.org/10.1016/j.neuron.2017.12.002>
- Maier, M., Peng, Y., Jiang, L., Seabrook, T. J., Carroll, M. C., & Lemere, C. A. (2008). Complement C3 deficiency leads to accelerated amyloid beta plaque deposition and neurodegeneration and modulation of the microglia/macrophage phenotype in amyloid precursor protein transgenic mice. *The Journal of Neuroscience: The Official Journal of the Society for Neuroscience*, *28*(25), 6333–6341. <https://doi.org/10.1523/JNEUROSCI.0829-08.2008>
- Manich, G., Recasens, M., Valente, T., Almolda, B., González, B., & Castellano, B. (2019). Role of the CD200-CD200R Axis During Homeostasis and Neuroinflammation. *Neuroscience*, *405*, 118–136. <https://doi.org/10.1016/j.neuroscience.2018.10.030>
- Martinez, F. O., & Gordon, S. (2014). The M1 and M2 paradigm of macrophage activation: Time for reassessment. *F1000prime Reports*, *6*, 13. <https://doi.org/10.12703/P6-13>
- Masuda, T., Sankowski, R., Staszewski, O., Böttcher, C., Amann, L., Sagar, Scheiwe, C., Nessler, S., Kunz, P., van Loo, G., Coenen, V. A., Reinacher, P. C., Michel, A., Sure, U., Gold, R., Grün, D., Priller, J., Stadelmann, C., & Prinz, M. (2019a). Spatial and temporal heterogeneity of mouse and human microglia at single-cell resolution. *Nature*, *566*(7744), 388–392. <https://doi.org/10.1038/s41586-019-0924-x>
- Masuda, T., Sankowski, R., Staszewski, O., Böttcher, C., Amann, L., Sagar, Scheiwe, C., Nessler, S., Kunz, P., van Loo, G., Coenen, V. A., Reinacher, P. C., Michel, A., Sure, U., Gold, R., Grün, D., Priller, J., Stadelmann, C., & Prinz, M. (2019b). Spatial and

- temporal heterogeneity of mouse and human microglia at single-cell resolution. *Nature*, 566(7744), 388–392. <https://doi.org/10.1038/s41586-019-0924-x>
- Masuda, T., Sankowski, R., Staszewski, O., & Prinz, M. (2020). Microglia Heterogeneity in the Single-Cell Era. *Cell Reports*, 30(5), 1271–1281. <https://doi.org/10.1016/j.celrep.2020.01.010>
- McNab, F., Mayer-Barber, K., Sher, A., Wack, A., & O'Garra, A. (2015). Type I interferons in infectious disease. *Nature Reviews Immunology*, 15(2), 87–103. <https://doi.org/10.1038/nri3787>
- McWhirter, S. M., Fitzgerald, K. A., Rosains, J., Rowe, D. C., Golenbock, D. T., & Maniatis, T. (2004). IFN-regulatory factor 3-dependent gene expression is defective in Tbk1-deficient mouse embryonic fibroblasts. *Proceedings of the National Academy of Sciences*, 101(1), 233–238. <https://doi.org/10.1073/pnas.2237236100>
- Menassa, D. A., & Gomez-Nicola, D. (2018). Microglial Dynamics During Human Brain Development. *Frontiers in Immunology*, 9, 1014. <https://doi.org/10.3389/fimmu.2018.01014>
- Michaelis, M., Nieswandt, B., Stegner, D., Eilers, J., & Kraft, R. (2015). STIM1, STIM2, and Orai1 regulate store-operated calcium entry and purinergic activation of microglia. *Glia*, 63(4), 652–663. <https://doi.org/10.1002/glia.22775>
- Mildner, A., Schmidt, H., Nitsche, M., Merkler, D., Hanisch, U. K., Mack, M., Heikenwalder, M., Brück, W., Priller, J., & Prinz, M. (2007). Microglia in the adult brain arise from Ly-6ChiCCR2+ monocytes only under defined host conditions. *Nature Neuroscience*, 10(12), 1544–1553. <https://doi.org/10.1038/nn2015>
- Minieri, L., Pivonkova, H., Caprini, M., Harantova, L., Anderova, M., & Ferroni, S. (2013). The inhibitor of volume-regulated anion channels DCPIB activates TREK potassium channels in cultured astrocytes. *British Journal of Pharmacology*, 168(5), 1240–1254. <https://doi.org/10.1111/bph.12011>
- Mongin, A. A. (2016). Volume-regulated anion channel – a frenemy within the brain. *Pflügers Archiv: European Journal of Physiology*, 468(3), 421–441. <https://doi.org/10.1007/s00424-015-1765-6>
- Moreland, J. G., Davis, A. P., Bailey, G., Nauseef, W. M., & Lamb, F. S. (2006). Anion Channels, Including CIC-3, Are Required for Normal Neutrophil Oxidative Function, Phagocytosis, and Transendothelial Migration *. *Journal of Biological Chemistry*, 281(18), 12277–12288. <https://doi.org/10.1074/jbc.M511030200>
- Naguro, I., Umeda, T., Kobayashi, Y., Maruyama, J., Hattori, K., Shimizu, Y., Kataoka, K., Kim-Mitsuyama, S., Uchida, S., Vandewalle, A., Noguchi, T., Nishitoh, H., Matsuzawa, A., Takeda, K., & Ichijo, H. (2012). ASK3 responds to osmotic stress and regulates

- blood pressure by suppressing WNK1-SPAK/OSR1 signaling in the kidney. *Nature Communications*, 3(1), 1285. <https://doi.org/10.1038/ncomms2283>
- Nimmerjahn, A., Kirchhoff, F., & Helmchen, F. (2005). Resting microglial cells are highly dynamic surveillants of brain parenchyma in vivo. *Science (New York, N.Y.)*, 308(5726), 1314–1318. <https://doi.org/10.1126/science.1110647>
- Norris, G. T., & Kipnis, J. (2018). Immune cells and CNS physiology: Microglia and beyond. *Journal of Experimental Medicine*, 216(1), 60–70. <https://doi.org/10.1084/jem.20180199>
- Nunes, P., Cornut, D., Bochet, V., Hasler, U., Oh-Hora, M., Waldburger, J.-M., & Demaurex, N. (2012). STIM1 Juxtaposes ER to Phagosomes, Generating Ca²⁺ Hotspots that Boost Phagocytosis. *Current Biology*, 22(21), 1990–1997. <https://doi.org/10.1016/j.cub.2012.08.049>
- Okabe, Y., & Medzhitov, R. (2016). Tissue biology perspective on macrophages. *Nature Immunology*, 17(1), 9–17. <https://doi.org/10.1038/ni.3320>
- Ousingsawat, J., Wanitchakool, P., Kmit, A., Romao, A. M., Jantarajit, W., Schreiber, R., & Kunzelmann, K. (2015). Anoctamin 6 mediates effects essential for innate immunity downstream of P2X7 receptors in macrophages. *Nature Communications*, 6(1), 6245. <https://doi.org/10.1038/ncomms7245>
- Paludan, S. R., & Bowie, A. G. (2013). Immune sensing of DNA. *Immunity*, 38(5), 870–880. <https://doi.org/10.1016/j.immuni.2013.05.004>
- Paolicelli, R. C., Bisht, K., & Tremblay, M.-È. (2014). Fractalkine regulation of microglial physiology and consequences on the brain and behavior. *Frontiers in Cellular Neuroscience*, 8, 129. <https://doi.org/10.3389/fncel.2014.00129>
- Paolicelli, R. C., Bolasco, G., Pagani, F., Maggi, L., Scianni, M., Panzanelli, P., Giustetto, M., Ferreira, T. A., Guiducci, E., Dumas, L., Ragozzino, D., & Gross, C. T. (2011). Synaptic pruning by microglia is necessary for normal brain development. *Science (New York, N.Y.)*, 333(6048), 1456–1458. <https://doi.org/10.1126/science.1202529>
- Parkhurst, C. N., Yang, G., Ninan, I., Savas, J. N., Yates, J. R., Lafaille, J. J., Hempstead, B. L., Littman, D. R., & Gan, W.-B. (2013). Microglia promote learning-dependent synapse formation through brain-derived neurotrophic factor. *Cell*, 155(7), 1596–1609. <https://doi.org/10.1016/j.cell.2013.11.030>
- Patir, A., Shih, B., McColl, B. W., & Freeman, T. C. (2019). A core transcriptional signature of human microglia: Derivation and utility in describing region-dependent alterations associated with Alzheimer's disease. *Glia*, 67(7), 1240–1253. <https://doi.org/10.1002/glia.23572>

- Pedersen, S. F., Kapus, A., & Hoffmann, E. K. (2011). Osmosensory Mechanisms in Cellular and Systemic Volume Regulation. *Journal of the American Society of Nephrology*, 22(9), 1587–1597. <https://doi.org/10.1681/ASN.2010121284>
- Pedersen, S. F., Klausen, T. K., & Nilius, B. (2015). The identification of a volume-regulated anion channel: An amazing Odyssey. *Acta Physiologica*, 213(4), 868–881. <https://doi.org/10.1111/apha.12450>
- Perregaux, D. G., Laliberte, R. E., & Gabel, C. A. (1996). Human monocyte interleukin-1beta posttranslational processing. Evidence of a volume-regulated response. *The Journal of Biological Chemistry*, 271(47), 29830–29838. <https://doi.org/10.1074/jbc.271.47.29830>
- Planells-Cases, R., Lutter, D., Guyader, C., Gerhards, N. M., Ullrich, F., Elger, D. A., Kucukosmanoglu, A., Xu, G., Voss, F. K., Reincke, S. M., Stauber, T., Blomen, V. A., Vis, D. J., Wessels, L. F., Brummelkamp, T. R., Borst, P., Rottenberg, S., & Jentsch, T. J. (2015). Subunit composition of VRAC channels determines substrate specificity and cellular resistance to Pt-based anti-cancer drugs. *The EMBO Journal*, 34(24), 2993–3008. <https://doi.org/10.15252/emj.201592409>
- Plant, T. D. (2014). TRPs in mechanosensing and volume regulation. *Handbook of Experimental Pharmacology*, 223, 743–766. https://doi.org/10.1007/978-3-319-05161-1_2
- Platanias, L. C. (2005). Mechanisms of type-I- and type-II-interferon-mediated signalling. *Nature Reviews Immunology*, 5(5), 375–386. <https://doi.org/10.1038/nri1604>
- Platt, C. D., Chou, J., Houlihan, P., Badran, Y. R., Kumar, L., Bainter, W., Poliani, P. L., Perez, C. J., Dent, S. Y. R., Clapham, D. E., Benavides, F., & Geha, R. S. (2017). Leucine-rich repeat containing 8A (LRRC8A)-dependent volume-regulated anion channel activity is dispensable for T-cell development and function. *The Journal of Allergy and Clinical Immunology*, 140(6), 1651-1659.e1. <https://doi.org/10.1016/j.jaci.2016.12.974>
- Podleśny-Drabiniok, A., Marcora, E., & Goate, A. M. (2020). Microglial Phagocytosis: A Disease-Associated Process Emerging from Alzheimer's Disease Genetics. *Trends in Neurosciences*, 43(12), 965–979. <https://doi.org/10.1016/j.tins.2020.10.002>
- Priller, J., Flügel, A., Wehner, T., Boentert, M., Haas, C. A., Prinz, M., Fernández-Klett, F., Prass, K., Bechmann, I., de Boer, B. A., Frotscher, M., Kreutzberg, G. W., Persons, D. A., & Dirnagl, U. (2001). Targeting gene-modified hematopoietic cells to the central nervous system: Use of green fluorescent protein uncovers microglial engraftment. *Nature Medicine*, 7(12), 1356–1361. <https://doi.org/10.1038/nm1201-1356>
- Prinz, M., Jung, S., & Priller, J. (2019). Microglia Biology: One Century of Evolving Concepts. *Cell*, 179(2), 292–311. <https://doi.org/10.1016/j.cell.2019.08.053>

- Qiu, Z., Dubin, A. E., Mathur, J., Tu, B., Reddy, K., Miraglia, L. J., Reinhardt, J., Orth, A. P., & Patapoutian, A. (2014). SWELL1, a plasma membrane protein, is an essential component of volume-regulated anion channel. *Cell*, *157*(2), 447–458. <https://doi.org/10.1016/j.cell.2014.03.024>
- Ransohoff, R. M. (2016). A polarizing question: Do M1 and M2 microglia exist? *Nature Neuroscience*, *19*(8), 987–991. <https://doi.org/10.1038/nn.4338>
- Rappert, A., Biber, K., Nolte, C., Lipp, M., Schubel, A., Lu, B., Gerard, N., Gerard, C., Boddeke, H., & Kettenmann, H. (2002). Secondary Lymphoid Tissue Chemokine (CCL21) Activates CXCR3 to Trigger a Cl⁻ Current and Chemotaxis in Murine Microglia. *Journal of Immunology (Baltimore, Md. : 1950)*, *168*, 3221–3226. <https://doi.org/10.4049/jimmunol.168.7.3221>
- Rizzo, F. R., Musella, A., De Vito, F., Fresegna, D., Bullitta, S., Vanni, V., Guadalupi, L., Stampanoni Bassi, M., Buttari, F., Mandolesi, G., Centonze, D., & Gentile, A. (2018). Tumor Necrosis Factor and Interleukin-1 β Modulate Synaptic Plasticity during Neuroinflammation. *Neural Plasticity*, *2018*, 8430123. <https://doi.org/10.1155/2018/8430123>
- Robertson, K. A., & Ghazal, P. (2016). Interferon Control of the Sterol Metabolic Network: Bidirectional Molecular Circuitry-Mediating Host Protection. *Frontiers in Immunology*, *7*, 634. <https://doi.org/10.3389/fimmu.2016.00634>
- Rosales, C., & Uribe-Querol, E. (2017). Phagocytosis: A Fundamental Process in Immunity. *BioMed Research International*, *2017*, 9042851. <https://doi.org/10.1155/2017/9042851>
- Ruparelia, N., Chai, J. T., Fisher, E. A., & Choudhury, R. P. (2017). Inflammatory processes in cardiovascular disease: A route to targeted therapies. *Nature Reviews Cardiology*, *14*(3), 133–144. <https://doi.org/10.1038/nrcardio.2016.185>
- Salter, M. W., & Stevens, B. (2017). Microglia emerge as central players in brain disease. *Nature Medicine*, *23*(9), 1018–1027. <https://doi.org/10.1038/nm.4397>
- Sawada, A., Takihara, Y., Kim, J. Y., Matsuda-Hashii, Y., Tokimasa, S., Fujisaki, H., Kubota, K., Endo, H., Onodera, T., Ohta, H., Ozono, K., & Hara, J. (2003). A congenital mutation of the novel gene LRRC8 causes agammaglobulinemia in humans. *The Journal of Clinical Investigation*, *112*(11), 1707–1713. <https://doi.org/10.1172/JCI18937>
- Schlichter, L. C., Mertens, T., & Liu, B. (2011). Swelling activated Cl⁻ channels in microglia: Biophysics, pharmacology and role in glutamate release. *Channels*, *5*(2), 128–137. <https://doi.org/10.4161/chan.5.2.14310>
- Schneider, L., Klausen, T. K., Stock, C., Mally, S., Christensen, S. T., Pedersen, S. F., Hoffmann, E. K., & Schwab, A. (2008). H-ras transformation sensitizes volume-

- activated anion channels and increases migratory activity of NIH3T3 fibroblasts. *Pflugers Archiv: European Journal of Physiology*, 455(6), 1055–1062. <https://doi.org/10.1007/s00424-007-0367-3>
- Schneider, W. M., Chevillotte, M. D., & Rice, C. M. (2014). Interferon-Stimulated Genes: A Complex Web of Host Defenses. *Annual Review of Immunology*, 32, 513–545. <https://doi.org/10.1146/annurev-immunol-032713-120231>
- Schober, A. L., Wilson, C. S., & Mongin, A. A. (2017). Molecular composition and heterogeneity of the LRRC8-containing swelling-activated osmolyte channels in primary rat astrocytes. *The Journal of Physiology*, 595(22), 6939–6951. <https://doi.org/10.1113/JP275053>
- Schwab, A., Fabian, A., Hanley, P. J., & Stock, C. (2012). Role of Ion Channels and Transporters in Cell Migration. *Physiological Reviews*, 92(4), 1865–1913. <https://doi.org/10.1152/physrev.00018.2011>
- Seki, Y., Feustel, P. J., Keller, R. W., Tranmer, B. I., & Kimelberg, H. K. (1999). Inhibition of ischemia-induced glutamate release in rat striatum by dihydrokinate and an anion channel blocker. *Stroke*, 30(2), 433–440. <https://doi.org/10.1161/01.str.30.2.433>
- Shi, Q., Chowdhury, S., Ma, R., Le, K. X., Hong, S., Caldarone, B. J., Stevens, B., & Lemere, C. A. (2017). Complement C3 deficiency protects against neurodegeneration in aged plaque-rich APP/PS1 mice. *Science Translational Medicine*. <https://www.science.org/doi/abs/10.1126/scitranslmed.aaf6295>
- Shi, Y., & Holtzman, D. M. (2018). Interplay between innate immunity and Alzheimer's disease: APOE and TREM2 in the spotlight. *Nature Reviews. Immunology*, 18(12), 759–772. <https://doi.org/10.1038/s41577-018-0051-1>
- Siegal, F. P., Kadowaki, N., Shodell, M., Fitzgerald-Bocarsly, P. A., Shah, K., Ho, S., Antonenko, S., & Liu, Y. J. (1999). The nature of the principal type 1 interferon-producing cells in human blood. *Science (New York, N.Y.)*, 284(5421), 1835–1837. <https://doi.org/10.1126/science.284.5421.1835>
- Sierra, A., Castro, F. de, Río-Hortega, J. del, Iglesias-Rozas, J. R., Garrosa, M., & Kettenmann, H. (2016). The “Big-Bang” for modern glial biology: Translation and comments on Pío del Río-Hortega 1919 series of papers on microglia. *Glia*, 64(11), 1801–1840. <https://doi.org/10.1002/glia.23046>
- Sierra, A., Paolicelli, R. C., & Kettenmann, H. (2019). Cien Años de Microglía: Milestones in a Century of Microglial Research. *Trends in Neurosciences*, 42(11), 778–792. <https://doi.org/10.1016/j.tins.2019.09.004>
- Smits, G., & Kajava, A. V. (2004). LRRC8 extracellular domain is composed of 17 leucine-rich repeats. *Molecular Immunology*, 41(5), 561–562. <https://doi.org/10.1016/j.molimm.2004.04.001>

- Sofroniew, M. V. (2014). Astrogliosis. *Cold Spring Harbor Perspectives in Biology*, 7(2), a020420. <https://doi.org/10.1101/cshperspect.a020420>
- Sofroniew, M. V. (2015). Astrocyte barriers to neurotoxic inflammation. *Nature Reviews Neuroscience*, 16(5), 249–263. <https://doi.org/10.1038/nrn3898>
- Solis, A. G., Bielecki, P., Steach, H. R., Sharma, L., Harman, C. C. D., Yun, S., Palm, N. W., de Zoete, M. R., Warnock, J. N., To, S. D. F., York, A. G., Mack, M., Schwartz, M. A., Cruz, Charles. S. D., Jackson, R., & Flavell, R. A. (2019). Mechanosensation of Cyclical Force by PIEZO1 is Essential for Innate Immunity. *Nature*, 573(7772), 69–74. <https://doi.org/10.1038/s41586-019-1485-8>
- Stevens, B., Allen, N. J., Vazquez, L. E., Howell, G. R., Christopherson, K. S., Nouri, N., Micheva, K. D., Mehalow, A. K., Huberman, A. D., Stafford, B., Sher, A., Litke, A. M., Lambris, J. D., Smith, S. J., John, S. W. M., & Barres, B. A. (2007). The classical complement cascade mediates CNS synapse elimination. *Cell*, 131(6), 1164–1178. <https://doi.org/10.1016/j.cell.2007.10.036>
- Strange, K., Yamada, T., & Denton, J. S. (2019). A 30-year journey from volume-regulated anion currents to molecular structure of the LRRC8 channel. *Journal of General Physiology*, 151(2), 100–117. <https://doi.org/10.1085/jgp.201812138>
- Stuhlmann, T., Planells-Cases, R., & Jentsch, T. J. (2018). LRRC8/VRAC anion channels enhance β -cell glucose sensing and insulin secretion. *Nature Communications*, 9, 1974. <https://doi.org/10.1038/s41467-018-04353-y>
- Sun, L., Wu, J., Du, F., Chen, X., & Chen, Z. J. (2013). Cyclic GMP-AMP Synthase Is a Cytosolic DNA Sensor That Activates the Type I Interferon Pathway. *Science*. <https://www.science.org/doi/abs/10.1126/science.1232458>
- Swanton, T., Cook, J., Beswick, J. A., Freeman, S., Lawrence, C. B., & Brough, D. (2018). Is Targeting the Inflammasome a Way Forward for Neuroscience Drug Discovery? *SLAS Discovery: Advancing Life Sciences R & D*, 23(10), 991–1017. <https://doi.org/10.1177/2472555218786210>
- Syeda, R., Qiu, Z., Dubin, A. E., Murthy, S. E., Florendo, M. N., Mason, D. E., Mathur, J., Cahalan, S. M., Peters, E. C., Montal, M., & Patapoutian, A. (2016). LRRC8 proteins form volume-regulated anion channels that sense ionic strength. *Cell*, 164(3), 499–511. <https://doi.org/10.1016/j.cell.2015.12.031>
- Takaoka, A., Wang, Z., Choi, M. K., Yanai, H., Negishi, H., Ban, T., Lu, Y., Miyagishi, M., Kodama, T., Honda, K., Ohba, Y., & Taniguchi, T. (2007). DAI (DLM-1/ZBP1) is a cytosolic DNA sensor and an activator of innate immune response. *Nature*, 448(7152), 501–505. <https://doi.org/10.1038/nature06013>
- Tinevez, J.-Y., Perry, N., Schindelin, J., Hoopes, G. M., Reynolds, G. D., Laplantine, E., Bednarek, S. Y., Shorte, S. L., & Eliceiri, K. W. (2017). TrackMate: An open and

- extensible platform for single-particle tracking. *Methods*, 115, 80–90. <https://doi.org/10.1016/j.ymeth.2016.09.016>
- Ulrich, J. D., Finn, M. B., Wang, Y., Shen, A., Mahan, T. E., Jiang, H., Stewart, F. R., Piccio, L., Colonna, M., & Holtzman, D. M. (2014). Altered microglial response to A β plaques in APPPS1-21 mice heterozygous for TREM2. *Molecular Neurodegeneration*, 9, 20. <https://doi.org/10.1186/1750-1326-9-20>
- Velichko, A. K., Petrova, N. V., Luzhin, A. V., Strelkova, O. S., Ovsyannikova, N., Kireev, I. I., Petrova, N. V., Razin, S. V., & Kantidze, O. L. (2019). Hypoosmotic stress induces R loop formation in nucleoli and ATR/ATM-dependent silencing of nucleolar transcription. *Nucleic Acids Research*, 47(13), 6811–6825. <https://doi.org/10.1093/nar/gkz436>
- Vilalta, A., & Brown, G. C. (2018). Neurophagy, the phagocytosis of live neurons and synapses by glia, contributes to brain development and disease. *The FEBS Journal*, 285(19), 3566–3575. <https://doi.org/10.1111/febs.14323>
- Volk, A. P. D., Heise, C. K., Hougén, J. L., Artman, C. M., Volk, K. A., Wessels, D., Soll, D. R., Nauseef, W. M., Lamb, F. S., & Moreland, J. G. (2008). CIC-3 and ICISwell are Required for Normal Neutrophil Chemotaxis and Shape Change. *The Journal of Biological Chemistry*, 283(49), 34315–34326. <https://doi.org/10.1074/jbc.M803141200>
- Voss, F. K., Ullrich, F., Münch, J., Lazarow, K., Lutter, D., Mah, N., Andrade-Navarro, M. A., Kries, J. P. von, Stauber, T., & Jentsch, T. J. (2014). Identification of LRRC8 Heteromers as an Essential Component of the Volume-Regulated Anion Channel VRAC. *Science*, 344(6184), 634–638. <https://doi.org/10.1126/science.1252826>
- Wakselman, S., Béchade, C., Roumier, A., Bernard, D., Triller, A., & Bessis, A. (2008). Developmental neuronal death in hippocampus requires the microglial CD11b integrin and DAP12 immunoreceptor. *The Journal of Neuroscience: The Official Journal of the Society for Neuroscience*, 28(32), 8138–8143. <https://doi.org/10.1523/JNEUROSCI.1006-08.2008>
- Wang, Y., Cella, M., Mallinson, K., Ulrich, J. D., Young, K. L., Robinette, M. L., Gilfillan, S., Krishnan, G. M., Sudhakar, S., Zinselmeyer, B. H., Holtzman, D. M., Cirrito, J. R., & Colonna, M. (2015). TREM2 lipid sensing sustains the microglial response in an Alzheimer's disease model. *Cell*, 160(6), 1061–1071. <https://doi.org/10.1016/j.cell.2015.01.049>
- Wang, Y., Szretter, K. J., Vermi, W., Gilfillan, S., Rossini, C., Cella, M., Barrow, A. D., Diamond, M. S., & Colonna, M. (2012). IL-34 is a tissue-restricted ligand of CSF1R required for the development of Langerhans cells and microglia. *Nature Immunology*, 13(8), 753–760. <https://doi.org/10.1038/ni.2360>

- Wang, Y., Ulland, T. K., Ulrich, J. D., Song, W., Tzaferis, J. A., Hole, J. T., Yuan, P., Mahan, T. E., Shi, Y., Gilfillan, S., Cella, M., Grutzendler, J., DeMattos, R. B., Cirrito, J. R., Holtzman, D. M., & Colonna, M. (2016). TREM2-mediated early microglial response limits diffusion and toxicity of amyloid plaques. *The Journal of Experimental Medicine*, *213*(5), 667–675. <https://doi.org/10.1084/jem.20151948>
- Weintz, G., Olsen, J. V., Frühauf, K., Niedzielska, M., Amit, I., Jantsch, J., Mages, J., Frech, C., Dölken, L., Mann, M., & Lang, R. (2010). The phosphoproteome of toll-like receptor-activated macrophages. *Molecular Systems Biology*, *6*, 371. <https://doi.org/10.1038/msb.2010.29>
- Wes, P. D., Holtman, I. R., Boddeke, E. W. G. M., Möller, T., & Eggen, B. J. L. (2016). Next generation transcriptomics and genomics elucidate biological complexity of microglia in health and disease. *Glia*, *64*(2), 197–213. <https://doi.org/10.1002/glia.22866>
- Westman, J., & Grinstein, S. (2021). Determinants of Phagosomal pH During Host-Pathogen Interactions. *Frontiers in Cell and Developmental Biology*, *8*, 1781. <https://doi.org/10.3389/fcell.2020.624958>
- White, M. M., & Aylwin, M. (1990). Niflumic and flufenamic acids are potent reversible blockers of Ca²⁺(+)-activated Cl⁻ channels in *Xenopus* oocytes. *Molecular Pharmacology*, *37*(5), 720–724.
- Wilson, C. S., Dohare, P., Orbeta, S., Nalwalk, J. W., Huang, Y., Ferland, R. J., Sah, R., Scimemi, A., & Mongin, A. A. (2021). Late adolescence mortality in mice with brain-specific deletion of the volume-regulated anion channel subunit LRRC8A. *The FASEB Journal*, *35*(10), e21869. <https://doi.org/10.1096/fj.202002745R>
- Wlodarczyk, A., Holtman, I. R., Krueger, M., Yogev, N., Bruttger, J., Khorrooshi, R., Benmamar-Badel, A., de Boer-Bergsma, J. J., Martin, N. A., Karram, K., Kramer, I., Boddeke, E. W., Waisman, A., Eggen, B. J., & Owens, T. (2017). A novel microglial subset plays a key role in myelinogenesis in developing brain. *The EMBO Journal*, *36*(22), 3292–3308. <https://doi.org/10.15252/emboj.201696056>
- Wolf, S. A., Boddeke, H. w. g. m., & Kettenmann, H. (2017). Microglia in Physiology and Disease. *Annual Review of Physiology*, *79*(1), 619–643. <https://doi.org/10.1146/annurev-physiol-022516-034406>
- World Health Organisation. (2021). *Noncommunicable diseases: Mortality*. <https://www.who.int/data/gho/data/themes/topics/topic-details/GHO/ncd-mortality>
- Xie, X., Zhang, D., Zhao, B., Lu, M.-K., You, M., Condorelli, G., Wang, C.-Y., & Guan, K.-L. (2011). I κ B kinase epsilon and TANK-binding kinase 1 activate AKT by direct phosphorylation. *Proceedings of the National Academy of Sciences of the United States of America*, *108*(16), 6474–6479. <https://doi.org/10.1073/pnas.1016132108>

- Yamada, T., & Strange, K. (2018). Intracellular and extracellular loops of LRRC8 are essential for volume-regulated anion channel function. *The Journal of General Physiology*, *150*(7), 1003–1015. <https://doi.org/10.1085/jgp.201812016>
- Yang, J., Vitery, M. del C., Chen, J., Osei-Owusu, J., Chu, J., & Qiu, Z. (2019). Glutamate-Releasing SWELL1 Channel in Astrocytes Modulates Synaptic Transmission and Promotes Brain Damage in Stroke. *Neuron*, *102*(4), 813-827.e6. <https://doi.org/10.1016/j.neuron.2019.03.029>
- Yona, S., Kim, K.-W., Wolf, Y., Mildner, A., Varol, D., Breker, M., Strauss-Ayali, D., Viukov, S., Guilliams, M., Misharin, A., Hume, D. A., Perlman, H., Malissen, B., Zelzer, E., & Jung, S. (2013). Fate mapping reveals origins and dynamics of monocytes and tissue macrophages under homeostasis. *Immunity*, *38*(1), 79–91. <https://doi.org/10.1016/j.immuni.2012.12.001>
- Zhang, H., Deng, Z., Zhang, D., Li, H., Zhang, L., Niu, J., Zuo, W., Fu, R., Fan, L., Ye, J.-H., & She, J. (2018). High expression of leucine-rich repeat-containing 8A is indicative of a worse outcome of colon cancer patients by enhancing cancer cell growth and metastasis. *Oncology Reports*, *40*(3), 1275–1286. <https://doi.org/10.3892/or.2018.6556>
- Zhang, Y., Jin, Y., Behr, M. J., Feustel, P. J., Morrison, J. P., & Kimelberg, H. K. (2005). Behavioral and histological neuroprotection by tamoxifen after reversible focal cerebral ischemia. *Experimental Neurology*, *196*(1), 41–46. <https://doi.org/10.1016/j.expneurol.2005.07.002>
- Zhang, Y., Xie, L., Gunasekar, S. K., Tong, D., Mishra, A., Gibson, W. J., Wang, C., Fidler, T., Marthaler, B., Klingelutz, A., Abel, E. D., Samuel, I., Smith, J. K., Cao, L., & Sah, R. (2017). SWELL1 is a regulator of adipocyte size, insulin signalling and glucose homeostasis. *Nature Cell Biology*, *19*(5), 504–517. <https://doi.org/10.1038/ncb3514>
- Zhang, Y., Zhang, H., Feustel, P. J., & Kimelberg, H. K. (2008). DCPIB, a specific inhibitor of Volume Regulated Anion Channels (VRACs), reduces infarct size in MCAo and the release of glutamate in the ischemic cortical penumbra. *Experimental Neurology*, *210*(2), 514–520. <https://doi.org/10.1016/j.expneurol.2007.11.027>
- Zhao, Y., Wu, X., Li, X., Jiang, L.-L., Gui, X., Liu, Y., Sun, Y., Zhu, B., Piña-Crespo, J. C., Zhang, M., Zhang, N., Chen, X., Bu, G., An, Z., Huang, T. Y., & Xu, H. (2018). TREM2 Is a Receptor for β -Amyloid that Mediates Microglial Function. *Neuron*, *97*(5), 1023-1031.e7. <https://doi.org/10.1016/j.neuron.2018.01.031>
- Zhou, C., Chen, X., Planells-Cases, R., Chu, J., Wang, L., Cao, L., Li, Z., López-Cayuqueo, K. I., Xie, Y., Ye, S., Wang, X., Ullrich, F., Ma, S., Fang, Y., Zhang, X., Qian, Z., Liang, X., Cai, S.-Q., Jiang, Z., ... Xiao, H. (2020). Transfer of cGAMP into Bystander Cells via LRRC8 Volume-Regulated Anion Channels Augments STING-Mediated Interferon

Responses and Anti-viral Immunity. *Immunity*, 52(5), 767-781.e6.
<https://doi.org/10.1016/j.immuni.2020.03.016>

Zhou, J.-J., Luo, Y., Chen, S.-R., Shao, J.-Y., Sah, R., & Pan, H.-L. (2020). LRRC8A-dependent volume-regulated anion channels contribute to ischemia-induced brain injury and glutamatergic input to hippocampal neurons. *Experimental Neurology*, 332, 113391. <https://doi.org/10.1016/j.expneurol.2020.113391>

Zhu, Y., An, X., Zhang, X., Qiao, Y., Zheng, T., & Li, X. (2019). STING: A master regulator in the cancer-immunity cycle. *Molecular Cancer*, 18(1), 152. <https://doi.org/10.1186/s12943-019-1087-y>

Zierler, S., Frei, E., Grissmer, S., & Kerschbaum, H. H. (2008). Chloride influx provokes lamellipodium formation in microglial cells. *Cellular Physiology and Biochemistry: International Journal of Experimental Cellular Physiology, Biochemistry, and Pharmacology*, 21(1–3), 55–62. <https://doi.org/10.1159/000113747>


Appendix

Review: Is Targeting the Inflammasome a Way Forward for Neuroscience Drug Discovery?

Published July 3, 2018: <https://journals.sagepub.com/doi/10.1177/2472555218786210>

Review co-first authored by me alongside Tess Swanton. I wrote the following sections: Glial Cells and Neuroinflammation, IL-1 β in Neuroinflammation, Inflammation and neuronal function, Injury Phases and Potential Points of Therapeutic Intervention in CNS Disease, as well as sections tackling inflammasomes in Parkinson's disease, amyotrophic lateral sclerosis and acute brain trauma. James Beswick wrote the section on NLRP3 inhibitors.

Is Targeting the Inflammasome a Way Forward for Neuroscience Drug Discovery?


SLAS Discovery
1–27
© 2018 Society for Laboratory
Automation and Screening
DOI:
10.1177/2472555218786210
slasdisc.sagepub.com

Tessa Swanton^{1*}, James Cook^{1*} , James A. Beswick², Sally Freeman², Catherine B. Lawrence¹, and David Brough¹ 

Abstract

Neuroinflammation is becoming increasingly recognized as a critical factor in the pathology of both acute and chronic neurological conditions. Inflammasomes such as the one formed by NACHT, LRR, and PYD domains containing protein 3 (NLRP3) are key regulators of inflammation due to their ability to induce the processing and secretion of interleukin 1 β (IL-1 β). IL-1 β has previously been identified as a potential therapeutic target in a variety of conditions due to its ability to promote neuronal damage under conditions of injury. Thus, inflammasome inhibition has the potential to curtail inflammatory signaling, which could prove beneficial in certain diseases. In this review, we discuss the evidence for inflammasome contributions to the pathology of neurodegenerative conditions such as Alzheimer's disease and Parkinson's disease, epilepsy, and acute degeneration following brain trauma or stroke. In addition, we review the current landscape of drug development targeting the NLRP3 inflammasome.

Keywords

inflammation, neurodegenerative diseases, inflammasome, interleukin, NLRP3

Introduction

Inflammation and Inflammasomes

Inflammation is a host response to injury and infection and is generally considered beneficial. However, inflammation is becoming recognized as a contributor to disease. This is well illustrated by the recent Canakinumab Anti-inflammatory Thrombosis Outcomes Study (CANTOS), where patients with a history of myocardial infarction were treated with canakinumab, a monoclonal antibody targeting the pro-inflammatory cytokine interleukin-1 β (IL-1 β).¹ In the CANTOS trial, it was found that canakinumab treatment reduced the rate of recurrent cardiovascular events and cancer mortality, in addition to improving many other clinical outcomes.¹ IL-1 β and other IL-1 family members are strongly implicated in inflammatory disease.^{2,3} IL-1 β is produced as an inactive precursor (pro-IL-1 β) by cells of the innate immune system, such as monocytes and macrophages, in response to pathogen-associated molecular patterns (PAMPs) or damage-associated molecular patterns (DAMPs). PAMPs are molecular motifs carried by pathogens (e.g., lipopolysaccharide [LPS] from Gram-negative bacteria). DAMPs are endogenous molecules released from dead cells or modified during disease (e.g., highmobility group box 1 [HMGB1]). These

danger signals are recognized by pattern recognition receptors (PRRs) (e.g., tolllike receptors [TLRs]) on the membranes of innate immune cells and induce signaling pathways (e.g., nuclear factor kappa-light-chain-enhancer of activated B cells [NF- κ B]) that result in the upregulation of pro-IL-1 β . A major mechanism by which pro-IL-1 β is cleaved to an active secreted form of IL-1 β is via the formation of large cytoplasmic multimeric protein complexes called inflammasomes.⁴

Inflammasomes are typically composed of a sensor (a cytosolic PRR) and an adaptor protein called apoptosis-associated speck-like protein containing a caspase-recruitment domain (CARD) (ASC), and an effector such as the protease caspase-1.⁴ The most commonly studied inflammasome is composed of the cytosolic PRR NACHT, LRR,

¹Division of Neuroscience and Experimental Psychology, School of Biological Sciences, Faculty of Biology, Medicine and Health, Manchester

Academic Health Science Centre, University of Manchester, Manchester, UK

²Division of Pharmacy and Optometry, School of Health Sciences,

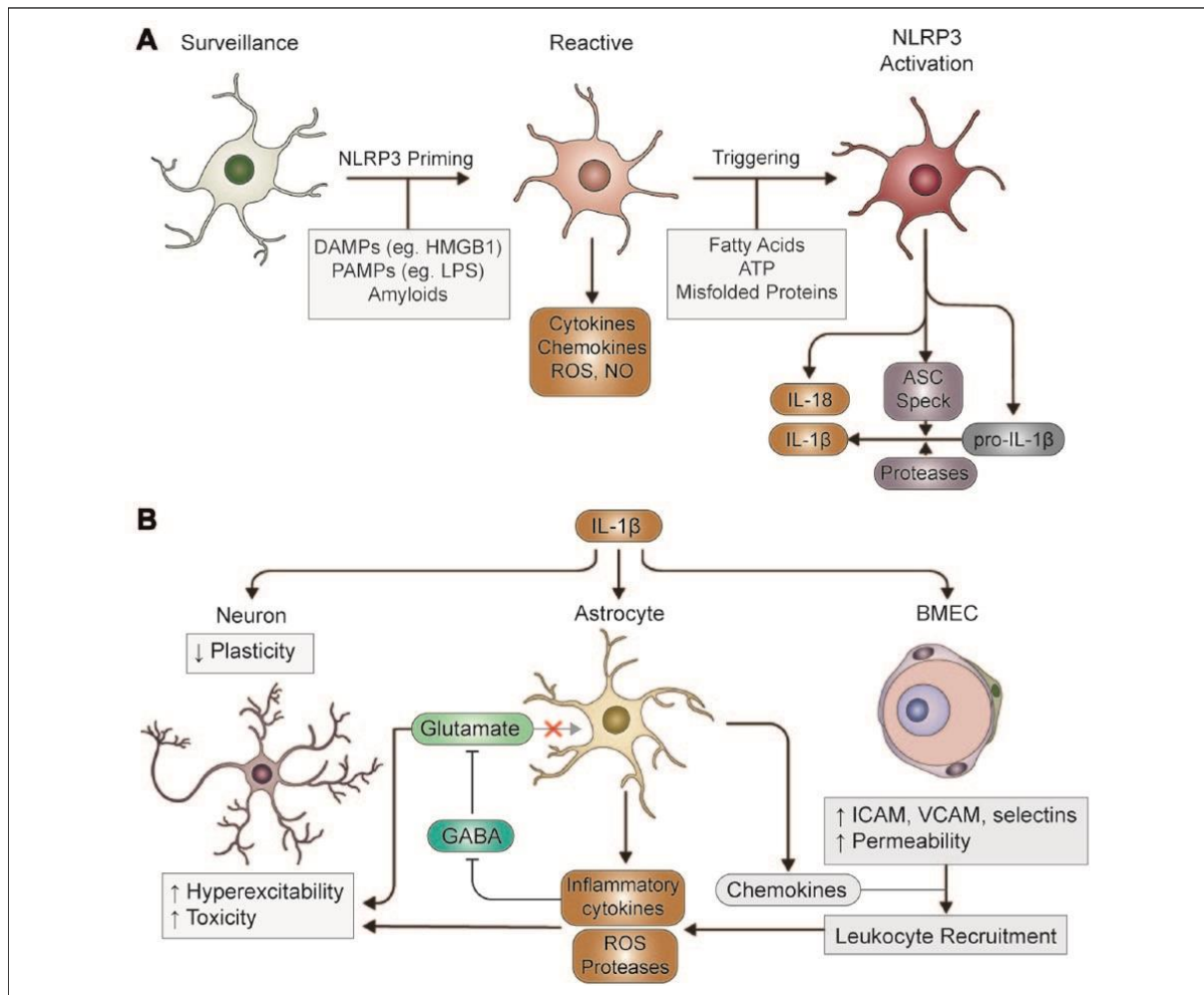


Figure 1. Production and action of IL-1 β in neuroinflammation. **(A)** Microglia sense DAMPs and PAMPs following infection or neuron injury, which promote reactive phenotypes and the release of pro-inflammatory factors. Certain DAMPs or PAMPs may also result in NLRP3 priming. However, the inflammasome may not be activated until the cell receives a second, triggering stimulus. Following inflammasome activation, mature IL-1 β and ASC specks are released. During pyroptosis, pro-IL-1 β may also be released and subsequently cleaved by extracellular ASC specks or other proteases. **(B)** IL-1 β promotes neurotoxicity and abnormal excitability by acting on a wide variety of cell types to promote neuroinflammation and modulate synaptic transmission. ATP = adenosine triphosphate; BMEC = brain microvascular endothelial cell; ICAM = intercellular adhesion molecule; VCAM = vascular cell adhesion

Faculty of Biology, Medicine and Health, Manchester Academic Health Science Centre, University of Manchester, Manchester, UK [†]These authors contributed equally to this work.

Received March 12, 2018, and in revised form June 11, 2018. Accepted for publication June 11, 2018.

Corresponding Author:

David Brough, Division of Neuroscience and Experimental Psychology,

School of Biological Sciences, Faculty of Biology, Medicine and Health, Manchester Academic Health Science Centre, University of Manchester, AV Hill Building, Oxford Rd., Manchester, M13 9PT, UK. Email: david.brough@manchester.ac.uk molecule.

and PYD domains containing protein 3 (NLRP3). In a PAMP or DAMP primed cell in which pro-IL-1 β and NLRP3 have been expressed, an additional encounter with another PAMP or DAMP is typically required to induce formation of the NLRP3 inflammasome (**Fig. 1A**).⁴ Upon activation, NLRP3 undergoes a conformational change and interacts with never in mitosis A-related kinase 7 (NEK7).^{5,6} The adaptor protein ASC is then recruited and undergoes oligomerization into large inflammasome specks upon which pro-caspase-1 is recruited and activated.^{7,8} Caspase-1 then cleaves pro-IL-1 β to a mature active form, which is then released from the cell to promote inflammation.⁹ Posttranslational modifications involving NLRP3 phosphorylation and deubiquitination are crucial for inflammasome assembly.^{10–13} K⁺ efflux is now widely accepted as an

essential step in the activation of NLRP3 inflammasomes,¹⁴ and recent studies from us and others suggest an involvement of Cl⁻ channels.^{15–17} Caspase-1 also drives a rapid inflammatory form of programmed cell death called pyroptosis, in which cell lysis occurs and pro-inflammatory mediators are released.¹⁸

Pyroptosis requires the caspase-1-dependent cleavage of gasdermin D (GSDMD) and the formation of plasma membrane pores by the cleaved GSDMD N-terminus.^{19,20} The secretion of IL-1 β is poorly characterized, and we recently speculated that membrane pore formation may represent the secretory mechanism semianalogous to the mechanism used by the unconventionally secreted fibroblast growth factor 2 (FGF2).⁹ The inflammasome specks can themselves also be released from pyroptotic cells and can further contribute to inflammation in the extracellular space.^{21,22}

Glial Cells and Neuroinflammation

The brain was long believed to be an immune-privileged organ, in which inflammation only occurred following infiltration of immune cells from the periphery due to blood–brain barrier (BBB) breakdown.²³ However, it is now understood that the brain possesses resident immune cells, known as microglia, which are able to initiate and sustain an inflammatory response.²⁴ In the healthy brain, microglia exist in a lattice-like organization; each microglial cell curates an individual section of the parenchyma, which it constantly monitors with long, motile processes.²⁵ In this state, microglia are said to appear “ramified,” which refers to the highly branched process morphology, and are now termed “surveillance microglia,” in an attempt to diverge away from the use of “resting,” which implies an inactive, nonfunctional state.²⁶ Microglia also facilitate synaptic development and plasticity by secreting brain-derived neurotrophic factor (BDNF) and by actively pruning synaptic terminals, making them critical for development and learning.^{27,28}

As immune-competent cells microglia express a variety of PRRs that allow them to sense diverse PAMPs and DAMPs and evoke an innate immune response. TLRs 1–9, are present in microglia, along with numerous co-receptors, such as CD14, CD36, CD33, and triggering receptor expressed on myeloid cells 2 (TREM2), in addition to inflammasome components such as NLRP3.²⁹ Many proteins found to be misfolded or aggregated in neurodegenerative diseases, such as amyloid- β (A β), α -synuclein, and superoxide dismutase 1 (SOD1), as well as DAMPs released from dying cells, provoke innate immune responses through microglial PRRs.^{30–32} Moreover, certain aggregated protein species have been reported to activate the inflammasome in primed microglia.^{33–35} PRR ligands and other signaling factors activate a wide range of transcriptional programs in microglia, which

promote a reactive phenotype that is distinct from that of surveillance microglia.²⁶ For example, in response to LPS, like peripheral macrophages, reactive microglia can evoke inflammatory, cytotoxic (M1-like) responses.^{36,37} Alternatively, challenges such as IL-4 or IL-13 can activate transcriptional profiles that enhance the phagocytic, anti-inflammatory activity of microglia (M2-like), thereby promoting tissue repair.^{36–40} However, recent profiling studies have highlighted considerable heterogeneity in microglial responses both in the context of disease and under homeostatic conditions, which do not readily conform to the M1/M2 model.^{41–44} As such, microglia are considered highly dynamic cells, with their transcriptional profile being regulated in a time- and context-dependent manner.⁴⁵ Nonetheless, many forms of neurodegeneration may be caused, perpetuated, or exacerbated by inappropriate skewing of the microglial response toward excessive release of inflammatory cytokines, such as tumor necrosis factor α (TNF- α) and IL-1 β . Often, this is accompanied by production of reactive oxygen species (ROS) and neurotoxic enzymes that promote neuronal damage.⁴⁶ Microglia are therefore regarded as key players in determining disease progression, and thus modulating microglial behavior may present novel therapeutic avenues in many diseases.

Astrocytes are the most numerous cell type in the brain, and primarily support neuron function via regulation of the extracellular environment, secretion of trophic factors, and maintenance of the BBB.⁴⁷ Astrocytes express scavenger receptors, complement receptors, and are suggested to express TLRs 2–5 and 9.⁴⁸ However, recent studies utilizing PCR and RNA-sequencing have found that TLR3 is the only TLR significantly expressed by astrocytes, with the remainder predominantly found on microglia.^{49,50} Astrocytes are also suggested to express inflammasome sensors NLRP3,^{51–53} NLRP2,⁵⁴ and NLR family CARD domain containing protein 4 (NLRC4),⁵³ as well as ASC.⁵⁵ The role of astrocyte-mediated inflammation in brain disease is controversial, and many studies now indicate that the protective or toxic function of astrocytes is highly context and stimulus dependent.^{56–58} In response to brain injuries, astrocytes undergo a variety of responses, including extension of processes, hypertrophy, and in more severe settings, proliferation followed by assembly of a dense “glial scar.”^{59,60} This behavior, termed gliosis, protects adjacent neural networks by confining toxic factors and inflammatory cells to the injured region.^{59,61} Elimination of reactive astrocytes in acute injury is therefore generally counterproductive, increasing damage and impeding repair.⁶² However, astrocytes also produce chemokines, particularly CCL2, CXCL1, CXCL2, and CXCL10, as well as certain cytokines, ROS, and proteases that may exacerbate neuronal damage (**Fig. 1**).^{57,63} Building on these opposing observations, Liddel et al.⁵⁸ propose an astrocyte activation model

analogous to the M1/2 designation, termed A1 (toxic) and A2 (protective), based on transcriptional profiling. Interestingly, induction of the A1 phenotype is dependent on cytokines and complement factors released primarily by microglia, and elimination of microglia largely prevents astrocyte activation in response to LPS *in vivo*.⁵⁸ Furthermore, postmortem analysis of human brain tissue revealed that A1 astrocytes predominate in active amyotrophic lateral sclerosis (ALS), multiple sclerosis (MS), and Alzheimer's disease (AD). Together with analyses of TLR localization, these results underscore the importance of microglia in orchestrating central nervous system (CNS) inflammation and astrocytes as critical effector cells.

IL-1 β and Neuroinflammation

The production of IL-1 β by microglia or infiltrating peripheral cells can have various effects depending on the cell type on which it acts (**Fig. 1**).⁶⁴ *In vitro* studies have identified hundreds of IL-1 β -responsive genes in astrocytes, including complement components, adhesion molecules, growth factors, and chemokines.^{58,63,65,66} While microglia are not considered primary targets of IL-1 β , *in vitro* data indicate that IL-1 β may nonetheless affect microglia indirectly via astrocyte-derived factors.⁶⁷ As such, both chronic and acute elevation of IL-1 β *in vivo* result in pronounced reactive astrogliosis and microgliosis.^{68–70} Vascular endothelial cells also respond to IL-1 β stimulation with upregulation of chemokines and adhesion molecules, which can affect the function of the BBB.^{67,71} It is well documented that IL-1 β elevation can promote the influx of peripheral neutrophils and monocytes from the circulation across the BBB,^{68–70,72–75} which is dependent on both endothelial cell and astrocyte responses (**Fig. 1**).^{64,72,73} Invading leukocytes have the potential to exacerbate inflammation by producing further cytokines, ROS, and proteases that increase tissue damage, as well as stimulating lymphocyte recruitment.^{76,77} As peripheral immune cells are suggested to contribute to the pathogenesis of AD,^{78,79} MS,⁸⁰ epilepsy,⁸¹ stroke, and traumatic brain injury (TBI),^{82–85} it is feasible that IL-1 β -dependent responses are detrimental in this regard.

Despite the potential neurotoxicity of reactive glia and invading leukocytes, IL-1 β elevation alone is not normally sufficient to cause overt neurodegeneration.^{2,69} Instead, it has been suggested that IL-1 β only promotes toxicity in the presence of additional cytokines, toxins, or existing CNS injury.² In support of this idea, co-administration of IL-1 β with excitotoxins, or following ischemic or traumatic insults, exacerbates neuronal loss, while inhibition by neutralizing antibodies or IL-1 receptor antagonist (IL-1Ra) is protective.⁸⁶ While this would support a pathological role of IL-1 β , it has been argued that IL-

1 β is also critical for CNS repair. In the cuprizone model of demyelination, mice lacking IL-1 β exhibit defective remyelination, possibly due to the role of IL-1 β in regulating the differentiation of oligodendrocyte precursors.^{87,88} Similarly, in a model of Parkinson's disease (PD), dopaminergic neuron recovery following injury is reduced in IL-1 β knockout animals, which may reflect lack of trophic support from reactive glia.⁸⁹

Inflammation and Neuronal Function

Inflammatory cytokines have direct effects on neuronal function and synaptic transmission, which may contribute to the neurocognitive symptoms associated with certain diseases. While physiological concentrations of IL-1 β are involved in hippocampal long-term potentiation (LTP) and memory formation, aberrant elevation of IL-1 β has the opposite effect, suppressing LTP.^{90–92} Accordingly, treatment with LPS, which induces activation of microglia and robust upregulation of IL-1 β in the hippocampus, impairs performance in memory tasks,⁹³ which may occur partially through suppression of BDNF signaling.⁹⁴ Furthermore, it was recently demonstrated that both aging and prior exposure to IL-1 β sensitizes hippocampal synapses to IL-1 β -dependent LTP inhibition,⁹⁵ and that mice lacking NLRP3 are resistant to age-related cognitive impairment.⁹⁶ Rats lacking NLRP1 have also been demonstrated to be resistant to age-related cognitive deficits.⁹⁷ Together, these studies provide a compelling mechanism linking neuroinflammation to cognitive decline.

Inflammation also affects neuronal excitability (**Fig. 1**). First, various reports have indicated that inhibitory γ -aminobutyric acid (GABA) tone can be suppressed by a number of inflammatory cytokines, including IL-1 β and IL-6.^{98–102} Second, IL-1 β signaling increases the amplitude of *N*-methyl α -aspartate (NMDA) and α -amino-3-hydroxy-5-methyl-4-isoxazolepropionic acid (AMPA) receptor-induced currents in a variety of neuronal subtypes.^{98,103,104} Third, pathophysiological levels of IL-1 β inhibit glutamate uptake by astrocytes, leading to raised extracellular glutamate concentrations.^{105,106} These effects all promote neuronal hyperexcitability and are thought to provide a link between inflammation and epileptic seizure generation.¹⁰⁷ Similarly, inflammation may also be a key mechanism of epileptogenesis following acute head trauma,¹⁰⁸ and in the development of chronic neuropathic pain after nerve injury.⁹⁸ Excitability also has a profound impact upon the pathology of both acute and chronic CNS diseases, where excitotoxicity is a key mechanism of neuronal death.^{86,109} Stroke, TBI, and spinal cord injury (SCI) are all thought to involve an acute excitotoxic component, which may be potentiated by IL-1 β .⁸⁶ There is also evidence to support a role of glutamate excitotoxicity in PD, Huntington's disease (HD), ALS, AD, and HIV-

associated dementia, which may partially explain the detrimental effects of neuroinflammation in these diseases.⁸⁶

Contribution of Inflammasomes to CNS Disease

Alzheimer's Disease

AD is a neurodegenerative disease associated with progressive neuronal loss in areas of the brain associated with memory and higher cortical function, most notably the hippocampus and neocortex.¹¹⁰ Consequently, AD patients show severe signs of dementia and cognitive decline, symptoms that worsen over time. Extracellular A β plaques and tau-containing neurofibrillary tangles are the pathological hallmarks of the disease found within the brain.^{110–112} A β plaques are largely composed of A β ₄₀ and A β ₄₂ peptides that are generated by amyloidogenic processing of amyloid precursor protein (APP). Among these species, A β ₄₂ has the highest propensity to aggregate and form oligomers and fibrils that are toxic to neurons.^{113–117}

Neuroinflammation is now also gaining acceptance as a core component of AD pathology, and there is evidence to suggest a role for the NLRP3, NLRP1, and NLRC4 inflammasomes in AD (**Table 1**).^{34,53,118–121} Perhaps the most direct evidence implicating inflammation in AD has come from genome-wide association studies (GWAS) identifying polymorphisms within genes of the innate immune system that are associated with an increased risk of developing AD. Such polymorphisms have been identified in the gene encoding complement receptor 1 (CR1), which plays an important regulatory role in the complement system and has been suggested to promote phagocytic clearance of A β by microglia.^{122,123} AD-

associated polymorphisms have also been identified within the gene encoding TREM2, another receptor involved in microglial phagocytosis, and within human leukocyte antigen-D-related beta 1 (*HLA-DR-B1*) and 5 (*HLA-DR-B5*).^{124,125} *HLA-DR-B1* and *HLA-DR-B5* encode the major histocompatibility complex II (MHC II) beta chain paralogues β 1 and β 5, which are responsible for the presentation of foreign antigens to cells of the adaptive immune system. As such, *HLA-DR* expression is commonly used as a marker of activated immune cells.¹²⁶ *HLA-DR*-positive microglia are found in abundance within the AD brain, particularly around amyloid plaques, suggesting that A β is a source of immune activation in AD.^{127–129}

In addition to the previously discussed roles of IL-1 β in neuronal injury, there are a number of specific mechanisms by which IL-1 β is thought to be detrimental in AD. For example, IL-1 β has been shown to promote the production of S100 β , a cytokine that is overexpressed in the AD brain predominantly by astrocytes and is thought to contribute to neuritic dystrophy.^{130,131} In human endothelial cells, glial cells, and neurons, IL-1 β can upregulate APP expression.^{132–134} IL-1 β also enhances the activity of several protein kinases involved in the phosphorylation of tau, including mitogen-activated protein kinase p38 (MAPK-p38), glycogen synthase kinase 3 β (GSK3 β) and cyclin-dependent kinase5 (Cdk5), suggesting that IL-1 β may promote the formation of neurofibrillary tangles.^{135–138}

Upon interaction with the scavenger receptor CD36 on the surface of microglia, fibrillar A β activates NF- κ B signaling by promoting the assembly of a CD36-TLR4-TLR6 heterotrimer.³¹

Table 1. Summary of Evidence Implicating Inflammasomes in Neurological and Neurodegenerative Conditions.

Disease	Inflammasome	Evidence*	Reference
Alzheimer's disease	NLRP3	Fibrillar A β activates NF- κ B signaling in microglia, priming microglia for NLRP3 inflammasome activation.	31, 139
		Fibrillar A β enhances the production of total IL-1 β and active caspase-1 in LPS-primed microglia and BMDMs.	34
		Increased protein expression of cleaved caspase-1 and total IL-1 β is seen within brain tissue of APP/PS1 mice.	118
		Elevated protein expression of active caspase-1 and total IL-1 is seen within postmortem hippocampal and cortical tissue of AD patients.	118
		APP/PS1 mice deficient in NLRP3 or caspase-1 show reduced amyloid burden within the brain and perform better in memory tasks.	118
	ASC promotes A β aggregation both in vitro and in vivo. ASC specks are found within the core of A β plaques isolated from postmortem brain tissue of AD patients and APP/PS1 mice.	121	
	NLRP1	NLRP1 protein expression is upregulated in brain tissue of APP/PS1 mice.	119

		A β ₄₂ oligomers increase NLRP1 mRNA and protein expression levels and promote neuronal pyroptosis in cultured rat cortical neurons.	119
		siRNA-mediated knockdown of NLRP1 or caspase-1 within the brains of APP/PS1 mice enhances neuronal survival and protects APP/PS1 mice from learning and memory deficits.	119
	NLRC4	NLRC4 expression is upregulated at the mRNA and protein level in postmortem brain tissue of AD patients.	120
		LPC activates NLRC4- and NLRP3-dependent IL-1 β secretion in microglia and astrocytes.	53
Parkinson's disease	NLRP3	Monomeric and fibrillar α -synuclein activate NF- κ B signaling in human monocytes, upregulating mRNA and protein expression of pro IL-1 β .	35
		Fibrillar, but not monomeric, induces pro-IL-1 β cleavage and the release of active IL-1 β from human monocytes.	35, 164
		Enhanced survival of dopaminergic neurons within the substantia nigra of MPTP-treated mice deficient in NLRP3.	165
		Dopamine negatively regulates the NLRP3 inflammasome through DRD1. MPTP-treated mice deficient in DRD1 and NLRP3 are protected from dopaminergic neuronal loss, whereas dopaminergic neuronal loss is exacerbated in MPTP-treated mice deficient in DRD1.	165
		Caspase-1 cleaves α -synuclein at its C-terminus promoting α -synuclein aggregation.	167
Multiple sclerosis	NLRP3	EAE development is impaired in NLRP3, ASC, or caspase-1-deficient EAE mice. Increased mRNA expression of NLRP3 is seen within the spinal cord of EAE mice.	184–186 184
		IL-1 β and IL-18 promote the differentiation of Th1 and Th17 cells; reduced production of IFN- γ and IL-17 is seen within the spinal cord of NLRP3-deficient EAE mice.	184
		NLRP3-deficient EAE mice show an impaired ability to recruit peripheral immune cells into the CNS; downregulated mRNA expression of chemokine molecule–receptor pairs in Th1/Th17 cells and APCs is seen in NLRP3-deficient EAE mice.	184, 188
	NLRC4	Mice deficient in both NLRP3 and NLRC4 show reduced demyelination and neuroinflammation in the cuprizone model of MS.	53
		LPC engages both NLRP3 and NLRC4 and induces the release of active IL-1 β in mouse astrocytes and microglia.	53
		Astrocytes within MS lesions from postmortem brain tissue of MS patients stain positively for NLRC4. Astrocytes from mouse corpus callosum tissue also stain positively for NLRC4 following cuprizone treatment.	53
Amyotrophic lateral sclerosis	NLRP3	NLRP3 protein expression and IL-1 β mRNA expression are enhanced in symptomatic SOD1 ^{G93A} mice.	207
		Caspase-1 or IL-1 β -deficient SOD1 ^{G93A} mice show prolonged survival.	33
		Aggregated SOD1 and TDP-43 enhance the production of total IL-1 β by microglia.	33, 209, 210
		17 β -Estradiol treatment reduces the protein expression of NLRP3, ASC, IL-1 β , and active caspase-1 within the spinal cord, improving motor performance, and prolongs survival in SOD1 ^{G93A} mice.	212
		Increased ASC and NLRP3 staining within the spinal cord of sALS patients, which is largely localized to astrocytes.	51

(continued)

Table 1. (continued)

Disease	Inflammasome	Evidence*	Reference
Stroke	NLRP3, NLRP1	mRNA and protein expression of NLRP3 and NLRP1 is upregulated within the brain of rodent models of ischemic or hemorrhagic stroke.	230–236
		NLRP3-deficient mice are protected from ischemic brain damage, BBB breakdown, and neurological deficits following MCAo.	233
		Neutralization of NLRP1 impairs NLRP1 inflammasome assembly and the production of mature IL-1 β within mouse brains following thromboembolic stroke.	238

	AIM2, NLRP3	AIM2 and NLRP3 mRNA expression is upregulated within the brain in rodent MCAo models.	236
		AIM2- or NLRP3-deficient MCAo mice show less severe brain tissue damage and perform better in neurological performance tests.	237
Acute brain trauma	NLRP1	IL-1 β and IL-18 are upregulated at the mRNA and protein level within the brain and CSF of TBI and SCI patients.	243–247
		ASC neutralization protects against CNS injury in rodent models of TBI and SCI.	250, 251
		NLRP1, ASC, and active caspase-1 protein expression is upregulated in the CSF of patients with moderate to severe TBI.	253
		NLRP1 is found within exosomes isolated from the CSF of patients with SCI.	255
		NLRP1 protein expression is upregulated in spinal cord motor neurons of rats following experimental SCI.	251, 256
		Downregulated protein expression of NLRP1 in response to HO-1 overexpression in rat spinal cord neurons is neuroprotective in experimental SCI.	256
	NLRP3	NLRP3 protein expression is upregulated in the CSF of pediatric TBI patients and correlates with worse outcome.	257
		NLRP3, caspase-1, and ASC expression is upregulated at the mRNA and protein level in rodent models of TBI and SCI.	258, 261, 262
		Mice lacking NLRP3 show reduced brain tissue damage and are protected from cognitive deficits following experimental TBI.	259
		The NLRP3 inflammasome inhibitor MCC950 ameliorates neurological deficit following experimental CCI in mice.	260
Epilepsy	NLRP3	NLRP3, active caspase-1, and IL-1 β protein expression is upregulated within the hippocampus of SE rat models.	273
		NLRP3 knockdown within the brain of SE rats is neuroprotective and has anticonvulsant effects.	273
		The caspase-1 inhibitor VX-765 has anticonvulsant effects in experimental partial seizure models.	275
	NLRP1	NLRP1 and active caspase-1 protein expression is elevated in postmortem hippocampal tissue of TLE patients.	276
		NLRP1 knockdown within the brain of rodent TLE models is neuroprotective and has anticonvulsant effects.	276

*Only evidence supporting the role of inflammasomes in each disease is listed.

Furthermore, fibrillar A β has also been shown to promote NLRP3-mediated IL-1 β release in LPS-primed microglia and bone marrow-derived macrophages (BMDMs), an effect that is absent in LPS-primed BMDMs isolated from NLRP3- or ASC-deficient mice.³⁴ Thus, it is suggested that A β can provide both the first and second signals for activation of the NLRP3 inflammasome. Activation of this pathway by A β upregulates IL-1 β mRNA expression and thus primes microglia for IL-1 β production.^{31,139} In vivo evidence further supports a role for the NLRP3 inflammasome in the pathology of AD. Total IL-1 β and active caspase-1 expression is significantly upregulated in the brains of APP/PS1 mice and in postmortem brain tissue of AD patients.^{118,140} Furthermore, APP/PS1 mice deficient in either NLRP3 or caspase-1 show a reduction in cerebral A β ₄₀ and A β ₄₂ load and are protected from memory and learning deficits. Impaired activation of the NLRP3 inflammasome in APP/PS1 mice deficient in NLRP3 or caspase-1 is suggested to enhance the phagocytic capacity of microglia and subsequent clearance of A β , thus providing a potential explanation for the reduced amyloid burden seen in these mice.¹¹⁸ Recently, an

additional role for extracellular ASC specks in the seeding and spread of amyloid burden in AD was demonstrated. ASC specks released into the supernatant of LPS-primed, ATP-activated mouse microglia interact directly with A β ₄₂ peptides and promote their aggregation in vitro.¹²¹ In support of this, APP/PS1 mice deficient in ASC display reduced amyloid burden and are protected from memory loss. Furthermore, intrahippocampal injection of brain lysates derived from 16-month-old APP/PS1 mice into 3-month-old APP/PS1 mice yet to develop severe A β pathology accelerates both the level and distribution of A β pathology within this hemisphere at 8 months. Notably, this effect is absent in APP/PS1 mice deficient in ASC.¹²¹ In this same study, ASC specks were found within the core of A β plaques isolated from the hippocampus of patients with AD and from the brains of APP/PS1 mice, further supporting the notion that ASC promotes A β seeding.¹²¹

The NLRP1 inflammasome is also implicated in AD pathology (**Table 1**). Within the brain, NLRP1 is predominantly expressed by neurons, and its protein expression is significantly upregulated in the brains of APP/PS1 mice compared with those of wild-type mice.^{119,141} Cultured rat cortical neurons exhibit enhanced mRNA and protein expression of NLRP1 in response to oligomeric A β ₄₂, and siRNA-mediated knockdown of NLRP1 in these neurons significantly reduces A β -induced neuronal pyroptosis and IL-1 β release.¹¹⁹ Furthermore, knockdown of NLRP1 or caspase-1 within the brains of APP/PS1 mice is neuroprotective, with these mice showing greater neuronal survival in the hippocampus and cortex compared with APP/PS1 mice treated with control siRNA. These mice also demonstrate improvements in learning and memory.¹¹⁹

Several lines of evidence implicate a high-fat diet and aberrant lipid metabolism as risk factors for AD.¹⁴² The saturated fatty acid palmitate promotes the release of IL-1 β in astrocytes.¹²⁰ Furthermore, culturing rat cortical neurons in palmitate-treated astrocyte-conditioned media enhances A β ₄₂ production in these neurons, an effect that is ablated through transient silencing of NLRC4 in astrocytes.¹²⁰ In further support of a role for the NLRC4 inflammasome in AD, NLRC4 and ASC expression is upregulated at both the mRNA and protein level within the neocortex of AD patients postmortem.¹²⁰ The phospholipid lysophosphatidylcholine (LPC) is also implicated in AD. LPC promotes glial recruitment and activation, pro-inflammatory cytokine production, A β ₄₂ oligomerization, demyelination, and neuronal death.^{143–147} LPC is produced as a metabolite of phospholipase A2 (PLA₂)-mediated hydrolysis of phosphatidylcholine and is an important constituent of oxidized low-density lipoprotein (ox-LDL).¹⁴⁷ Elevated levels of PLA₂ have been found within the hippocampus of APP mice and human AD patients postmortem; thus, LPC levels are also likely to be elevated.^{148–151} Furthermore, PLA₂-deficient hAPP mice are protected against learning and memory deficits.¹⁵¹ LPC was recently shown to activate NLRP3 and NLRC4 inflammasome pathways in LPS-primed microglia and astrocytes.⁵³ This suggests that the potential role of LPC in AD may be mediated, at least in part, by co-activation of NLRC4 and NLRP3.

Parkinson's Disease

PD is a neurodegenerative disease that is associated with severe atrophy of dopaminergic neurons within the substantia nigra pars compacta, an area of the brain associated with motor function.¹⁵² As a result, PD patients experience tremors, muscle stiffness, and impaired voluntary movement, symptoms that are often accompanied by dementia and cognitive dysfunction.¹⁵³ Pathologically, PD is characterized by the buildup of α -synuclein aggregates within the brain.

α Synuclein aggregates accumulate within Lewy bodies that disrupt neuronal function and ultimately cause neuronal death.^{154–156} As such, specific mutations within the gene encoding α -synuclein are causal of familial PD.¹⁵⁷

Several lines of evidence suggest that inflammation also plays an important role in the pathology of PD. GWAS have identified polymorphisms within several inflammatory genes that are associated with PD risk, including human leukocyte antigen-D-related alpha (*HLA-DR-A*) and *HLADR-B5*, which encode specific MHC II molecule alpha and beta chains, respectively.^{158,159} *HLA-DR*-positive microglia are found in abundance within the substantia nigra of PD patients postmortem,^{127,160} accompanied by high levels of IL-1 β , IL-6, and TNF- α .^{127,161} Polymorphisms in IL-1 α , IL-1 β , and TNF- α are also associated with an increased risk of developing PD; however, the significance of these polymorphisms is yet to be established through GWAS.^{162,163}

Given their close association with *HLA-DR*-positive microglia within the PD brain, α -synuclein aggregates are considered key drivers of neuroinflammation in the disease.¹²⁷ In human monocytes, monomeric and fibrillar species of α -synuclein activate NF- κ B signaling upon interaction with TLR2, upregulating mRNA and protein expression of pro-IL-1 β . Furthermore, α -synuclein can also induce the processing and secretion of mature IL-1 β in human monocytes, though this property is exclusive to fibrillar species.^{35,164}

A commonly used experimental model of PD involves the administration of 1-methyl-4-phenyl-1,2,3,6-tetrahydropyridine (MPTP), which is directly toxic to nigral dopaminergic neurons. Mice deficient in NLRP3 are protected from MPTP-mediated dopaminergic neuronal loss within the substantia nigra, suggesting that the NLRP3 inflammasome might play an important role in PD-associated neurodegeneration.¹⁶⁵ Interestingly, dopamine has been shown to negatively regulate NLRP3 inflammasome activation in primary mouse BMDMs and astrocytes by promoting cyclic AMP (cAMP)-mediated ubiquitination and degradation of NLRP3.¹⁶⁵ Dopamine is thought to do this via activation of dopamine receptor D1 (DRD1), which is abundantly expressed by immune cells.^{165,166} Furthermore, mice deficient in DRD1 show enhanced levels of active caspase-1 within the brain following MPTP administration, accompanied by increased levels of total IL-1 β within serum. The extent of nigral dopaminergic neuronal loss is also exacerbated by DRD1 deficiency in mice administered MPTP compared with wild-type mice. However, mice deficient in both DRD1 and NLRP3 show dopaminergic neuronal loss comparable to that of wild-type mice in response to MPTP treatment.¹⁶⁵ Dopamine-mediated regulation of the NLRP3 inflammasome is thus likely to be an important

mechanism by which inflammation is controlled within the CNS.¹⁶⁵ However, given the deficit in dopaminergic signaling within the PD brain, this endogenous control over the NLRP3 inflammasome may be impaired in PD.^{152,165}

An alternative role for the inflammasome, but more specifically caspase-1, in promoting the aggregation of α synuclein has also been suggested.¹⁶⁷ In response to inflammasome-activating stimuli, caspase-1 cleaves α synuclein at residue 121 within its C-terminus, resulting in the production of a highly aggregation-prone species of α synuclein that are neurotoxic in vitro.¹⁶⁷ C-terminally truncated species of α -synuclein have a higher propensity to aggregate and are found in abundance within Lewy bodies. Such truncated species are more toxic to dopaminergic neurons.^{168–170} Furthermore, the caspase-1 inhibitor VX-765 is neuroprotective in a transgenic mouse model of multiple system atrophy (MSA), another neurodegenerative movement disorder that is characterized by the buildup of α synuclein aggregates within the brain. In this mouse model of MSA, VX-765 treatment significantly reduces striatal α -synuclein load, protects nigral dopaminergic neurons from α -synuclein-mediated neurotoxicity, and improves motor function.¹⁷¹ However, it is important to note that PD and MSA are distinct diseases and caution should be taken when applying these findings to PD.

Multiple Sclerosis

MS is an autoimmune disease characterized by CD4+ T-cell-mediated autoreactivity toward myelin, resulting in severe demyelination, axonal degeneration, and chronic inflammation within the CNS.¹⁷² These changes result in the clinical manifestation of a variety of neurological complications, including fatigue and problems with movement and vision.¹⁷³ Although inflammation is thought to be important in the pathology of MS, its role in the disease is not completely understood given that demyelination has also been shown to occur independently of inflammation.¹⁷² For example, peripheral immune infiltrates are generally found dispersed throughout the CNS rather than being specifically localized to MS lesions. Thus, it has been argued that these infiltrates may instead be involved in regeneration and repair.^{172,174}

Experimental autoimmune encephalitis (EAE) is a commonly used animal model for MS that is usually achieved through immunization with myelin peptides such as myelin oligodendrocyte glycoprotein (MOG), which evoke strong CD4+ T-cell-mediated immune responses that promote demyelination and inflammation within the CNS.¹⁷⁵ Th1 and Th17 cell responses are thought to be important in the pathology of EAE.¹⁷⁶ In EAE, following differentiation within the periphery, Th1 and Th17 cells are recruited into the

CNS and produce interferon gamma (IFN- γ) and IL-17, respectively, in response to antigen-presenting cells (APCs).¹⁷⁷ IFN- γ and IL-17 enhance the permeability of the BBB and promote the recruitment of peripheral immune cells into the CNS, which initiate immune responses toward myelin and bring about demyelination and axonal degeneration.¹⁷⁶

Evidence suggests that the NLRP3 inflammasome plays an important role in the recruitment of CD4+ Th1 and Th17 cells into the CNS and in the orchestration of Th1 and Th17 responses in EAE (**Table 1**). IL-1 β and another pro-inflammatory cytokine that is secreted following inflammasome activation, IL-18, are important for the differentiation of Th1 and Th17 cells.^{178–181} IL-1 β is expressed by macrophages and microglia in MS lesions isolated from the CNS tissue of MS patients postmortem and EAE rats.^{182,183} Furthermore, NLRP3 mRNA expression is upregulated within the spinal cord of EAE mice in response to MOG peptide and increases with disease progression.¹⁸⁴ EAE mice also show similar increases in caspase-1, IL-1 β , IL-6, TNF- α , and IFN- γ mRNA within blood.¹⁸⁵ In NLRP3-, ASC-, or caspase-1-deficient mice, the development of EAE in response to MOG peptide is impaired and there is a marked reduction in the recruitment of peripheral immune cells into the CNS.^{184–186} MOG-immunized mice deficient in NLRP3 also demonstrate a marked reduction in the production of IFN- γ and IL-17 within the spinal cord. These findings suggest that CD4+ Th1 and Th17 cell responses are dampened by NLRP3 deficiency in these mice, providing a potential explanation for the impaired development of EAE.¹⁸⁴ Similar findings have been demonstrated in MOG-treated EAE mice deficient in IL-1 α and IL-1 β , whereas the development of EAE in MOG-treated mice lacking the endogenous IL-1Ra is augmented.¹⁸⁷

CD4+ Th1 and Th17 cells isolated from the peripheral lymphoid organs of MOG-immunized EAE mice deficient in NLRP3 or ASC show downregulated mRNA levels of various genes involved in chemotaxis, including those encoding C-C chemokine receptor type 2 (CCR2) and C-X-C motif chemokine receptor 6 (CXCR6). mRNA levels of the corresponding chemotactic molecules (e.g., CCL7 and CXCL16) are also downregulated in APCs concomitantly in EAE mice deficient in NLRP3 or ASC. Thus, it is suggested that in EAE, activation of the NLRP3 inflammasome within the periphery promotes the infiltration of CD4+ T cells and APCs into the CNS by enhancing the expression of chemokine molecule and receptor pairs in these cells.¹⁸⁸

The development of EAE in rodents can occur both independently of NLRP3 and in a NLRP3-dependent manner, depending on the method and intensity of experimental immunization.^{189–191} Aggressive immunization methods used to achieve EAE do not require activation of the NLRP3 inflammasome, a

subtype of EAE referred to as type B EAE.¹⁸⁹ Interestingly, IFN- β , which is currently approved for the treatment of MS, is ineffective in type B EAE and has therefore been suggested to mediate its effects through the NLRP3 inflammasome.^{189,191} In line with this, IFN- β treatment has been shown to inhibit the production of total IL-1 β and active caspase-1 in LPS-primed splenocytes isolated from nonaggressively immunized EAE mice, and lower levels of total IL-1 β are also observed in the spleens of these mice.¹⁸⁹ As some MS patients are nonresponsive to IFN- β treatment, it is feasible that patient responsiveness to IFN- β treatment may be determined, at least in part, by the extent of NLRP3 inflammasome activation in patients. To investigate this, a patient cohort study was carried out to compare the expression of NLRP3 and IL-1 β in peripheral blood mononuclear cells (PBMCs) from IFN- β -responsive and nonresponsive MS patients.¹⁹² At baseline, the expression of NLRP3 and IL-1 β mRNA was significantly higher in the PBMCs of IFN- β -resistant MS patients. However, following IFN- β treatment, NLRP3 and IL-1 β mRNA expression significantly increased from baseline in the IFN- β -responsive group and remained unchanged in the IFN- β -resistant group. The authors suggest that the upregulated expression of NLRP3 and IL-1 β mRNA that was seen in the responsive group following IFN- β treatment was required for their response to treatment. In this same study, an association was found between a gain-of-function NLRP3 polymorphism (rs35929419) and IFN- β response, with the polymorphism being found at a higher prevalence in IFN- β -responsive patients.¹⁹² However, the significance of NLRP3 polymorphisms in the response to IFN- β treatment in MS patients is yet to be confirmed through GWASs. A role for the inflammasome has also been demonstrated in the cuprizone model of MS. Cuprizone is a copper chelator that is toxic to oligodendrocytes; 4-week treatment of cuprizone causes severe gliosis, neuroinflammation, and demyelination in C57BL/6 mice.¹⁹³ NLRC4 protein expression is abundant within astrocytes and, to a lesser degree, microglia in corpus callosum tissue sections of mice after 4 weeks of cuprizone treatment. In line with this, astrocytic NLRC4 protein expression is also elevated within MS lesions from postmortem brain tissue of patients with chronic MS.⁵³ Furthermore, in the cuprizone model of MS, mice deficient in both NLRP3 and NLRC4 demonstrate a significant reduction in gliosis and extent of demyelination, whereas disease phenotype is more severe in mice deficient in just NLRP3 or NLRC4.⁵³ As previously discussed, the phospholipid LPC, which promotes demyelination and is thought to be elevated in MS due to enhanced PLA₂ activity,^{143,194} promotes inflammasome activation in LPS-primed microglia and astrocytes by engaging both NLRP3 and NLRC4.⁵³ Together these findings suggest that both

NLRP3 and NLRC4 are important for MS-associated demyelination and that LPC may be an important mediator of this process.⁵³

Amyotrophic Lateral Sclerosis

ALS is a devastating neurodegenerative condition characterized by a steady loss of spinal motor neurons, leading to progressive motor impairment followed by death. The average survival is 3–5 years following diagnosis, and there are currently very few treatments. Familial ALS (fALS) is linked to variants in more than 30 separate genes, including in SOD1, fused in sarcoma (FUS), TAR DNA-binding protein 43 kDa (TDP-43), and the noncoding chromosome 9 open reading frame 72 (C9orf72) region.^{195–199} The cause of sporadic ALS (sALS) is not fully understood but is thought to be a multihit process arising through both genetic and environmental risk factors.²⁰⁰ Various environmental factors have been suggested to increase ALS risk, including excessive physical activity, military deployment, smoking, and exposure to neurotoxins.²⁰¹ However no definitive, reproducible associations have yet been established, which may reflect either genuine population differences, differences in study design, or low study power.²⁰¹ Due to the extreme variety in causative factors, ALS pathology is heterogeneous.¹⁹⁹ However, it is notable that aggregated protein inclusions in motor neurons are prevalent even in sALS cases and are commonly composed of TDP-43, as well as SOD1, FUS, and other products of ALS risk genes.²⁰²

ALS patients display evidence of an increased inflammatory profile in both the periphery and cerebrospinal fluid (CSF), and radiological studies have highlighted microglial reactivity along spinal motor tracts and in the motor cortex, which colocalize with structural abnormalities.^{203–205} However, microglial reactivity may be a response to motor neuron injury rather than a cause, and may be either beneficial or detrimental. Both rats and mice bearing the disease-causing human SOD1^{G93A} mutation are widely used as ALS models, and several studies using SOD1^{G93A} mice indicate that the microglial phenotype in the early stages of ALS is protective and promotes neuronal survival.^{206,207} Accordingly, when microglial reactivity is attenuated via P2X7 receptor inhibition, earlystage SOD1^{G93A} mice deteriorate faster than controls, whereas late presymptomatic mice experience prolonged survival.²⁰⁸ These observations highlight a switch in microglial behavior to a neurotoxic phenotype as the disease progresses, yet the molecular basis of this transition is poorly understood. Sequencing and protein studies have demonstrated upregulated protein expression of NLRP3, in addition to upregulated IL-1 β mRNA, in symptomatic but not presymptomatic mice.²⁰⁷

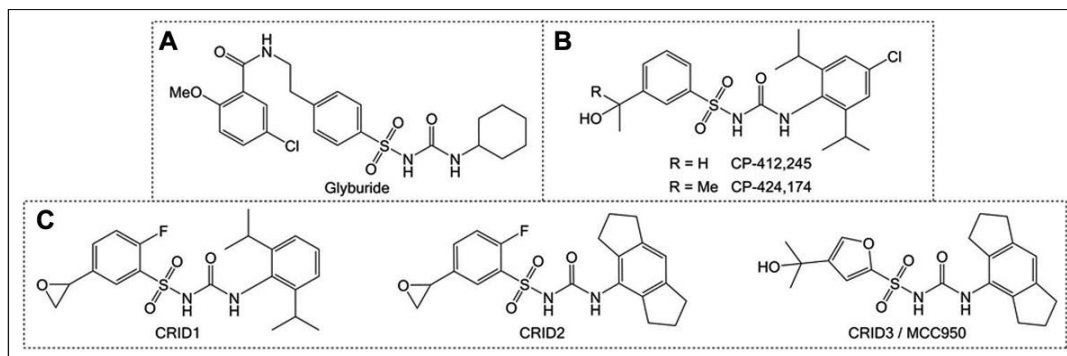


Figure 2. Diarylsulfonylurea inhibitors of the inflammasome. **(A)** Structure of the antidiabetic drug glyburide.²⁸⁴ **(B)** Structures of the early CP compounds.²⁸⁴ **(C)** Structures of the CRID compounds, including MCC950.^{282,287}

Deep RNA sequencing of SOD1^{G93A} microglia by Chiu et al.⁴¹ found evidence of a progressive alteration in microglial phenotype, but one which deviated significantly from both the classical M1 and M2 states. Thus, a unique neurodegeneration-specific signature appears to predominate in SOD1-related ALS.

Various reports suggest that inflammasomes may contribute to ALS pathology (Table 1). In mice, aggregated SOD1^{G93A} is released by severely injured neurons in the later stages of progression and activates ASC-dependent mature IL-1 β release in microglia.³³ TDP-43, which is often misfolded in ALS and frontotemporal dementia (FTD), also activates NLRP3-dependent IL-1 β secretion in microglia, as well as increasing secretion of TNF- α .^{209,210} In vivo, several groups have reported cleaved caspase-1 in spinal homogenates of mice bearing SOD1 mutations.^{33,51,211} Furthermore, SOD1^{G93A} mice lacking either IL-1 β or caspase-1 display slower loss of motor neurons and extended survival.³³ More recently, ASC and NLRP3 staining was observed in spinal cord tissue from sALS patients, which primarily localized to astrocytes.⁵¹ Thus, inflammasome activation may occur in both human cases and animal models of ALS. Nonetheless, the significance of individual inflammasome components in ALS pathogenesis remains to be demonstrated. While ALS mice lacking caspase-1 experience longer survival, it is unclear which inflammasome is responsible for caspase-1 activity in the SOD1^{G93A} model.³³ It is also important from a therapeutic angle that no studies have so far tested the efficacy of specific inflammasome inhibitors in ALS models. However Heitzer et al.²¹² administered 17 β -estradiol, which is known to suppress expression of inflammasome components,²¹³ to symptomatic SOD1^{G93A} mice. 17 β -Estradiol treatment improves motor performance and extended survival, as well as reducing the expression of NLRP3, ASC, mature IL-1 β , and active caspase-1 in the spinal cord.²¹²

Overall, studies to date suggest a potential involvement of the inflammasome in the course of ALS (Table 1). However, there are several prominent

gaps in our understanding of the precise consequences of each inflammasome for disease progression. A recent clinical trial assessing IL-1Ra treatment in ALS patients failed to demonstrate any improvement in motor scores, though the study's primary outcome was tolerability.²¹⁴ Due to the complex and heterogeneous pathology of ALS, it seems likely that disease stage and individual mutations will radically influence the benefits of inflammasome inhibition. Thus, more studies are required to investigate the efficacy of direct inflammasome modulation in ALS models.

Stroke

Stroke is a neurovascular disease that is caused by an interruption in blood flow to the brain, resulting in cerebral hypoxia. Given the high metabolic demand of the brain, these hypoxic conditions bring about rapid cell death, irreversible brain damage, and subsequent loss of brain function. Ischemic stroke is the most common form of stroke and is caused by either thrombotic (e.g., an atherosclerotic plaque) or embolic blockage of a cerebral blood vessel. In hemorrhagic stroke, a cerebral blood vessel becomes ruptured, resulting in the leakage of blood either into the brain, in the case of intracerebral hemorrhage (ICH), or into the subarachnoid space, in the case of subarachnoid hemorrhage (SAH). In addition to interrupted cerebral blood flow, hemorrhagic stroke is also characterized by the formation of a neurotoxic hematoma.²¹⁵

Rapid inflammatory responses are seen during the acute phase of stroke. DAMPs, including ATP, HMGB1, and heat shock protein (HSP), are released from necrotic tissue poststroke and promote the recruitment of microglia, neutrophils, lymphocytes, and macrophages to the site of ischemic injury.^{216–218} Enhanced immune cell activation and pro-inflammatory cytokine production are seen within both the ischemic core and the peri-infarct region, which is most commonly referred to as the “inflammatory penumbra.”^{219–221} Of these pro-inflammatory cytokines, evidence suggests that IL-1 is a particularly important mediator of poststroke neuronal injury.²

In the commonly used middle cerebral artery occlusion (MCAo) model of ischemic stroke, mice deficient in both IL-1 α and IL-1 β or the IL-1 receptor (IL-1R1) are protected from neuronal injury.^{222,223} Furthermore, administration of recombinant IL-1 β into the brains of rats undergoing transient MCAo promotes postischemic neuronal injury,²²⁴ whereas administration of IL-1Ra is neuroprotective in the MCAo model and in rodent models of SAH.^{225,226} Such findings have led to the testing of IL-1Ra in phase II clinical trials for ischemic stroke and SAH. IL-1Ra was not associated with significant toxicity issues in these studies, and as such, the efficacy of IL-1Ra in stroke patients is now being tested in phase III clinical trials.^{227–229}

The evidence implicating IL-1 in poststroke brain injury suggests a role for the inflammasomes. NLRP3 mRNA and protein expression within the brain of rodents is upregulated following experimental induction of ischemic and hemorrhagic stroke.^{230–236} The mRNA expression of the inflammasome sensors NLRP1, absent in melanoma 2 (AIM2), and NLRC4, as well as the protein expression of NLRP1, also appears to be upregulated within the brain in rodent MCAo models of ischemic stroke.^{231,236} NLRP3-deficient mice are protected from ischemic brain damage, BBB breakdown, and neurological deficits following MCAo.²³³ However, work by Denes et al.²³⁷ suggests that the NLRP3 inflammasome is not important for the acute injury after MCAo in mice; rather, the injury is regulated by AIM2 and NLRC4 inflammasomes. In this study, NLRP3-deficient mice that underwent MCAo were not protected from ischemic brain injury or neurological deficits, whereas ASC-, NLRC4-, or AIM2-deficient mice

were.²³⁷ Further studies are required to explain the discrepancies between these studies and to elucidate the mechanisms by which the AIM2 and NLRC4 inflammasomes may be activated in stroke. Antibody-mediated neutralization of NLRP1 has been shown to reduce the expression of IL-1 β and active caspase-1 within the brain following thromboembolic stroke in mice. However, NLRP1 neutralization does not reduce infarct volume, suggesting that other inflammasomes may be more important in this model.²³⁸

Free heme, a toxic metabolite of hemoglobin, is released into the brain parenchyma following cerebral vessel rupture and is thought to have detrimental effects in hemorrhagic stroke.²²⁶ Heme induces oxidative stress in brain tissue, which in turn promotes neuronal and endothelial cell death, with the latter resulting in the breakdown of the BBB and infiltration of peripheral immune cells into the CNS.²³⁹ In line with this, heme oxygenase 1 (HO-1), an enzyme responsible for the breakdown of heme, is abundantly expressed around the bleed site following SAH and is found in close proximity to IL-1 α -expressing microglia.²²⁶

Furthermore, treatment of LPS-primed mixed glial cultures with heme, the oxidation product of heme, induces the processing and release of mature IL-1 α but not IL-1 β . In hippocampal organotypic slices, heme treatment induces neuronal death concomitantly with IL-1 α expression, an effect that is ablated with IL-1Ra treatment, suggesting that the neurotoxic effect of heme may in part be mediated through IL-1 α .²²⁶ Conversely, free heme has been shown to activate the NLRP3 inflammasome in LPS-primed BMDMs and induce the release of mature IL-1 β . Furthermore, the production of total IL-1 β within the peritoneal cavity of mice is also enhanced in response to intraperitoneal injection of heme and mice deficient in either NLRP3, ASC, or caspase-1 are protected from hemolysis-induced lethality.²⁴⁰ Thus, in addition to DAMPs released from necrotic tissue, heme may also serve as an important DAMP for the release of IL-1 α and IL-1 β following hemorrhagic stroke.

Acute Brain Trauma

TBI and SCI are neuropathological events resulting from direct physical trauma to the head or vertebrae, respectively. Following the primary trauma, a series of cascades initiate the “secondary” injury, whereby inflammatory, excitotoxic, and oxidative stress drives neuronal loss and neurological impairment.^{241,242} DAMPs released by necrotic cells following the initial hemorrhage drive an inflammatory response that is likely protective in the initial phase.²⁴² mRNA and protein expression of IL-1 β and IL-18 is upregulated within the brain and CSF of TBI and SCI patients, and is accompanied by the recruitment of leukocytes to the site of injury, which may transform the initial protective response to aggravate damage.^{243–247} Exogenous administration of IL-1 β following experimental TBI increases neuronal apoptosis, whereas neutralization of IL-1 β decreases neutrophil infiltration, lesion volume, and cognitive deficits in controlled cortical impact (CCI) models.^{248,249} Furthermore, neutralization of the inflammasome component ASC is protective in rodent models of TBI and SCI.^{250,251}

NLRP1 expressed by both neurons and microglia may be a contributor to neuronal pyroptosis following acute injury.²⁵² In patients with moderate to severe TBI, increases in NLRP1, ASC, and caspase-1 protein expression in the CSF have been reported, with higher levels correlating with unfavorable outcomes.²⁵³ However, only one study has directly and specifically addressed the role of NLRP1 in TBI. Brickler et al.²⁵⁴ reported that mice lacking NLRP1 or ASC are not protected against motor impairment following CCI, despite decreases in IL-1 β and IL-18 production. However, two previous reports indicate that IL-1 β contributes primarily to cognitive deficits following

TBI, which were not measured by the former study, and that motor deficits are unaffected by IL-1 β neutralization.^{248,249} Thus, motor deficit alone may not be fully indicative of the extent of brain trauma and does not rule out a role of inflammasomes in cognitive outcome.

NLRP1 is also present in exosomes isolated from the CSF of patients following SCI, and rodent models demonstrate NLRP1 protein expression and activation in spinal cord motor neurons following experimental SCI.^{255,250,256} Antibody-mediated ASC neutralization results in reduced IL-1 β production, tissue damage, and motor deficits, supporting a role of inflammasomes in SCI.²⁵⁰ However, ASC neutralization is a rather broad approach and does not specifically implicate NLRP1 in SCI pathology. HO-1 is expressed in rat spinal cord neurons after SCI and downregulates NLRP1 by modulating endoplasmic reticulum stress signaling.²⁵⁶ When overexpressed in spinal cord motor neurons prior to SCI, HO-1 reduces NLRP1 expression, which correlates with decreased neuronal loss and motor recovery.²⁵⁶ Thus, while NLRP1 has a potential role in CNS trauma, direct evidence for its involvement is lacking and will require further study. Several lines of evidence now also support a role of the NLRP3 inflammasome in the pathogenesis of TBI. A recent study in pediatric TBI patients reports elevated protein expression of NLRP3 in the CSF up to 72 h postinjury, which correlates with worse outcome.²⁵⁷ NLRP3, active caspase-1, and ASC mRNA and protein expression is also increased following experimental CCI in rats, accompanied by enhanced production of IL-1 β and IL-18.²⁵⁸ Furthermore, Irrera et al.²⁵⁹ demonstrate that NLRP3-deficient mice exhibit reduced tissue damage after TBI and score better in cognitive tests than wild-type controls. Accordingly, lack of NLRP3 reduces expression of the pro-apoptotic protein BAX in the hippocampus at 7 days postinjury, indicating that NLRP3 may contribute to the spread of neuronal death and to neurological deficit.²⁵⁹ The selective NLRP3 inhibitor MCC950 (**Fig. 2C**) partially ameliorates neurological deficit at 72 h in mice following experimental CCI, and reduces activation of caspase-3, which may reflect protection against pro-apoptotic signaling.²⁶⁰

Rodent models of SCI have also demonstrated robust upregulation of NLRP3, ASC, and caspase-1 protein within spinal cord tissue, though these findings have yet to be verified in human patients.^{212,261,262} Jiang et al.²⁶² found that BAY 11-7082, which inhibits NF- κ B signaling, and A438079, an inhibitor of P2X7 receptor-dependent NLRP3 inflammasome activation, improve motor recovery in mice following spinal cord compression injury. Faster recovery in these mice was accompanied by reduced neutrophil recruitment; reduced spinal cord levels of IL-1 β , IL-18, and active caspase-1; and reduced neuronal apoptosis. However, no studies have directly addressed NLRP3

involvement using either genetic models or specific inhibitors such as MCC950. Therefore, a definitive role for NLRP3 in experimental SCI remains to be demonstrated.

Epilepsy

Epilepsy is a neurological disorder associated with episodic seizures that range in severity and frequency.²⁶³ Generally speaking, epileptic seizures are thought to occur due to an imbalance between excitatory and inhibitory signaling in the brain. The etiology of epilepsy is largely unclear, but genetics and comorbidities such as stroke, brain trauma, and infection have all been associated with an increased risk of epilepsy.²⁶⁴ Evidence suggests that neuroinflammation may also be a core component of epilepsy, and in light of what has been previously discussed, it is feasible that neuroinflammation links epilepsy to these comorbidities.² IL-1 β and IL-6 immunoreactivity is seen in rodent brains following the induction of an experimental seizure, alongside concomitant upregulated mRNA expression of these cytokines and their receptors on neurons.^{265–269} Of these cytokines, IL-1 β is thought to be of particular importance in epilepsy. Recombinant IL-1Ra treatment inhibits the onset of experimentally induced seizures in rodents, an effect that is absent in mice deficient in IL-1R1.²⁷⁰ In rodent models of febrile seizures, IL-1 β protein levels are elevated within the brain and are associated with increased seizure risk.²⁷¹ The role of IL-1 β and other pro-inflammatory mediators in epilepsy is yet to be fully established. However, these cytokines are thought to enhance the excitability of neurons, lower the threshold for the onset of seizures, and contribute to synaptic remodeling to allow for the generation of hyperexcitable neuronal circuits.²⁷²

A role for the NLRP3 inflammasome in epilepsy was first demonstrated by Meng et al.²⁷³ Status epilepticus (SE) is a condition associated with prolonged or frequently occurring seizures of short duration.²⁷⁴ Experimental rat models of SE involving electrical stimulation of the amygdala show elevated hippocampal levels of NLRP3, active caspase-1, and IL-1 β compared with sham controls.²⁷³ siRNA-mediated knockdown of NLRP3 within the brain of SE rats enhances neuronal survival within the hippocampus and reduces the onset, duration, and severity of seizures, also implying a role for NLRP3 in epileptogenesis.²⁷³ Furthermore, the caspase-1 inhibitor VX-765 has anticonvulsant activity in rodent experimental partial seizure models by reducing the production of IL-1 β , and as such, its use for the treatment of drug-resistant partial epilepsy has been tested in clinical trials.²⁷⁵ Evidence also suggests an involvement for the NLRP1 inflammasome in epilepsy (**Table 1**). Elevated protein levels of NLRP1 and caspase-1 are seen within the hippocampus of patients

with temporal lobe epilepsy (TLE), a form of epilepsy associated with hippocampal neuronal atrophy.²⁷⁶ Furthermore, genetically silencing NLRP1 within the brain of rodent TLE models reduces the severity and occurrence of seizures and enhances neuronal survival within the hippocampus.²⁷⁶

Injury Phases and Potential Points of Therapeutic Intervention in CNS Disease

It is critical to the development of inflammasome-targeting therapies to understand at what stage in disease inflammasome activation is most detrimental. In stroke models, administration of IL-1Ra and caspase-1 inhibitors is protective only up to 3 h poststroke.^{277,278} Therefore, any benefits of inflammasome inhibition are likely to be limited to this acute time window. It appears feasible, given prior preclinical data, that if inflammasome inhibition could be accomplished, the reduction in IL-1 β levels might favor reduced neutrophil recruitment and attenuated neuronal damage. However, preclinical validation of this strategy in stroke, TBI, and SCI models will first be required.

In neurodegenerative conditions such as AD, PD, and ALS, in which there is marked proteotoxic involvement, the picture is less clear. These diseases all involve a period of clinical latency, followed by gradual onset of symptoms as neurons are progressively lost.^{201,279,280} Inflammasomes could act during the latent phase to drive the underlying pathological changes that occur prior to overt neurodegeneration, or alternatively could act as downstream effectors exacerbating neuronal demise in response to the primary pathology. This is a critical distinction in determining whether inflammasome inhibition might be prophylactic or therapeutic in these conditions. In AD, there is evidence that NLRP3 could act at all disease stages, via ASC-mediated nucleation of A β plaques, as well as IL-1 β -driven tau aggregation and cognitive decline.^{121,135–138} Similarly, in PD, caspase-1 can promote α -synuclein aggregation,¹⁶⁷ and in a reciprocal manner, fibrillar α -synuclein can also promote activation of the NLRP3 inflammasome.^{35,164} Pharmacological targeting of the inflammasome pathway could therefore potentially delay PD and AD onset if given sufficiently early in the disease course, or slow the disease progression by ameliorating neuronal death. In ALS, there is relatively little evidence specifically addressing the temporal involvement of inflammasomes. In the SOD1^{G93A} model, caspase-1 deficiency lengthens survival but does not delay disease onset.³³ This suggests that, at least in SOD1-related pathologies, inflammasome activation is an accompanying rather than an initiating event and might therefore be targeted to slow ALS progression. However, as ALS comprises a particularly heterogeneous set of pathologies, more research is

required to determine whether other forms of familial and sporadic ALS might be similarly tractable.

MS is still more complex, with some patients experiencing distinct attacks separated by quiescent periods (relapsing-remitting), while others present with progressive disease that does not remit (primary progressive).²⁸¹ Inflammasome deficiency can reduce the severity of demyelination in EAE and delay disease progression, suggesting an involvement in the early stages of EAE.^{184–186} There is also some evidence that NLRP3 inhibitors can attenuate the severity of EAE.²⁸²

Given the role of IL-1 β in the development of Th1 and Th17 responses,^{178–181} it is possible that inflammasome inhibition might help reduce the infiltration of inflammatory immune cells and ameliorate demyelination in MS. However, due to inherent differences between EAE and clinical MS, the translational value of these results remains to be established.

Given that there are several different types of epilepsy disorders and that our current knowledge of the pathological processes involved in epilepsy is lacking, it is hard to conclude at this stage whether inflammasome inhibition would be beneficial in epilepsy. Inflammasomes have been implicated both in the onset of seizures and in epileptogenesis;²⁷³ thus, further research is warranted in order to understand when therapeutic intervention might prove useful.

Inflammasome Inhibitors

Given the role of the NLRP3 inflammasome in the discussed diseases, there is great potential in developing NLRP3 inflammasome inhibitors as therapeutics for such conditions. We recently published a comprehensive review of small-molecule inhibitors of the NLRP3 pathway, and their potential for therapeutic intervention in neurological disorders.²⁸³ A few biological inhibitors of IL-1 β are already utilized clinically, including riloncept (Arcalyst), canakinumab (Ilaris), and anakinra (Kineret). However, these inhibitors target solely IL-1 and, as a result, have no effect on other inflammasome-mediated processes, such as pyroptosis and IL-18 release. Moreover, the BBB penetration of these therapeutics is slow; thus, their utility may be limited to peripheral inflammatory diseases. On the other hand, small-molecule inhibitors of the NLRP3 inflammasome will likely be more cost-effective, and of greater use in CNS indications due to greater BBB permeability. Some promising small molecules are discussed below, illustrating the various approaches taken to inhibiting the NLRP3 inflammasome.

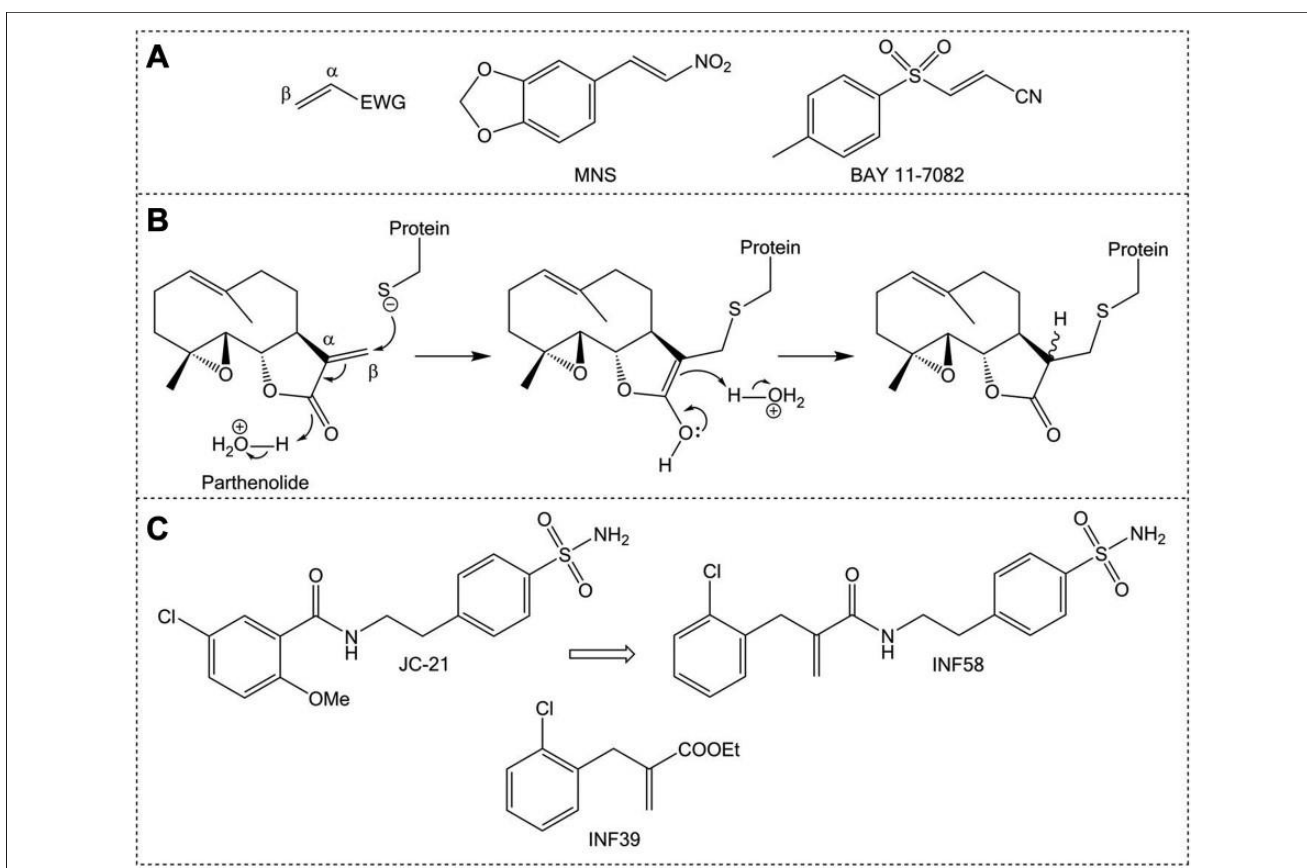


Figure 3. Michael acceptors in inflammasome inhibitors. **(A)** The generalized structure of a Michael acceptor drug, with α - and β -carbon atoms defined. The structures of Michael acceptor-containing inhibitors of the NLRP3 inflammasome: MNS²⁹³ and BAY 11-7082.²⁹⁴ **(B)** General mechanism of protein alkylation through a cysteine residue of a protein attacking the β -carbon of the Michael acceptor present in parthenolide, another reported inhibitor of the NLRP3 inflammasome.^{294,311} **(C)** Structure of the known inflammasome inhibitor JC-21,²⁹⁶ and the JC-21-inspired electrophilic warhead INF58,²⁹⁵ with incorporation of an acrylamide Michael acceptor. The structure of the latest lead compound of this series, INF39, is also shown.²⁹⁷

From Glyburide to MCC950: The CRID Story

A promising series of inhibitors was inspired by the discovery of the antidiabetic sulfonylurea glyburide (**Fig. 2A**) as an inhibitor of IL-1 β production.²⁸⁴ Following the discovery of the inflammasome,²⁸⁵ glyburide was found to act via inhibition of NLRP3 inflammasome assembly.²⁸⁶ Early compounds CP-412,245 and CP-424,174 took inspiration from the glyburide structure, with a diarylsulfonylurea motif incorporated (**Fig. 2B**). The CP compounds inhibit NLRP3 inflammasome-dependent posttranslational IL-1 β processing with IC₅₀ values of around 250 nM.²⁸⁴

Subsequent mechanism of action studies suggested glutathione *S*-transferase omega 1 (GSTO1) as a possible target of two diarylsulfonylurea-containing cytokine release inhibitory drugs (CRIDs), CRID1 and CRID2, which also inhibit the release of IL-1 β (**Fig. 2C**).^{287,288} The related analogue CRID3 was also reported in this study, with structural features taken from CP-424,174 and CRID2. CRID3, also known as MCC950, is a selective small molecule inhibitor of NLRP3 with an IC₅₀ of 7.5 nM against NLRP3

inflammasome activation in BMDMs (**Fig. 2C**).^{282,287,289} In vivo, MCC950 reduces IL-1 β production and attenuates symptoms of EAE.²⁸² MCC950 also abrogates neonatal lethality in a mouse model of cryopyrin-associated periodic syndrome (CAPS), an autoinflammatory disease that is caused by gain-of-function mutations in NLRP3.²⁸² MCC950 also inhibits inflammasome activation and microglial activation in the APP/PS1 mouse model of AD.²⁹⁰ Thus, MCC950 is an interesting potential therapeutic for NLRP3-associated diseases.

The precise biological target for MCC950 is yet to be elucidated. Unlike glyburide, MCC950 does not target ATP-sensitive K⁺ channels,²⁸² with K⁺ efflux an event common to all NLRP3 activators.¹⁴ Ca²⁺ signaling is also implicated in NLRP3 activation;²⁹¹ however, MCC950 has little effect on the ATP-induced increase of intracellular Ca²⁺.²⁸² MCC950 inhibits the NLRP3-induced oligomerization of ASC, yet does not interfere with either the NLRP3/NLRP3 or NLRP3/ASC interaction.²⁸²

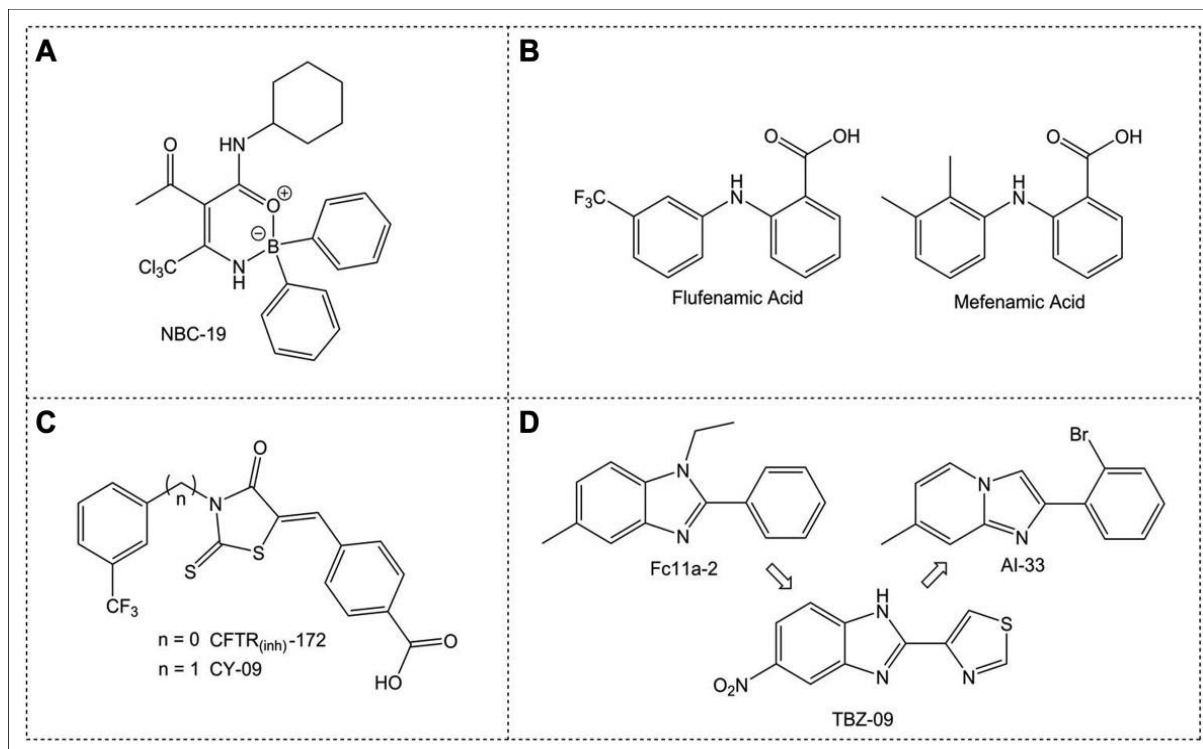


Figure 4. Structures of NLRP3 inflammasome inhibitors. **(A)** Structure of NBC-19, a leading representative of the novel oxazaborine which inhibit the NLRP3 inflammasome through inhibition of VRAC.scaffold with key features including the CCl_3 and amide functionality.¹⁵²⁹⁹ **(CB)** Structure of the chloride channel blocker CFTR Structures of the NSAIDs flufenamic and mefenamic acid, $_{(\text{inh})}$ -172, which inhibits NLRP3 activation, and the close analogue CY-09, which inhibits the ATPase activity of NLRP3, with no effect on CFTR.³⁰⁶ **(D)** Structure of Fc11a-2, identified from a screen of synthetic molecules to inhibit IL-1 β release. TBZ-09 was a leading compound when a range of Fc11a-2 analogues was screened. Subsequent screening of alternatives to the core chemical scaffold of TBZ-09 yielded AI-33.

Michael Acceptors in NLRP3 Inflammasome Inhibitors

Compounds containing α,β -unsaturated carbonyl groups are called Michael acceptors (named after Arthur Michael), which react with nucleophiles at the β -carbon of the alkene (**Fig. 3A**). Michael acceptors are present in a number of drugs that are covalent modifiers of their target protein (suicide substrates). Michael acceptors are present in a number of reported NLRP3 inflammasome inhibitors.²⁹² 3,4-methylenedioxy- β -nitrostyrene (MNS) and BAY 11-7082 (**Fig. 3A**) selectively inhibit the NLRP3 inflammasome independently of any effect on the NF- κ B pathway in the priming stage by binding the ATPase region of the NLRP3 NACHT domain, with the Michael acceptor moieties being indispensable.^{293,294} Parthenolide (**Fig. 3B**), which has reported inhibitory activity against NLRP3, NLRP1, and NLRC4 inflammasome-dependent IL-1 β release, is another example of an inhibitor with a Michael acceptor. The broad activity of parthenolide was found to be due to alkylation of both the caspase-1 p20 subunit and NLRP3.²⁹⁴

A series of electrophilic Michael acceptor warheads inhibit ATPase activity of NLRP3 as well as caspase-1 activity.²⁹² Despite fine tuning of reactivity to avoid

cytotoxic effects, the lead compounds of this initial study do retain some cytotoxicity, with a follow-up exploring less reactive acrylamide-based warheads.²⁹⁵ In an interesting merging strategy, the electrophilic warhead was combined with structural motifs from the reported NLRP3 inflammasome inhibitor JC-21, itself an analogue of an intermediate in the synthesis of glyburide (**Fig. 3C**).²⁹⁶ The resulting compound, INF58, is able to inhibit the ATPase activity of NLRP3, though with a relatively modest IC_{50} of 74 μM .²⁹⁵ INF39 is the latest leading compound of this series (**Fig. 3C**), with an IC_{50} of around 10 μM , representing an irreversible, nontoxic inhibitor of the NLRP3 inflammasome that has undergone preliminary in vitro absorption, distribution, metabolism, excretion (ADME) studies.²⁹⁷

NBC Compounds

Since the discovery of MCC950, the landscape for NLRP3 inhibition has broadened. Boron is an unusual element in drugs, with only one medicine in the clinic that contains boron, Velcade (or bortezomib), which is used to treat multiple myeloma.²⁹⁸ We recently published our novel boron compound (NBC) series of inflammasome inhibitors based on an oxazaborine ring scaffold (exhibited by NBC-19; **Fig. 4A**).^{299,300} 2-

Aminoethoxy diphenylborinate (2APB) is a small-molecule inhibitor of Ca^{2+} signaling used to probe the involvement of Ca^{2+} in inflammasome activation.^{301–304} Though 2APB likely affects the NLRP3 inflammasome independently of Ca^{2+} ,³⁰⁵ the potential to develop 2APB as an NLRP3 inflammasome inhibitor is limited by its influence on Ca^{2+} homeostasis. A screen of a library of 2APB analogues suggests that boron is essential for inhibitory activity against IL-1 β release, with the most active compounds consisting of a diarylborinic acid moiety and oxazaborine ring. Subsequently, several analogues were synthesized and screened, with the lead compounds also incorporating the trichloromethyl (CCl_3) group, as well as an amide functionality as present in NBC-19 (**Fig. 4A**). This series of molecules effectively inhibit ASC speck formation and IL-1 β release both in vitro and in vivo in a mouse model of peritonitis.²⁹⁹ Importantly, these inhibitors appear to have no effect on Ca^{2+} signaling, with their inhibitory activity against IL-1 β release independent of Ca^{2+} . Thus, the NBC series represents a unique chemical scaffold for the development of NLRP3-targeting therapeutics.

Chloride Channels: A Potential Target?

Recent work has suggested that Cl^- channel inhibition could be a good therapeutic angle for NLRP3 inhibition.^{15–17} We demonstrated that nonsteroidal anti-inflammatory drugs (NSAIDs) based on a fenamate scaffold could be repurposed as NLRP3 inhibitors (**Fig. 4B**).¹⁵ The fenamate scaffold, exemplified by mefenamic and flufenamic acid, consists of two aromatic rings separated by an amine linker, with a carboxylic acid located in the position next (ortho) to the amine linker of one of the rings. The fenamates appear to inhibit the NLRP3 inflammasome through blocking Cl^- channels, with pharmacology suggesting the volume-regulated anion channel (VRAC).¹⁵ Further work is required to explore this approach of NLRP3 inflammasome inhibition.

Another Cl^- channel inhibitor, the cystic fibrosis transmembrane conductance regulator inhibitor $\text{CFTR}_{(\text{inh})}$ -172, specifically inhibited NLRP3 activation in LPS/ATP-treated BMDMs independently of any effect on CFTR (**Fig. 4C**).³⁰⁶ Given the CFTR-independent nature of this effect, several $\text{CFTR}_{(\text{inh})}$ -172 analogues were screened, which had no CFTR inhibitory activity.³⁰⁶ One analogue, CY-09, exhibited NLRP3-specific inhibition of a magnitude similar to $\text{CFTR}_{(\text{inh})}$ -172 (**Fig. 4C**).³⁰⁶ CY-09 has no effect on LPS-induced priming, nigericin-induced K^+ efflux, or VRAC-dependent Cl^- efflux, but does inhibit NLRP3 oligomerization and subsequently inflammasome assembly. The proposed mechanism for CY-09 against NLRP3 is via inhibition of the ATP binding region of the NLRP3 NACHT domain, which prevents the ATPase activity necessary for NLRP3

self-association.^{306,307} In vivo, CY-09 is protective against NLRP3-dependent pathologies, both abrogating neonatal lethality in a mouse model of CAPS and reversing metabolic disorders in diabetic mice.³⁰⁶ Interestingly CY-09 also inhibits caspase-1 activation and IL-1 β production in synovial fluid cells from patients with gout, suggesting that CY-09 or its analogues may represent a potential therapeutic in NLRP3-dependent diseases.³⁰⁶

Inhibiting NLRP3 Inflammasome Dissociation

In a search for small molecules with anti-inflammatory activity, a series of compounds were screened, yielding Fc11a-2 as an inhibitor of ATP-induced IL-1 β release at 10 μM (**Fig. 4D**).³⁰⁸ Fc11a-2 also dose dependently reduces the symptoms of dextran sodium sulfate (DSS)-induced experimental colitis in mice.³⁰⁸ Inhibition of inflammasome activation by Fc11a-2 is through suppression of caspase-1 release from the ASC/NLRP3 complex.³⁰⁸ Structurally similar thiabendazole analogues³⁰⁹ can also act as anti-inflammatory agents.³¹⁰ An early lead, TBZ-09, inhibits the release of IL-1 β and exhibits the structural feature of an electron withdrawing group (EWG) at position 5 of the benzimidazole core (**Fig. 4D**). A broader series was synthesized consisting of analogues retaining an EWG in this position, as well as alternatives to the benzimidazole scaffold.³¹⁰ The most potent compound of this series, AI-33 (**Fig. 4D**), has an IC_{50} of only around 10 μM ; however, this series does represent a potential new approach to inhibiting NLRP3-dependent IL-1 β release.

Summary

Inflammasomes have emerging roles in a variety of neurodegenerative conditions, and their inhibition may be an effective strategy for future therapeutics. Given the recent acceleration in advances surrounding the regulation, mechanism of action, and inhibition of inflammasomes, clinical manipulation of the pathway is becoming increasingly feasible. This is particularly evident in the discovery of existing drugs that target NLRP3. However, due to the multiphasic progression of many conditions, care must be taken to identify the disease stages at which inflammasome-directed therapies will be effective. It is also important to note from a translational standpoint that preclinical data are generally produced in laboratory mice under specified pathogen-free conditions. Therefore, the physiological importance of proteins with immunological functions such as inflammasomes may be masked in such studies. As humans exist in a far “dirtier”, more immunologically challenging environment, careful assessment of the potential impact of inflammasome

inhibition on host–microbe interactions and pathogen resistance is required. At present, there are minimal data regarding side effects from inflammasome-targeting treatments specifically, though the CANTOS trial does note a slightly increased incidence of fatal infection in canakinumab recipients.¹ However, canakinumab targets all IL-1 β irrespective of its origin. Immunosuppression might therefore be minimized by targeting specific inflammasomes, such as NLRP3, while leaving others, such as NLRC4 and AIM2, functional, thus preserving some aspects of the inflammasome response.

Work continues on a number of series in order to improve potency and pharmacokinetic properties, while attempting to limit off-target and cytotoxic effects. These small-molecule inhibitors of the NLRP3 inflammasome offer some promise in the development of potential anti-inflammatory therapeutics in the treatment of diseases involving the NLRP3-dependent release of IL-1 β .

Declaration of Conflicting Interests


The authors declared no potential conflicts of interest with respect to the research, authorship, and/or publication of this article.

Funding

The authors disclosed receipt of the following financial support for the research, authorship, and/or publication of this article: T.S. is funded by the Alzheimer's society. J.C. and J.A.B. are funded by MRC DTP studentships.

ORCID iDs

James Cook  <https://orcid.org/0000-0002-1905-4928>

David Brough  <https://orcid.org/0000-0002-2250-2381>

References

- Ridker, P. M.; Everett, B. M.; Thuren, T.; et al. Antiinflammatory Therapy with Canakinumab for Atherosclerotic Disease. *N. Engl. J. Med.* **2017**, *377*, 1119–1131.
- Allan, S. M.; Tyrrell, P. J.; Rothwell, N. J. Interleukin-1 and Neuronal Injury. *Nat. Rev. Immunol.* **2005**, *5*, 629–640.
- Dinarello, C. A. Interleukin-1 in the Pathogenesis and Treatment of Inflammatory Diseases. *Blood* **2011**, *117*, 3720–3732.
- Broz, P.; Dixit, V. M. Inflammasomes: Mechanism of Assembly, Regulation and Signalling. *Nat. Rev. Immunol.* **2016**, *16*, 407–420.
- He, Y.; Zeng, M. Y.; Yang, D.; et al. NEK7 Is an Essential Mediator of NLRP3 Activation Downstream of Potassium Efflux. *Nature* **2016**, *530*, 354–357.
- Shi, H.; Wang, Y.; Li, X.; et al. NLRP3 Activation and Mitosis Are Mutually Exclusive Events Coordinated by NEK7, a New Inflammasome Component. *Nat. Immunol.* **2016**, *17*, 250–258.
- Lu, A.; Magupalli, V. G.; Ruan, J.; et al. Unified Polymerization Mechanism for the Assembly of ASC-Dependent Inflammasomes. *Cell* **2014**, *156*, 1193–1206.
- Dick, M. S.; Sborgi, L.; Ruhl, S.; et al. ASC Filament Formation Serves as a Signal Amplification Mechanism for Inflammasomes. *Nat. Commun.* **2016**, *7*, 11929.
- Brough, D.; Pelegrin, P.; Nickel, W. An Emerging Case for Membrane Pore Formation as a Common Mechanism for the Unconventional Secretion of FGF2 and IL-1 β . *J. Cell Sci.* **2017**, *130*, 3197–3202.
- Stutz, A.; Kolbe, C. C.; Stahl, R.; et al. NLRP3 Inflammasome Assembly Is Regulated by Phosphorylation of the Pyrin Domain. *J. Exp. Med.* **2017**, *214*, 1725–1736.
- Juliana, C.; Fernandes-Alnemri, T.; Kang, S.; et al. NonTranscriptional Priming and Deubiquitination Regulate NLRP3 Inflammasome Activation. *J. Biol. Chem.* **2012**, *287*, 36617–36622.
- Lopez-Castejon, G.; Luheshi, N. M.; Compan, V.; et al. Deubiquitinases Regulate the Activity of Caspase-1 and Interleukin-1 β Secretion via Assembly of the Inflammasome. *J. Biol. Chem.* **2013**, *288*, 2721–2733.
- Song, N.; Liu, Z. S.; Xue, W.; et al. NLRP3 Phosphorylation Is an Essential Priming Event for Inflammasome Activation. *Mol. Cell.* **2017**, *68*, 185–197.
- Munoz-Planillo, R.; Kuffa, P.; Martinez-Colon, G.; et al. K(+) Efflux Is the Common Trigger of NLRP3 Inflammasome Activation by Bacterial Toxins and Particulate Matter. *Immunity* **2013**, *38*, 1142–1153.
- Daniels, M. J.; Rivers-Auty, J.; Schilling, T.; et al. Fenamate NSAIDs Inhibit the NLRP3 Inflammasome and Protect against Alzheimer's Disease in Rodent Models. *Nat. Commun.* **2016**, *7*, 12504.
- Domingo-Fernandez, R.; Coll, R. C.; Kearney, J.; et al. The Intracellular Chloride Channel Proteins CLIC1 and CLIC4 Induce IL-1 β Transcription and Activate the NLRP3 Inflammasome. *J. Biol. Chem.* **2017**, *292*, 12077–12087.
- Tang, T.; Lang, X.; Xu, C.; et al. CLICs-Dependent Chloride Efflux Is an Essential and Proximal Upstream Event for NLRP3 Inflammasome Activation. *Nat. Commun.* **2017**, *8*, 202.
- Bergsbaken, T.; Fink, S. L.; Cookson, B. T. Pyroptosis: Host Cell Death and Inflammation. *Nat. Rev. Microbiol.* **2009**, *7*, 99–109.
- Shi, J.; Zhao, Y.; Wang, K.; et al. Cleavage of GSDMD by Inflammatory Caspases Determines Pyroptotic Cell Death. *Nature* **2015**, *526*, 660–665.
- Kayagaki, N.; Stowe, I. B.; Lee, B. L.; et al. Caspase-11 Cleaves Gasdermin D for Non-Canonical Inflammasome Signalling. *Nature* **2015**, *526*, 666–671.
- Franklin, B. S.; Bossaller, L.; De Nardo, D.; et al. The Adaptor ASC Has Extracellular and “Prionoid” Activities That Propagate Inflammation. *Nat. Immunol.* **2014**, *15*, 727–737.
- Baroja-Mazo, A.; Martin-Sanchez, F.; Gomez, A. I.; et al. The NLRP3 Inflammasome Is Released as a Particulate Danger Signal That Amplifies the Inflammatory Response. *Nat. Immunol.* **2014**, *15*, 738–748.
- Galea, I.; Bechmann, I.; Perry, V. H. What Is Immune Privilege (Not)? *Trends Immunol.* **2007**, *28*, 12–18.
- Aloisi, F. Immune Function of Microglia. *Glia* **2001**, *36*, 165–179.
- Nimmerjahn, A.; Kirchhoff, F.; Helmchen, F. Resting Microglial Cells Are Highly Dynamic Surveillants of Brain Parenchyma In Vivo. *Science* **2005**, *308*, 1314–1318.

26. Hanisch, U.-K.; Kettenmann, H. Microglia: Active Sensor and Versatile Effector Cells in the Normal and Pathologic Brain. *Nat. Neurosci.* **2007**, *10*, 1387–1394.
27. Paolicelli, R. C.; Bolasco, G.; Pagani, F.; et al. Synaptic Pruning by Microglia Is Necessary for Normal Brain Development. *Science* **2011**, *333*, 1456–1458.
28. Parkhurst, C. N.; Yang, G.; Ninan, I.; et al. Microglia Promote Learning-Dependent Synapse Formation through Brain-Derived Neurotrophic Factor. *Cell* **2013**, *155*, 1596–1609.
29. Kettenmann, H.; Hanisch, U.-K.; Noda, M.; et al. Physiology of Microglia. *Physiol. Rev.* **2011**, *91*, 461–553.
30. Jin, J.-J.; Kim, H.-D.; Maxwell, J. A.; et al. Toll-Like Receptor 4-Dependent Upregulation of Cytokines in a Transgenic Mouse Model of Alzheimer's Disease. *J. Neuroinflammation* **2008**, *5*, 23.
31. Stewart, C. R.; Stuart, L. M.; Wilkinson, K.; et al. CD36 Ligands Promote Sterile Inflammation through Assembly of a Toll-Like Receptor 4 and 6 Heterodimer. *Nat. Immunol.* **2010**, *11*, 155–161.
32. Fellner, L.; Irschick, R.; Schanda, K.; et al. Toll-Like Receptor 4 Is Required for α -Synuclein Dependent Activation of Microglia and Astroglia. *Glia* **2013**, *61*, 349–360.
33. Meissner, F.; Molawi, K.; Zychlinsky, A. Mutant Superoxide Dismutase 1-Induced IL-1 β Accelerates ALS Pathogenesis. *Proc. Natl. Acad. Sci. U.S.A.* **2010**, *107*, 13046–13050.
34. Halle, A.; Hornung, V.; Petzold, G. C.; et al. The NALP3 Inflammasome Is Involved in the Innate Immune Response to Amyloid- β . *Nat. Immunol.* **2008**, *9*, 857–865.
35. Codolo, G.; Plotegher, N.; Pozzobon, T.; et al. Triggering of Inflammasome by Aggregated α -Synuclein, an Inflammatory Response in Synucleinopathies. *PLoS One* **2013**, *8*, e55375.
36. Martinez, F. O.; Gordon, S. The M1 and M2 Paradigm of Macrophage Activation: Time for Reassessment. *F1000Prime Rep.* **2014**, *6*, 13.
37. Butovsky, O.; Talpalar, A. E.; Ben-Yaakov, K.; et al. Activation of Microglia by Aggregated β -Amyloid or Lipopolysaccharide Impairs MHC-II Expression and Renders Them Cytotoxic Whereas IFN- γ and IL-4 Render Them Protective. *Mol. Cell. Neurosci.* **2005**, *29*, 381–393.
38. Ponomarev, E. D.; Maresz, K.; Tan, Y.; et al. CNS-Derived Interleukin-4 Is Essential for the Regulation of Autoimmune Inflammation and Induces a State of Alternative Activation in Microglial Cells. *J. Neurosci.* **2007**, *27*, 10714–10721.
39. Doyle, A. G.; Herbein, G.; Montaner, L. J.; et al. Interleukin-13 Alters the Activation State of Murine Macrophages In Vitro: Comparison with Interleukin-4 and Interferon- γ . *Eur. J. Immunol.* **1994**, *24*, 1441–1445.
40. Stein, M.; Keshav, S.; Harris, N.; et al. Interleukin 4 Potently Enhances Murine Macrophage Mannose Receptor Activity: A Marker of Alternative Immunologic Macrophage Activation. *J. Exp. Med.* **1992**, *176*, 287–292.
41. Chiu, I. M.; Morimoto, E. T. A.; Goodarzi, H.; et al. A Neurodegeneration-Specific Gene-Expression Signature of Acutely Isolated Microglia from an Amyotrophic Lateral Sclerosis Mouse Model. *Cell Rep.* **2013**, *4*, 385–401.
42. Keren-Shaul, H.; Spinrad, A.; Weiner, A.; et al. A Unique Microglia Type Associated with Restricting Development of Alzheimer's Disease. *Cell* **2017**, *169*, 1276–1290.e17.
43. Morganti, J. M.; Riparip, L.-K.; Rosi, S. Call Off the Dog(ma): M1/M2 Polarization Is Concurrent Following Traumatic Brain Injury. *PLoS One* **2016**, *11*, e0148001.
44. Kim, C. C.; Nakamura, M. C.; Hsieh, C. L. Brain Trauma Elicits Non-Canonical Macrophage Activation States. *J. Neuroinflammation* **2016**, *13*, 117.
45. Ransohoff, R. M. A Polarizing Question: Do M1 and M2 Microglia Exist? *Nat. Neurosci.* **2016**, *19*, 987–991.
46. Heneka, M. T.; Kummer, M. P.; Latz, E. Innate Immune Activation in Neurodegenerative Disease. *Nat. Rev. Immunol.* **2014**, *14*, 463–477.
47. Sofroniew, M. V.; Vinters, H. V. Astrocytes: Biology and Pathology. *Acta Neuropathol.* **2010**, *119*, 7–35.
48. Farina, C.; Aloisi, F.; Meinl, E. Astrocytes Are Active Players in Cerebral Innate Immunity. *Trends Immunol.* **2007**, *28*, 138–145.
49. Zhang, Y.; Chen, K.; Sloan, S. A.; et al. An RNA-Sequencing Transcriptome and Splicing Database of Glia, Neurons, and Vascular Cells of the Cerebral Cortex. *J. Neurosci.* **2014**, *34*, 11929–11947.
50. McCarthy, G. M.; Bridges, C. R.; Blednov, Y. A.; et al. CNS Cell-Type Localization and LPS Response of TLR Signaling Pathways. *F1000Research* **2017**, *6*, 1144.
51. Johann, S.; Heitzer, M.; Kanagaratnam, M.; et al. NLRP3 Inflammasome Is Expressed by Astrocytes in the SOD1 Mouse Model of ALS and in Human Sporadic ALS Patients. *Glia* **2015**, *63*, 2260–2273.
52. Du, R. H.; Wu, F. F.; Lu, M.; et al. Uncoupling Protein 2 Modulation of the NLRP3 Inflammasome in Astrocytes and Its Implications in Depression. *Redox Biol.* **2016**, *9*, 178–187.
53. Freeman, L.; Guo, H.; David, C. N.; et al. NLR Members NLRC4 and NLRP3 Mediate Sterile Inflammasome Activation in Microglia and Astrocytes. *J. Exp. Med.* **2017**, *214*, 1351–1370.
54. Minkiewicz, J.; de Rivero Vaccari, J. P.; Keane, R. W. Human Astrocytes Express a Novel NLRP2 Inflammasome. *Glia* **2013**, *61*, 1113–1121.
55. Couturier, J.; Stancu, I.-C.; Schakman, O.; et al. Activation of Phagocytic Activity in Astrocytes by Reduced Expression of the Inflammasome Component ASC and Its Implication in a Mouse Model of Alzheimer Disease. *J. Neuroinflammation* **2016**, *13*, 20.
56. Sofroniew, M. V. Astrogliosis. *Cold Spring Harb. Perspect. Biol.* **2014**, *7*, a020420.
57. Zamanian, J. L.; Xu, L.; Foo, L. C.; et al. Genomic Analysis of Reactive Astrogliosis. *J. Neurosci.* **2012**, *32*, 6391–6410.
58. Liddelow, S. A.; Guttenplan, K. A.; Clarke, L. E.; et al. Neurotoxic Reactive Astrocytes Are Induced by Activated Microglia. *Nature* **2017**, *541*, 481–487.
59. Wanner, I. B.; Anderson, M. A.; Song, B.; et al. Glial Scar Borders Are Formed by Newly Proliferated, Elongated Astrocytes That Interact to Corral Inflammatory and Fibrotic Cells via STAT3-Dependent Mechanisms after Spinal Cord Injury. *J. Neurosci.* **2013**, *33*, 12870–12886.
60. Burda, J. E.; Sofroniew, M. V. Reactive Gliosis and the Multicellular Response to CNS Damage and Disease. *Neuron* **2014**, *81*, 229–248.

61. Horng, S.; Therattil, A.; Moyon, S.; et al. Astrocytic Tight Junctions Control Inflammatory CNS Lesion Pathogenesis. *J. Clin. Invest.* **2017**, *127*, 3136–3151.
62. Anderson, M. A.; Burda, J. E.; Ren, Y.; et al. Astrocyte Scar Formation Aids Central Nervous System Axon Regeneration. *Nature* **2016**, *532*, 195–200.
63. Sofroniew, M. V. Astrocyte Barriers to Neurotoxic Inflammation. *Nat. Rev. Neurosci.* **2015**, *16*, 249–263.
64. Dickens, A. M.; Tovar-Y-Romo, L. B.; Yoo, S.-W.; et al. Astrocyte-Shed Extracellular Vesicles Regulate the Peripheral Leukocyte Response to Inflammatory Brain Lesions. *Sci. Signal.* **2017**, *10*, eaai7696.
65. John, G. R.; Lee, S. C.; Song, X.; et al. IL-1-Regulated Responses in Astrocytes: Relevance to Injury and Recovery. *Glia* **2005**, *49*, 161–176.
66. Teh, D. B. L.; Prasad, A.; Jiang, W.; et al. Transcriptome Analysis Reveals Neuroprotective Aspects of Human Reactive Astrocytes Induced by Interleukin 1 β . *Sci. Rep.* **2017**, *7*, 13988.
67. Krasnow, S. M.; Knoll, J. G.; Verghese, S. C.; et al. Amplification and Propagation of Interleukin-1 β Signaling by Murine Brain Endothelial and Glial Cells. *J. Neuroinflammation* **2017**, *14*, 133.
68. Proescholdt, M.; Chakravarty, S.; Foster, J.; et al. Intracerebroventricular but Not Intravenous Interleukin1 β Induces Widespread Vascular-Mediated Leukocyte Infiltration and Immune Signal mRNA Expression Followed by Brain-Wide Glial Activation. *Neuroscience* **2002**, *112*, 731–749.
69. Shaftel, S. S.; Carlson, T. J.; Olschowka, J. A.; et al. Chronic Interleukin-1 β Expression in Mouse Brain Leads to Leukocyte Infiltration and Neutrophil-Independent Blood Brain Barrier Permeability without Overt Neurodegeneration. *J. Neurosci.* **2007**, *27*, 9301–9309.
70. Rivera-Escalera, F.; Matousek, S. B.; Ghosh, S.; et al. Interleukin-1 β Mediated Amyloid Plaque Clearance Is Independent of CCR2 Signaling in the APP/PS1 Mouse Model of Alzheimer's Disease. *Neurobiol. Dis.* **2014**, *69*, 124–133.
71. Stanimirovic, D. B.; Wong, J.; Shapiro, A.; et al. Increase in Surface Expression of ICAM-1, VCAM-1 and E-Selectin in Human Cerebromicrovascular Endothelial Cells Subjected to Ischemia-Like Insults. *Acta Neurochir. Suppl.* **1997**, *70*, 12–16.
72. Bernardes-Silva, M.; Anthony, D. C.; Issekutz, A. C.; et al. Recruitment of Neutrophils across the Blood–Brain Barrier: The Role of E- and P-Selectins. *J. Cereb. Blood Flow Metab.* **2001**, *21*, 1115–1124.
73. Argaw, A. T.; Asp, L.; Zhang, J.; et al. Astrocyte-Derived VEGF-A Drives Blood-Brain Barrier Disruption in CNS Inflammatory Disease. *J. Clin. Invest.* **2012**, *122*, 2454–2468.
74. Ferrari, C. C.; Depino, A. M.; Prada, F.; et al. Reversible Demyelination, Blood-Brain Barrier Breakdown, and Pronounced Neutrophil Recruitment Induced by Chronic IL-1 Expression in the Brain. *Am. J. Pathol.* **2004**, *165*, 1827–1837.
75. Depino, A.; Ferrari, C.; Pott Godoy, M. C.; et al. Differential Effects of Interleukin-1 β on Neurotoxicity, Cytokine Induction and Glial Reaction in Specific Brain Regions. *J. Neuroimmunol.* **2005**, *168*, 96–110.
76. Kim, J. Y.; Park, J.; Chang, J. Y.; et al. Inflammation after Ischemic Stroke: The Role of Leukocytes and Glial Cells. *Exp. Neurobiol.* **2016**, *25*, 241–251.
77. Allen, C.; Thornton, P.; Denes, A.; et al. Neutrophil Cerebrovascular Transmigration Triggers Rapid Neurotoxicity through Release of Proteases Associated with Decondensed DNA. *J. Immunol.* **2012**, *189*, 381–392.
78. Zenaro, E.; Pietronigro, E.; Della Bianca, V.; et al. Neutrophils Promote Alzheimer's Disease-Like Pathology and Cognitive Decline via LFA-1 Integrin. *Nat. Med.* **2015**, *21*, 880–886.
79. Baik, S. H.; Cha, M. Y.; Hyun, Y. M.; et al. Migration of Neutrophils Targeting Amyloid Plaques in Alzheimer's Disease Mouse Model. *Neurobiol. Aging* **2014**, *35*, 1286–1292.
80. Baecher-Allan, C.; Kaskow, B. J.; Weiner, H. L. Multiple Sclerosis: Mechanisms and Immunotherapy. *Neuron* **2018**, *97*, 742–768.
81. Fabene, P. F.; Navarro Mora, G.; Martinello, M.; et al. A Role for Leukocyte-Endothelial Adhesion Mechanisms in Epilepsy. *Nat. Med.* **2008**, *14*, 1377–1383.
82. Vemuganti, R.; Dempsey, R. J.; Bowen, K. K. Inhibition of Intercellular Adhesion Molecule-1 Protein Expression by Antisense Oligonucleotides Is Neuroprotective after Transient Middle Cerebral Artery Occlusion in Rat. *Stroke* **2004**, *35*, 179–184.
83. Shultz, S. R.; Bao, F.; Weaver, L. C.; et al. Treatment with an Anti-CD11d Integrin Antibody Reduces Neuroinflammation and Improves Outcome in a Rat Model of Repeated Concussion. *J. Neuroinflammation* **2013**, *10*, 793.
84. Utagawa, A.; Bramlett, H. M.; Daniels, L.; et al. Transient Blockage of the CD11d/CD18 Integrin Reduces Contusion Volume and Macrophage Infiltration after Traumatic Brain Injury in Rats. *Brain Res.* **2008**, *1207*, 155–163.
85. Bao, F.; Shultz, S. R.; Hepburn, J. D.; et al. A CD11d Monoclonal Antibody Treatment Reduces Tissue Injury and Improves Neurological Outcome after Fluid Percussion Brain Injury in Rats. *J. Neurotrauma* **2012**, *29*, 2375–2392.
86. Fogal, B.; Hewett, S. J. Interleukin-1 β : A Bridge between Inflammation and Excitotoxicity? *J. Neurochem.* **2008**, *106*, 1–23.
87. Mason, J. L.; Suzuki, K.; Chaplin, D. D.; et al. Interleukin1 β Promotes Repair of the CNS. *J. Neurosci.* **2001**, *21*, 7046–7052.
88. Vela, J. M.; Molina-Holgado, E.; Arévalo-Martín, Á.; et al. Interleukin-1 Regulates Proliferation and Differentiation of Oligodendrocyte Progenitor Cells. *Mol. Cell. Neurosci.* **2002**, *20*, 489–502.
89. Parish, C. L.; Finkelstein, D. I.; Tripianichkul, W.; et al. The Role of Interleukin-1, Interleukin-6, and Glia in Inducing Growth of Neuronal Terminal Arbors in Mice. *J. Neurosci.* **2002**, *22*, 8034–8041.
90. Curran, B.; O'Connor, J. J. The Pro-Inflammatory Cytokine Interleukin-18 Impairs Long-Term Potentiation and NMDA Receptor-Mediated Transmission in the Rat Hippocampus In Vitro. *Neuroscience* **2001**, *108*, 83–90.
91. Bellinger, F. P.; Madamba, S.; Siggins, G. R. Interleukin 1 β Inhibits Synaptic Strength and Long-Term Potentiation in the Rat CA1 Hippocampus. *Brain Res.* **1993**, *628*, 227–234.
92. del Rey, A.; Balschun, D.; Wetzel, W.; et al. A Cytokine Network Involving Brain-Borne IL-1 β , IL-1 α , IL-18, IL-6, and TNF α Operates during Long-Term

- Potentiation and Learning. *Brain Behav. Immun.* **2013**, *33*, 15–23.
93. Tanaka, S.; Kondo, H.; Kanda, K.; et al. Involvement of Interleukin-1 in Lipopolysaccharide-Induced Microglial Activation and Learning and Memory Deficits. *J. Neurosci. Res.* **2011**, *89*, 506–514.
 94. Tong, L.; Prieto, G. A.; Kramar, E. A.; et al. Brain-Derived Neurotrophic Factor-Dependent Synaptic Plasticity Is Suppressed by Interleukin-1 via p38 Mitogen-Activated Protein Kinase. *J. Neurosci.* **2012**, *32*, 17714–17724.
 95. Prieto, G. A.; Snigdha, S.; Baglietto-Vargas, D.; et al. Synapse-Specific IL-1 Receptor Subunit Reconfiguration Augments Vulnerability to IL-1 β in the Aged Hippocampus. *Proc. Natl. Acad. Sci. U.S.A.* **2015**, *112*, E5078–E5087.
 96. Youm, Y. H.; Grant, R. W.; McCabe, L. R.; et al. Canonical Nlrp3 Inflammasome Links Systemic Low-Grade Inflammation to Functional Decline in Aging. *Cell Metab.* **2013**, *18*, 519–532.
 97. Mawhinney, L. J.; de Vaccari Rivero, J.; Dale, G. A.; et al. Heightened Inflammasome Activation Is Linked to Age-Related Cognitive Impairment in Fischer 344 Rats. *BMC Neurosci.* **2011**, *12*, 123.
 98. Kawasaki, Y.; Zhang, L.; Cheng, J.-K.; et al. Cytokine Mechanisms of Central Sensitization: Distinct and Overlapping Role of Interleukin-1, Interleukin-6, and Tumor Necrosis Factor in Regulating Synaptic and Neuronal Activity in the Superficial Spinal Cord. *J. Neurosci.* **2008**, *28*, 5189–5194.
 99. Clarkson, B. D. S.; Kahoud, R. J.; McCarthy, C. B.; et al. Inflammatory Cytokine-Induced Changes in Neural Network Activity Measured by Waveform Analysis of High-Content Calcium Imaging in Murine Cortical Neurons. *Sci. Rep.* **2017**, *7*, 9037.
 100. Wang, S.; Cheng, Q.; Malik, S.; et al. Interleukin-1 β Inhibits Gamma-Aminobutyric Acid Type A (GABA(A)) Receptor Current in Cultured Hippocampal Neurons. *J. Pharmacol. Exp. Ther.* **2000**, *292*, 497–504.
 101. Rossi, S.; Studer, V.; Motta, C.; et al. Inflammation Inhibits GABA Transmission in Multiple Sclerosis. *Mult. Scler. J.* **2012**, *18*, 1633–1635.
 102. Zhu, G.; Okada, M.; Yoshida, S.; et al. Effects of Interleukin-1 β on Hippocampal Glutamate and GABA Releases Associated with Ca²⁺-Induced Ca²⁺-Releasing Systems. *Epilepsy Res.* **2006**, *71*, 107–116.
 103. Viviani, B.; Bartesaghi, S.; Gardoni, F.; et al. Interleukin1 β Enhances NMDA Receptor-Mediated Intracellular Calcium Increase through Activation of the Src Family of Kinases. *J. Neurosci.* **2003**, *23*, 8692–8700.
 104. Liu, T.; Jiang, C.-Y.; Fujita, T.; et al. Enhancement by Interleukin-1 β of AMPA and NMDA Receptor-Mediated Currents in Adult Rat Spinal Superficial Dorsal Horn Neurons. *Mol. Pain* **2013**, *9*, 16.
 105. Chao, C. C.; Hu, S. X.; Ehrlich, L.; et al. Interleukin-1 and Tumor Necrosis Factor- α Synergistically Mediate Neurotoxicity: Involvement of Nitric Oxide and of N-Methyl-D-Aspartate Receptors. *Brain Behav. Immun.* **1995**, *9*, 355–365.
 106. Fogal, B.; Li, J.; Lobner, D.; et al. System Xc Activity and Astrocytes Are Necessary for Interleukin-1 β -Mediated Hypoxic Neuronal Injury. *J. Neurosci.* **2007**, *27*, 10094–10105.
 107. Riazi, K.; Galic, M. A.; Pittman, Q. J. Contributions of Peripheral Inflammation to Seizure Susceptibility: Cytokines and Brain Excitability. *Epilepsy Res.* **2010**, *89*, 34–42.
 108. Webster, K. M.; Sun, M.; Crack, P.; et al. Inflammation in Epileptogenesis after Traumatic Brain Injury. *J. Neuroinflammation* **2017**, *14*, 10.
 109. Bading, H. Therapeutic Targeting of the Pathological Triad of Extrasynaptic NMDA Receptor Signaling in Neurodegenerations. *J. Exp. Med.* **2017**, *214*, 569–578.
 110. Braak, H.; Braak, E. Neuropathological Stageing of Alzheimer-Related Changes. *Acta Neuropathol.* **1991**, *82*, 239–259.
 111. Kosik, K. S.; Joachim, C. L.; Selkoe, D. J. Microtubule-Associated Protein Tau (Tau) Is a Major Antigenic Component of Paired Helical Filaments in Alzheimer Disease. *Proc. Natl. Acad. Sci. U.S.A.* **1986**, *83*, 4044–4048.
 112. Selkoe, D. J. The Cell Biology of Beta-Amyloid Precursor Protein and Presenilin in Alzheimer's Disease. *Trends Cell Biol.* **1998**, *8*, 447–453.
 113. Mori, H.; Takio, K.; Ogawara, M.; et al. Mass Spectrometry of Purified Amyloid Beta Protein in Alzheimer's Disease. *J. Biol. Chem.* **1992**, *267*, 17082–17086.
 114. Burdick, D.; Soreghan, B.; Kwon, M.; et al. Assembly and Aggregation Properties of Synthetic Alzheimer's A β Amyloid Peptide Analogs. *J. Biol. Chem.* **1992**, *267*, 546–554.
 115. Miller, D. L.; Papayannopoulos, I. A.; Styles, J.; et al. Peptide Compositions of the Cerebrovascular and Senile Plaque Core Amyloid Deposits of Alzheimer's Disease. *Arch. Biochem. Biophys.* **1993**, *301*, 41–52.
 116. Roher, A. E.; Lowenson, J. D.; Clarke, S.; et al. BetaAmyloid-(1-42) Is a Major Component of Cerebrovascular Amyloid Deposits: Implications for the Pathology of Alzheimer Disease. *Proc. Natl. Acad. Sci. U.S.A.* **1993**, *90*, 10836–10840.
 117. Dahlgren, K. N.; Manelli, A. M.; Blaine Stine, W.; et al. Oligomeric and Fibrillar Species of Amyloid- β Peptides Differentially Affect Neuronal Viability. *J. Biol. Chem.* **2002**, *277*, 32046–32053.
 118. Heneka, M. T.; Kummer, M. P.; Stutz, A.; et al. NLRP3 Is Activated in Alzheimer's Disease and Contributes to Pathology in APP/PS1 Mice. *Nature* **2013**, *493*, 674–678.
 119. Tan, M. S.; Tan, L.; Jiang, T.; et al. Amyloid- β Induces NLRP1-Dependent Neuronal Pyroptosis in Models of Alzheimer's Disease. *Cell Death Dis.* **2014**, *5*, e1382.
 120. Liu, L.; Chan, C. IPAF Inflammasome Is Involved in Interleukin-1 β Production from Astrocytes, Induced by Palmitate; Implications for Alzheimer's Disease. *Neurobiol. Aging* **2014**, *35*, 309–321.
 121. Venegas, C.; Kumar, S.; Franklin, B. S.; et al. Microglia-Derived ASC Specks Crossseed Amyloid- β in Alzheimer's Disease. *Nature* **2017**, *552*, 355–361.
 122. Lambert, J.-C.; Heath, S.; Even, G.; et al. Genome-Wide Association Study Identifies Variants at CLU and CR1 Associated with Alzheimer's Disease. *Nat. Genet.* **2009**, *41*, 1094–1099.
 123. Crehan, H.; Hardy, J.; Pocock, J. Blockage of CR1 Prevents Activation of Rodent Microglia. *Neurobiol. Dis.* **2013**, *54*, 139–149.

124. Guerreiro, R.; Wojtas, A.; Bras, J.; et al. TREM2 Variants in Alzheimer's Disease. *N. Engl. J. Med.* **2013**, *368*, 117–127.
125. Lambert, J. C.; Ibrahim-Verbaas, C. A.; Harold, D.; et al. Meta-Analysis of 74,046 Individuals Identifies 11 New Susceptibility Loci for Alzheimer's Disease. *Nat. Genet.* **2013**, *45*, 1452–1458.
126. Lechler, R. I.; Bal, V.; Rothbard, J. B.; et al. Structural and Functional Studies of HLA-DR Restricted Antigen Recognition by Human Helper T Lymphocyte Clones by Using Transfected Murine Cell Lines. *J. Immunol.* **1988**, *141*, 3003–3009.
127. McGeer, P. L.; Itagaki, S.; Boyes, B. E.; et al. Reactive Microglia Are Positive for HLA-DR in the Substantia Nigra of Parkinson's and Alzheimer's Disease Brains. *Neurology* **1988**, *38*, 1285–1291.
128. Itagaki, S.; McGeer, P. L.; Akiyama, H.; et al. Relationship of Microglia and Astrocytes to Amyloid Deposits of Alzheimer Disease. *J. Neuroimmunol.* **1989**, *24*, 173–182.
129. Meyer-Luehmann, M.; Spire-Jones, T. L.; Prada, C.; et al. Rapid Appearance and Local Toxicity of Amyloid- β Plaques in a Mouse Model of Alzheimer's Disease. *Nature* **2008**, *451*, 720–724.
130. Van Eldik, L. J.; Griffin, W. S. T. S100 β Expression in Alzheimer's Disease: Relation to Neuropathology in Brain Regions. *BBA Mol. Cell Res.* **1994**, *1223*, 398–403.
131. Sheng, J. G.; Ito, K.; Skinner, R. D.; et al. In Vivo and In Vitro Evidence Supporting a Role for the Inflammatory Cytokine Interleukin-1 as a Driving Force in Alzheimer Pathogenesis. *Neurobiol. Aging* **1996**, *17*, 761–766.
132. Goldgaber, D.; Harris, H. W.; Hla, T.; et al. Interleukin 1 Regulates Synthesis of Amyloid Beta-Protein Precursor mRNA in Human Endothelial Cells. *Proc. Natl. Acad. Sci. U.S.A.* **1989**, *86*, 7606–7610.
133. Rogers, J. T.; Leiter, L. M.; McPhee, J.; et al. Translation of the Alzheimer Amyloid Precursor Protein mRNA Is Up-Regulated by Interleukin-1 through 5'-Untranslated Region Sequences. *J. Biol. Chem.* **1999**, *274*, 6421–6431.
134. Forloni, G.; Demicheli, F.; Giorgi, S.; et al. Expression of Amyloid Precursor Protein mRNAs in Endothelial, Neuronal and Glial Cells: Modulation by Interleukin-1. *Brain Res. Mol. Brain Res.* **1992**, *16*, 128–134.
135. Sheng, J. G.; Zhu, S. G.; Jones, R. A.; et al. Interleukin-1 Promotes Expression and Phosphorylation of Neurofilament and Tau Proteins In Vivo. *Exp. Neurol.* **2000**, *163*, 388–391.
136. Griffin, W. S. T.; Liu, L.; Li, Y.; et al. Interleukin-1 Mediates Alzheimer and Lewy Body Pathologies. *J. Neuroinflammation* **2006**, *3*, 5.
137. Ojala, J. O.; Sutinen, E. M.; Salminen, A.; et al. Interleukin-18 Increases Expression of Kinases Involved in Tau Phosphorylation in SH-SY5Y Neuroblastoma Cells. *J. Neuroimmunol.* **2008**, *205*, 86–93.
138. Kitazawa, M.; Cheng, D.; Tsukamoto, M. R.; et al. Blocking IL-1 Signaling Rescues Cognition, Attenuates Tau Pathology, and Restores Neuronal β -Catenin Pathway Function in an Alzheimer's Disease Model. *J. Immunol.* **2011**, *187*, 6539–6549.
139. El Khoury, J. B.; Moore, K. J.; Means, T. K.; et al. CD36 Mediates the Innate Host Response to β -Amyloid. *J. Exp. Med.* **2003**, *197*, 1657–1666.
140. Griffin, W. S.; Stanley, L. C.; Ling, C.; et al. Brain Interleukin 1 and S-100 Immunoreactivity Are Elevated in Down Syndrome and Alzheimer Disease. *Proc. Natl. Acad. Sci. U.S.A.* **1989**, *86*, 7611–7615.
141. Kummer, J. A.; Broekhuizen, R.; Everett, H.; et al. Inflammasome Components NALP 1 and 3 Show Distinct but Separate Expression Profiles in Human Tissues Suggesting a Site-Specific Role in the Inflammatory Response. *J. Histochem. Cytochem.* **2007**, *55*, 443–452.
142. Di Paolo, G.; Kim, T.-W. Linking Lipids to Alzheimer's Disease: Cholesterol and Beyond. *Nat. Rev. Neurosci.* **2011**, *12*, 284–296.
143. Ousman, S. S.; David, S. Lysophosphatidylcholine Induces Rapid Recruitment and Activation of Macrophages in the Adult Mouse Spinal Cord. *Glia* **2000**, *30*, 92–104.
144. Lauber, K.; Bohn, E.; Kröber, S. M.; et al. Apoptotic Cells Induce Migration of Phagocytes via Caspase-3-Mediated Release of a Lipid Attraction Signal. *Cell* **2003**, *113*, 717–730.
145. Sheikh, A. M.; Nagai, A. Lysophosphatidylcholine Modulates Fibril Formation of Amyloid Beta Peptide. *FEBS J.* **2011**, *278*, 634–642.
146. Sheikh, A. M.; Michikawa, M.; Kim, S. U.; et al. Lysophosphatidylcholine Increases the Neurotoxicity of Alzheimer's Amyloid β 1–42 Peptide: Role of Oligomer Formation. *Neuroscience* **2015**, *292*, 159–169.
147. Stock, C.; Schilling, T.; Schwab, A.; et al. Lysophosphatidylcholine Stimulates IL-1 β Release from Microglia via a P2X7 Receptor-Independent Mechanism. *J. Immunol.* **2006**, *177*, 8560–8568.
148. Stephenson, D.; Rash, K.; Smalstig, B.; et al. Cytosolic Phospholipase A2 Is Induced in Reactive Glia Following Different Forms of Neurodegeneration. *Glia* **1999**, *27*, 110–128.
149. Colangelo, V.; Schurr, J.; Ball, M. J.; et al. Gene Expression Profiling of 12633 Genes in Alzheimer Hippocampal CA1: Transcription and Neurotrophic Factor Down-Regulation and Up-Regulation of Apoptotic and Pro-Inflammatory Signaling. *J. Neurosci. Res.* **2002**, *70*, 462–473.
150. Farooqui, A. A. Inhibitors of Brain Phospholipase A2 Activity: Their Neuropharmacological Effects and Therapeutic Importance for the Treatment of Neurologic Disorders. *Pharmacol. Rev.* **2006**, *58*, 591–620.
151. Sanchez-Mejia, R. O.; Newman, J. W.; Toh, S.; et al. Phospholipase A2 Reduction Ameliorates Cognitive Deficits in a Mouse Model of Alzheimer's Disease. *Nat. Neurosci.* **2008**, *11*, 1311–1318.
152. Damier, P.; Hirsch, E. C.; Agid, Y.; et al. The Substantia Nigra of the Human Brain: II. Patterns of Loss of Dopamine-Containing Neurons in Parkinson's Disease. *Brain* **1999**, *122*, 1437–1448.
153. Postuma, R. B.; Berg, D.; Stern, M.; et al. MDS Clinical Diagnostic Criteria for Parkinson's Disease. *Mov. Disord.* **2015**, *30*, 1591–1601.
154. Serpell, L. C.; Berriman, J.; Jakes, R.; et al. Fiber Diffraction of Synthetic Alpha-Synuclein Filaments Shows Amyloid-Like Cross-Beta Conformation. *Proc. Natl. Acad. Sci. U.S.A.* **2000**, *97*, 4897–4902.
155. Goedert, M. Alpha-Synuclein and Neurodegenerative Diseases. *Nat. Rev. Neurosci.* **2001**, *2*, 492–501.

156. Spillantini, M. G.; Schmidt, M. L.; Lee, V. M.-Y.; et al. Alpha-Synuclein in Lewy Bodies. *Nature* **1997**, *388*, 839–840.
157. Polymeropoulos, M. H.; Lavedan, C.; Leroy, E.; et al. Mutation in the α -Synuclein Gene Identified in Families with Parkinson's Disease. *Science* **1997**, *276*, 2045–2047.
158. Hamza, T. H.; Zabetian, C. P.; Tenesa, A.; et al. Common Genetic Variation in the HLA Region Is Associated with Late-Onset Sporadic Parkinson's Disease. *Nat. Genet.* **2010**, *42*, 781–785.
159. Nalls, M. A.; Plagnol, V.; Hernandez, D. G.; et al. Imputation of Sequence Variants for Identification of Genetic Risks for Parkinson's Disease: A Meta-Analysis of Genome-Wide Association Studies. *Lancet* **2011**, *377*, 641–649.
160. Orr, C. F.; Rowe, D. B.; Mizuno, Y.; et al. A Possible Role for Humoral Immunity in the Pathogenesis of Parkinson's Disease. *Brain* **2005**, *128*, 2665–2674.
161. Mogi, M.; Harada, M.; Kondo, T.; et al. Interleukin-1 β , Interleukin-6, Epidermal Growth Factor and Transforming Growth Factor- α Are Elevated in the Brain from Parkinsonian Patients. *Neurosci. Lett.* **1994**, *180*, 147–150.
162. Schulte, T.; Schöls, L.; Müller, T.; et al. Polymorphisms in the Interleukin-1 Alpha and Beta Genes and the Risk for Parkinson's Disease. *Neurosci. Lett.* **2002**, *326*, 70–72.
163. Wahner, A. D.; Sinsheimer, J. S.; Bronstein, J. M.; et al. Inflammatory Cytokine Gene Polymorphisms and Increased Risk of Parkinson Disease. *Arch. Neurol.* **2007**, *64*, 836–840.
164. Freeman, D.; Cedillos, R.; Choyke, S.; et al. Alpha-Synuclein Induces Lysosomal Rupture and Cathepsin Dependent Reactive Oxygen Species Following Endocytosis. *PLoS One* **2013**, *8*, e62143.
165. Yan, Y.; Jiang, W.; Liu, L.; et al. Dopamine Controls Systemic Inflammation through Inhibition of NLRP3 Inflammasome. *Cell* **2015**, *160*, 62–73.
166. Meredith, E. J.; Chamba, A.; Holder, M. J.; et al. Close Encounters of the Monoamine Kind: Immune Cells Betray Their Nervous Disposition. *Immunology* **2005**, *115*, 289–295.
167. Wang, W.; Nguyen, L. T. T.; Burlak, C.; et al. Caspase-1 Causes Truncation and Aggregation of the Parkinson's Disease-Associated Protein α -Synuclein. *Proc. Natl. Acad. Sci. U.S.A.* **2016**, *113*, 9587–9592.
168. Li, W.; West, N.; Colla, E.; et al. Aggregation Promoting C-Terminal Truncation of Alpha-Synuclein Is a Normal Cellular Process and Is Enhanced by the Familial Parkinson's Disease-Linked Mutations. *Proc. Natl. Acad. Sci. U.S.A.* **2005**, *102*, 2162–2167.
169. Periquet, M.; Fulga, T.; Myllykangas, L.; et al. Aggregated α -Synuclein Mediates Dopaminergic Neurotoxicity In Vivo. *J. Neurosci.* **2007**, *27*, 3338–3346.
170. Prasad, K.; Beach, T. G.; Hedreen, J.; et al. Critical Role of Truncated α -Synuclein and Aggregates in Parkinson's Disease and Incidental Lewy Body Disease. *Brain Pathol.* **2012**, *22*, 811–825.
171. Bassil, F.; Fernagut, P.-O.; Bezard, E.; et al. Reducing C-Terminal Truncation Mitigates Synucleinopathy and Neurodegeneration in a Transgenic Model of Multiple System Atrophy. *Proc. Natl. Acad. Sci. U.S.A.* **2016**, *113*, 9593–9598.
172. Lassmann, H. The Pathology of Multiple Sclerosis and Its Evolution. *Philos. Trans. R. Soc. B Biol. Sci.* **1999**, *354*, 1635–1640.
173. Compston, A.; Coles, A. Multiple Sclerosis. *Lancet* **2008**, *372*, 1502–1517.
174. Shaw, P. J.; Smith, N. M.; Ince, P. G.; et al. Chronic Periphlebitis Retinae in Multiple Sclerosis. A Histopathological Study. *J. Neurol. Sci.* **1987**, *77*, 147–152.
175. Constantinescu, C. S.; Farooqi, N.; O'Brien, K.; et al. Experimental Autoimmune Encephalomyelitis (EAE) as a Model for Multiple Sclerosis (MS). *Br. J. Pharmacol.* **2011**, *164*, 1079–1106.
176. Fletcher, J. M.; Lalor, S. J.; Sweeney, C. M.; et al. T Cells in Multiple Sclerosis and Experimental Autoimmune Encephalomyelitis. *Clin. Exp. Immunol.* **2010**, *162*, 1–11.
177. O'Connor, R. A.; Prendergast, C. T.; Sabatos, C. A.; et al. Cutting Edge: Th1 Cells Facilitate the Entry of Th17 Cells to the Central Nervous System during Experimental Autoimmune Encephalomyelitis. *J. Immunol.* **2008**, *181*, 3750–3754.
178. Ito, A.; Matejuk, A.; Hopke, C.; et al. Transfer of Severe Experimental Autoimmune Encephalomyelitis by IL-12- and IL-18-Potentiated T Cells Is Estrogen Sensitive. *J. Immunol.* **2003**, *170*, 4802–4809.
179. Langrish, C. L.; Chen, Y.; Blumenschein, W. M.; et al. IL-23 Drives a Pathogenic T Cell Population That Induces Autoimmune Inflammation. *J. Exp. Med.* **2005**, *201*, 233–240.
180. Rao, D. A.; Tracey, K. J.; Pober, J. S. IL-1 and IL-1 Are Endogenous Mediators Linking Cell Injury to the Adaptive Alloimmune Response. *J. Immunol.* **2007**, *179*, 6536–6546.
181. Ben-Sasson, S. Z.; Hu-Li, J.; Quiel, J.; et al. IL-1 Acts Directly on CD4 T Cells to Enhance Their Antigen-Driven Expansion and Differentiation. *Proc. Natl. Acad. Sci. U.S.A.* **2009**, *106*, 7119–7124.
182. Brosnan, C. F.; Cannella, B.; Battistini, L.; et al. Cytokine Localization in Multiple Sclerosis Lesions: Correlation with Adhesion Molecule Expression and Reactive Nitrogen Species. *Neurology* **1995**, *45*, S16–S21.
183. Prins, M.; Eriksson, C.; Wierinckx, A.; et al. Interleukin1 β and Interleukin-1 Receptor Antagonist Appear in Grey Matter Additionally to White Matter Lesions during Experimental Multiple Sclerosis. *PLoS One* **2013**, *8*, e83835.
184. Gris, D.; Ye, Z.; Iocca, H. A.; et al. NLRP3 Plays a Critical Role in the Development of Experimental Autoimmune Encephalomyelitis by Mediating Th1 and Th17 Responses. *J. Immunol.* **2010**, *185*, 974–981.
185. Furlan, R.; Martino, G.; Galbiati, F.; et al. Caspase-1 Regulates the Inflammatory Process Leading to Autoimmune Demyelination. *J. Immunol.* **1999**, *163*, 2403–2409.
186. Shaw, P. J.; Lukens, J. R.; Burns, S.; et al. Cutting Edge: Critical Role for PYCARD/ASC in the Development of Experimental Autoimmune Encephalomyelitis. *J. Immunol.* **2010**, *184*, 4610–4614.
187. Matsuki, T.; Nakae, S.; Sudo, K.; et al. Abnormal T Cell Activation Caused by the Imbalance of the IL-1/IL-1R Antagonist System Is Responsible for the Development of Experimental Autoimmune Encephalomyelitis. *Int. Immunol.* **2006**, *18*, 399–407.

188. Inoue, M.; Williams, K. L.; Gunn, M. D.; et al. NLRP3 Inflammasome Induces Chemotactic Immune Cell Migration to the CNS in Experimental Autoimmune Encephalomyelitis. *Proc. Natl. Acad. Sci. U.S.A.* **2012**, *109*, 10480–10485.
189. Inoue, M.; Williams, K. L.; Oliver, T.; et al. Interferon Therapy Against EAE Is Effective Only When Development of the Disease Depends on the NLRP3 Inflammasome. *Sci. Signal.* **2012**, *5*, ra38.
190. Inoue, M.; Shinohara, M. L. NLRP3 Inflammasome and MS/EAE. *Autoimmune Dis.* **2013**, *2013*, 859145.
191. Inoue, M.; Chen, P. H.; Siecinski, S.; et al. An Interferon- β Resistant and NLRP3 Inflammasome-Independent Subtype of EAE with Neuronal Damage. *Nat. Neurosci.* **2016**, *19*, 1599–1609.
192. Malhotra, S.; Río, J.; Urcelay, E.; et al. NLRP3 Inflammasome Is Associated with the Response to IFN- β in Patients with Multiple Sclerosis. *Brain* **2015**, *138*, 644–652.
193. Hiremath, M. M.; Saito, Y.; Knapp, G. W.; et al. Microglial/Macrophage Accumulation during Cuprizone-Induced Demyelination in C57BL/6 Mice. *J. Neuroimmunol.* **1998**, *92*, 38–49.
194. Kalyvas, A.; David, S. Cytosolic Phospholipase A2 Plays a Key Role in the Pathogenesis of Multiple Sclerosis-Like Disease. *Neuron* **2004**, *41*, 323–335.
195. Kabashi, E.; Valdmanis, P. N.; Dion, P.; et al. TARDBP Mutations in Individuals with Sporadic and Familial Amyotrophic Lateral Sclerosis. *Nat. Genet.* **2008**, *40*, 572–574.
196. Blair, I. P.; Williams, K. L.; Warraich, S. T.; et al. FUS Mutations in Amyotrophic Lateral Sclerosis: Clinical, Pathological, Neurophysiological and Genetic Analysis. *J. Neurol. Neurosurg. Psychiatry* **2010**, *81*, 639–645.
197. Renton, A. E.; Majounie, E.; Waite, A.; et al. A Hexanucleotide Repeat Expansion in C9ORF72 Is the Cause of Chromosome 9p21-Linked ALS-FTD. *Neuron* **2011**, *72*, 257–268.
198. DeJesus-Hernandez, M.; Mackenzie, I. R.; Boeve, B. F.; et al. Expanded GGGGCC Hexanucleotide Repeat in Noncoding Region of C9ORF72 Causes Chromosome 9p-Linked FTD and ALS. *Neuron* **2011**, *72*, 245–256.
199. Robberecht, W.; Philips, T. The Changing Scene of Amyotrophic Lateral Sclerosis. *Nat. Rev. Neurosci.* **2013**, *14*, 248–264.
200. van Es, M. A.; Hardiman, O.; Chio, A.; et al. Amyotrophic Lateral Sclerosis. *Lancet* **2017**, *390*, 2084–2098.
201. Hardiman, O.; Al-Chalabi, A.; Chio, A.; et al. Amyotrophic Lateral Sclerosis. *Nat. Rev. Dis. Prim.* **2017**, *3*, 17071.
202. Blokhuis, A. M.; Groen, E. J. N.; Koppers, M.; et al. Protein Aggregation in Amyotrophic Lateral Sclerosis. *Acta Neuropathol.* **2013**, *125*, 777–794.
203. Alshikho, M. J.; Zürcher, N. R.; Loggia, M. L.; et al. Glial Activation Colocalizes with Structural Abnormalities in Amyotrophic Lateral Sclerosis. *Neurology* **2016**, *87*, 2554–2561.
204. Zürcher, N. R.; Loggia, M. L.; Lawson, R.; et al. Increased In Vivo Glial Activation in Patients with Amyotrophic Lateral Sclerosis: Assessed with [(11)C]-PBR28. *Neuroimage. Clin.* **2015**, *7*, 409–414.
205. Turner, M.; Cagnin, A.; Turkheimer, F.; et al. Evidence of Widespread Cerebral Microglial Activation in Amyotrophic Lateral Sclerosis: An [(11)C](R)-PK11195 Positron Emission Tomography Study. *Neurobiol. Dis.* **2004**, *15*, 601–609.
206. Liao, B.; Zhao, W.; Beers, D. R.; et al. Transformation from a Neuroprotective to a Neurotoxic Microglial Phenotype in a Mouse Model of ALS. *Exp. Neurol.* **2012**, *237*, 147–152.
207. Cunha, C.; Santos, C.; Gomes, C.; et al. Downregulated Glia Interplay and Increased miRNA-155 as Promising Markers to Track ALS at an Early Stage. *Mol. Neurobiol.* **2018**, *55*, 4207–4224.
208. Apolloni, S.; Amadio, S.; Parisi, C.; et al. Spinal Cord Pathology Is Ameliorated by P2X7 Antagonism in a SOD1 Mutant Mouse Model of Amyotrophic Lateral Sclerosis. *Dis. Model. Mech.* **2014**, *7*, 1101–1109.
209. Zhao, W.; Beers, D. R.; Bell, S.; et al. TDP-43 Activates Microglia through NF- κ B and NLRP3 Inflammasome. *Exp. Neurol.* **2015**, *273*, 24–35.
210. Leal-Lasarte, M. M.; Franco, J. M.; Labrador-Garrido, A.; et al. Extracellular TDP-43 Aggregates Target MAPK/MAK/ MRK Overlapping Kinase (MOK) and Trigger Caspase-3/ IL-18 Signaling in Microglia. *FASEB J.* **2017**, *31*, 2797–2816.
211. Pasinelli, P.; Houseweart, M. K.; Brown, R. H.; et al. Caspase-1 and -3 Are Sequentially Activated in Motor Neuron Death in Cu,Zn Superoxide Dismutase-Mediated Familial Amyotrophic Lateral Sclerosis. *Proc. Natl. Acad. Sci. U.S.A.* **2000**, *97*, 13901–13906.
212. Heitzer, M.; Kaiser, S.; Kanagaratnam, M.; et al. Administration of 17 β -Estradiol Improves Motoneuron Survival and Down-Regulates Inflammasome Activation in Male SOD1(G93A) ALS Mice. *Mol. Neurobiol.* **2017**, *54*, 8429–8443.
213. Slowik, A.; Beyer, C. Inflammasomes Are Neuroprotective Targets for Sex Steroids. *J. Steroid Biochem. Mol. Biol.* **2015**, *153*, 135–143.
214. Maier, A.; Deigendesch, N.; Müller, K.; et al. Interleukin-1 Antagonist Anakinra in Amyotrophic Lateral Sclerosis—A Pilot Study. *PLoS One* **2015**, *10*, e0139684.
215. Corbyn, Z. Stroke—Statistics: A Growing Global Burden. *Nature* **2014**, *510*, S2–S3.
216. Rock, K. L.; Kono, H. The Inflammatory Response to Cell Death. *Annu. Rev. Pathol. Mech. Dis.* **2008**, *3*, 99–126.
217. Gelderblom, M.; Leyboldt, F.; Steinbach, K.; et al. Temporal and Spatial Dynamics of Cerebral Immune Cell Accumulation in Stroke. *Stroke* **2009**, *40*, 1849–1857.
218. Chen, G. Y.; Nuñez, G. Sterile Inflammation: Sensing and Reacting to Damage. *Nat. Rev. Immunol.* **2010**, *10*, 826–837.
219. Gauberti, M.; Montagne, A.; Marcos-Contreras, O. A.; et al. Ultra-Sensitive Molecular MRI of Vascular Cell Adhesion Molecule-1 Reveals a Dynamic Inflammatory Penumbra after Strokes. *Stroke* **2013**, *44*, 1988–1996.
220. Amantea, D.; Nappi, G.; Bernardi, G.; et al. Post-Ischemic Brain Damage: Pathophysiology and Role of Inflammatory Mediators. *FEBS J.* **2009**, *276*, 13–26.
221. Amantea, D.; Bagetta, G.; Tassorelli, C.; et al. Identification of Distinct Cellular Pools of Interleukin-1 β during the Evolution of the Neuroinflammatory Response Induced by Transient Middle Cerebral Artery Occlusion in the Brain of Rat. *Brain Res.* **2010**, *1313*, 259–269.

222. Boutin, H.; LeFeuvre, R. A.; Horai, R.; et al. Role of IL-1 α and IL-1 β in Ischemic Brain Damage. *J. Neurosci.* **2001**, *21*, 5528–5534.
223. Touzani, O.; Boutin, H.; LeFeuvre, R.; et al. Interleukin-1 Influences Ischemic Brain Damage in the Mouse Independently of the Interleukin-1 Type I Receptor. *J. Neurosci.* **2002**, *22*, 38–43.
224. Yamasaki, Y.; Matsuura, N.; Shozuhara, H.; et al. Interleukin-1 as a Pathogenetic Mediator of Ischemic Brain Damage in Rats. *Stroke* **1995**, *26*, 676–681.
225. Relton, J. K.; Rothwell, N. J. Interleukin-1 Receptor Antagonist Inhibits Ischaemic and Excitotoxic Neuronal Damage in the Rat. *Brain Res. Bull.* **1992**, *29*, 243–246.
226. Greenhalgh, A. D.; Brough, D.; Robinson, E. M.; et al. Interleukin-1 Receptor Antagonist Is Beneficial after Subarachnoid Haemorrhage in Rat by Blocking HaemDriven Inflammatory Pathology. *Dis. Model. Mech.* **2012**, *5*, 823–833.
227. Emsley, H. C. A. A Randomised Phase II Study of Interleukin-1 Receptor Antagonist in Acute Stroke Patients. *J. Neurol. Neurosurg. Psychiatry* **2005**, *76*, 1366–1372.
228. Singh, N.; Hopkins, S. J.; Hulme, S.; et al. The Effect of Intravenous Interleukin-1 Receptor Antagonist on Inflammatory Mediators in Cerebrospinal Fluid after Subarachnoid Haemorrhage: A Phase II Randomised Controlled Trial. *J. Neuroinflammation* **2014**, *11*, 1.
229. McCann, S. K.; Cramond, F.; Macleod, M. R.; et al. Systematic Review and Meta-Analysis of the Efficacy of Interleukin-1 Receptor Antagonist in Animal Models of Stroke: An Update. *Transl. Stroke Res.* **2016**, *7*, 395–406.
230. Fann, D. Y.-W.; Lee, S. Y.; Manzanero, S.; et al. Intravenous Immunoglobulin Suppresses NLRP1 and NLRP3 Inflammasome-Mediated Neuronal Death in Ischemic Stroke. *Cell Death Dis.* **2013**, *4*, e790.
231. Fann, D. Y.-W.; Santro, T.; Manzanero, S.; et al. Intermittent Fasting Attenuates Inflammasome Activity in Ischemic Stroke. *Exp. Neurol.* **2014**, *257*, 114–119.
232. Zhang, N.; Zhang, X.; Liu, X.; et al. Chrysophanol Inhibits nalp3 Inflammasome Activation and Ameliorates Cerebral Ischemia/Reperfusion in Mice. *Mediators Inflamm.* **2014**, *2014*, 370530.
233. Yang, F.; Wang, Z.; Wei, X.; et al. NLRP3 Deficiency Ameliorates Neurovascular Damage in Experimental Ischemic Stroke. *J. Cereb. Blood Flow Metab.* **2014**, *34*, 660–667.
234. Ma, Q.; Chen, S.; Hu, Q.; et al. NLRP3 Inflammasome Contributes to Inflammation after Intracerebral Hemorrhage. *Ann. Neurol.* **2014**, *75*, 209–219.
235. Wang, X.; Li, R.; Wang, X.; et al. Umbelliferone Ameliorates Cerebral Ischemia–Reperfusion Injury via Upregulating the PPAR Gamma Expression and Suppressing TXNIP/NLRP3 Inflammasome. *Neurosci. Lett.* **2015**, *600*, 182–187.
236. Lammerding, L.; Slowik, A.; Johann, S.; et al. Poststroke Inflammasome Expression and Regulation in the Peri-Infarct Area by Gonadal Steroids after Transient Focal Ischemia in the Rat Brain. *Neuroendocrinology* **2016**, *103*, 460–475.
237. Denes, A.; Coutts, G.; Lénárt, N.; et al. AIM2 and NLRC4 Inflammasomes Contribute with ASC to Acute Brain Injury Independently of NLRP3. *Proc. Natl. Acad. Sci. U.S.A.* **2015**, *112*, 4050–4055.
238. Abulafia, D. P.; de Rivero Vaccari, J. P.; Lozano, J. D.; et al. Inhibition of the Inflammasome Complex Reduces the Inflammatory Response after Thromboembolic Stroke in Mice. *J. Cereb. Blood Flow Metab.* **2009**, *29*, 534–544.
239. Lok, J.; Leung, W.; Murphy, S.; et al. Intracranial Hemorrhage: Mechanisms of Secondary Brain Injury. *Acta Neurochir. Suppl.* **2011**, *111*, 63–69.
240. Dutra, F. F.; Alves, L. S.; Rodrigues, D.; et al. Hemolysis-Induced Lethality Involves Inflammasome Activation by Heme. *Proc. Natl. Acad. Sci. U.S.A.* **2014**, *111*, E4110–E4118.
241. Dorsett, C. R.; McGuire, J. L.; DePasquale, E. A. K.; et al. Glutamate Neurotransmission in Rodent Models of Traumatic Brain Injury. *J. Neurotrauma* **2017**, *34*, 263–272.
242. Simon, D. W.; McGeachy, M. J.; Bayir, H.; et al. The FarReaching Scope of Neuroinflammation after Traumatic Brain Injury. *Nat. Rev. Neurol.* **2017**, *13*, 171–191.
243. Hutchinson, P. J.; O’Connell, M. T.; Rothwell, N. J.; et al. Inflammation in Human Brain Injury: Intracerebral Concentrations of IL-1 α , IL-1 β , and Their Endogenous Inhibitor IL-1ra. *J. Neurotrauma* **2007**, *24*, 1545–1557.
244. Yatsiv, I.; Morganti-Kossmann, M. C.; Perez, D.; et al. Elevated Intracranial IL-18 in Humans and Mice after Traumatic Brain Injury and Evidence of Neuroprotective Effects of IL-18-Binding Protein after Experimental Closed Head Injury. *J. Cereb. Blood Flow Metab.* **2002**, *22*, 971–978.
245. Frugier, T.; Morganti-Kossmann, M. C.; O’Reilly, D.; et al. In Situ Detection of Inflammatory Mediators in Post Mortem Human Brain Tissue after Traumatic Injury. *J. Neurotrauma* **2010**, *27*, 497–507.
246. Hayakata, T.; Shiozaki, T.; Tasaki, O.; et al. Changes in CSF S100B and Cytokine Concentrations in Early-Phase Severe Traumatic Brain Injury. *Shock* **2004**, *22*, 102–107.
247. Holmin, S.; Höjeberg, B. In Situ Detection of Intracerebral Cytokine Expression after Human Brain Contusion. *Neurosci. Lett.* **2004**, *369*, 108–114.
248. Clausen, F.; Hånell, A.; Björk, M.; et al. Neutralization of Interleukin-1 β Modifies the Inflammatory Response and Improves Histological and Cognitive Outcome Following Traumatic Brain Injury in Mice. *Eur. J. Neurosci.* **2009**, *30*, 385–396.
249. Clausen, F.; Hånell, A.; Israelsson, C.; et al. Neutralization of Interleukin-1 β Reduces Cerebral Edema and Tissue Loss and Improves Late Cognitive Outcome Following Traumatic Brain Injury in Mice. *Eur. J. Neurosci.* **2011**, *34*, 110–123.
250. de Rivero Vaccari, J. P.; Lotocki, G.; Marcillo, A. E.; et al. A Molecular Platform in Neurons Regulates Inflammation after Spinal Cord Injury. *J. Neurosci.* **2008**, *28*, 3404–3414.
251. de Rivero Vaccari, J. P.; Lotocki, G.; Alonso, O. F.; et al. Therapeutic Neutralization of the NLRP1 Inflammasome Reduces the Innate Immune Response and Improves Histopathology after Traumatic Brain Injury. *J. Cereb. Blood Flow Metab.* **2009**, *29*, 1251–1261.
252. Walsh, J. G.; Muruve, D. A.; Power, C. Inflammasomes in the CNS. *Nat. Rev. Neurosci.* **2014**, *15*, 84–97.
253. Adamczak, S.; Dale, G.; de Rivero Vaccari, J. P.; et al. Inflammasome Proteins in Cerebrospinal Fluid of

- Brain Injured Patients as Biomarkers of Functional Outcome. *J. Neurosurg.* **2012**, *117*, 1119–1125.
254. Brickler, T.; Gresham, K.; Meza, A.; et al. Nonessential Role for the NLRP1 Inflammasome Complex in a Murine Model of Traumatic Brain Injury. *Mediators Inflamm.* **2016**, *2016*, 6373506.
255. De Rivero Vaccari, J. P.; Brand, F.; Adamczak, S.; et al. Exosome-Mediated Inflammasome Signaling after Central Nervous System Injury. *J. Neurochem.* **2016**, *136*, 39–48.
256. Lin, W.-P.; Xiong, G.-P.; Lin, Q.; et al. Heme Oxygenase-1 Promotes Neuron Survival through Down-Regulation of Neuronal NLRP1 Expression after Spinal Cord Injury. *J. Neuroinflammation* **2016**, *13*, 52.
257. Wallisch, J. S.; Simon, D. W.; Bayır, H.; et al. Cerebrospinal Fluid NLRP3 Is Increased after Severe Traumatic Brain Injury in Infants and Children. *Neurocrit. Care* **2017**, *27*, 44–50.
258. Liu, H.-D.; Li, W.; Chen, Z.-R.; et al. Expression of the NLRP3 Inflammasome in Cerebral Cortex after Traumatic Brain Injury in a Rat Model. *Neurochem. Res.* **2013**, *38*, 2072–2083.
259. Irrera, N.; Pizzino, G.; Calò, M.; et al. Lack of the Nlrp3 Inflammasome Improves Mice Recovery Following Traumatic Brain Injury. *Front. Pharmacol.* **2017**, *8*, 459.
260. Ismael, S.; Nasoohi, S.; Ishrat, T. MCC950, the Selective NLRP3 Inflammasome Inhibitor Protects Mice against Traumatic Brain Injury. *J. Neurotrauma* **2018**, *35*, 2018.
261. Zendedel, A.; Johann, S.; Mehrabi, S.; et al. Activation and Regulation of NLRP3 Inflammasome by Intrathecal Application of SDF-1a in a Spinal Cord Injury Model. *Mol. Neurobiol.* **2016**, *53*, 3063–3075.
262. Jiang, W.; Li, M.; He, F.; et al. Targeting the NLRP3 Inflammasome to Attenuate Spinal Cord Injury in Mice. *J. Neuroinflammation* **2017**, *14*, 207.
263. Duncan, J. S.; Sander, J. W.; Sisodiya, S. M.; et al. Adult Epilepsy. *Lancet* **2006**, *367*, 1087–1100.
264. Staley, K. Molecular Mechanisms of Epilepsy. *Nat. Neurosci.* **2015**, *18*, 367–372.
265. Minami, M.; Kuraishi, Y.; Yamaguchi, T.; et al. Convulsants Induce Interleukin-1 β Messenger RNA in Rat Brain. *Biochem. Biophys. Res. Commun.* **1990**, *171*, 832–837.
266. Minami, M.; Kuraishi, Y.; Satoh, M. Effects of Kainic Acid on Messenger RNA Levels of IL-1 Beta, IL-6, TNF Alpha and LIF in the Rat Brain. *Biochem. Biophys. Res. Commun.* **1991**, *176*, 593–598.
267. De Simoni, M. G.; Perego, C.; Ravizza, T.; et al. Inflammatory Cytokines and Related Genes Are Induced in the Rat Hippocampus by Limbic Status Epilepticus. *Eur. J. Neurosci.* **2000**, *12*, 2623–2633.
268. Ravizza, T.; Vezzani, A. Status Epilepticus Induces Time-Dependent Neuronal and Astrocytic Expression of Interleukin-1 Receptor Type I in the Rat Limbic System. *Neuroscience* **2006**, *137*, 301–308.
269. Lehtimäki, K. A.; Peltola, J.; Koskikallio, E.; et al. Expression of Cytokines and Cytokine Receptors in the Rat Brain after Kainic Acid-Induced Seizures. *Brain Res.* **2003**, *110*, 253–260.
270. Vezzani, A.; Moneta, D.; Conti, M.; et al. Powerful Anticonvulsant Action of IL-1 Receptor Antagonist on Intracerebral Injection and Astrocytic Overexpression in Mice. *Proc. Natl. Acad. Sci. U.S.A.* **2000**, *97*, 11534–11539.
271. Heida, J. G.; Pittman, Q. J. Causal Links between Brain Cytokines and Experimental Febrile Convulsions in the Rat. *Epilepsia* **2005**, *46*, 1906–1913.
272. Vezzani, A.; French, J.; Bartfai, T.; et al. The Role of Inflammation in Epilepsy. *Nat. Rev. Neurol.* **2011**, *7*, 31–40.
273. Meng, X.-F.; Tan, L.; Tan, M.-S.; et al. Inhibition of the NLRP3 Inflammasome Provides Neuroprotection in Rats Following Amygdala Kindling-Induced Status Epilepticus. *J. Neuroinflammation* **2014**, *11*, 212.
274. Vezzani, A.; Dingledine, R.; Rossetti, A. O. Immunity and Inflammation in Status Epilepticus and Its Sequelae: Possibilities for Therapeutic Application. *Expert Rev. Neurother.* **2015**, *15*, 1081–1092.
275. Maroso, M.; Balosso, S.; Ravizza, T.; et al. Interleukin1 β Biosynthesis Inhibition Reduces Acute Seizures and Drug Resistant Chronic Epileptic Activity in Mice. *Neurotherapeutics* **2011**, *8*, 304–315.
276. Tan, C.-C.; Zhang, J.-G.; Tan, M.-S.; et al. NLRP1 Inflammasome Is Activated in Patients with Medial Temporal Lobe Epilepsy and Contributes to Neuronal Pyroptosis in Amygdala Kindling-Induced Rat Model. *J. Neuroinflammation* **2015**, *12*, 18.
277. Ross, J.; Brough, D.; Gibson, R. M.; et al. A Selective, Non-Peptide Caspase-1 Inhibitor, VRT-018858, Markedly Reduces Brain Damage Induced by Transient Ischemia in the Rat. *Neuropharmacology* **2007**, *53*, 638–642.
278. Mulcahy, N. J.; Ross, J.; Rothwell, N. J.; et al. Delayed Administration of Interleukin-1 Receptor Antagonist Protects against Transient Cerebral Ischaemia in the Rat. *Br. J. Pharmacol.* **2003**, *140*, 471–476.
279. Poewe, W.; Seppi, K.; Tanner, C. M.; et al. Parkinson Disease. *Nat. Rev. Dis. Prim.* **2017**, *3*, 17013.
280. Scheltens, P.; Blennow, K.; Breteler, M. M. B.; et al. Alzheimer's Disease. *Lancet* **2016**, *388*, 505–517.
281. Dendrou, C. A.; Fugger, L.; Friese, M. A. Immunopathology of Multiple Sclerosis. *Nat. Rev. Immunol.* **2015**, *15*, 545–558.
282. Coll, R. C.; Robertson, A. A.; Chae, J. J.; et al. A Small Molecule Inhibitor of the NLRP3 Inflammasome for the Treatment of Inflammatory Diseases. *Nat. Med.* **2015**, *21*, 248–255.
283. Baldwin, A. G.; Brough, D.; Freeman, S. Inhibiting the Inflammasome: A Chemical Perspective. *J. Med. Chem.* **2016**, *59*, 1691–1710.
284. Perregaux, D. G.; McNiff, P.; Laliberte, R.; et al. Identification and Characterization of a Novel Class of Interleukin-1 Post-Translational Processing Inhibitors. *J. Pharmacol. Exp. Ther.* **2001**, *299*, 187–197.
285. Martinon, F.; Burns, K.; Tschopp, J. The Inflammasome: A Molecular Platform Triggering Activation of Inflammatory Caspases and Processing of proIL-Beta. *Mol. Cell* **2002**, *10*, 417–426.
286. Lamkanfi, M.; Mueller, J. L.; Vitari, A. C.; et al. Glyburide Inhibits the Cryopyrin/Nalp3 Inflammasome. *J. Cell Biol.* **2009**, *187*, 61–70.
287. Laliberte, R. E.; Perregaux, D. G.; Hoth, L. R.; et al. Glutathione S-Transferase Omega 1-1 Is a Target of Cytokine Release Inhibitory Drugs and May Be Responsible for Their Effect on Interleukin-1beta Posttranslational Processing. *J. Biol. Chem.* **2003**, *278*, 16567–16578.

288. Egger, J. F.; Gabel, C. A.; Zandi, K.; et al. Synthesis of Covalent [14C]-Labeled Diarylsulfonylurea (DASU) Inhibitors of the Processing and Release of IL-1. *J. Labelled Comp. Radiopharm.* **2002**, *45*, 785–794.
289. Coll, R. C.; O'Neill, L. A. J. The Cytokine Release Inhibitory Drug CRID3 Targets ASC Oligomerisation in the NLRP3 and AIM2 Inflammasomes. *PLoS One* **2011**, *6*, e29539.
290. Dempsey, C.; Rubio Araiz, A.; Bryson, K. J.; et al. Inhibiting the NLRP3 Inflammasome with MCC950 Promotes NonPhlogistic Clearance of Amyloid- β and Cognitive Function in APP/PS1 Mice. *Brain Behav. Immun.* **2017**, *61*, 306–316.
291. Horng, T. Calcium Signaling and Mitochondrial Destabilization in the Triggering of the NLRP3 Inflammasome. *Trends Immunol.* **2014**, *35*, 253–261.
292. Cocco, M.; Garella, D.; Di Stilo, A.; et al. Electrophilic Warhead-Based Design of Compounds Preventing NLRP3 Inflammasome-Dependent Pyroptosis. *J. Med. Chem.* **2014**, *57*, 10366–10382.
293. He, Y.; Varadarajan, S.; Muñoz-Planillo, R.; et al. 3,4-Methylenedioxy- β -Nitrostyrene Inhibits NLRP3 Inflammasome Activation by Blocking Assembly of the Inflammasome. *J. Biol. Chem.* **2014**, *289*, 1142–1150.
294. Juliana, C.; Fernandes-Alnemri, T.; Wu, J.; et al. AntiInflammatory Compounds Parthenolide and Bay 11-7082 Are Direct Inhibitors of the Inflammasome. *J. Biol. Chem.* **2010**, *285*, 9792–9802.
295. Cocco, M.; Miglio, G.; Giorgis, M.; et al. Design, Synthesis, and Evaluation of Acrylamide Derivatives as Direct NLRP3 Inflammasome Inhibitors. *ChemMedChem* **2016**, *11*, 1790–1803.
296. Marchetti, C.; Chojnacki, J.; Toldo, S.; et al. A Novel Pharmacologic Inhibitor of the NLRP3 Inflammasome Limits Myocardial Injury after Ischemia–Reperfusion in the Mouse. *J. Cardiovasc. Pharmacol.* **2014**, *63*, 316–322.
297. Cocco, M.; Pellegrini, C.; Martínez-Banaclocha, H.; et al. Development of an Acrylate Derivative Targeting the NLRP3 Inflammasome for the Treatment of Inflammatory Bowel Disease. *J. Med. Chem.* **2017**, *60*, 3656–3671.
298. Richardson, P.; Sonneveld, P.; Schuster, M.; et al. Bortezomib or High-Dose Dexamethasone for Relapsed Multiple Myeloma. *N. Engl. J. Med.* **2005**, *352*, 2487–2498.
299. Baldwin, A.; Rivers-Auty, J.; Daniels, M.; et al. Boron Based Inhibitors of the NLRP3 Inflammasome. *Cell Chem. Biol.* **2017**, *24*, 1321–1335.
300. Baldwin, A. G.; Tapia, V. S.; Swanton, T.; et al. Design, Synthesis and Evaluation of Oxazaborine Inhibitors of the NLRP3 Inflammasome. *ChemMedChem* **2018**, *13*, 312–320.
301. Compan, V.; Baroja-Mazo, A.; López-Castejón, G.; et al. Cell Volume Regulation Modulates NLRP3 Inflammasome Activation. *Immunity* **2012**, *37*, 487–500.
302. Rossol, M.; Pierer, M.; Raulien, N.; et al. Extracellular Ca²⁺ Is a Danger Signal Activating the NLRP3 Inflammasome through G Protein-Coupled Calcium Sensing Receptors. *Nat. Commun.* **2012**, *3*, 1329.
303. Lee, G.-S.; Subramanian, N.; Kim, A. I.; et al. The CalciumSensing Receptor Regulates the NLRP3 Inflammasome through Ca²⁺ and cAMP. *Nature* **2012**, *492*, 123–127.
304. Murakami, T.; Ockinger, J.; Yu, J.; et al. Critical Role for Calcium Mobilization in Activation of the NLRP3 Inflammasome. *Proc. Natl. Acad. Sci. U.S.A.* **2012**, *109*, 11282–11287.
305. Katsnelson, M. A.; Rucker, L. G.; Russo, H. M.; et al. K⁺ + Efflux Agonists Induce NLRP3 Inflammasome Activation Independently of Ca²⁺ Signaling. *J. Immunol.* **2015**, *194*, 3937–3952.
306. Jiang, H.; He, H.; Chen, Y.; et al. Identification of a Selective and Direct NLRP3 Inhibitor to Treat Inflammatory Disorders. *J. Exp. Med.* **2017**, *214*, 3219–3238.
307. Duncan, J. A.; Bergstralh, D. T.; Wang, Y.; et al. Cryopyrin/NALP3 Binds ATP/dATP, Is an ATPase, and Requires ATP Binding to Mediate Inflammatory Signaling. *Proc. Natl. Acad. Sci. U.S.A.* **2007**, *104*, 8041–8046.
308. Liu, W.; Guo, W.; Wu, J.; et al. A Novel Benzo[d]imidazole Derivate Prevents the Development of Dextran Sulfate Sodium-Induced Murine Experimental Colitis via Inhibition of NLRP3 Inflammasome. *Biochem. Pharmacol.* **2013**, *85*, 1504–1512.
309. Zhang, C.; Zhong, B.; Yang, S.; et al. Synthesis and Biological Evaluation of Thiabendazole Derivatives as

Anti-Angiogenesis and Vascular Disrupting Agents. *Bioorg. Med. Chem.* **2015**, *23*, 3774–3780.

310. Pan, L.; Hang, N.; Zhang, C.; et al. Synthesis and Biological Evaluation of Novel Benzimidazole Derivatives and Analogs Targeting the NLRP3 Inflammasome. *Molecules* **2017**, *22*, 213.

311. Avonto, C.; Tagliatela-Scafati, O.; Pollastro, F.; et al. An

NMR Spectroscopic Method to Identify and Classify Thiol-Trapping Agents: Revival of Michael Acceptors for Drug Discovery? *Angew. Chem. Int. Ed.* **2011**, *50*, 467–471.